Mechanisms of Visual Circuit Assembly in Zebrafish

Szydlo Shein, Andy

Awarding institution:
King's College London

Mechanisms of Visual Circuit Assembly in Zebrafish

Thesis for Degree of

Doctor of Philosophy

Andrea Szydlo-Shein

Supervisors:

Prof. Robert Hindges (Primary Supervisor)

Dr. Martin Meyer (Secondary Supervisor)

MRC Centre for Neurodevelopmental Disorders

Centre for Developmental Neurobiology

Institute of Psychiatry, Psychology & Neuroscience

King's College London

ABSTRACT

One of the most outstanding and unique features of the central nervous system is the complexity underlying its neural circuit assembly. Development of the vertebrate visual system is dependent on the correct morphological and functional connectivity between synaptic partners. Cell adhesion molecules expressed in specific cell types are known not only to mediate the connections between pre- and postsynaptic partners but to maintain them after they have been made. However, the full extent of the mechanism responsible for neuronal wiring within the retina and between the retina and its retinorecipient nuclei in the brain is still far from complete. During my PhD, I started bridging this knowledge gap by investigating the role of the synaptic adhesion protein, teneurin-4, in shaping the morphological and functional connectivity in the vertebrate visual system. Making use of a zebrafish CRISPR knockout combined with a wide range of techniques, including but not limited to, single cell labelling, *in vivo* functional and structural imaging we were able to assess the role of teneurin-4 (tenm4) in the assembly of defined retinal circuits, specifically in the correct morphological development of retinal ganglion cell (RGC) axonal arbors and tectal cell (TC) dendritic arbors in the tectum**.** Furthermore, we detect an aberrant distribution of the presynaptic protein synaptophysin in RGC axonal arbors, as well as of the postsynaptic density protein PSD-95 in TC dendritic arbors - suggesting a role for *tenm4* in synaptogenesis and/or synaptic organisation. Mutations in human TENM4 have been linked to bipolar disorder. Our findings therefore have the potential to lead to a better understanding of the aetiology of this disorder, as well as the general mechanisms involved in the creation of functional synaptic networks in healthy state

COVID-19 IMPACT STATEMENT

The current COVID-19 pandemic resulted in the closure of our research laboratories starting the 23rd of March 2020. Facilities then gradually re-opened in June 2020; however, access was severely limited with required equipment for the completion of this thesis remaining inaccessible. This has had a widespread impact on my research project. Planned work for this thesis impacted by the pandemic includes:

1) Access to the Fish Facility was limited and more importantly some fish lines were not breeding causing an extra delay on final experiments.
2) Functional analysis of the enlarged synapses in tenm4 mutant fish, which was an important element of my project. For this, I would have performed two-photon functional imaging on zebrafish larvae upon visual stimulation. The Nikon Imaging Centre did not allow training, therefore planned experiments on the two-photon microscope were not able to be done.
3) Finally, the understanding whether the phenotype observed throughout the project is cell autonomous or not was indispensable for the complete description of the overall phenotype. This required single cell transplants – where donor cells from a WT fish are transplanted into a tenm4 mutant fish and vice versa – and subsequent analysis of their development.

Therefore, the work presented here is based on data collected prior to the COVID-19 pandemic.

DECLARATION STATEMENT

The work presented in this thesis is the result of my own original research. Contribution of others involved is indicated in the text. However, I would like to use this space to highlight that initial functional data on the tenm4$^{10bp\Delta}$ mutant was collected **by Dr. Katherine Trevers.**

ACKNOWLEDGEMENTS

"Above all, don't fear difficult moments. The best comes from them" – Rita Levi-Montalcini

Firstly, I would like to thank my primary supervisor Prof. Robert Hindges - from whom I learnt so much. I am truly thankful to him for allowing me to take on a project so dear to me and forming me from a newby MSc student to the independent scientist I am today. I would also like thank the following people: my second supervisor Dr. Martin Meyer for his help, statistics lessons, and useful guidance throughout the PhD. My thesis committee, Dr. Darren Williams and Dr. Deepak Srivastava, whose assistance and dedicated involvement helped guide not only my research project but my development as a scientist. The BSU staff: Bruno, Thom, Jacqui, Sam, Dimi, Will and all my fish - working with them made these four years incredibly enjoyable, although no longer colleagues, the friendship will forever remain. A special thanks to Dr. Matt Grubb and Dr. Esther Bell, whose office doors were always open for scientific advice, encouragement, but most importantly sincere and valuable guidance, thank you both for being my lifeline throughout this adventure.

Rita, boop, every day with you made being away from home bearable. Thank you for being my colleague, my friend, my confidant, my home.

Tom, my love, your patience is inspiring. Growing with you, achieving this with you, and adventuring life with you is a dream come true. Thank you for being my main rock and form of support, for your patient, love…and for writing all my e-mails.

Zeidito, you planted the seed, and although you are no longer here to see the fruit it bore, I will forever be grateful to you for beginning this journey with me. Bobe, every call reenergised me and gave me the strength to keep going, I am proud to be your Rita Levi-Montalcini.

Tulip, Slope and GabOrly, thank you for always being role models and friends. We have conquered the world together, and I cannot wait to see what we do next. MaPa, there will never be enough words to thank you both. I am who I am because of the unconditional love and support you have given me. You are my best friends, my role models, and my heroes. This accomplishment is as much yours as it is mine.

TABLE OF CONTENTS

FIGURES

Chapter 1.

Chapter 2.

Chapter 3.

Chapter 4.

Chapter 5.

TABLES

ABBREVIATIONS

aa	Amino Acids
ACL	Amacrine Cell Layer
ACs	Amacrine Cells
AF	Arborisation Field
BCs	Bipolar Cells
BD	Bipolar Disorders
bsPVIN	bi-stratified Periventricular Neurons
CAMs	Cell Adhesion Molecules
CNS	Central Nervous System
Cntn6	Cell Adhesion Molecule Contactin-6
dpf	Days Post Fertilisation
DsR	DsRedExpress
E#	Embryonic Day
ECD	Extracellular Domain
EGF	Epidermal Growth Factors
EM	Electron Microscopy
GCL	Ganglion Cell Layer

GFP	Green Fluorescent Protein
GWAS	Genome Wide Association Studies
HCs	Horizontal Cells
hpf	Hours Post Fertilisation
ICD	Intracellular Domain
IHC	Immunohistochemistry
INL	Inner Nuclear Layer
IPL	Inner Plexiform Layer
ISH	in situ hybridisation
KD	Knockdown
KO	Knockout
MeOH	Methanol
MGCs	Müller Glia Cells
msPVIN	mono-stratified Periventricular Neurons
NDDs	Neurodevelopmental Disorders
NHL	NCL-1, HT2A and Lin-41
Nlgns	Neuroligins
NMJ	Neuromuscular Junction
Nrxns	Neurexins
nsPVIN	non-stratified Periventricular Neurons

O/N	Overnight
ON	Optic Nerve
ONL	Outer Nuclear Layer
OPL	Outer Plexiform Layer
OT	Optic Tectum
PH3	Phosphohistone-H3
PH3+	PH3-positive
ProK	Proteinase K
PRs	Photoreceptors
PSD	Postsynaptic density
PTVs	Piccolo-Bassoon Transport Vesicles
PVN	Periventricular Neurons
PVPN	Periventricular Projection Neurons
PyrN	Pyramidal Neurons
RGCs	Retinal Ganglion Cells
RPC	Retinal Progenitor Cells
SAC	Stratum Album Centrale
scRNA-seq	Single-Cell RNA-Sequencing
SCZ	Schizophrenia
SGC	Stratum Griseum Centrale

SGFS	Stratum Griseum et Fibrosum Superficiale
SGP	Stratum Griseum Periventriculare
SH3	Src-Homology 3
SIN	Superficial Interneurons
SO	Stratum Opticum
SPV	Stratum Periventriculare
STVs	Synaptic Transport Vesicles
Syp	Synaptophysin
TC	Tectal Cells
tenm1	Teneurin-1
tenm2	Teneurin-2
tenm3	Teneurin-3
tenm4	Teneurin-4
TLPN	Torus Longitudinalis
TMD	Transmembrane Domain
TPGN	Tegmentum
TUNEL	Terminal Transferase (TdT)-Mediated Deoxyuridine-Triphosphate
WT	Wildtype
YD	Tyrosine-Aspartat

CHAPTER 1.

INTRODUCTION

For a brain to be fully functional, it requires the appropriate and coordinated establishment of connections between billions of neurons. It is a precise connectivity pattern that eventually leads to function and behaviour and is known to be highly conserved between species. The functional outputs that arise from neural circuit information processing rely on the wiring of correct synaptic connections between different cells. This cell diversity varies from tens to thousands of neuronal types per region of the brain, differing in aspects such as morphology, physiology, and gene expression (Cook, 2003; Masland, 2012; Stevens, 1998). The formation of functional neural circuits during development is highly complex and involves a variety of processes such as axon growth and axon guidance (Hadjieconomou, Timofeev, & Salecker, 2011), synapse formation (Meyer & Smith, 2006), generation and positioning of correct neuronal types along the nervous system (F. J. Livesey & Cepko, 2001; R. Livesey & Cepko, 2001), and a variety of mechanisms that control the subcellular specificity of synaptic connections (Missaire & Hindges, 2015). Although some of the mechanisms have been identified, there are still many fundamental questions to be answered.

The purpose of this introductory chapter is to give the general background, which will be introduced in greater detail within each chapter. First, an overview of the organisation and development of the vertebrate visual system is provided. Then, the different types of cells in the retina and the tectum and their developmental are described. This is followed by an explanation of cell adhesion molecules, focusing on

Teneurins – a family of type II glycoproteins - and their role in regulating neuronal connectivity and circuit assembly. Finally, an outline of previous work done in the lab which led to this research project as well as the description of the aims and objectives of this thesis are defined.

1.1 VERTEBRATE VISUAL SYSTEM

Over the past decades, zebrafish have become an important vertebrate model in developmental neuroscience; they are prolific breeders, whose embryos develop rapidly, reaching sexual maturity within 3 months. This development occurs externally and in a well-defined staging series, which allows for the observation of embryonic development from the moment of fertilisation. During the first 24 hours of development, embryos do not develop pigmentation, allowing the visualisation of the developing organs. By 48 hours, common vertebrate specific body features can be seen, including a compartmentalised brain, eyes, and ears. Larvae hatch, are able to swim, and can freely search for food as soon as 5 days after fertilisation **(Figure 1.1)** (Bilotta & Saszik, 2001).

Sensory systems – specifically the visual system – are some of the most important models concerning the study of synaptic specificity and neural processing (Bilotta & Saszik, 2001). They are simpler models for studying more complex regions of the brain, and they are highly conserved across vertebrates in both structure and mechanisms leading to their development (Centanin & Wittbrodt, 2014). The zebrafish visual system, which is comparable to that of other vertebrates, continues to develop after hatching, which gives rise to the opportunity of linking development of the different visual structures with both physiological and behavioural aspects. It develops at an extraordinary pace resulting in a well-developed and functional system by 5 days post fertilisation (dpf) (Fleisch & Neuhauss, 2006).

The visual system plays a key role in most animals. It allows processing of sensory stimuli – such as identifying prey or predators in zebrafish - so it can elicit a

proper behavioural reaction. This entails the synchronised development of numerous neuronal types working in parallel neural circuits to process features of the visual input (Fleisch & Neuhauss, 2006) .

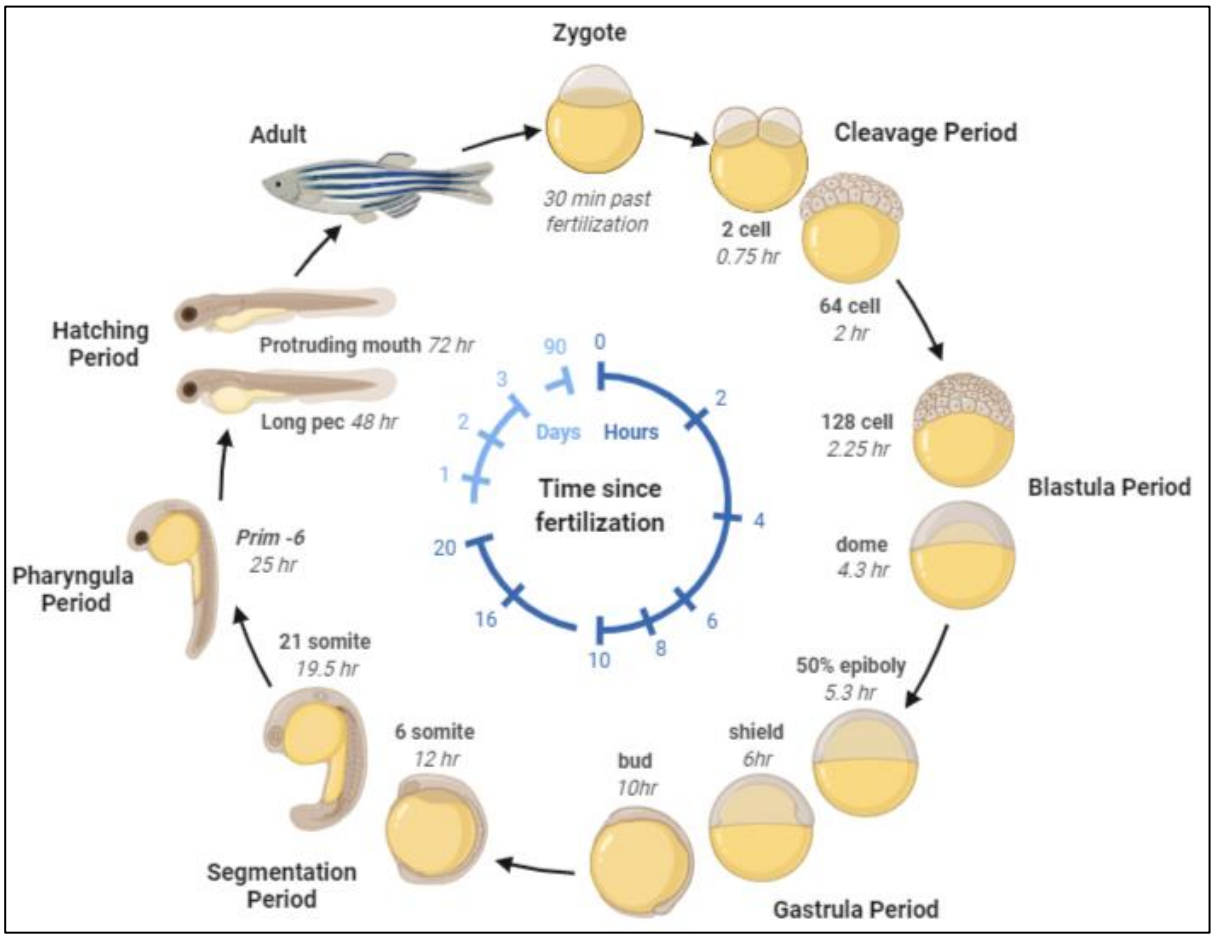

Figure 1.1 Zebrafish Development From Zygote to Adult. Zygote Period – the newly fertilised egg after completion of the first zygotic cell cycle. Cleavage Period – zygotic cell cyles 2-7 occur rapidly and synchronously. Blastula Period – rapid and metasynchronous cell cycles (8-9) occur, which give way to lengthened, asynchronous ones at the midblastula transition, then epibloy begins. Grasula Period – morphogenetic movements of involution, convergence, and extension form the epliblast, hypoblast, and embryonic axis. Segmentation period – Somites, pharyngeal arch primordia, and neuromeres develop, primary organogenesis and earliest movements take place, tail appears. Pharyngula Period – phylotypic stage of embryo, body axis straightens from its early curvature around the yolk sac; circulation, pigmentation, and fins begin development. Hatching period – completion of rapid morphogenesis of primary organ system, cartilage development in head and pectoral fin. Hatching occurs asynchronously across individuals. Adapted from (Hosen et al., 2013)

1.1.1 Retinal Development

Retinal development in zebrafish has been thoroughly studied; it originates from a pseudostratified neuroepithelium and develops into a laminated tissue. This neuroepithelium contains highly polarised elongated retinal progenitor cells (RPCs) which undergo apical division (Lee & Norden, 2013). They are known to be multipotent and to give rise to all the different retinal cell types (Agathocleous & Harris, 2009; He et al., 2012). In vertebrates, retinal subtypes are generated in a stereotyped manner. The “competence model” suggests that RPCs pass through different competence states with specific restriction on their developmental potential. Hence, each RPC division can give rise to a retinal cell subtype and/or another RPC with a more regulated potential **(Figure 1.2 A)** (Centanin & Wittbrodt, 2014). Developmentally, there is an overlap in retinal neurogenesis. Retinal ganglion cells (RGCs) are the first neurons to be born and they migrate to, and later occupy the innermost (basal) retinal layer (described below). Apically located cone photoreceptors (PRs) arise, together with the later born rod PRs, they create the outermost (apical) layer. Next, the inhibitory interneurons are generated, horizontal cells (HCs) and amacrine cells (ACs). Lastly, bipolar cells (BPs) and müller glia cells (MGCs) **(Figure 1.2 B)** (Centanin & Wittbrodt, 2014; He et al., 2012).

Visual information is captured by the eyes and pre-processed in the retina. Although only ~500µm thick – in zebrafish, (Ren, McCarthy, Zhang, Adolph, & Li, 2002) the vertebrate retina is made up of six main neuronal classes, which can be divided into more than 70 neuronal subtypes – species dependent (Harvard University Press, n.d.; Nguyen-Ba-Charvet & Chédotal, 2014): (1) PRs, (2) HCs, (3) BCs, (4) ACs, (5) RGCs, (6) MGCs - who provide metabolic and homeostatic support (**Figure**

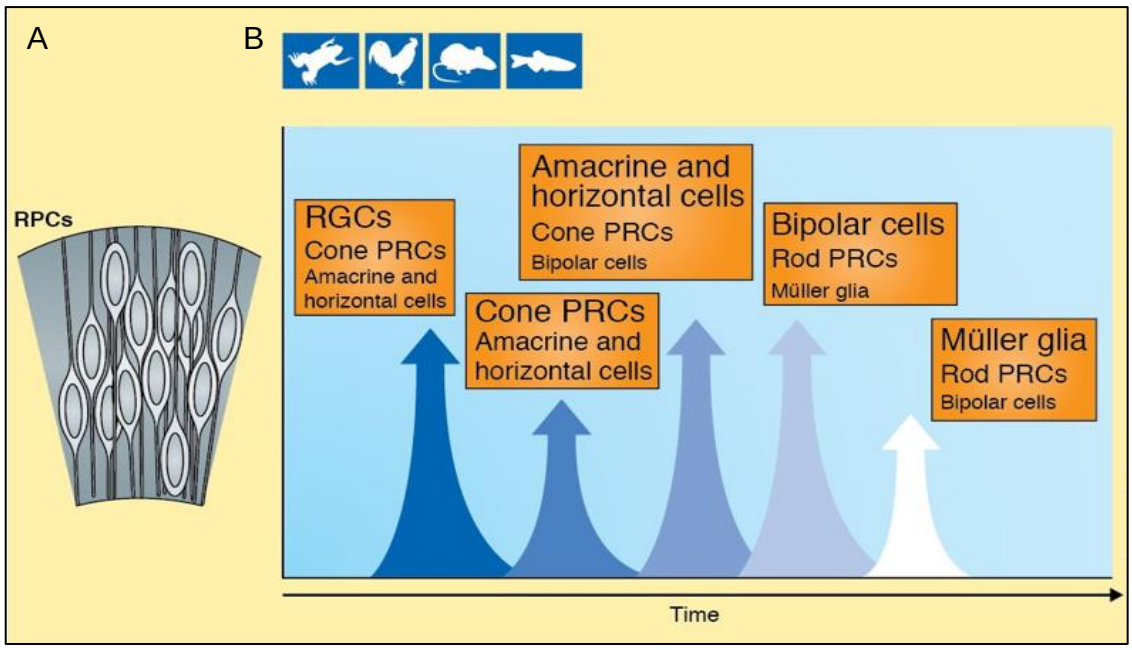

Figure 1.2 Neurogenesis in the vertebrate retina. A. The vertebrate retina originates from a pseudostratified neuroepithelium in which undifferentiated RPCs are connected to both apical and basal laminae. **B.** In vertebrates, retinal cell types are generated in a stereotyped time order**:** RGCs are the first to differentiate, then PRs, followed by ACs and HCs, and lastly BCs and MGCs. Adapted from (Centanin & Wittbrodt, 2014).

1.3 A). These six types of neurons are organised in a five-layered structure made up of three cellular layers and two synaptic layers. (1) The outer nuclear layer (ONL), containing PRs, (2) the inner nuclear layer (INL), containing cell bodies of HCs, BCs, ACs and MGCs, and (3) the ganglion cell layer (GCL) constituted of RGCs and some displaced ACs. The synaptic layers, in between the cellular layers, are where synaptic connections occur between the bordering retinal cell types, (4) the outer plexiform layer (OPL) made up of connections between PRs, BCs, and HCs, and (5) the inner plexiform layer (IPL) which consists of connections amongst ACs, BCs and RGCs (**Figure 1.3 B**).

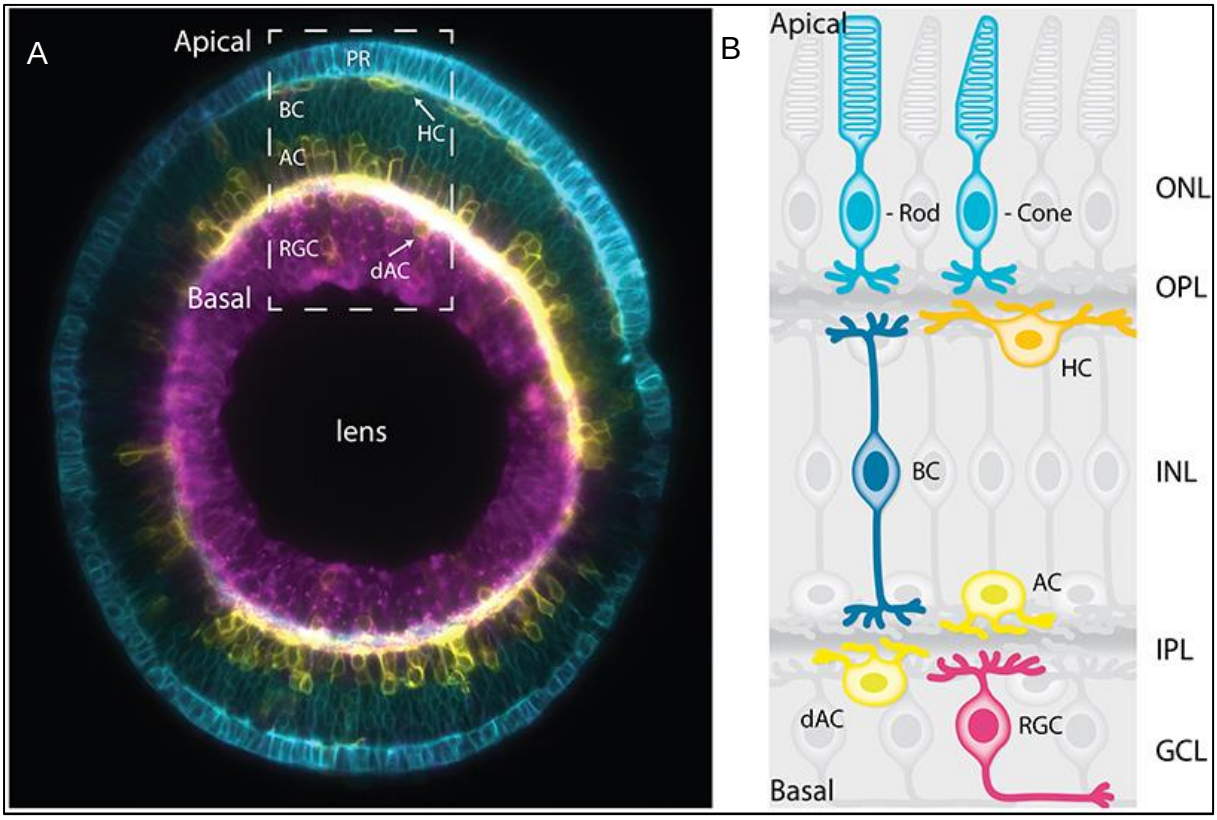

Figure 1.3 Vertebrate retina organisation. A. Sagittal section of a mature zebrafish retina *in vivo*, showing lamination of cell bodies. The retinal cells are labelled with a combination of membrane-tagged fluorescent proteins that allows that identification of all the major neuronal types. Cyan – PR and BCs; yellow – HCs and ACs; magenta – RGCs. Arrows indicate HCs and displaced ACs. **B.** Schematic representation of a cross-section of a mature retina in zebrafish showing lamination and cell bodies and their neurites. Cell bodies are organised into five layers from apical to basal; ONL, OPL, INL, IPL and GCL. Major retinal cell types: Cyan – PR; yellow – HCs; blue – BPs; light yellow – ACs; and magenta - RGCs. Adapted from (Amini, Rocha-Martins, & Norden, 2017).

1.1.2 Inner Plexiform Layer Development

There is a general understanding of how precise neuronal connectivity patterning occurs during development. It is known that synaptic connections can be

organised into different layers or laminae, this is evident within the CNS. Systems that are organised this way are great for studying how dendrites and axons target each other during synaptogenesis (J R Sanes & Yamagata, 1999).

As previously mentioned, the IPL is the layer in the retina where synaptic connections occur between RGCs and their presynaptic partners, ACs, and BCs. These synaptic connections are arranged into different laminae. Roughly, the IPL can be divided into two functionally distinct sublaminae: 1) ON circuits, positioned closer to RGCs – where cells depolarise as a response to an increase in light and, 2) OFF circuits, positioned closer to ACs and BPs – where cells hyperpolarise in response to the increase in light (Famiglietti & Kolb, 1976). These two main sublaminae are further subdivided into multiple strata. This strata is responsible for processing information about the visual scene (Lettvin, Maturana, McCulloch, & Pitts, 1959; Wässle, 2004; Werblin & Roska, 2004). Initial studies in cats suggested dendritic segregation into ON and OFF sublaminae happened because of selective elimination of branches following an initial overgrowth period (Chalupa & Günhan, 2004; Dann, Buhl, & Peichl, 1988; Ramoa, Campbell, & Shatz, 1988; H.-P. Xu & Tian, 2007). Later, through time-lapse imaging of a Brn3c:MGFP zebrafish line, it was shown by Mumm et al., (2006) that the IPL begins its stratification with a single layer made up primarily of RGC dendrites at the boundary between the GCL and the amacrine cell layer **(Figure 1.4 A**; 2.5 dpf). As development continues, the IPL expands along with the rest of the eye, RGC dendrites begin to innervate deeper areas of the IPL, which forms multiple dendritic strata **(Figure 1.4 A;** 3 dpf). Accompanying this, a subpopulation of ACs are born and embedded within this developing IPL. The cell bodies of these ACs function as a barrier to stop RGC dendrite outgrowth, forcing them to accumulate below the AC bodies. As the IPL continues to develop, the RGC dendrites are able to extend around

the AC cell bodies to innervate deeper regions of the IPL, and thus, creating multiple dendritic strata. By 6 dpf four different strata could be distinguished **(Figure 1.4 A;** 6dpf) and, the IPL can be considered as mature at 16 dpf when 5 different strata have been fully formed **.** Interestingly, RGC dendritic lamination mostly occurs in an "inside-out" manner, creating the inner IPL before the outer IPL – from GCL to INL **(Figure 1.4 B,C;** 2.5 dpf – 6 dpf**).** This takes an unexpected turn during the second week of development when the last strata appears between S^{70} and S^{40}, S^{55}, it is created by intercalation of new RGC dendritic branches which get inputs from a specific type of ACs (Mumm et al., 2006).

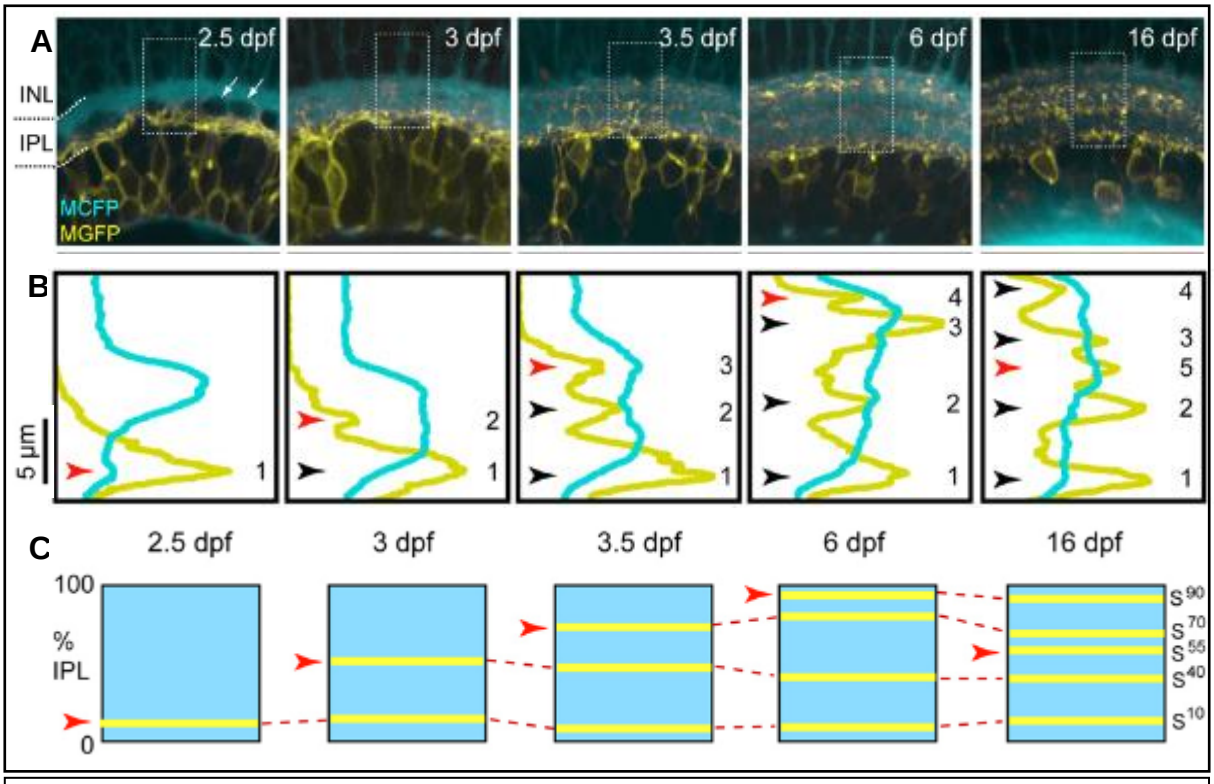

Figure 1.4 Inner plexiform layer development. A. Time-lapse images of a region of the retina in a Brn3c:MGFP zebrafish line. MGFP-positive RGCs from 2.5 dpf – 16 dpf showing IPL stratification development. **B.** Averaged fluorescent intensities within the boxed regions shown in A. Arrows indicate peaks in MGFP fluorescence, i.e.: strata; red arrows indicate development of new strata. Numbers indicate presumed sequence in the appearance of each peak. **C.** Location of each dendritic stratum expressed as a percentage of IPL thickness. Adapted from (Mumm et al., 2006).

1.1.3 Retinal Projections Leading to Optic Tectum Development

The processing of visual information in the tectum begins with the transmission of visual signals by RGC axons. RGCs form very long axons that in time make up the optic nerve (ON) which with they convey visual information to the primary visual centres in the brain (i.e. optic tectum (OT) in vertebrates, superior colliculus in mammals).

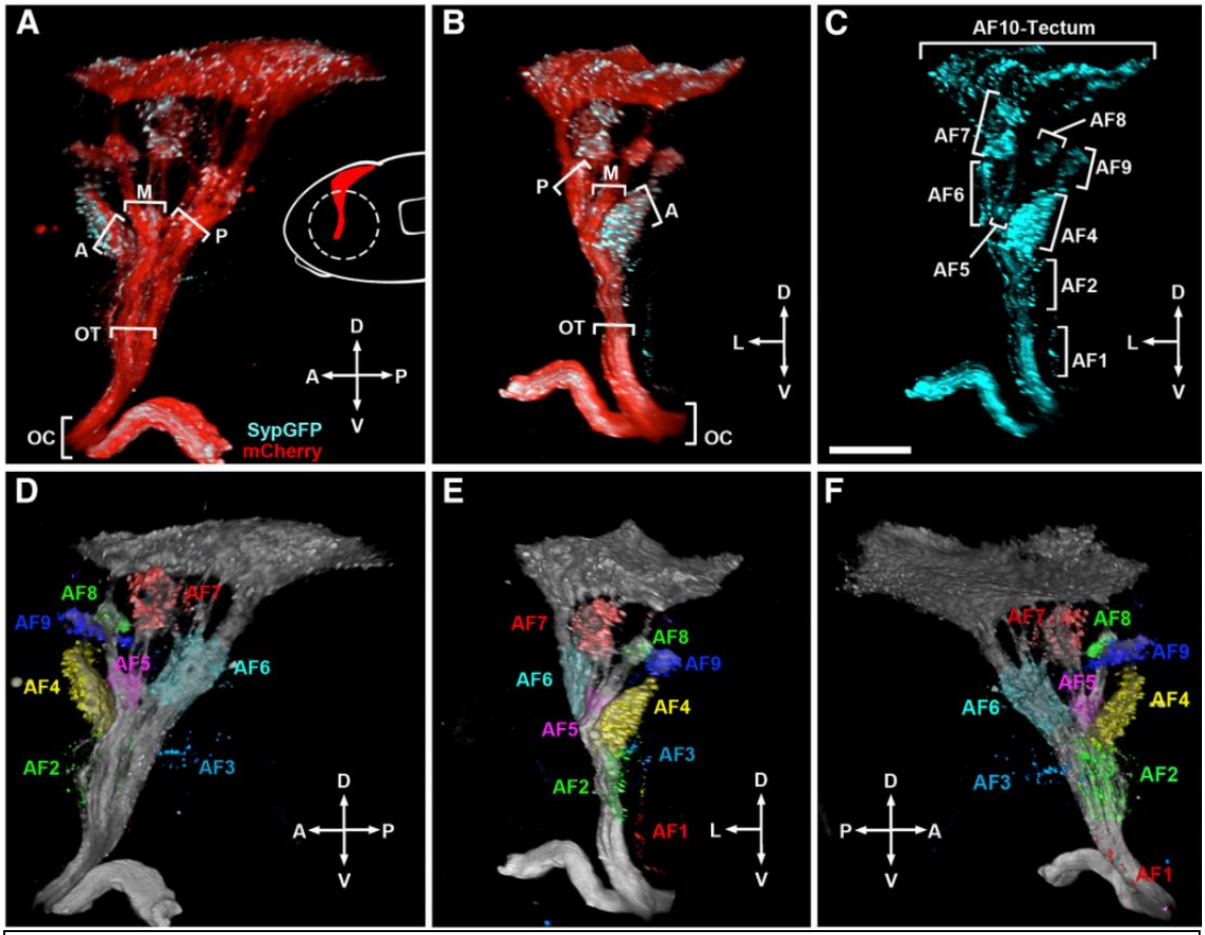

Figure 1.5 Arborisation fields formed by RGC axons. A. 3D reconstruction of a fixed 6 dpf larval brain with RGC expression (red). Note the optic chiasm (OC), main bundle of the optic tract (OT), and anterior (A), medial (M) and posterior (P) branches formed in the thalamus. The inset schematic side view of a larval zebrafish, dashed line is the contralateral eye. **B.** Frontal view of volume in (**A**). **C.** Syp-GFP channel of volume in (B). Brackets indicate distinct AFs formed by RGC axons. **C-F.** Lateral, frontal, and medial views of volume in B-D., with AF1-AF9 pseudo coloured. Scale bar is set at 50 µm. Adapted from (Robles et al., 2014).

RGCs differentiate at around 28 hpf (Nawrocki, 1985) Shortly after, they extend both dendritic and axonal processes. The initial axon leaves the retina and projects towards the midline at ~32 hpf, it crosses the midline at the optic chiasm between 34-36 hpf and begin to arborise. RGCs project to the ten different arborisation fields (**Figure 1.5;** AFs; AF1-10) in the diencephalon and the mesencephalon, which correspond to the neuropil areas of the retinorecipient brain nuclei (Robles, Laurell, & Baier, 2014). These fields are referred to numerically by the distance from the ventral surface. The development of the AFs is very orderly, with no sign of projections that must be removed later in the developmental process. At 44 hpf, the only area that is targeted by the RGC axons is the AF10 (OT), suggesting that this is their initial target, but by 52 hpf, a small group of axons deviate from their original course to form AF9. Between 55 and 72 hpf the rest of the AFs are established **(Table 1.1)**. By this time point the larvae have hatched and become free feeding (Burrill & Easter, 1994; Robles et al., 2014)**.** The development of dendritic and axonal arborisations, projections and synaptic connections will be discussed in detail within future sections.

Table 1.1 Development of the various AFs. Adapted from (Burrill & Easter, 1994)

AF	48 hpf	52-54 hpf	60 hpf	66 hpf	72 hpf	6-7 dpf
AF-1	NO	NO	YES	YES	YES	YES
AF-2	NO	NO	NO	YES	YES	YES
AF-3	NO	NO	NO	YES	YES	YES
AF-4	NO	NO	NO	YES	YES	YES
AF-5	NO	NO	YES	YES	YES	YES
AF-6	NO	NO	NO	YES	YES	YES
AF-7	NO	NO	YES	YES	YES	YES
AF-8	NO	NO	NO	NO	YES	YES
AF-9	NO	YES	YES	YES	YES	YES
AF-10	YES	YES	YSE	YES	YES	YES

1.1.4 Optic Tectum Development

Previously, it was mentioned that the OT, located in the midbrain, is the primary visual centre for visual processing in nonmammalian vertebrates. During embryonic development, the OT – which is conserved across vertebrates, is formed from a pseudostratified neuroepithelium into a complex, multi-layered structure. The process by which this happens is both complex and unique. The chick OT is formed at embryonic day 2 (E2), when the mesencephalic alar plate of the midbrain rapidly enlarges (Watanabe & Nakamura, 2000). Until E3.5, the tectal wall is comprised of a simple pseudostratified neuroepithelium with proliferating cells. By E4 a large migration of young neurons migrate from the ventricular zone, leading to lamination and thickening of the tectal wall (LaVail & Cowan, 1971; Mey & Thanos, 2000). After which there are three successive waves of migration forming the tectal laminae. The first wave forms the deeper layers of the *stratum griseum centrale* (SGC) and the *stratum griseum perventriculare* (SGP). The second wave forms the superficial layers of the *stratum griseum et fibrosum superficiale* (SGFS). The third and last wave of migration produces the remaining layers of the SGFS (LaVail & Cowan, 1971).

The zebrafish OT, is divided in two main areas, (1) a deep layer, called the *stratum periventriculare* (SPV) which contains cell bodies and (2) a superficial neuropil region containing dendrites of tectal cells (TCs) (Xiao & Baier, 2007). Most RGCs are known to innervate the SFGS, which has six subdivisions (SFGS1-6) (Robles et al., 2014) while others innervate the *stratum opticum* (SO), the SGC, the SPV and the interface between the *stratum album centrale* (SAC) and the SPV **(Figure 1.6)** (Nevin, Robles, Baier, & Scott, 2010).

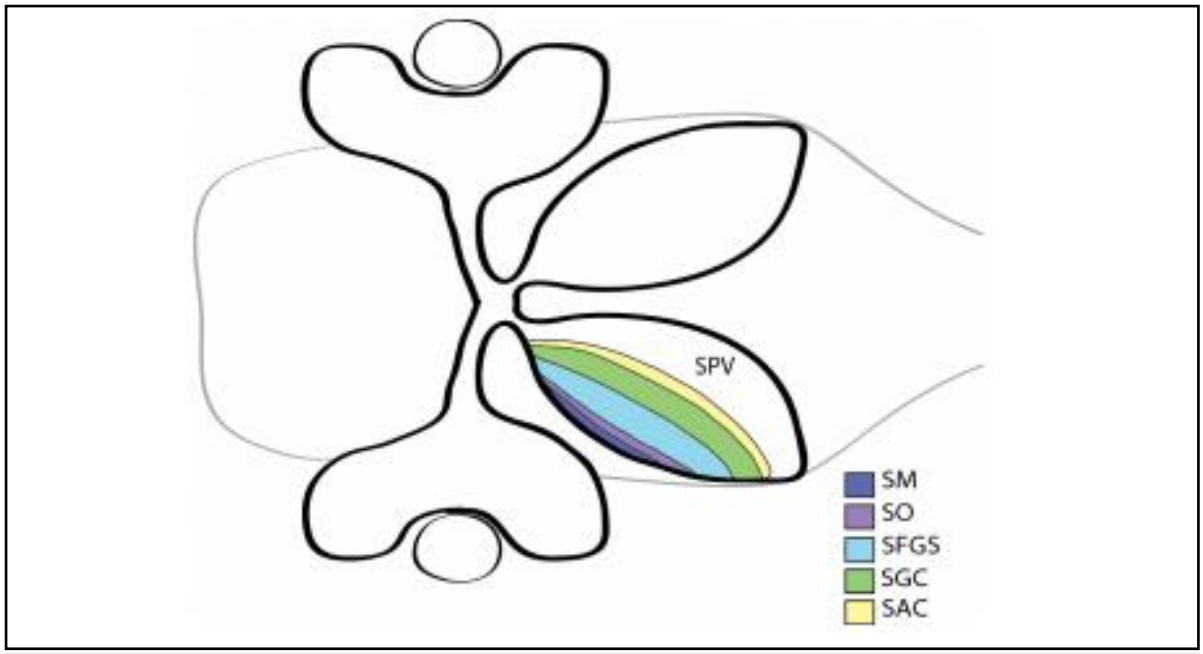

Figure 1.6 Schematic of OT laminae organisation. Dorsal view schematic of the larval zebrafish OT. Six tectal laminae coloured: blue – *stratum marginale* (SM); purple – *stratum opticum* (SO); cyan – *stratum fibrosum et griseum superficiale* (SFGS); *stratum griseum centrale* (SGC); and *stratum album centrale* (SAC) of the neuropil region. The deepest layer, containing cell bodies the *stratum periventriculare* (SPV). Adapted from (Rouse, 2015)

1.1.4.1 Development of Synaptic Layers in the Optic Tectum

The formation of the neuropil strata in both the IPL and the OT is regulated by both adhesive (Joshua R Sanes & Yamagata, 2009) and repulsive transmembrane proteins (Matsuoka et al., 2011). As previously mentioned, former developmental studies have verified that cell adhesion molecules (CAMs) expressed in specific retinal cell types mediate the connections between pre- and postsynaptic partners to form specific networks (Antinucci, Nikolaou, Meyer, & Hindges, 2013; Antinucci, Suleyman, Monfries, & Hindges, 2016; Duan et al., 2014).

In zebrafish, different subtypes of RGCs innervate each of the ten laminae in the OT. The lamination pattern although complex is not random. Each lamina has a different processing function varying from tuning of objects to size filtering. This laminar specificity is precise throughout development, once an axon reaches its position in a specific OT lamina, it develops a highly branched and flat arbor that does not cross over into neighbouring laminae (Xiao et al., 2011). In contrast to the retina, where dendrites are continuously rearranged within the IPL by the addition or elimination of branches and synapses, in the axonal arbors in the OT there is no noticeable change over time (Robles, Filosa, & Baier, 2013).

1.2 RETINOTECTAL PATHWAYS

Retinotectal pathways provide the perfect opportunity to explore the different mechanisms that underlie neural circuit formation and information processing. The retina, an isolated neural network, gives the opportunity to examine morphological, physiological, and developmental features as well as the molecular mechanisms underlying circuit assembly (Karlstrom et al., 1996). By 3 days post-fertilisation (dpf), developmental time point for hatching, the retina and its projections to the brain can be considered mature enough for visually evoked responses and motor behaviours to be solicited (Easter & Nicola, 1996; Niell & Smith, 2005). This provides a chance to compare the developmental processes of the visual system of morphological features to those of visual physiology and behaviour. Some of the morphological features include the arrangement of cells and their connections in parallel layers, the regular spacing of neurons within each of these layers, and the radial connections that run perpendicular to these. Physiologically, there are two mechanisms for parallel processing, the first, to be able to extract salient visual features, from the visual scene, such as colour, motion, and form - every small section of the visual world must be processed in multiple ways. Second, this mechanism has to be repeated across the entire visual field so that it can be processed (Joshua R Sanes & Zipursky, 2010). With time, studies in development have revealed some of the molecular mechanisms that are responsible for neural connectivity such as guidance molecules and synapse formation (Bilotta & Saszik, 2001). These are some of the subjects that will be described in the following pages.

1.2.1 Retinal Ganglion Cells

As mentioned before, RGCs are the sole output neurons of the retina with the OT being their primary visual target. In zebrafish, they are the first retinal neurons to develop at ~28 hours post fertilisation (hpf) and their axons reach the OT by ~2 dpf. Postmitotic RGCs migrate to the GCL and begin their structural and functional development. Before dendrites are developed, the cell body extends an axon, which makes its way into the visual targets. Primary processes tipped with growth cones emerge opposite the axon initial segment and shortly after a complex dendritic arbor begins to form with branching at different depths of the IPL. The first synaptic connections are established with ACs and later with BCs. The dendritic arborisation can be considered mature when it is confined to one of the sublaminae of the IPL (Sernagor, Eglen, & Wong, 2001).

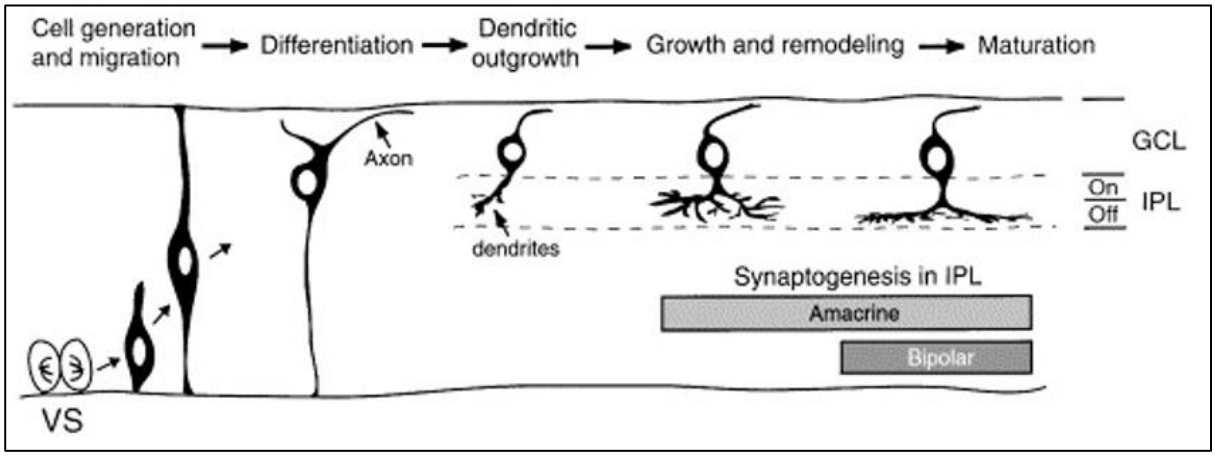

Figure 1.7 Schematic representation of the major stages in RGC development. Schematic represented from left (mitotic cell) to right (RGC synaptically confined to a specific IPL sublaminae). Adapted from (Sernagor et al., 2001).

1.2.1.1 Classification of RGC Subtypes

RGCs can be subdivided into dozens of subtypes based on anatomical, physiological, and molecular characteristics (Baden et al., 2016; Bae et al., 2018; Peng et al., 2019; Robles et al., 2014; N. M. Tran et al., 2019; Yan et al., 2020). Each subtype of RGC sends the output of a distinct visual computation by the retina which in turn is associated with a specific perceptual and behavioural function (Dhande & Huberman, 2014; Dhande, Stafford, Lim, & Huberman, 2015; Gollisch & Meister, 2010; Nikolaou et al., 2012; Robles et al., 2013). Because of this, the classification of these neurons has been of crucial importance over the past years. Although still far from complete, throughout the years, progress has been made regarding the classification of these cells. Neurons have been sparsely labelled using a mixture of techniques such as microinjections, transgenic animal lines and/or RNA sequencing (scRNA-seq) (Badea & Nathans, 2004; Coombs, van der List, Wang, & Chalupa, 2006; Kölsch et al., 2020; Kong, Fish, Rockhill, & Masland, 2005; Martersteck et al., 2017; Peng et al., 2019; Rheaume et al., 2018; Joshua R Sanes & Masland, 2015; Seung & Sümbül, 2014; Sun, Li, & He, 2002; N. M. Tran et al., 2019; Yan et al., 2020).

1.2.1.1.1 Morphological Criteria

Santiago Ramon y Cajal was a pioneer at describing with precision the anatomical aspects of neurons. By doing so he accomplished morphological characterisations from over 250 tissues and 1200 organs and systems (Garcia-Lopez, Garcia-Marin, & Freire, 2010). This included the vertebrate visual system, where RGCs where part of

his characterisation (S. R. y Cajal, 1893). Although revolutionary at his time, the classification of these cells has undergone a dramatic change over the past few years as a result of technological advancements. The morphological criteria frequently used to classify RGC is by soma size and dendritic and/or axonal field dimensions (Coombs et al., 2006).

From a morphological perspective, the characterisation of ~12 to ~22 distinct RGC subtypes were classified by their dendritic arborisation patterns in the mouse retina. It was thought that focusing solely on dendritic arborisation morphology would not produce precise data (Badea & Nathans, 2004; Coombs et al., 2006; Kong et al., 2005; Seung & Sümbül, 2014; Sun et al., 2002). By combining both dendritic and axonal arborisation patterns of zebrafish RGCs, more than 50 and possibly up to 82 different RGC types were identified by morphology alone **(Figure 1.8)** (Robles et al., 2014).

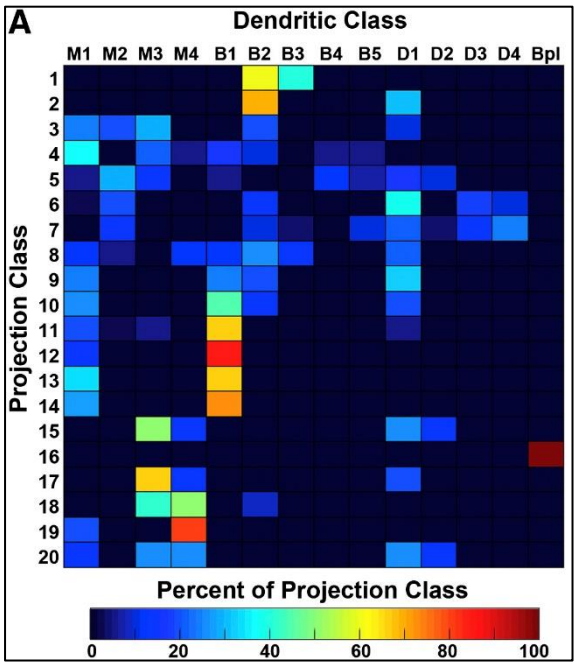

Figure 1.8 RGC subtypes by morphology in zebrafish. Contribution of RGCs with specific dendritic morphologies to each axonal projection patter. Each row sums to 100%. Eighty-two colourised squared represent distinct RGC population with unique combinations of dendritic and axonal morphologies. Seventy-five of these were observed in multiple samples. Adapted from (Robles et al., 2014).

1.2.1.1.2 Functional Criteria

For many years, *in vivo* studies of brain cell dynamics depended exclusively on electrical recordings of neuronal activity. These were done by either intracellular recordings of membrane potential dynamics or extracellular recordings of neuronal spike patterns. The invention of the two-photon excited fluorescence laser scanning microscopy (two-photon imaging) allowed the optical studies of both brain cell morphology and function *in vivo* **(Figure 1.9)** (Helmchen, 2009).

To begin to understand the different physiological subtypes of RGCs, two-photon calcium imaging was performed in the ventral retina of mice whilst presenting a variety of visual stimuli. This allowed the characterisation of RGC response types leading to the discovery of ~32 functionally distinct groups. Subsequently, anatomical and immunohistochemical (IHC) analysis was done to further specify the identified types (Baden et al., 2016).

1.2.1.1.3 Molecular Criteria

The field of biology has, over the last decade, been revolutionised. RNA sequencing has allowed the opportunity to study entire transcriptomes extensively and therefore has encouraged many important discoveries. The ability to isolate single cells, capture their transcripts, and generate sequencing libraries in which the transcripts can be mapped to individual cells, has allowed for scRNA-seq to assess properties of cell populations and biological systems at an extraordinary resolution (Olsen & Baryawno, 2018).

Recent studies have begun to use scRNA-seq to create comprehensive molecular taxonomies of RGCs in zebrafish, mice, non-human primates and humans (Kölsch et al., 2020; Peng et al., 2019; Rheaume et al., 2018; N. M. Tran et al., 2019; Yan et al., 2020). Using single cell transcriptomics, a comprehensive molecular catalogue of RGC in zebrafish was assembled. Transcription factors, cell recognition molecules and neuropeptides found to be expressed in one or few of the RGC clusters can now be used as markers for individual cell types, leading to the identification of ~33 transcriptionally distinct RGC subtypes **(Figure 1.10)** (Kölsch et al., 2020).

One of the central goals in the classification of RGCs has been classifying the diverse cell types by combining morphological, physiological, and molecular properties. Recent studies in mice, such as the one described in the previous section, have shown correlation between these two of three aspects (Baden et al., 2016; Bae et al., 2018; N. M. Tran et al., 2019). In zebrafish, reporter lines expressing specific transcription factors allowed, for the first time, the study of these three aspects together (Kölsch et al., 2020).

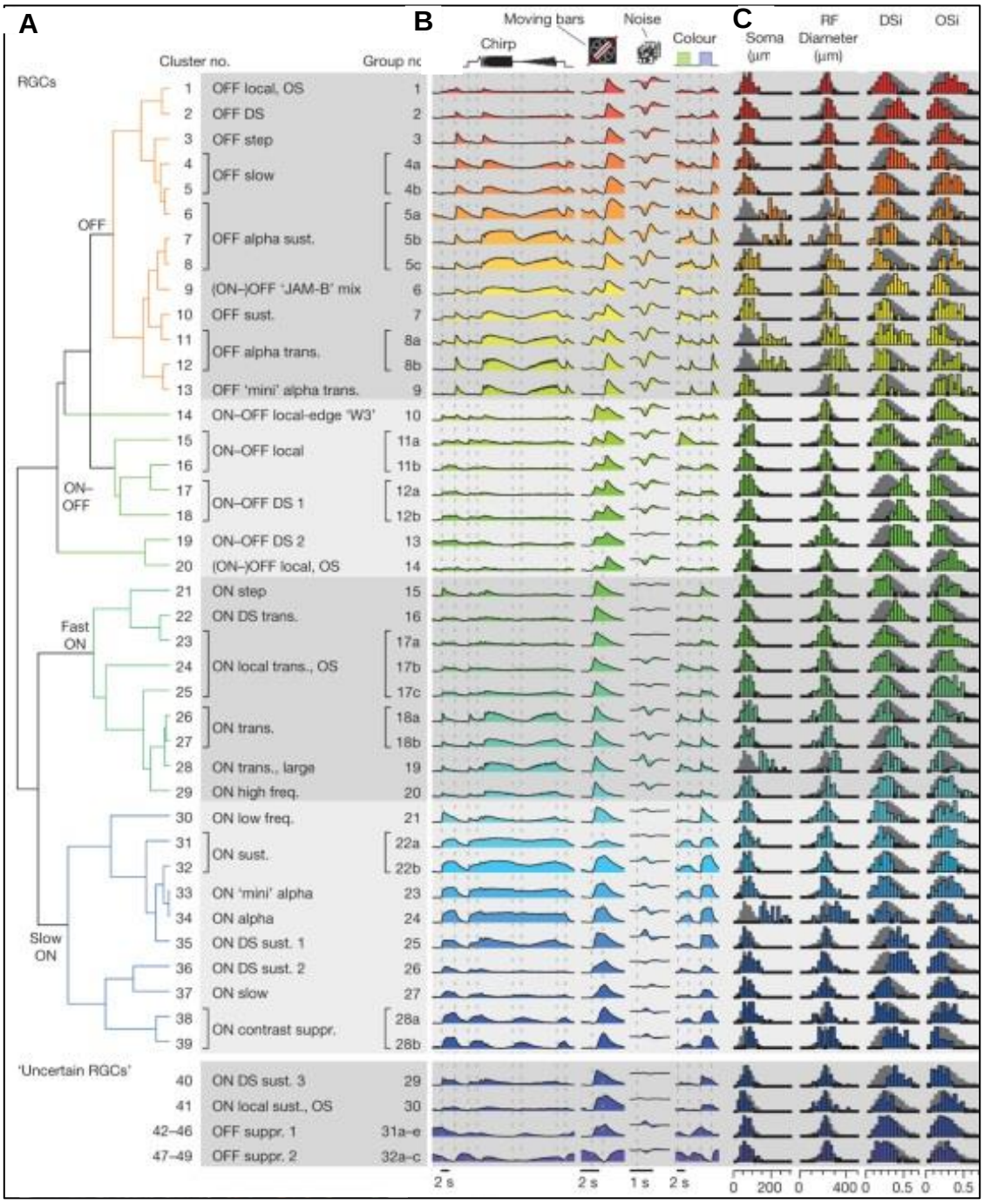

Figure 1.9 Functional RGC types of the mouse retina. A. Clusters of RGC subtypes, 28 RGC groups in total. **B.** Cluster-mean Ca^{2+} responses to the stimuli presented. **C.** Different selected metrics, from left to right: region of interest (soma) area, receptive field (RF) diameter, direction-selectivity index (DSi) and orientation-selectivity index (OSi). Adapted from (Baden et al., 2016).

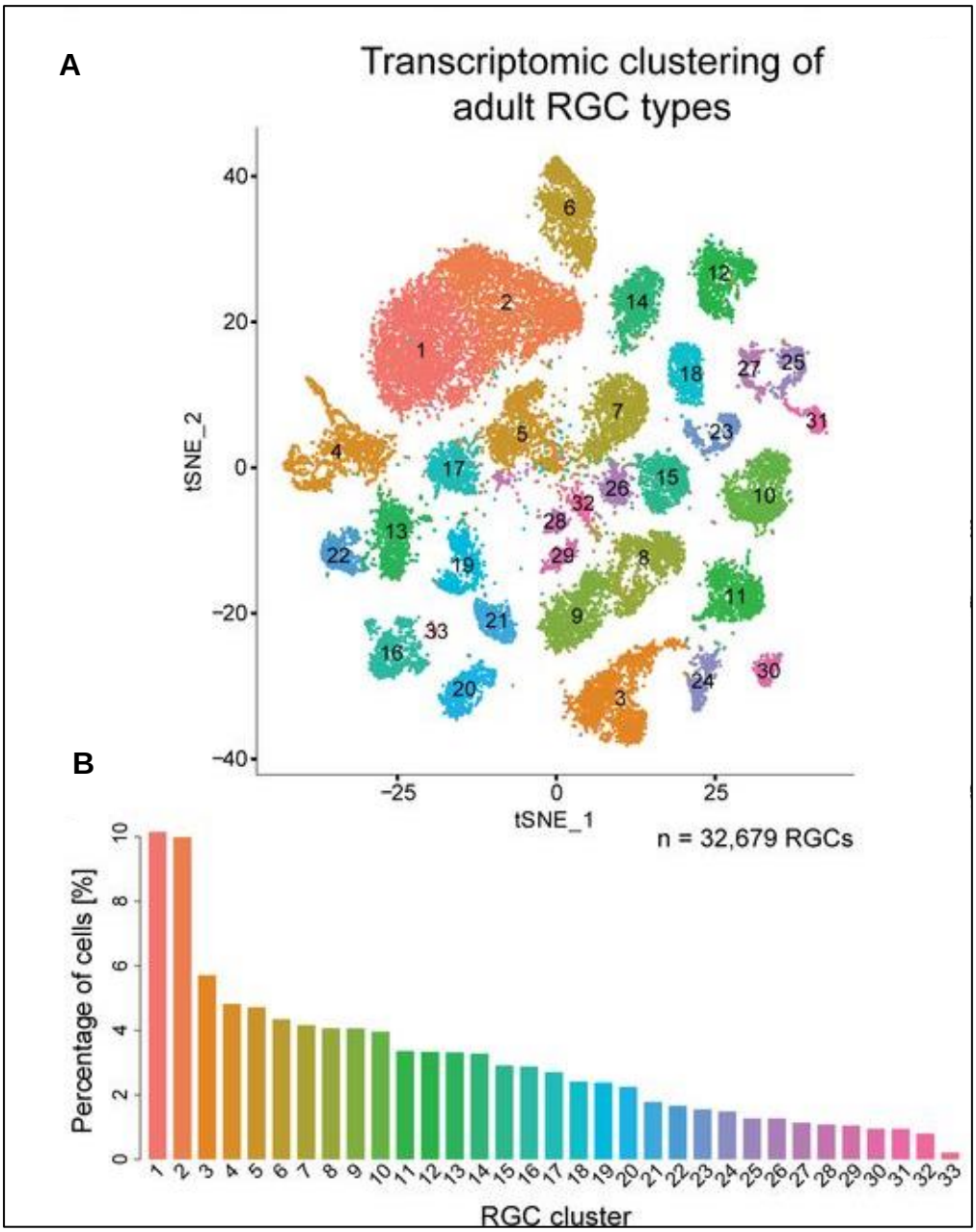

Figure 1.10 Molecular RGC types of zebrafish. A. t-distributed stochastic neighbour embedding (tSNE) visualisation of 33 transcription clusters (colours) of 32,679 adult zebrafish RGCs (points). Clusters are numbered in the order of decreasing relative frequency. **B.** Relative frequency (y-axis) of RGC clusters (x-axis), ordered from highest to lowest. Clusters are coloured as A. Adapted from (Kölsch et al., 2020).

1.2.1.2 Arborisations of RGCs

Neurons are born as spherical cells; however, their biology requires a highly polarised morphology. Throughout development, they extend tubular-like processes away from the cell body to establish connections with their targets. These elongating neuronal processes (axonal and dendritic), possess growth cones distally. Growth cones have a complex cytoskeletal structure. Cytoskeleton dynamics play a key role in neurite elongation, dendrite, and axon specification and most importantly it underlies growth cone motility. Growth cones have many other central functions that guarantee the correct development of the nervous system – including axon growth and pathfinding and the recognition of synaptic targets (Pinto-Costa & Sousa, 2021). The pathway RGC dendrites and axons must navigate within the retina and from the retina to the OT respectively, is not straightforward. RGC growth cones must navigate through a variety of different environments before reaching their final synaptic target (Holt, 1989).

1.2.1.2.1 Dendritic Arborisations of RGCs

Growing dendrites are very dynamic and undergo constant rearrangement throughout development by both adding and removing growing branches (Sernagor et al., 2001). These processes ramify into the different depths of the IPL creating complex dendritic arborisations and reaching maturation when they establish synaptic connections with ACs, BCs (Dreher & Robinson, 1991). Although this process is the same across all RGCs, there are variations in the rate at which the arborisations develop according to the subtype of the RGC (Ault & Leventhal, 1994; Dann et al., 1988). Both intrinsic

programmes - which are genetically encoded, and external influences - such as target dependent factors, are thought to play a role in regulating dendritic development (Sernagor et al., 2001).

The intrinsic programme states that despite there being diversity of patterns in RGC dendritic arborisations, cells with similar functions in the retina also share close similarities to each other. Furthermore, the different dendritic branching patterns of diverse subclasses are comparable amongst species. Because of this, the intrinsic programme theory proposes that there may be inherent similarities in gene expression that regulates the morphologies of RGC subtypes (Montague & Friedlander, 1991)

The external influence can occur from visual targets in the brain or within the retina itself. The latter can vary from diffusible or contact-mediated factors such as cell surface adhesion molecules. For a RGC to survive, it relies on forming contacts with its targets. There are different target-derived factors which influence RGC dendritic branching patterns, for example neurotrophins - which are important regulators of neuronal survival development, function, and plasticity - affect RGC dendritic outgrowth, remodelling and maintenance (Bosco & Linden, 1999; Lom & Cohen-Cory, 1999). Neurotransmission also plays a fundamental role in this. Certain neurotransmitters, such as acetylcholine, affect neurite outgrowth, dendritic branch length and number (Lipton, Frosch, Phillips, Tauck, & Aizenman, 1988; Sernagor et al., 2001). Developing dendrites of both invertebrate and vertebrate neurons are responsive to extrinsic signals that can not only stimulate or inhibit outgrowth but can also act as cues for directional growth. Some of these include Wnt and Dishevelled which increase the dendrite complexity and arborisation (Rosso, Sussman, Wynshaw-Boris, & Salinas, 2005); the receptor tyrosine kinases EphB1-3, which promotes dendritic complexity (Hoogenraad, Milstein, Ethell, Henkemeyer, & Sheng, 2005) and

Slit and Robo which have a role in dendritic differentiation, growth, regulation and branching and elongation of dendrites (Furrer, Vasenkova, Kamiyama, Rosado, & Chiba, 2007).

1.2.1.2.2. Axonal Arborisations of RGCs

Morphological and functional identities are provided to neurons via progenitor and precursor cells. This is achieved through its intrinsic specification programme which helps regulate mechanisms such as transcription factors, which not only regulate the expression of cell surface molecules but control morphogenesis and branch patterning of axons (Jan & Jan, 2010).

RGC axons navigate from the retina to their different targets in a stereotyped and error-free manner. Once they reach their specific visual targets in the brain, they form stereotypical planar axonal arbors with which they create synaptic connections with TCs (Baier, 2013; Xiao & Baier, 2007). The molecular mechanisms that could underlie the creation of these axonal arbors can be divided into one of the following groups: (1) intrinsic regulation of branching patterns (Jan & Jan, 2010), (2) neurite guidance by extracellular cues and (3) local cell-cell recognition.

It is also known that through these intrinsic factors, neurites can position themselves within their corresponding target layer. This leads to the idea that the final morphology of a neuron does not require guidance or external interactions but is generated by a cell-autonomous branching programme that results in specific synapse formation due to spatial proximity of presynaptic axons and postsynaptic dendrites (Baier, 2013).

Growing axons navigate to their targets by gradients of both attractant and repellent molecular cues. Through these extracellular cues, axons and dendrites are guided into spatial proximity with each other. Short-range repulsion and/or attraction by extracellular matrix molecules (i.e. Tenascin family molecules) define go and no-go areas for growing RGCs into the OT (Becker, Schweitzer, Feldner, Becker, & Schachner, 2003; Perez & Halfter, 1993). This is similar to what is observed in long-range axon guidance.

Transmembrane adhesion molecules have been identified as fundamental players in target recognition. Homophilic cell-cell recognition has been found to be essential for the specificity of synaptic partner matching and to ensure laminar targeting between dendrites and axons (Missaire & Hindges, 2015). Dynamic regulation of cell adhesion molecules is crucial to ensure a layer-specific targeting where laminae develop sequentially during development (Antinucci et al., 2013; Huberman, Clandinin, & Baier, 2010; Melnattur & Lee, 2011; M Yamagata & Sanes, 1995).

Each AF sublaminae is innervated by different subtypes of RGC. Although vastly branched, they are flat within the plane of their respective lamina, meaning that they do not cross over into neighbouring laminae **(Figure 1.11)** (Xiao & Baier, 2007; Xiao et al., 2011). In zebrafish, there are 22 stereotyped projection patterns by which RGCs transmit visual information to these AF in unique combinations. By doing this, they distribute visual inputs into different areas of the brain. The majority of RGCs ~97% terminate in the AF10 - the neuropil of the OT (Robles et al., 2013). RGCs axonal laminar selection occurs during the initial growth into the tectum.

In conclusion, in zebrafish, the vast majority of RGC axons target a specific sublaminae of the OT (Robles et al., 2013; Xiao & Baier, 2007). RGC axons form topographic connections with TCs . Studies in the mammalian visual system demonstrated that there is a correlation between the type of RGC and the lamination pattern its axon has (Y. K. Hong, Kim, & Sanes, 2011; Huberman, Feller, & Chapman,

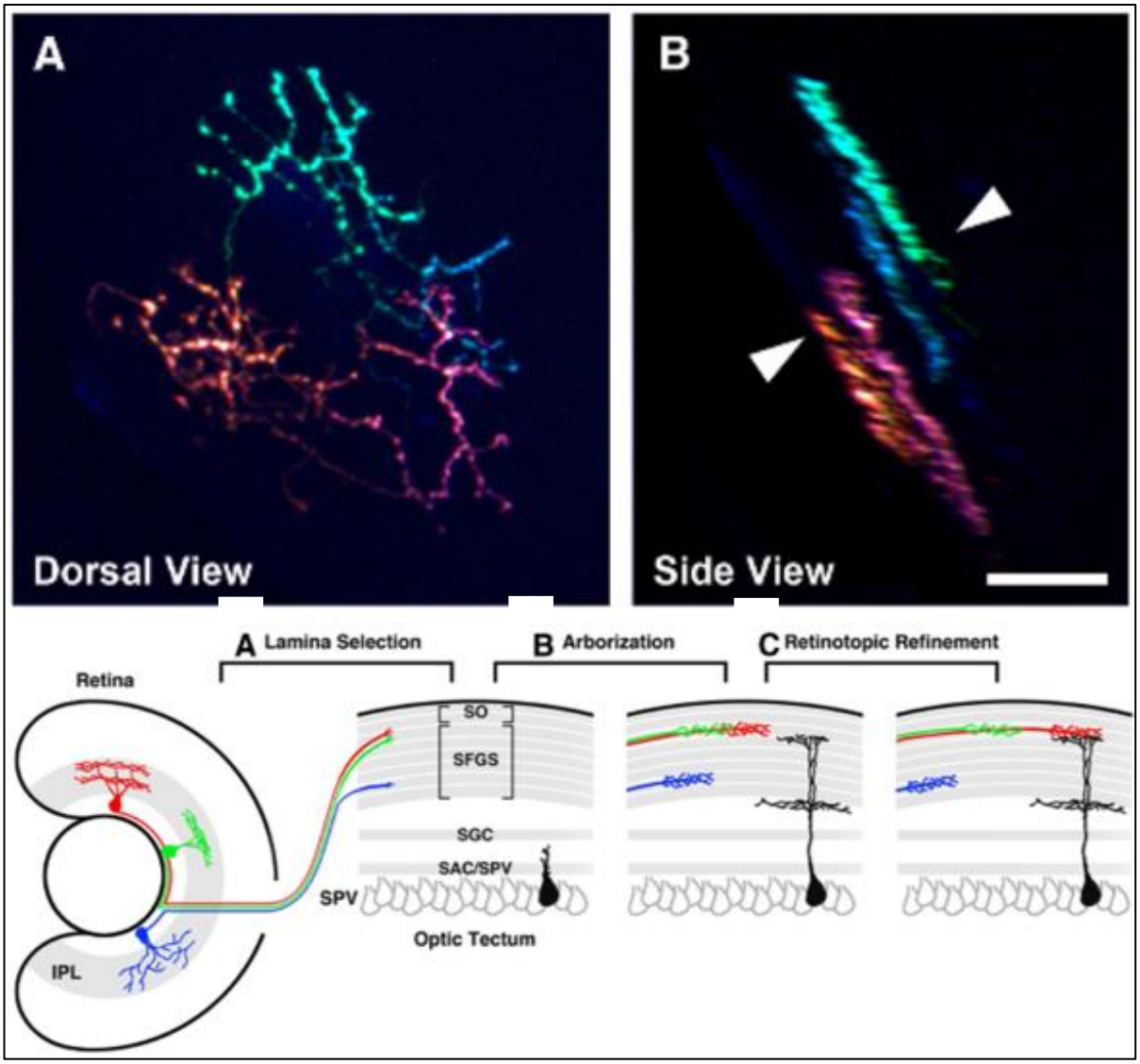

Figure 1.11 RGC axonal arborisation organised into thin sublaminae. A. Top view of a 7 dpf zebrafish larva. Four axons with unique colour profiles are labelled. **B.** Side view of image volume in A. **C.** RGC subtypes with different dendritic morphologies in the IPL (coloured in red, green, and blue) select specific retinotopic and sublaminar positions within the layers of the tectum. **D.** Relative laminar positions are maintained as axons form branched, planar arbors. **E.** Relative laminar positions remain unchanged. Scale bars set at 20 μm. Adapted from (Robles et al., 2013)

2008; Huberman et al., 2009; Kim, Zhang, Meister, & Sanes, 2010). Within this midbrain structure the RGCs form planar arbors (Xiao & Baier, 2007; Xiao et al., 2011) where processing of information begins with the transmission of visual signals by these RGC axons from the retina.

1.2.2 Cell Type Diversity in the OT

Information processing in the OT flows mainly from superficial layers to deeper layers. Most of the RGCs enter the OT through superficial layers, where they create glutamatergic synaptic connections with TC dendrites. The information continues through dendrites of periventricular neurons (PVNs) into the deeper layers of the OT (Kinoshita, Ito, Urano, Ito, & Yamamoto, 2006; Kinoshita & Ito, 2006). Here, the information gets transferred from interneurons to either other interneurons or to TC projection neurons which target the midbrain and hindbrain. These connections can be either GABAergic or glutamatergic and a small percentage of PVNs are known to be cholinergic. The outputs from these deeper layers govern behavioural responses (Kinoshita et al., 2006; Kinoshita & Ito, 2006).

Studies done in adult goldfish revealed 14 types of tectal cells characterised morphologically by the cell body position and dendritic arborisation(Meek & Schellart, 1978). This was later expanded to larval zebrafish. Through transgenic lines, three more neurons were identified, periventricular projection neurons (PVPNs), periventricular interneurons (PVINs) and superficial interneurons (SINs). PVINs can be subdivided into non-stratified PVINs (nsPVINs), mono-stratified PVINs (msPVINs) or bi-stratified PVINs (bsPVINs) depending on the morphology of their dendritic

arborisation (**Figure 1.12**) (Nevin et al., 2010), tectal pyramidal neurons (PyrN), tectal neurons with projections to the *torus longitudinalis* (TLPN), and tectal neurons with

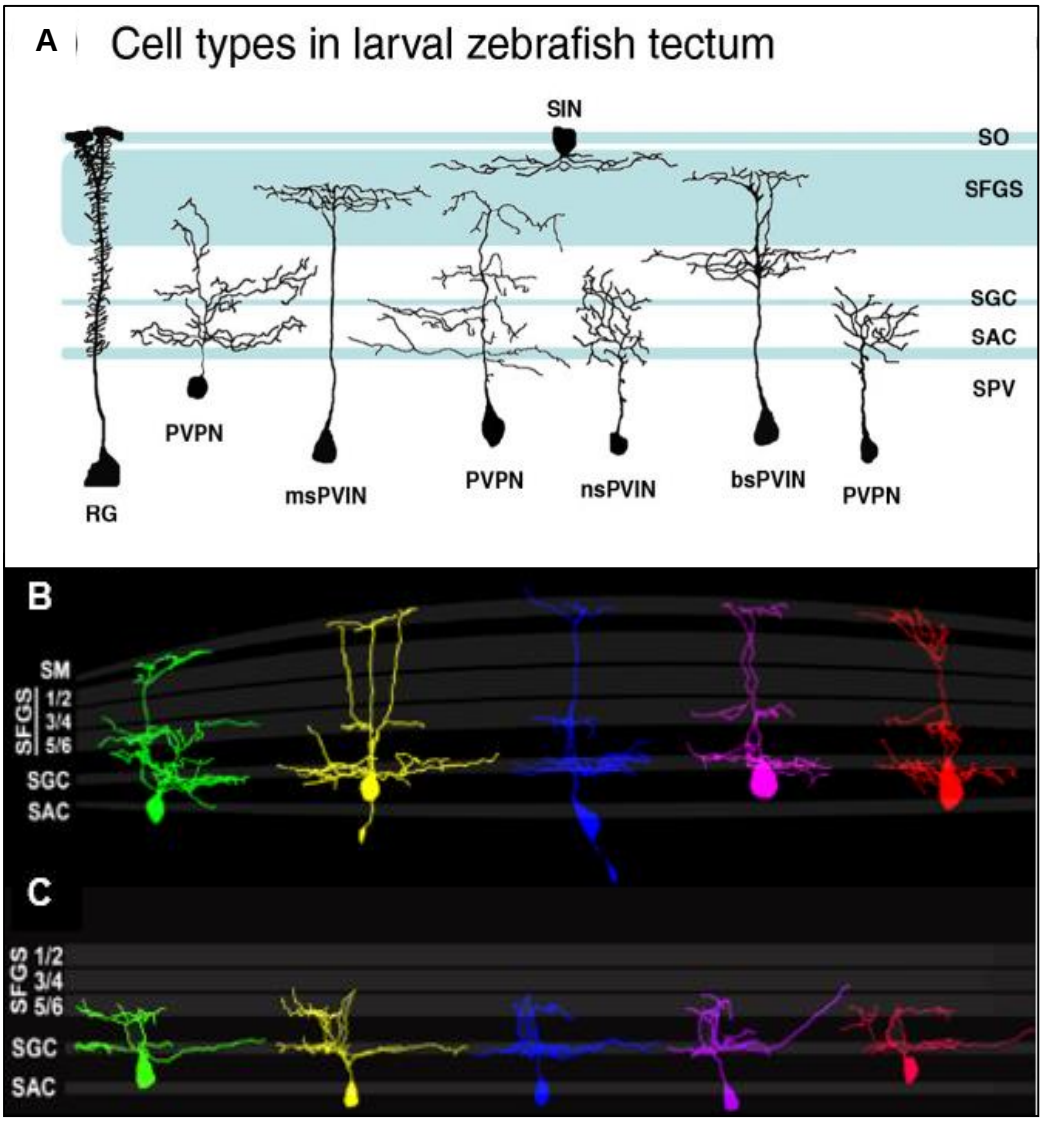

Figure 1.12 Cell type diversity in the zebrafish OT. A. Sampling of neuron morphologies observed in the larval zebrafish tectum. Including RG, PVPNs, PVINs, SINs. Note the diverse dendrite morphologies of both projection neurons and interneurons in the tectum. In particular, PVINs have been observed containing arbors that are non-stratified, mono-stratified or bi-stratified. **B.** Skeletonised tracings of five PyrNs. Light shading indicates tectal sublayers indicated at the left. Note morphological variability and the asymmetric morphology of PyNs located at the edges of the tectal NP. **C.** Skeletonised tracings of proximal/tectal neurite arbor formed by TLPNs in the NP. Despite morphological variability, all TLPNs form arbors mostly restricted to the SGC and deep SFGS layers, both of which are retinorecipient layers. Adapted from (DeMarco et al., 2020; Nevin et al., 2010)

ipsilateral descending projections to the *tegmentum* (TGPN) (compare **Figure 1.12 A**, **Figure 1.12 B, Figure 1.12 C).** (DeMarco, Xu, Baier, & Robles, 2020). It is important to state that many of these newly found cell types have a strong resemblance to those found in adult goldish.

1.2.3 Information Processing

Light enters the eye through the cornea and the lens where it is captured by the PRs and converted into electrochemical signals before it is sent through feature-specific parallel channels to the primary visual centres in the brain (Baier, 2013; Gebhardt, Baier, & Del Bene, 2013; Rodieck, n.d.; Schulte & Bumsted-O'Brien, 2008). PRs – located in the ONL, respond to light by hyperpolarising and initially send these signals to BCs, which function as interneurons. The information is then transmitted to the inner retina, where the axons of BCs make synaptic connections in the IPL, with both RGCs - the sole output neurons of the retina, and ACs - inhibitory neurons, whose main function is to shape and regulate RGC responses. The IPL is where most image processing takes place (Demb & Singer, 2015; Werblin & Roska, 2004). Lastly, RGC axons exit the eye forming the optic nerve, via which all information about the visual scene must be passed (Stevens, 1998), to reach the higher visual nuclei.

Information processing in the retina has three main stages. First, it decomposes the output from the PRs into ~12 different parallel information channels based on ~12 anatomical types of BCs that make synaptic connections to the PRs. Second, it connects these different channels to specific types of RGCs. Third, it combines the activity of both BCs and ACs to create the different encodings of the

visual world, which will consequently be transmitted to the brain (Masland, 2012). The complex but methodical organisation of RGCs and their synapses allows the efficient processing of visual stimuli (Wu, 2010). However, the formation of these vertical networks is not enough for the processing of visual stimuli; additionally, it has been discovered that retinal neurons are arranged in regular arrays in the horizontal plane, creating a “retinal mosaic” which allows the sampling of the entire visual field (Dhande & Huberman, 2014; Nguyen-Ba-Charvet & Chédotal, 2014). RGCs, encode different features of the visual scene depending on their subtype; each subtype tiles the retinal surface in a uniform and regular fashion making sure that the whole retina is sensitive to all the different types of visual features and thus covers every visual image completely (Anishchenko et al., 2010). The different subtypes of RGCs sample the visual scene through different size apertures established by the size of their dendritic field. Functionally, receptive fields that are created from the same subtype of RGCs sample the visual scene uniformly and can therefore provide a consistent map of the visual space (Wässle, 2004).

As previously mentioned, each retinal axon projects into a specific layer. It is also known that each of these retinorecipient laminae that are formed are topographically organised. RGC axons project to each layer in a visuotopic order, this leads to the retinotectal map actually being six parallel maps piled on top of each other. The topographic projections from the retina to the tectum have a specific order, RGCs in the temporal retina project into the anterior tectum; RGCs in the nasal retina develop into the posterior tectum; objects in the dorsal retina are mapped in the ventral tectum; and lastly the objects ventral retina project into the dorsal tectum (Nevin et al., 2010; Robles et al., 2014).

1.3 NEURONAL CONNECTIVITY

Synapses are specialised sites of contact which enable electrochemical signalling between neurons and their different targets – neurons, muscles, or glands. They typically are made up of (a) an axonal presynaptic compartment, (b) the synaptic cleft, and (c) a dendritic postsynaptic compartment (Waites, Craig, & Garner, 2005). The axonal presynaptic compartment is characterised by an accumulation of neurotransmitter-filled synaptic vesicles and by active zones –specialised domains where synaptic vesicles release these neurotransmitters into the synaptic cleft. The dendritic postsynaptic compartment, referred to as the postsynaptic density (PSD) is mainly involved in both, the clustering and anchoring of a variety of proteins, which include different receptors, ion channels, and cell adhesion molecules (CAMs) (Garner, Zhai, Gundelfinger, & Ziv, 2002).

1.3.1 Cell-Adhesion Molecules in Neuronal Connectivity

CAMs are known to hold together the pre- and postsynaptic compartment by extending from the cytoplasm of the postsynaptic cell into the synaptic cleft, ensuring the apposition of the active zone and the PSD. Although these features are known to be common in synapses throughout the brain, differences such as size and organisation can be found depending on the type and function of the specific synapse.

Regarding development, the specificity of how synaptic partner matching occurs amongst the millions of other neuronal and glial processes is a matter of astounding complexity. Generally, there are two main models that attempt to explain how this

synaptic specificity occurs (H. Cline, 2003; Huberman et al., 2008): one relies on patterns between correlated activity between neurons (Katz & Shatz, 1996; Psychology Press, n.d.), the other on mechanisms controlled by molecular cues (Benson, Colman, & Huntley, 2001; Sperry, 1963). Over the past years, it has become clear that the role of neuronal activity alone in refining synaptic partner matching is not enough for the precise specification of all the synaptic connections within the CNS. As a matter of fact, evidence shows that the expression of different recognition molecules is essential for the shaping of these precise neural circuits (Jontes & Phillips, 2006; Shapiro & Colman, 1999; Shen & Scheiffele, 2010). Within the molecular cue model, there are three classes of molecular mechanisms that could plausibly generate synaptic specificity: (1) intrinsic regulation of branching patterns, (2) neurite guidance by extracellular cues, and (3) local cell-cell recognition (Baier, 2013).

CAMs are membrane-bound cell surface molecules that encompass a varied group of transmembrane molecules. They have been implicated in both cell-cell or cell-extracellular matrix interactions – depending on their homophilic and/or heterophilic adhesion properties (Missaire & Hindges, 2015; Sakurai, 2017). Axon growth and guidance (Dickson, 2002), target recognition (Masahito Yamagata, Sanes, & Weiner, 2003) and synaptogenesis (Washbourne et al., 2004) are just some of the processes in which CAMs have been implicated.

1.3.2 Synapse Formation

Synaptogenesis is a complex and highly organised process by which functional synapses arise between neurons. Although it mainly occurs during development it is not exclusive to this stage, there is evidence of synapse formation and synapse plasticity taking place throughout adulthood. When comparing excitatory synapse formation versus inhibitory synapse formation, it has been found that the first occurs very rapidly whereas the latter is delayed – in the rodent cortex, for example, excitatory synaptogenesis happens very rapidly and peaks within the second postnatal week, while inhibitory synaptogenesis peaks at the end of the second week and well into the third week of postnatal development **(Figure 1.13)**. This is a highly unsynchronised process with the formation of synapses within a same neuron being formed over different time ranging from minutes to hours (Ahmari, Buchanan, & Smith, 2000; Friedman, Bresler, Garner, & Ziv, 2000; Sabo, Gomes, & McAllister, 2006; Shapira et al., 2003; Washbourne, Bennett, & McAllister, 2002).

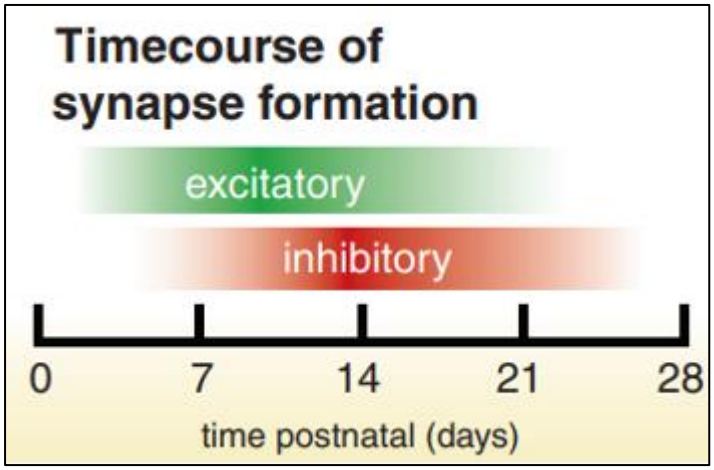

Figure 1.13 Time course of synapse formation in the rodent cortex. Excitatory synapse formation begins during the first postnatal week; inhibitory synapse formation begins during the second postnatal week. Eyes and ear canals open near the end of the second postnatal week. Adapted from (Bury & Sabo, 2010)

Synapses can initiate at axo-dendritic, axo-somatic, or axo-axonal sites. At first, recognition of an appropriate partner must be made. This is followed by the

establishment of physical contact, which leads to controlled changes in morphology and molecular content, such as recruitment of molecular components like synaptic vesicles and active zone proteins – essential for mature synapse formation. Lastly, synapses are formed and synaptic proteins are sorted to their appropriate location as the contact site differentiates into a functional synapse (Washbourne et al., 2004). Therefore, it can be said that synaptogenesis can be divided into three main phases, (1) neuronal contact, (2) synaptic precursor transport and (3) stopping of synaptic precursors **(Figure 1.14)**.

1.3.2.1 Neuronal Contact

During development, neurites extend from the surface of an undeveloped neuron through a highly active membrane protrusion - the growth cone. They are present at tips of developing axons and dendrites and guide them to their targets where they contact specific dendritic arbors or somas. Once contact is made, it activates a cascade of events through CAMs, which are known to be crucial for the establishment of stable cell-cell contact and correct assembly of synapses (Garner et al., 2002; Gordon-Weeks & Fischer, 2000; Washbourne, 2015). In theory, synaptogenesis can be generated by axonal growth cones contacting dendrites, dendritic growth cones with axons or dendritic shaft filopodia contacting nearby axons or vice versa. Most of these contacts are not stabilised and need other intrinsic factors to do so and allow a synapse to form. Once this contact is stabilised, synapse formation is mediated by different transmembrane proteins that can interact across the space which will develop into the synaptic cleft. These CAMs, such as Neuroligins (Nlgns) and Neurexins

(Nrxns) are known to be essential in triggering synapse formation and act as signal transducers **(Figure 1.14 A)** (Bury & Sabo, 2010; Fu, Washbourne, Ortinski, & Vicini, 2003; Scheiffele, 2003; Washbourne et al., 2002, 2004).

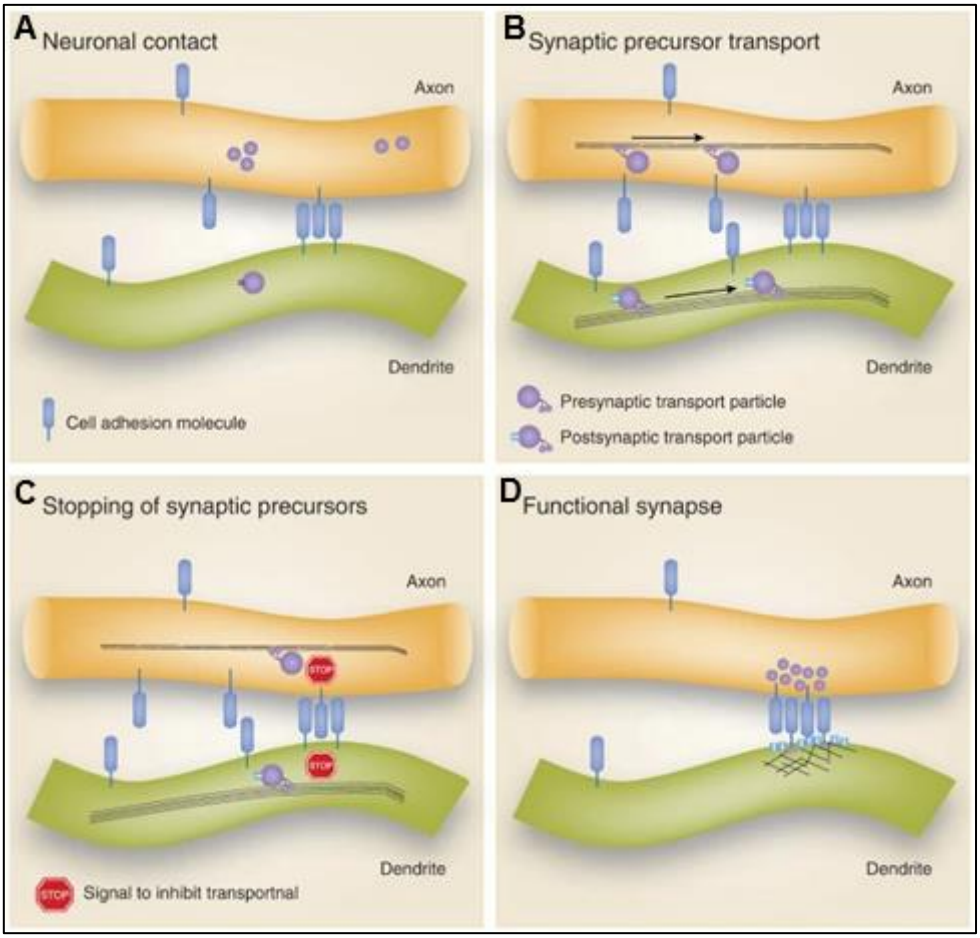

Figure 1.14 Synapse assembly A. First neuronal contact triggers a cascade of events through CAMs. **B.** Recruitment of pre- and postsynaptic proteins to the site of contact. **C.** Kinases, are in control of the synaptic precursor stopping to create **D.** A functional synapse. Adapted from (Washbourne, 2015).

1.3.2.2 Synaptic Precursor Transport

The transformation of these contact sites to functional synapses involves the quick recruitment of both pre- and postsynaptic components followed by a quick stabilisation. It requires the delivery of specialised proteins to the right place at the right time. Presynaptically, the main elements of synaptic vesicles and active zone machinery move in clusters alongside other proteins and can then be recruited to new sites of contact (Ahmari et al., 2000; Bury & Sabo, 2010; Washbourne et al., 2002; Zhai et al., 2001). There are two main specific clusters which are known to participate in this process: (1) Synaptic vesicle protein transport vesicles (STVs), and (2) piccolo-bassoon transport vesicles (PTVs) (Bury & Sabo, 2010). Postsynaptically, different components of the scaffold PSD are recruited separately after the initial contact is made.

Active zone proteins are transported to growing synapses through PTVs, and proteins associated with synaptic vesicles are transported there through STVs. Once they have been assembled in the cell body, both PTVs and STVs are transferred to the axon where they move around in both retrograde and anterograde directions. Sites where STVs repeatedly pause are more likely to develop into synapses. The initial axodendritic contact is considered to trigger a cascade of intracellular events which modifies STV transport within the axon, by recruiting STVs to the actual site of contact. It is thought that the primary mechanisms by which synaptogenic signals induce the stable accumulation of STVs at nascent presynaptic terminals is through “the regulation of pausing” – the accumulation of synaptic proteins at synaptogenesis sites entails moving precursors to stop and presynaptic terminals seem to form preferentially at STV pause sites **(Figure 1.14 B)** (Sabo et al., 2006). It is thought that

because STV pause sites are established before dendritic contact and in the absence of glia, they are intrinsic to axons. (Ahmari et al., 2000; Nakata, Terada, & Hirokawa, 1998; Sabo et al., 2006).

1.3.2.3 Stopping of Synaptic Precursors

Once the synaptic precursors reach the stable synaptic site they must stop and be maintained there to form a functional synapse. Scaffold molecules are involved in recruiting and keeping synaptic components at the mature synapse. Other proteins, such as kinases, are in control of the synaptic precursor stopping at the correct place to create the synapses (Washbourne, 2015). These proteins act as stop signals to allow the PTVs and STVs to stop at the correct place (**Figure 1.14 C)**.

CAMs have been shown to be involved not only in initial contact formation and specific target recognition, but also synapse assembly and plasticity (Shen & Bargmann, 2003; Shen, 2004; Masahito Yamagata et al., 2003; Masahito Yamagata, Weiner, & Sanes, 2002). CAMs have been known to interact with the cytoskeleton and scaffolding proteins, therefore they can recruit receptors and different signalling molecules which are necessary for the assembly of synapses (Waites et al., 2005).

Through neurodevelopmental disorders (NDDs) Genome Wide Association (GWAS) studies it has been found that most of the disorder-associated genes are involved in neuronal cell adhesion and synaptic scaffolding. Linking this to synapse formation, it suggests that cell adhesion is key for the correct formation of healthy and

functional synapses (Bukalo & Dityatev, 2012; Washbourne et al., 2004). The specificity of synaptic CAMs is established through the structural organisation of their extracellular domains – they project into the synaptic cleft, allowing the binding and forming of transsynaptic complexes which provide mechanical stability (Missler, Südhof, & Biederer, 2012; Washbourne, 2015). To generate all the different cell interactions and the specificity of synaptic partner matching, CAMs must act in a combinatorial manner. New protein families involved in a variety of fine scale neural wiring processes such as neurite outgrown, axon pathfinding, cell type specific dendrite morphogenesis and synaptic specificity have been discovered (Antinucci et al., 2013; Cheung, Trevers, Reyes-Corral, Antinucci, & Hindges, 2019; Dharmaratne et al., 2012; W. Hong, Mosca, & Luo, 2012; Leamey et al., 2007; Merlin et al., 2013; Mosca & Luo, 2014). Teneurins, also known as Ten-m/Odz, have recently been added to this list.

1.4 TENEURINS

Discovered originally in *Drosophila melanogaster* in the 90's, Teneurins belong to a family of phylogenetically conserved type II glycoproteins that have been implicated in the correct development of neural circuitry (R P Tucker & Chiquet-Ehrismann, 2006; Young & Leamey, 2009). They were initially named Odd Oz (Odz), because of the oddless pair-rule phenotype that was discovered in mutants. However, they were

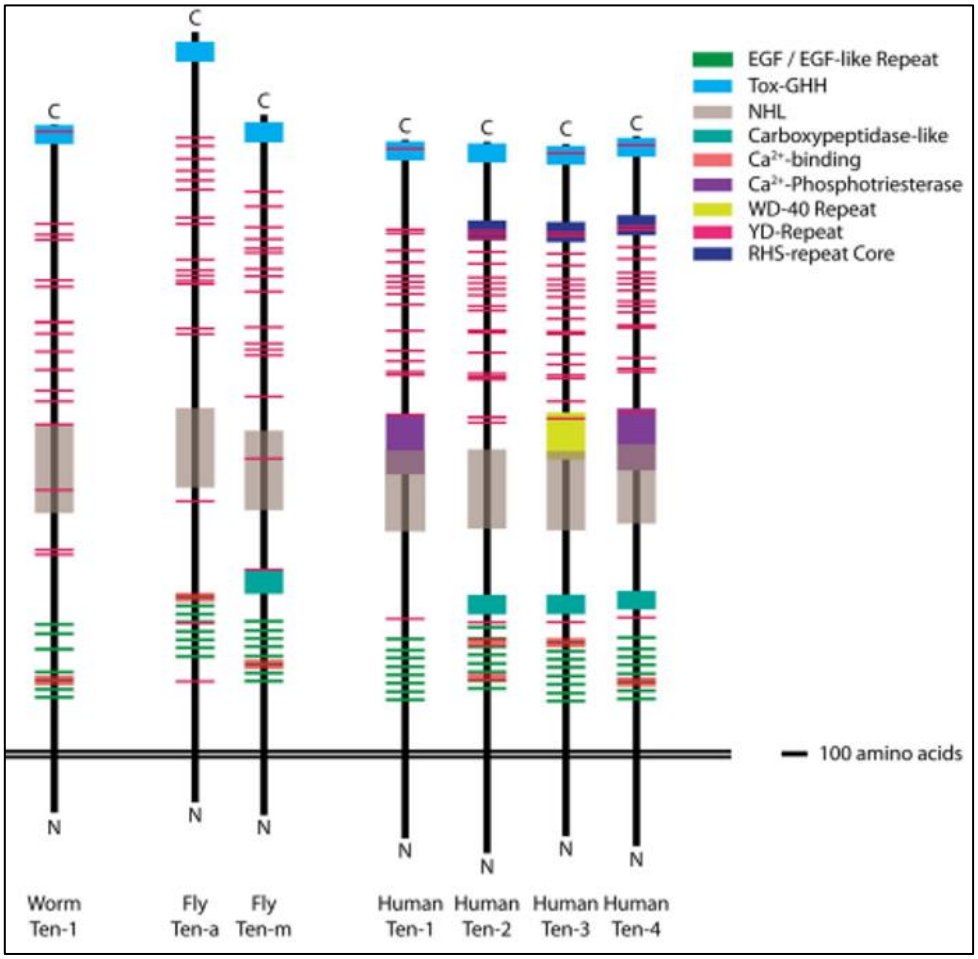

Figure 1.15 Molecular structure of Teneurins. Diagram of the domain organization of the C. elegans Ten-1, the Drosophila Ten-m and Ten-a, and the human Ten-1, Ten-2, Ten-3, and Ten-4 proteins. The transmembrane domains are aligned as the reference point to facilitate comparison between the extracellular domains of each homolog. Each domain is color-coded (key) and scaled by size (scale = 100 amino acids). Adapted from (Mosca, 2015)

initially described as cell surface proteins and as pair-rule genes, but with time they were proved to be type II transmembrane proteins (Baumgartner & Wides, 2019; Levine et al., 1994). Teneurins have been found both in invertebrates and vertebrates; *Caenorhabditis elegans* possess a single teneurin (ten-1), *Drosophila melanogaster* have two (Ten-a and Ten-m) while all vertebrates have four paralogs (tenm1-4). Sequence similarity between paralogs is high, with human teneurin paralogs sharing between 58-70% sequence identity **(Figure 1.15)** (Jackson et al., 2018). The four Teneurin paralogues can be predominantly found in the CNS, although not exclusively, where they have complementary expression patterns throughout development (Ben-Zur, Feige, Motro, & Wides, 2000; Kenzelmann-Broz, Tucker, Leachman, & Chiquet-Ehrismann, 2010; Zhou et al., 2003).

1.4.1 Teneurin Structure

Teneurins are large proteins, with a molecular weight of 300 kDa, they are composed of 2500 to 2800 amino acids (aa). They are made up of a smaller N-terminal intracellular domain (ICD) of ~400 aa – which is capable of signalling and transcriptional regulation as well as interacting with the cytoskeleton (Bagutti, Forro, Ferralli, Rubin, & Chiquet-Ehrismann, 2003; Nunes et al., 2005). A single hydrophobic membrane-spanning helical transmembrane domain (TMD) of 34 aa, and a very large C-terminal extracellular domain (ECD) of ~2400 aa (B P Rubin, Tucker, Martin, & Chiquet-Ehrismann, 1999; Tan et al., 2012; R P Tucker & Chiquet-Ehrismann, 2006). A significant functional role has recently been found for the C-terminal ECD named TCAP for "teneurin C-terminal associated peptide", which acts as a neuromodulatory peptide after being processed (L. Wang et al., 2005). The ICD is highly conserved across

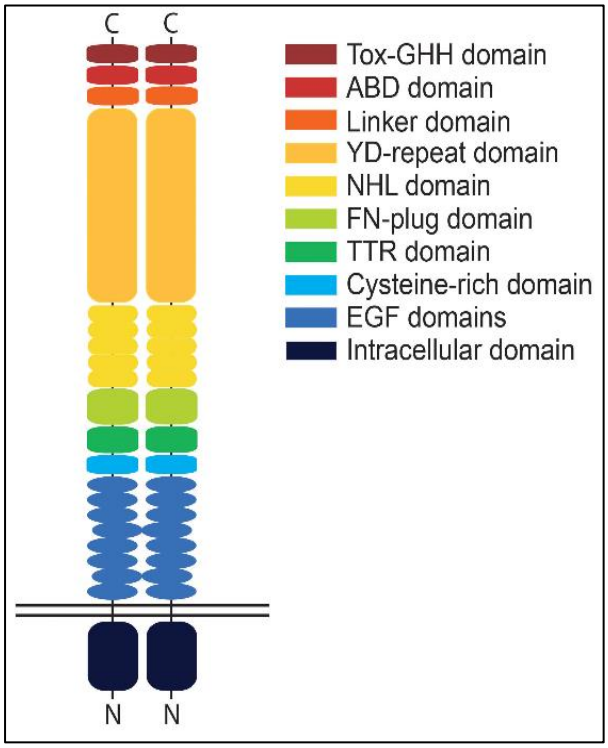

Figure 1.16 Schematic illustration of a teneurin dimer. Teneurins possess a single transmembrane domain, a small intracellular domain, and a relatively large extracellular domain. Depicted is a cis-dimer with identified protein domains indicated in different colours. The extracellular domain consists of the EGF domain, cysteine-rich domain, TTR (transthyretin-related) domain, FN (fibronectin)-plug domain, NHL domain, YD (tyrosine-aspartate)-repeat domain, internal linker domain, ABD (antibiotic-binding domain-like) domain and the Tox-GHH domain. Domains are only representative and not to relative scale. Adapted from (Cheung et al., 2019)

vertebrates and is composed of two EF-hand like calcium binding motifs, two proline-rich stretches which function as binding sites for Src-homology 3 (SH3) proteins, as well as several conserved tyrosine residues - two of which are predicted to be phosphorylation sites (Leachman, 2010). Different studies have shown that the ICD of both tenm1 and tenm2 translocate to the nucleus if they are processed by proteolytic cleavage where they interact with transcription factors and/or cytoskeletal adaptor proteins (Kenzelmann, Chiquet-Ehrismann, Leachman, & Tucker, 2008). In all Teneurins, the ECD is characterised by eight epidermal growth factors (EGF)-like repeats, several tyrosine-aspartate (YD)-repeats, and five NHL (NCL-1, HT2A and Lin-41) repeats **(Figure 1.15; Figure 1.16)**. They can interact in *trans* both homo- and heterophilically through their NHL domains and can make homo- and heterodimers in *cis* by establishing disulphide bonds between two of their EGF-like repeats (Cheung et al., 2019; Feng et al., 2002; Oohashi et al., 1999)**.** Lastly, the primary proteolytic processing appears to take place at a furin cleave site found between the TMD and the first EGF-like repeat **(Figure 1.17)** (Cheung et al., 2019; Kenzelmann et al., 2008;

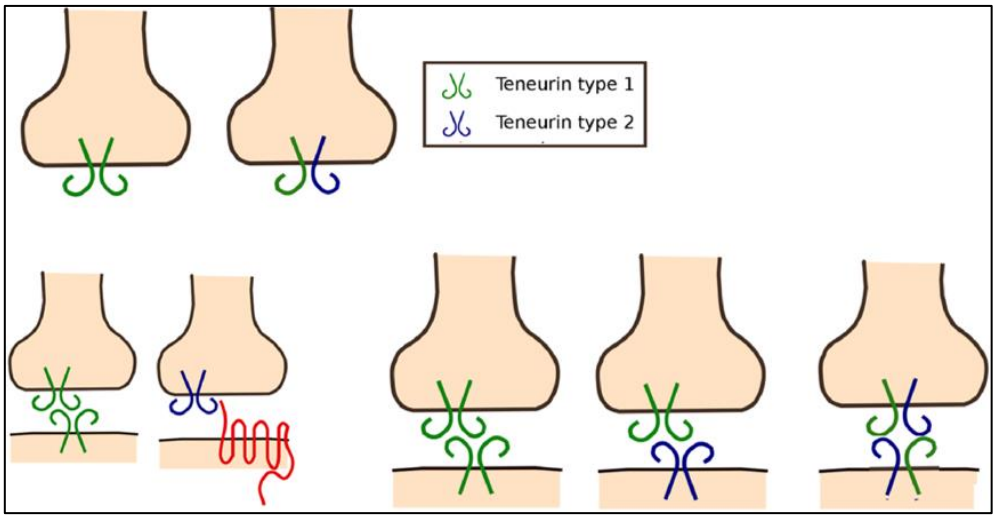

Figure 1.17 Teneurin homo- and heterophilic interactions A. Same or different Teneurins can be expressed by the same cell **B.** They can interact with the same Teneurin or with other CAMs or **C.** they can express and interact with the same Teneurin, different Teneurin or express and interact with different Teneurins. Drawing by Lucia de Andes, Hindges Lab, unpublished.

Kenzelmann-Broz et al., 2010; Leamey & Sawatari, 2014; R P Tucker & Chiquet-Ehrismann, 2006; Richard P Tucker, Kenzelmann, Trzebiatowska, & Chiquet-Ehrismann, 2007; Young & Leamey, 2009).

1.4.2 Expression of Teneurins During Development

Teneurins have been found to be predominantly expressed during development in the CNS. Alongside this, they are known to be expressed in non-neuronal tissues that are implicated in aspects such as pattern formation, cell migration and muscle attachment (R P Tucker & Chiquet-Ehrismann, 2006). Their expression in the CNS has been observed across different species. In mice, Zhou et al., (Zhou et al., 2003) demonstrated that all four paralogues are expressed in distinct neuronal populations that sometimes overlapped across the CNS – cortex, thalamus, hippocampus, and cerebellum. The expression of t*enm3* is in the retinogeniculate and the retinocollicular pathways. *Tenm3* is expressed in a high-medial to low-lateral gradient, which concurs topographically with high-ventral to low-dorsal retinal gradient – high expressing areas target each other (Dharmaratne et al., 2012). It has also been proved that it shows a gradient expression in the GCL, dorsal lateral geniculate nucleus and superior colliculus. *Tenm2* on the other hand has a uniform expression pattern in similar regions – dorsal lateral geniculate nucleus, superior colliculus and the primary visual cortex (Young et al., 2013). In chicks, expression patterns of *tenm1* are found in the developing visual and olfactory systems. Signal from ISH showed strong expression in the mitral cell layer and the ganglion cell layer on the olfactory bulb as well as the ganglion cell layer and inner nuclear layer (with weaker expression) of the retina. The OT showed widespread expression but is clearly seen in large neurons of the stratum griseum centrale (Kenzelmann et al., 2008; Minet, Rubin, Tucker, Baumgartner, & Chiquet-Ehrismann, 1999). *Tenm4* expression in the chick embryo changes throughout development, at E4 faint expression is seen in the optic fiber layer of the retina and in the diencephalon – near the optic stalk. Expression changes and at E7

is seen in limited bundles of axons in the optic fiber layer of the nasal retina. By E10 the expression is seen in the occipital part of the OT and by E12 showed high expression in the optic tract. Lastly, at E17 - stage at which the chick brain resemble adult brains - a gradient expression of *tenm4* can be seen in the retina, more temporal parts of the retina had higher expressions of neurons in the GCL (Kenzelmann-Broz et al., 2010; Richard P Tucker, Martin, Kos, & Chiquet-Ehrismann, 2000). In zebrafish, the expression of Teneurins is visible in embryos since 24 hpf, this being particularly evident for tenm1, tenm3 and tenm4, where they are expressed along the visual pathway, specifically in the OT and the retina (Cheung et al., 2019; Mieda, Kikuchi, Hirate, Aoki, & Okamoto, 1999). *Tenm3,* for example, is expressed in the retina within the GCL and the INL. At 2 dpf higher expression is seen in the ventral part of the retina, and from 3 dpf to 5 dpf it acquires a sparse expression pattern. In the 3 dpf OT, *tenm3* is highly expressed in the medial portion of the stratum periventriculare and between 3 dpf and 5 dpf, the medial to lateral gradient gradually decreases, leading to a salt and pepper expression pattern (Antinucci et al., 2013). Comparably, strong expression of *tenm4* is apparent from 24 hpf, this is evident in the forming retina, midbrain and hindbrain **(Figure 1.18 A,F,K; Figure 1.19 A)**. The expression begins to localise in the inner layers of the retina, olfactory bulb and OT between 2 dpf and 3 dpf **(Figure 1.18 B,G,L,C,H,M; Figure 1.19. B,B',C,C')** and persists over 4 dpf and 5 dpf **(Figure 1.18. D,I,N,E,J,O; Figure 1.19. D,D',E,E')** (Cheung et al., 2019). This supports the role that Teneurins have a role in directing the functional connectivity of RGCs and ACs in the developing visual system. Depending on the paralogue, Teneurins show overlapping expression patterns, suggesting that they may have an important role in creating specific synaptic matching between pre- and postsynaptic cells (W. Hong et al., 2012; Mosca, Hong, Dani, Favaloro, & Luo, 2012).

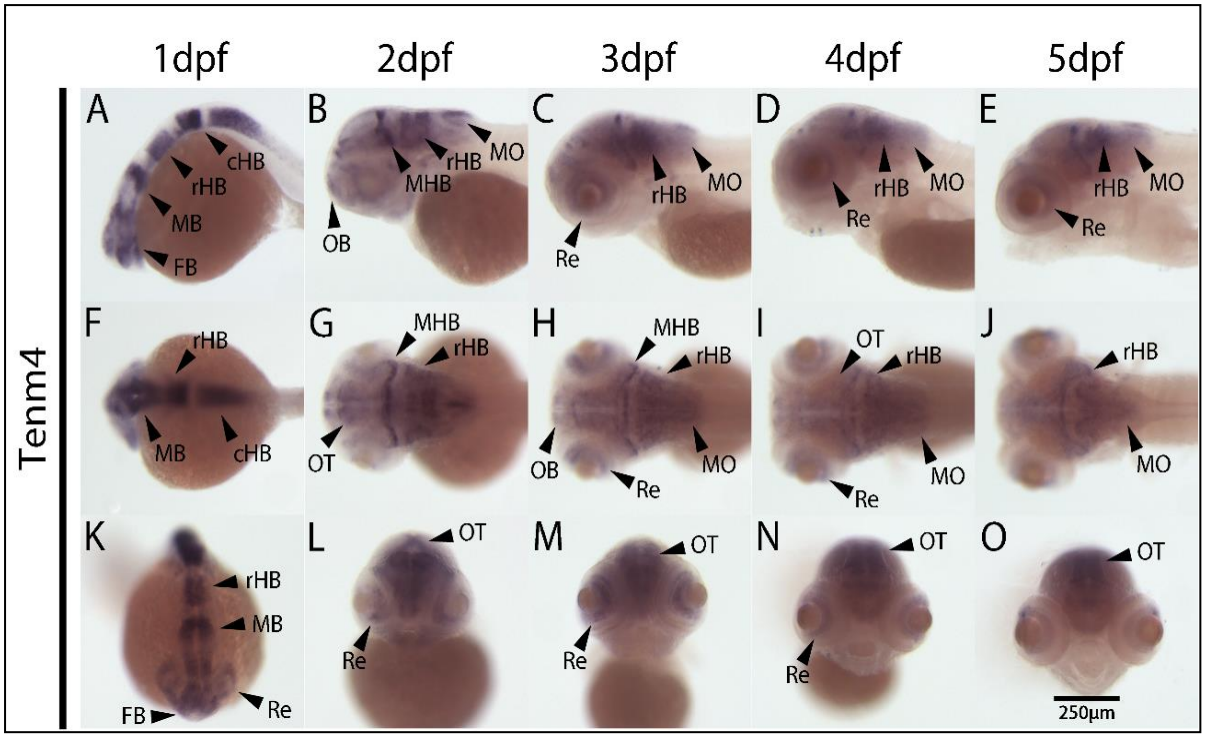

Figure 1.18. Wholemount expression of *tenm4* during zebrafish development. *Tenm4* expression during 1–5 dpf from lateral **(A–E)**, dorsal **(F–J)** and frontal **(K–O)** perspectives. A, Anterior; cHB, caudal Hindbrain; D, Dorsal; FB, Forebrain; MB, Midbrain; MHB, Mid-Hindbrain Boundary; MO, Medulla Oblongata; OB, Olfactory Bulb; OT, Optic Tectum; P, Posterior; rHB, rostral Hindbrain; Re, Retina; V, Ventral. Scale bars set at 250 µm. (Cheung et al., 2019)

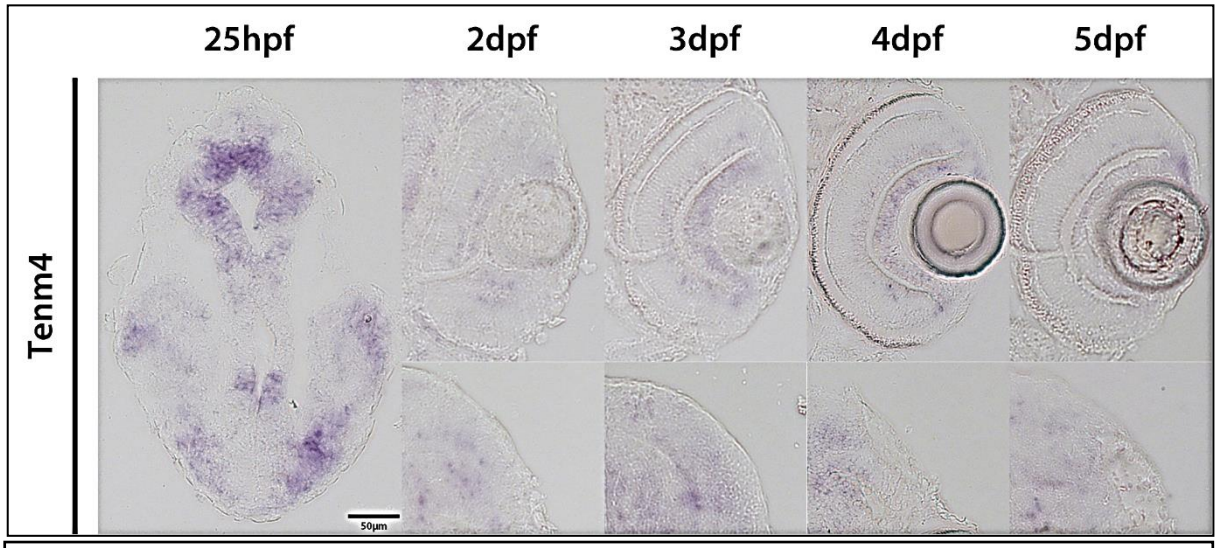

Figure 1.19. Sectioned expression of *tenm4* during zebrafish development. *Tenm4* expression during 1–5 dpf from sectioned zebrafish larvae. **A.** Dorsal view**, B – E.** Retina, clear salt, and pepper expression pattern in GCL and ACL, **B'-E'.** OT, clear salt, and pepper expression pattern throughout. Scale bars set at 50µm. (Cheung et al., 2019)

1.4.3 Teneurin Function

As previously discussed, in both *in vitro* and *in vivo* studies, it has been found that Teneurins, throughout neurodevelopment, are expressed at synapses and promote neurite outgrowth and cell adhesion, and as previously stated can interact both homophilically and heterophilically (Beckmann, Schubert, Chiquet-Ehrismann, & Müller, 2013; Boucard, Maxeiner, & Südhof, 2014; Leamey et al., 2008; Leamey & Sawatari, 2014; Mosca et al., 2012; Oohashi et al., 1999; B P Rubin et al., 1999; Beatrix P. Rubin, Tucker, Brown-Luedi, Martin, & Chiquet-Ehrismann, 2002). Beckmann et al., (2013) proved that by deleting and swapping tenm-1 and tenm-2 domains, that teneurins use their NHL domain to select homophilic teneurins from adjacent cells. Similarly, by altering teneurin expression in *Drosophila,* Mosca et. al., (2012), increased the failure rate of innervation between neurons at the NMJ, this occurred when knocking down teneurins in both the neurons and the muscle, or just in one of the two, supporting the idea of a homophilic interaction between the pre- and postsynaptic *Drosophila* teneurins.

Initially, most work on Teneurins was done *in vitro*, but a major drawback was the inability to observe and study the natural complexity of organ systems – where the monitoring of various biological effects is possible. Tenm2, for example, is known to be expressed in a spatial and temporal pattern that corresponds with the development of the thalamofugal visual pathway. Through *in vitro* studies, it was shown that the ECD of tenm2 was concentrated at sites of cell-cell contact in neuroblastoma cells, this suggests a role of homophilic interaction of tenm2 in developing visual system (Beatrix P. Rubin et al., 2002). Tenm4, was shown to be localised and accumulated in

growth cones of Neuro-2A neurites in a time-dependent manner. Before neurite outgrowth began, tenm4 expression was localised at the cell body, expression levels became stronger along the neurites as outgrowth began and accumulation of the protein was observed in growth cones. Through *in vitro* KO experiments, it was proved that tenm4 promotes filopodia-like formation, as well as being involved in neurite outgrowth through the focal adhesion kinase signalling pathway (Suzuki et al., 2014).

To further investigate the roles of Teneurins throughout development, *in vivo* studies began to be used. The main findings so far have been the involvement of these molecules in the synaptic partner matching in different circuits of the developing nervous system. In *Drosophila* it was shown that Teneurins (ten-m and ten-a) play a role in target choice within the olfactory system and the neuromuscular junction (NMJ) (W. Hong et al., 2012; Mosca et al., 2012). Within the olfactory system, both Ten-m and Ten-a were found to be highly expressed by an overlapping subset of olfactory receptor neurons as well as their postsynaptic partners – the projection neurons. Through gain-of-function and loss-of-function experiments, they were shown to promote synaptic partner matching between these two neurons through homophilic interactions in the antennal lobe (W. Hong et al., 2012) - this is done by homophilic attraction. Regarding the NMJ, Ten-a is expressed pre-synaptically whilst Ten-m is expressed post-synaptically. Through knockdown (KD) experimentsin *Drosophila* it was found that synaptic partner matching within the NMJ is mediated through heterophilic interaction between the two different teneurin paralogues. KD of ten-m and/or ten-a caused severe synaptic changes both morphologically (cytoskeletal defects) or physiological (synaptic transmission differences). This shows that proper synaptic development requires both pre- and postsynaptic Teneurins (Mosca et al., 2012).

As previously described, vertebrates Teneurins are highly expressed throughout the visual system, therefore *in vivo* experiments have mostly concentrated on this system (Leamey & Sawatari, 2014). Our lab has taken advantage of this model and shown that tenm3 is required for correct morphological and physiological development and connectivity of RGCs. Tenm3 is expressed in RGCs, their presynaptic partners the ACs and postsynaptic partners in the OT. KO of tenm3 led to severe RGC dendrite stratification defects in the retina, with particular defects found within the IPL. This was also observed by a subset of RGC axons in the OT having some laminar arborisation errors. Lastly, through functional imaging, it was shown that there was a deficit in the development of orientation selective RGCs in the OT, showing that tenm3 plays a vital role in the functional wiring of the vertebrate visual (Antinucci et al., 2013). Finally, in mice, Teneurins are involved in a variety of processes such as directing the formation of the thalamostriatal pathway and that orchestrating the assembly of complexly distributed circuits in the mammalian brain, including entorhinal and hippocampal projections (Berns, DeNardo, Pederick, & Luo, 2018). In mice lacking tenm3, behavioural aspects such as motor skill acquisition were proved to be delayed (H. Tran, Sawatari, & Leamey, 2015). Alongside this, other experiments showed that Tenm3 has an important regulatory role in the correct development of binocular maps. When it comes to binocular vision, it is necessary for both eyes to be topographically mapped as well as aligned with the projections from the other eye. In mice lacking tenm3, a severe impairment in this binocular vision was observed – where uncrossed projections from the eye to the brain mapped aberrantly, whilst crossed projections mapped normally. This proved that tenm3 is necessary to regulate the mapping of ipsilateral projections from the retina. KD of tenm2 also led to a decrease in ipsilateral RGCs projecting their axons to the dorsal lateral geniculate

nucleus and the superior colliculus, proving that tenm2 is also required for the correct function of binocular vision (Leamey et al., 2007; Young et al., 2013). It was also shown that Tenm3 acts both pre- and postsynaptically in neurons in the hippocampus for precise topographic projections. Loss of function experiments revealed for example that homophilic attraction is necessary for CA1 neurons to reach their subiculum targets. When eliminating tenm3 proximal CA1 neurons spread throughout the entire subiculum instead of projecting only to distal tenm3 positive targets.

Primarily, work on the teneurin family has been focused on tenm3. Because of this, it can be said, that, in comparison to the other Teneurins, its roles, particularly within the vertebrate visual system, are largely understood. As mentioned before, Teneurins are highly conserved and share a high percentage of sequence similarity, therefore it can be inferred that the other paralogues may have similar functions. In this study we focus on tenm4 and its role in visual circuit assembly *in vivo.*

1.4.4 Teneurins in Neurodevelopmental Disorders

NDDs are a group of complex conditions involving some form of disruption during brain development (Thapar, Cooper, & Rutter, 2017) which have a significant socioeconomic impact. They are associated with dysfunction of neuronal activity due to perturbations at the synapse level (Ardiles, Grabrucker, Scholl, Rudenko, & Borsello, 2017), because of this they can also be referred to as diseases of the synapse or synaptopathies.

Through different GWAS studies, Teneurin mutations have been linked to significant susceptibility in a variety of these NDD. The human chromosomal regions

of *teneurin-1 (tenm1)* and *teneurin-2 (tenm2)* (Xq25 and 5q34, respectively) are linked to intellectual disability (Minet et al., 1999; Paoloni-Giacobino, Bottani, & Dahoun, 1999). Rare variants in c.521C>A/p.Ala174Asp in *tenm1* seems to contribute to autism spectrum disorder (Nava et al., 2012). *TENM3* has been identified as a plausible candidate for late onset cerebellar ataxia (Storey et al., 2009). Lastly, the genomic locus of *teneurin-4 (tenm4)* (11q14.1 and 11q14-21, respectively) is associated with the susceptibility of bipolar disorder (BD) and schizophrenia (SCZ) (Psychiatric GWAS Consortium Bipolar Disorder Working Group, 2011; Sklar, Ripke, Scott, Andreassen, & Cichon, 2011; Xue et al., 2018). Recent GWAS studies have found a notorious genetic overlap between SCZ and BD, with risk of BD associated to a family history of SCZ (Fanous et al., 2012; Lichtenstein et al., 2009). Particular focus will be given to bipolar disorders and schizophrenia because of their implication with the TENM4 gene.

In RNA-seq data of human tissue, including: brain, cerebrum, heart, liver, kidney, and testis, it was shown that *TENM4* is highly expressed in human brain tissue, and that it exhibited a higher specificity to the brain than to other tissues in the study. The expression of *TENM4* was highest in the brains of mice and monkeys, hinting that high expression is evolutionarily maintained in mammals (Xue et al., 2018).

1.4.4.1 Bipolar Disorder

Ranked as the 17th leading cause of disability among all diseases worldwide, it is characterised by the presence of recurring manic or hypomanic episodes which alternate with depressive ones. BD affects approximately 2.5% of the global population. It is known that genetic factors play a key role in the aetiology of this

disorder, but the biochemical factors behind the predisposition remain to be fully understood (Carvalho, Firth, & Vieta, 2020; Manji et al., 2003). Although genetic studies throughout the years have been inconsistent, they have repeatedly found various genes that are involved in cellular metabolic activities, ion exchange, synaptic development and differentiation, as well as genes regulating myelination, neurotransmission and neuronal plasticity (Barnett & Smoller, 2009; Faraone, Glatt, & Tsuang, 2003; Maletic & Raison, 2014). Originally, it was thought that the pathophysiology of BD was linked to problems in neurotransmission, however, advances in the field have been made and changed the focus onto a network of interconnected limbic, striatal and fronto-cortical neurotransmitter neuronal circuits (Bowden, Swann, & Calabrese, 1997; Manji et al., 2003; Psychiatric GWAS Consortium Bipolar Disorder Working Group, 2011; Sklar et al., 2011).

TENM4 has been associated with BD in a recent GWAS study, where 10 genome-wide significant single-nucleotide polymorphisms (SNPs) in the *TENM4* gene, on chromosome 11q14.1 (Psychiatric GWAS Consortium Bipolar Disorder Working Group, 2011; Sklar et al., 2011). Recent studies have described rare *TENM4* variants which might contribute to the aetiology of BP (Ament et al., 2015).

1.4.4.2 Schizophrenia

Ranked as the 11th cause of global burden of disease and affecting approximately 1% of the world's population, SCZ is a NDD mainly characterised by delusion and hallucinations, leading to reduced life expectancy by an average of 20-25 years. The fundamental neurobiology of SCZ, its pathophysiology - or disease mechanism - have

not been established. It has been thought that SCZ can be associated with cortical volumetric reduction of the brain (Weinberg et al., 2016), decreased neocortical and hippocampal formation volumes (Adriano, Caltagirone, & Spalletta, 2012) as well as increased synaptic pruning (Sekar et al., 2016).

Tenm4 has been implicated in a rodent model of SCZ (Neary, Perez, Peterson, Lodge, & Carless, 2017), and through exome sequencing Xue et al., (Xue et al., 2018), found a novel missense mutation (c.6724C>T,p.R2242C) in the *TENM4* gene. *TENM4* is located within the schizophrenia disorder 2 (SCZD2) locus, a region previously linked to SCZ at 11q14-21. Additional investigation into TENM4 exons adjacent to the p.R2242C mutations found two additional missense mutations in various sporadic SCZ patients. The mutations found in this study were located within a YD region in the ECD of *TENM4* protein, which is essential for homophilic and heterophilic interactions as well as for signal transduction for transmembrane proteins (Xue et al., 2018).

1.5 Previous Work

To investigate the roles of Tenm4 during development a tenm4 KO transgenic zebrafish line was previously created in the Hindges Lab. Using CRISPR gene editing technology, a 10 bp deletion was made in the exon encoding the TD (exon 2/3). This led to frameshift, which subsequently led to a premature stop codon causing a loss of the entire ECD **(Figure 1.20)** - this mutation will be known from here on as tenm4$^{10bp\Delta}$ mutant. Because of the positioning of the deletion, it is assumed that there is a nonsense-directed decay of mRNA, resulting therefore in a viable knockout model for tenm4. Importantly, both larvae and adult tenm4$^{10bp\Delta}$ mutants are viable and do not display visible morphological abnormalities.

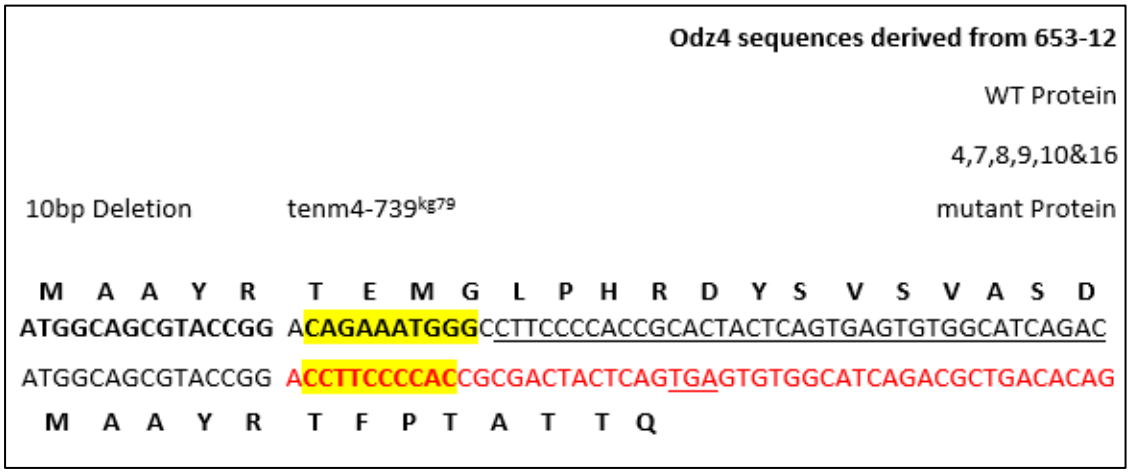

Figure 1.20 Tenm4 CRISPR KO. A 10 bp deletion was made in the exon encoding the transmembrane domain causing a frameshift which consequently led to a stop codon resulting in the elimination of the entire extracellular domain.

As an initial analysis of this zebrafish line, functional imaging of RGC axons in the OT was done on 4dpf zebrafish larvae (Kathrin Trevers, Hindges Lab) – as mentioned before, by this time point, visually evoked responses can be elicited. This

was done to address the overall functionality of the tenm4$^{\Delta 10bp}$ mutant, by using a genetically encoded reporter of presynaptic function (SyGCaMP3) we were able to record visually evoked activity in the population of RGCs axons innervating the tectum of both WT and tenm4$^{\Delta 10bp}$ mutant background zebrafish (*tg(isl2b:Gal4;UAS:SyGCaMP3)).* By combining *in vivo* imaging of SyGCaMP3 responses with patterned visual stimulation - differently orientated moving black and white bars were randomly presented - we were able to record stimulus-evoked calcium influx in the tectum. Functional imaging of the contralateral RGC axons revealed an increase in the number of visually responsive voxels within our tenm4$^{\Delta 10bp}$ mutant group (**Figure 1.21;** n=5). Using unbiased voxel-wise analysis of the SyGCaMP3 signals, significant differences were observed in direction-selective responses as well as the overall visual responses, but not in orientation selective responses. Based on these results, our attention was drawn towards connectivity in the visual system of the tenm4$^{\Delta 10bp}$ mutant larvae – from morphology to function, to better understand the significant results uncovered through this experiment.

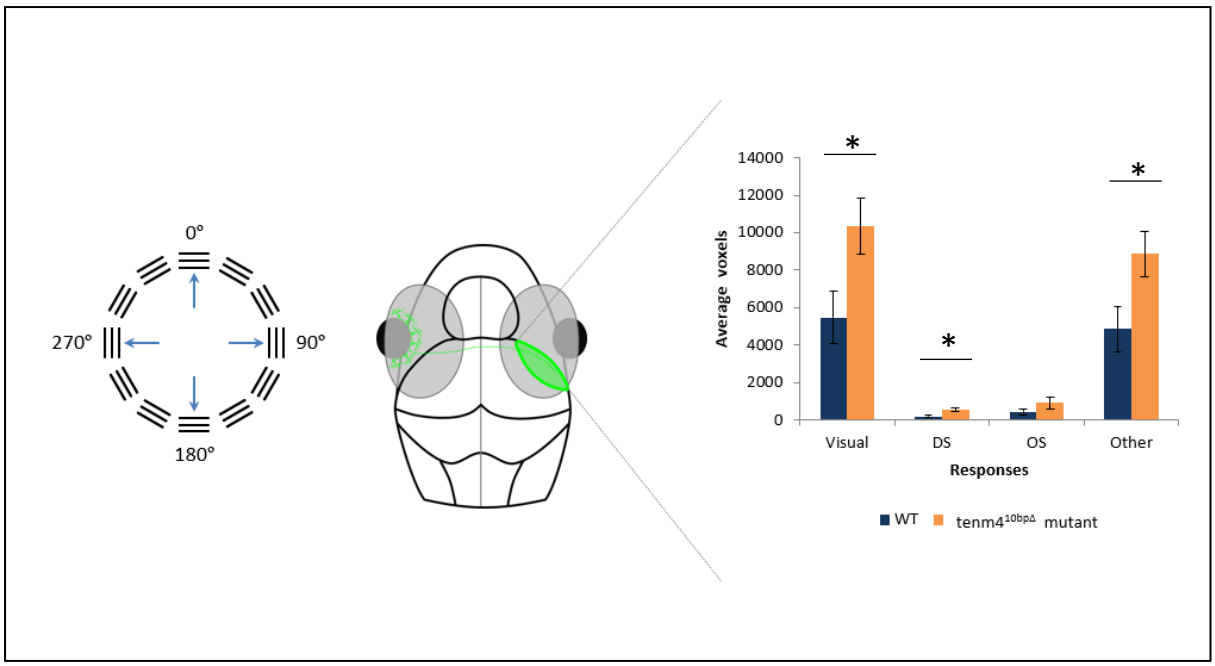

Figure 1.21 Functional imaging of a 4 dpf tenm4$^{10bp\Delta}$ mutant larvae. Black and white bars moving in different orientations were presented to 4 dpf tg*(isl2b:Gal4;UAS:SyGCaMP3)* zebrafish larva in WT and tenm4$^{\Delta 10bp}$ mutant backgrounds. Imaging of RGC responses was done on the contralateral OT. An increase of visually responsive voxels was seen in the tenm4$^{\Delta 10bp}$ mutant larva. Visual corresponds to all visual stimuli – includes direction selectivity (DS), orientation selectivity (OS) and all other stimulus (Other). There was a significant difference in DS, Visual and Other, but not OS.

1.6 Aims of the Project

Studying the different roles of Teneurins during visual circuit assembly and synaptic partner matching could lead to a better understanding of the aetiology of BD and SCZ, as well as the general mechanisms involved in the creation of functional synaptic networks in healthy states. During my PhD project, I focused on the role that Teneurin-4 plays in specifying the wiring of visual circuits in the developing zebrafish larvae. The main aim that drove this research study was to investigate the potential morphological or synaptic targeting phenotypes that could justify the differences observed in visual responses by the *tenm4* mutant zebrafish larvae. To investigate this, I have made use of the immense knowledge that has been gathered over the last decades on the development, structure, and function of the vertebrate visual system to understand the role that tenm4 has in mechanisms of visual circuit assembly. Several experimental approaches implemented had to be optimised, varying from immunohistochemical analysis to morphological characterisation.

Firstly, the role of *tenm4* in the developing retina of larval zebrafish is described (see Chapter 3) Secondly, a morphological assessment was performed on RGCs axonal arbours to see whether *tenm4* is required for the correct development of these cells as well as understanding what their role is in synaptogenesis (see Chapter 4). Lastly, a characterisation of developing tectal cells was presented (see Chapter 5). In the discussion, I elaborate on the significance of this project as well as the limitations of the results presented in this thesis (see Chapter 6).

CHAPTER 2.

MATERIAL AND METHODS

2.1 ZEBRAFISH

Zebrafish were raised according to standard procedures at 28.5ºC with 14 hours ON/ 10 hours OFF light cycle. Embryo collection was synchronised to these times and they were maintained in 1X Danieau solution [58 mM NaCl + 0.7 mM KCl + 0.4 mM MgSO4 + 0.6 Mm Ca(NO3)2 + 5 mM HEPES, pH 7.6]. Zebrafish husbandry for all lines used in this study was done at the King's College London Zebrafish Facility. **Table 2.1** shows all the transgenic lines used in this study. Larvae used for *in vivo* and fixed tissue imaging of morphological and molecular features (not including functional experiments) were treated in 200 µm PTU (1-Phenyl-2-Thiourea; Sigma) and Danieau solution to prevent pigmentation in embryos. Details regarding each line are given in individual chapters.

* The *tenm4* $^{10bp\Delta}$ *mutant* – using CRISPR gene editing technology, a 10 bp deletion was created in the (2/3) exon encoding the transmembrane domain of Tenm-4 which led to a reading frame shift and subsequently to a premature stop codon causing the loss of the entire extracellular domain. This line was generated in the Ekkwill (EKK) zebrafish wildtype background (WT).

All animal procedures were approved by the local Animal Welfare and Ethics Review Body (King's College London) and were carried out in accordance with the Animals (Scientific Procedures) act 1986 under license from the United Kingdom Home Office.

Table 2.1 Zebrafish lines used for this thesis.	
Fish line	**Experiment**
AB	Tectal cell morphological analysis
Crystal Mutants (nacre-/-;alb-/-;roy-/-)[1]	Single cell functional imaging
Ekkwill	RGC morphological analysis; IHC
Tg(isl2b:Gal4)^{zc60Tg} [2]	IPL stratification
Tg(isl2b:Gal4-VP16, myl7:EGFP)^{zc60Tg}	IPL stratification
tenm4$^{\Delta 10bp}$ mutant *	RGC morphological analysis; IHC
Tg(isl2b:Gal4-VP16, myl7:EGFP)^{zc60Tg}; tenm4$^{\Delta 10bp}$ mutant	IPL stratification
tenm4$^{\Delta 10bp}$ mutant; nacre-/-;alb-/-;roy-/-	Single cell functional imaging
Tg(UAS:GFP;mitfa+/-)^{kca33Tg}	IPL stratification; Tectal cell morphological analysis
Tg(UAS:tagRFP-CAAX)^{zf456Tg} [3]	IPL stratification/tectal cell morphological analysis

[1] Antinucci and Hindges, 2016
[2] Ben Fredj et al., 2010
[3] Hunter et al., 2013

2.2 IMMUNOHISTOCHEMESTRY

2.2.1 TUNEL Assay

The DeadEnd™ Fluorometric TUNEL (terminal deoxynucleotidyl transferase (TdT)-mediated deoxyuridine-triphosphate (dTUP) nick end-labelling) System (Promega) was used to identify cells that were undergoing apoptosis.

2.2.1.1 TUNEL assay: Cryosections

Prior to sectioning, embryos were fixed in 4% PFA in 1X PBS O/N at 4ºC, they were then rinsed two times for 10 minutes in 1.5 ml 1X PBS and washed with 1.5 ml 0.05% sodium azide in 1X PBS. Subsequently, they were placed for 10 minutes in an ascending concentration of 1.5 ml sucrose in 1X PBS at 5%, 15% and 30% sucrose. Fresh 30% sucrose in 1X PBS was added and embryos were kept at 4ºC O/N.

The next morning, embryos were incubated in 1.5 ml of a previously molten solution made up of 15% sucrose, 7.5% gelatine in 1X PBS at 37ºC for one hour. This was replaced with 1.5 ml of fresh solution for a further hour at 37ºC. Embedding molds were prewarmed in a container in the water bath at 37ºC. Several embryos were transferred into the prewarmed molds and topped up with fresh molten gelatine solution, they were then oriented as required under a dissection microscope. The gelatine was allowed to harden at 4ºC for one hour. Molds were then snap frozen in an isopentane bath in dry ice.

Cryosections were cut using Microm HM 560 Cryostat at 14 µm (-30/-40ºC) and SuperFrost® Plus slides used to collect the sections. Slides were left out to dry overnight at RT and then placed in 1X PBS (37ºC) to degelatinise sections for 5 – 10 minutes or until gelatine was completely off.

Cryosections were postfixed in a coplin jar with 4% PFA in 1X PBS for 15 minutes and washed twice in 1X PBS. After ProK permeabilisation (15ng/ml) at RT for 5 minutes slides were washed three times in 1X PBS, re-fixed in 4% PFA in 1X PBS, then washed again in 1X PBS. The tissue was equilibrated at RT for 10 minutes with Equilibration Buffer. rTdT reaction mix (45 µl Equilibration Buffer + 5 µl Nucleotide Mix + 1 µl rTdT enzyme) was added to the sections and plastic coverslips placed for even labelling; they were kept at 37º in a container inside the water bath for 60 minutes. Slides were immersed in a coplin jar with 2X SSC for 15 minutes to stop the reaction and washed two times in 1X PBS and one time in 1X PBSTw (1% Tween-20). For negative controls, the same procedure was done except the Incubation Buffer was made up without the rTdT enzyme (45 µl Equilibration Buffer + 5 µl Nucleotide Mix). Lastly, Fluoromount – G (Thermofisher) was used as mounting medium and glass cover slips placed. Imaging was done on a ZEISS LSM 800 confocal microscope and cells were quantified on ImageJ (Schneider et al., 2012) through the cell counter plugin.

2.2.1.2 TUNEL assay: Wholemount

Larvae were fixed overnight (O/N) in 1.5 ml 4% paraformaldehyde (PFA) in 1X PBS at 4ºC. Subsequently, larvae were dehydrated in an ascending series of 1.5 ml methanol

(MeOH) starting at 25% MeOH in 1X PBS until 100% MeOH. Each increase was done for 5 minutes on a shaker. Finally, dehydrated larvae were stored in 100% methanol (MeOH) at -20ºC.

Before their use, larvae were rehydrated in 1.5 ml of descending MeOH in 1X PBS series inverse of above, then rinsed in 1X PBST (1X PBS + 0.8% TritonX-100) and treated with proteinase K (ProK) (15ng/ml) - the length of this step varies depending on the developmental stage **(Table 2.2).**

Table 2.2 Proteinase K treatment for wholemount larvae

Developmental Stage	Concentration	Incubation Time
3 dpf	2:1000	30 minutes
4 dpf	3:1000	25 minutes
5 dpf	4:1000	20 minutes

Larvae were washed in 1.5 ml 1X PBS four times for 5 minutes each, fixed in 4% PFA in 1X PBST (1X PBS + 0.8% TritonX-100) for 10 minutes at RT on a shaker and washed on a shaker in 1X PBST (1X PBS + 0.8% TritonX-100) four times for 5 minutes each. Subsequently, embryos were equilibrated O/N at on a shaker at RT with Equilibration Buffer. rTdT incubation buffer (45 µl Equilibration Buffer + 5 µl Nucleotide Mix + 1 µl rTdT Enzyme) was added to the Eppendorf tubes and kept on a shaker at 4ºC O/N. Larvae were immersed in 1.5 ml 2X SSC for 20 minutes on a shaker at RT to stop the reaction, washed 2 times in 1X PBS for 5 minutes each and one time in PBST (1X PBS + 0.8% TritonX-100) for 5 minutes. They were then incubated in

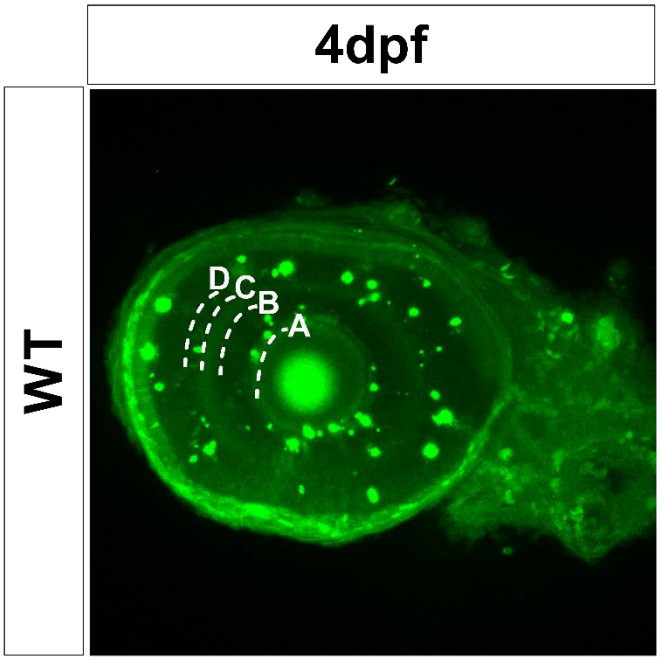

Figure 2.1 TUNEL analysis.

Cells counted from line **A.** to line **B.** were considered to be in the GCL. Cells counted from line **C.** in line **D.** were considered to be in the region where ACs are located. Cells outside of line **D.** were considered as rest of retina. Scale bars set at 10 µm.

1:1000 Hoechst 33258 in 1X PBS for 30 minutes at RT. Lastly larvae were rinsed three times for 5 minutes each in 1X PBS and one time for 5 minutes in 1X PBST (1X PBS + 0.8% TritonX-100). Larvae were rinsed in an ascending glycerol in 1X PBS series of 1.5 ml - 25%, 50% and 70% for 5 minutes each step. Imaging was done on a ZEISS LSM 800 confocal microscope and cells were quantified on ImageJ (Schneider et al., 2012) through the cell counter plugin. **Figure 2.1.** describes parameters used for dividing the retina into sections for cell counts.

2.2.2 PH3 Staining

Anti-phospho-Histone H3 (Ser10) Antibody, Mitosis Marker is a Rabbit Polyclonal Antibody for detection of Histone H3 phosphorylated at serine 10. This was used to detect mitotic cells in the retina of developing zebrafish. Protocols used are below.

2.2.2.1 PH3 staining: Cryosections

Cryosections were acquired following the same steps as **2.2.1.1**, following the degelatination step, cryosections were blocked in 1.5 ml blocking reagent (5% Normal Goat Serum + 1mg/ml BSA + PBST (0.1% TritonX-100) for one hour at RT. After blocking, the slides were incubated with 1 ml of the primary antibody (rabbit anti-PH3 1:1000, Millipore) in 0.4% blocking reagent O/N at 4ºC. They were then washed with 1 ml 1X PBST (1X PBS + 0.1% TritonX-100) three times for 30 minutes each and incubated in secondary antibody (goat anti-rabbit Alexa 546, 1:200, Invitrogen) in 0.4% blocking reagent at 4ºC O/N. Secondary antibodies were washed with 1X PBST (1X PBS + 0.1% TritonX-100) three times for 30 minutes each. Lastly, fluoromount was used to mount coverslips. Imaging was done on a ZEISS LSM 800 confocal microscope and cells were quantified on ImageJ (Schneider et al., 2012) through the cell counter plugin.

2.2.2.2 PH3 staining: Wholemount

Larvae were prepared following the same steps as **2.2.1.2,** after rehydration through an ascending series of 1.5 ml MeOh starting at 75% MeOH in 1X PBS until 100% 1X PBS; larvae were fixed for 20 minutes in 1.5 ml 4% PFA in 1X PBS, washed several times in 1X PBST (1X PBS + 0.8% TritonX-100) and then blocked for 1 hour at RT in 1.5 ml of blocking reagent (5% Normal Goat Serum + 1mg/ml bovine serum albumin in 1X PBST(1X PBS + 0.8% TritonX-100)). Primary antibodies (rabbit anti-PH3 1:1000, Millipore) were diluted in the blocking reagent and larvae incubated at 4ºC O/N.

Larvae were then rinsed twice in 1.5 ml 1X PBST (1X PBS + 0.8% TritonX-100) and washed four times for 15 minutes in 1.5 ml 1X PBST (1X PBS + 0.1% TritonX-100) . Antibody blocking was repeated by incubating larvae for 1 hour in 1.5 ml blocking reagent at room temperature (RT). Secondary antibodies (goat anti-rabbit Alexa 546, 1:200, Invitrogen) were added in blocking reagent and larvae were kept at 4ºC O/N. Larvae were rinsed in an ascending glycerol in 1X PBS series starting at 25% until 70%. Larvae were then mounted in 1% low melting point (LMP) agarose (Sigma) in 1X PBS for subsequent imaging. Imaging was done on a ZEISS LSM 800 confocal microscope and cells were quantified on ImageJ (Schneider et al., 2012) through the cell counter plugin.

2.3 SINGLE CELL LABELLING

To mosaically label cells for morphological analysis , the UAS:GAL4 system was used. The specifics of which will be described in each of the following sections.

2.3.1 Microinjections

Microinjections were done between the 1- and 4-cell stage using a Zeiss Stemi SV 6 long working distance stereomicroscope, a Kanetic micromanipulator, and an Intracel Picospritzer III pneumatic microinjector with a foot pedal; needles were 10 mm diameter capillary glass and an Intracel pipette-holder with the outer diameter matched to that of the capillary glass. After embryos were transferred to microinjection plates

using a 2.5 ml plastic pipette, the tip of the microinjection needle was broken off with ultra-fine forceps to reach an appropriate diameter. The needle was loaded with 2-4 µl of injection solution. After injection, embryos were then transferred into sterilised petri dishes with fresh 1X Danieau or Danieau + PTU solution and placed in the incubator at 28.5°C on a 14-hour ON /10-hour OFF light cycle until imaging was done.

2.3.2 Plasmids

All plasmid DNAs used for this thesis **(Table 2.3)** were prepared using a Midiprep kit (Qiagen®) and will be described in following sections.

Table 2.3 Plasmid DNAs used for this thesis

Plasmid	Use
Ath5:Gal4[4]	RGC specific promoter
FoxP2:Gal4	FoxP2-positive tectal cells
UAS:Syp-GFP DsRed Express[5]	Presynaptic vesicle marker
UAS:FingR-PSD95-GFP mKate2	Postsynaptic density marker

2.3.3 Single Cell Labelling of RGCs

[4] Gift from Prof. Steve Wilson, UCL, UK
[5] Gift from Professor. Martin Meyer, KCL, UK

To mosaically label RGCs for morphological analysis, an activator plasmid containing GAL4 driven by an upstream *ath5* promoter (Ath5:Gal4[6]) was co-injected with an effector plasmid where dual expression of a cytosolic red fluorescent protein (DsRed Express) to mark arbour structure, and a fusion of the synaptic vesicle protein synaptophysin (Syp) with green fluorescent protein (GFP) to mark presynaptic vesicles was under the control of five UAS repeats (UAS:Syp-GFP DsRedExpress[7]) (MEYER AND SMITH, 2006). The mixed plasmids were injected at a concentration of 30 ng/µl each in 1X Danieau solution.

2.3.4 Single Cell Labelling of tectal cells

Sparse labelling of tectal cells for morphological analysis was achieved by using a FoxP2 enhancer to drive Gal4 (FoxP2:Gal4[8]). FoxP2 is a forkhead domain transcription factor with high expression along the CNS, including the optic tectum in zebrafish. In addition, the injection mix contained the responder plasmid UAS:FingR-PSD95-GFP mKate2 [9] (to label postsynaptic densities) and Tol2 mRNA for genomic integration. The PSD95 plasmid contains a self-regulatory element by having zinc finger binding sites 5' to the UAS. The constructs were injected with the following concentrations: FoxP2:Gal4 and UAS:FingR-PSD95-GFP mKate2 at 30ng/µl and the Tol2 mRNA at 50 ng/µl in 1X Danieau solution.

[6] Gift from Prof. Steve Wilson, UCL, UK
[7] Gift from Professor. Martin Meyer, KCL, UK
[8] Gift from Professor Martin Meyer, KCL, UK
[9] Gift from Professor Jason Rihel, UCL, UK

2.4 IMAGING

Prior to imaging, 3 to 5 dpf larvae were immobilised with LMP agarose (Sigma) in either 1X PBS or 1X Danieau **(Table 2.4)** for cryosections and wholemount larvae respectively and mounted dorsal side up on custom-made chambers - a silicone border was made around a glass microscope slide to allow LMP agarose (Sigma) and Danieau to stay in place.

Table 2.4 Percentage of LMP agarose

PH3	1% LMP agarose in PBS
TUNEL	1% LMP agarose in PBS
RGC morphology	2% LMP agarose in Danieau
Tectal cell morphology	2% LMP agarose in Danieau

2.4.1 Confocal Imaging of Fixed Tissue

Imaging for IHC was performed using a ZEISS LSM 800 confocal microscope equipped with an 20X air objective (Carl Zeiss). 488 nm laser excitation light was used to elicit GFP fluorescence and 405 nm laser excitation light was used to elicit Hoechst 33258 signal. Z-stacks were generated from images taken at 1.00 µm intervals using the following settings (512x512 pixel, 8 speed, 2X averaging). All images were acquired and manipulated in the same way.

2.4.2 *In Vivo* Confocal Imaging

Imaging was performed using an LSM 710 confocal microscope equipped with a spectral detection scan head and a 20x/1.0 NA water-immersion objective (Carl Zeiss). Optical sections were obtained at 0.66 µm intervals through the Z-axis and 1 AU pinhole aperture. Maximum intensity projections and 3D rotated images were generated using either ImageJ (Schneider et al., 2012) or IMARIS 8.0 (Bitplane).

2.5 GENOTYPING

Fin clips from tenm4 $^{10bp\Delta}$ mutant adult zebrafish were taken after anaesthetising them in a solution with 22.5 ml Tricaine and 7 ml per litre Lidocaine. Genomic DNA was extracted using 50 µl Gruenwald's Buffer (10 mM Tris-HCL pH 8.2 + 10mM EDTA pH 8.0 + 200mM NaCL + 0.5% SDS) + 1% ProK (20 mg/ml) and incubating overnight. PCR was run with GoTaq® Flexi DNA Polymerase **(Table 2.5)** following the steps outlined in **Table 2.6** with primers outlined in **Table 2.7**. After PCR, DNA was run on a 5% agarose (Sigma) gel (7.5g agarose + 150ml 1X TAE) with Ethidium Bromide. A 314 bp fragment was amplified, and subsequently sequenced for verification of the deletion. The 10 bp deletion sequence expected is: CAGAAATGGG.

Table 2.5 GoTaq® Flexi master mix	
Reagent	1X Reaction
5x GoTaq Flexi Buffer	4µl.
dNTPs (40mM) – 10mM each	0.5µl.
Fwd Primer (10mM)	0.5µl.
Rev Primer (10mM)	0.5µl.
$MgCl_2$	1µl.
DNA Template	1µl.
Taq	0.2µl.
DMSO	1/0µl.
ddH_2o	11.3/12.3µl.

Table 2.6 PCR procedure		
	Temperature	**Time**
Denature	95°C	5 minutes
Denature	95°C	30 seconds
Annealing	58°C	30 seconds
Extension	72°C	45 seconds
	33 Cycles	
Final Extension	72°C	5 minutes
Hold	4°C	

Table 2.7 Primers for tenm4$^{\Delta 10bp}$ mutant genotyping	
Forward Primer	GAAAATGCAAGCTTGTTTTATGTTC
Reverse Primer	GAACTGCGGCCGGATTTG

2.6 ANALYSIS

2.6.1 Morphological Analysis

2.6.1.1 IPL Stratification

To determine the IPL stratification profile of RGCs dendrites, rectangular 10µm-wide ROIs were drawn across the IPL using ImageJ (Schneider et al., 2012). The Plot Profile function was applied to the ROIs to calculate fluorescence intensity traces across the IPL depth. The traces obtained from multiple larvae were then normalised, averaged and graphed using GraphPad (Prism software).

2.6.1.2 RGC and TC Morphology

RGCs were imaged as described in section **2.3.1**, Z-stacks acquired during imaging were imported into IMARIS (Bitplane) for analysis. First, the *"surface object"* function was used to create an alternative channel and reduce background noise. Followed by the *"filaments object"* function being used to outline the axon and its arborisation as well as to determine the measurements for branch length and number. The *"spot object"* function was used manually to quantify the number of puncta in each RGC, and the *"measurement points object"* function for acquisition of puncta length. Lastly the *"surface object"* function was used again to calculate the volume for every punctum. All steps and objects were initially done with manual settings and then repeated with automatic detection for corroboration of manual results. Specific parameters were taken into consideration throughout the analysis: For the *"filament object"*, the first point was always placed at the first branching point where the RGC begins ramification. Finally, measurements for puncta length were taken from point "a" – start of the synapse, to point "b" – end of the synapse, always following the direction of the branch.

Data obtained through IMARIS (Bitplane) was statistically analysed and graphed using GraphPad (Prism).

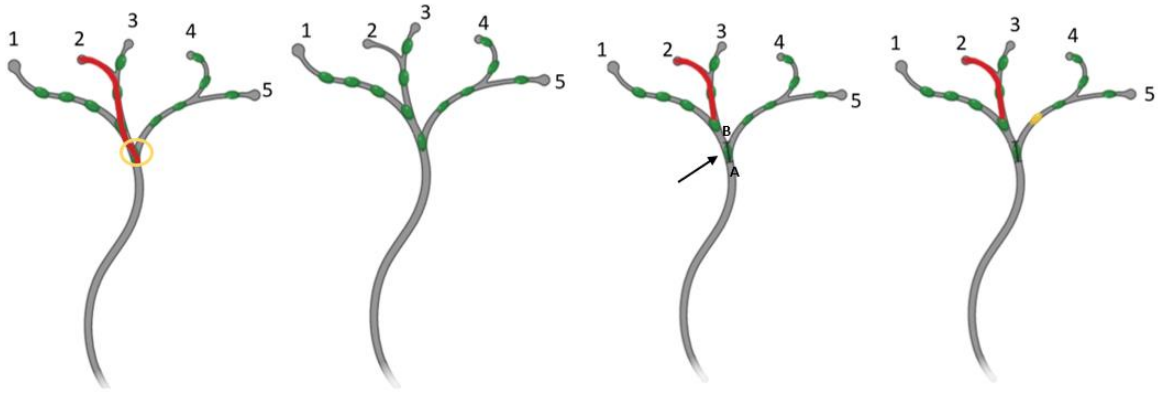

Figure 2.2 IMARIS (Bitplane) measurements. A. "Filament object" function used for branch measurements outlined in red. Yellow circle is marking the branching point where measurements began. **B**. "Spots object" function for puncta number quantification represented by green dots. **C.** "Filament object" function used for puncta length marked by black arrow. **D.** "Surface object" used for puncta volume measurements represented by yellow dot.

Sholl analysis (Ferreira et al., 2014), is a plugin for ImageJ (Schneider et al., 2012) used to describe the complexity of neuronal arbours. Images were first converted from multichannel images to grayscale, this is done because composites cannot be thresholded. The start-up ROI was positioned at the first branch point of the cell. The parameters were kept the same throughout the images, these include: the starting radius, the ending radius, and the radius step size. The data obtained was transferred, statistically analysed and graphed using GraphPad (Prism).

2.6.4 Statistical Analysis

Statistical analysis and tests were carried out using GraphPad (Prism). Before performing statistical tests, sample distributions were checked for normality with either the Shapiro-Wilk test or D'Agostino-Pearson normality test. The criteria for statistical significance were set at $p < 0.05$ with a 95% confidence interval. Details regarding each statistical test used can be found summarised in **Table 2.8** for Chapter 3 results, **Table 2.9** for Chapter 4 results and **Table 2.10** for Chapter 5 results. Note that no statistical test was used to predetermine sample sizes for the experiments, but n numbers are similar to those generally used throughout the field.

Table 2.8 Statistical test for experiments in Chapter 3

Experiment	Statistical Test
PH3 Staining	Unpaired t-test
TUNEL Assay	Unpaired t-test
IPL Stratification	Two-way ANOVA

Table 2.9 Statistical test for experiments in Chapter 4	
Experiment	**Statistical Test**
Branch Number	Unpaired t-test
Branch Length	Unpaired t-test
Puncta Number	Unpaired t-test
Puncta Length	Unpaired t-test
Puncta Volume	Unpaired t-test
Sholl Analysis	Two-way ANOVA/ Unpair t-test
Development	Unpaired t-test

Table 2.10 Statistical test for experiments in Chapter 5	
Experiment	**Statistical Test**
Branch Number	Unpaired t-test
Branch Length	Unpaired t-test
Puncta Number	Unpaired t-test
Puncta Volume	Unpaired t-test
Sholl Analysis	Two-way ANOVA/ Unpaired t-test

CHAPTER 3.

ROLE OF TENEURIN-4 IN THE DEVELOPING VERTEBRATE RETINA

3.1 Cell Proliferation and Apoptosis During Retinal Development

Over the years, the retina has become a valuable model in which to study various aspects of development, such as cell cycle, neurogenesis, and circuit assembly. In multicellular organisms, cell cycle regulation is a fundamental element of cellular function. This process is crucial for the correct development, organogenesis, and tissue homeostasis. The coordination and balance of cell growth, cell division and cell death are essential for normal embryonic and therefore tissue development. A balance must be reached between new cell growth and the elimination of existing cells by programmed cell death. For these cells to survive, they must compete for growth and survival factors which guarantee stability between the addition and elimination of cells (Hipfner & Cohen, 2004).

Eye morphogenesis in zebrafish larvae closely resembles other vertebrates and humans. It develops from three embryological tissues: (1) Neuroectoderm, (2) Surface ectoderm, and (3) Mesenchyme. For the purposes of this thesis, we will only be concentrating on the (1) Neuroectoderm. The neuroectoderm gives rise to the neural retina, retinal pigment, epithelium, optic stalk, ciliary body, iris dilator and sphincter muscles (Richardson, Tracey-White, Webster, & Moosajee, 2017). The rate of zebrafish retinal development is remarkable, as it changes from a proliferative neuroepithelium into a functional retina over 2.5 days. Before neurogenesis begins,

the neural retain contains a group of proliferating retinal progenitor cells (RPCs) which form a pseudostratified neuroepithelium; each RPC makes contact with both the basal and apical laminae. Between 24 hpf and 36 hpf, the retina enters a rapid proliferation stage. RGCs are the first type to differentiate, followed by amacrine cells (ACs) and bipolar cells (BCs) by 48 hpf; and lastly by photoreceptors (PRs), horizontal cells (HCs) and muller glial cells (MCs) by 72 hpf. Whilst neurogenesis is still happening within the retina, the already formed RGC axons exit the eye between 32 hpf and 34 hpf, and the optic nerves gradually form (Burrill & Easter, 1994, 1995; Centanin & Wittbrodt, 2014; Cepko, Austin, Yang, Alexiades, & Ezzeddine, 1996; Schmitt & Dowling, 1999; B. Xu et al., 2020)

The coordination and balance amongst cell growth, cell division and cell death are essential for normal embryonic development. This balance must be reached between new cell growth and the elimination of existing cells by programmed cell death. Intricate mechanisms, which will be spoken about later, guarantee that cells do not evade these rules and thus reach homeostasis by preventing uncontrolled proliferation (Hipfner & Cohen, 2004).

Cell death is essential for the morphogenesis of a developing embryo as well as one of the major factors for achieving homeostasis in adult tissue and organs. There are two general mechanisms that can cause cell death: necrosis and apoptosis. Necrosis is a passive form of simultaneous cell death, where a specific organ is compromised, and the entire organism is affected to some extent (Daly & Sandell, 2000). Apoptosis is a programmed cell death which occurs mostly, but not only, during embryonic development of multicellular organisms (Glücksmann, 1965; Oppenheim et al., 2001) and represents one of the most common mechanisms to regulate the size of cell populations during development (Vecino, Hernández, & García, 2004).

Apoptosis is a highly conserved mechanism characterised by cellular shrinkage, membrane blebbing, nuclear condensation, fragmentation, and nuclear collapse (Cole & Ross, 2001; Taylor, Cullen, & Martin, 2008). The whole process is coordinated by the caspase family (cysteine proteases), which target hundreds of proteins involved in cell demolition. Apoptosis is a highly studied subject, in mammalian retinal development, for example, apoptosis spreads over the retina in consecutive waves and induces a remarkable amount of cell loss (Remé, Grimm, Hafezi, Wenzel, & Williams, 2000); in the postnatal period of rats and mice, RGCs are reduced by about 50% (Biehlmaier, Neuhauss, & Kohler, 2001; Perry, Henderson, & Linden, 1983; Potts, Dreher, & Bennett, 1982; Williams, Piñon, Linden, & Pinto, 1990). This has not been found in zebrafish. Apoptosis in the zebrafish retina seems to serve as a mechanism for the formation of precise retinal neuronal networks. It seems to occur after mitotic waves during specific developmental processes, or in later in life where there are residual mitotic regions instead of as a method for removing large numbers of excess cells (Dyer & Cepko, 2001; Linden, Rehen, & Chiarini, 1999).

As previously stated (see Chapter 1) there is an increase of visually responsive voxels in the Tenm4$^{\Delta 10bp}$ mutant larvae. We hypothesise that (1) an increase of mitotic RGCs, or (2) an increase of apoptotic ACs, could lead to an imbalance in cell numbers within the retina, preventing ACs (main inhibitory neurons of the retina) to fulfill their role in shaping and modulating RGC responses. ISH data shows the expression of *tenm4* within the retina localised specifically in a subset of RGCs and ACs (**Figure 1.16** and **1.17** ; Chapter 1. Introduction). Understanding the relationship between RGC and AC numbers undergoing apoptosis could begin to shed light to the mechanisms that tenm4 has within the developing CNS.

3.2 Cell proliferation is Not Affected Upon Teneurin-4 Deletion

Previously, the Hindges lab identified an increase of visual responsive voxels in the axons of RGCs at 4 days post fertilisation (dpf) in the Tenm4$^{\Delta 10bp}$ mutant larvae by performing calcium functional imaging (Chapter 1). Wanting to understand the underlying cause of this, we came up with various hypothesis. One possibility to explain the increase of responses could be based in an enlarged number of RGC numbers within the tenm4 $^{\Delta 10bp}$ mutant fish retina. As it was previously stated in Chapter 1, RGCs are the sole output neurons of the retina, and ACs are inhibitory neurons which shape and modulate the responses of these RGCs. We therefore hypothesised, if there is a higher number of RGCs undergoing mitosis, but ACs stay within normal numbers or even undergo less proliferation, then ACs would not be able to fulfil their role of inhibiting RGC responses because of the imbalance amongst the two cell type populations.

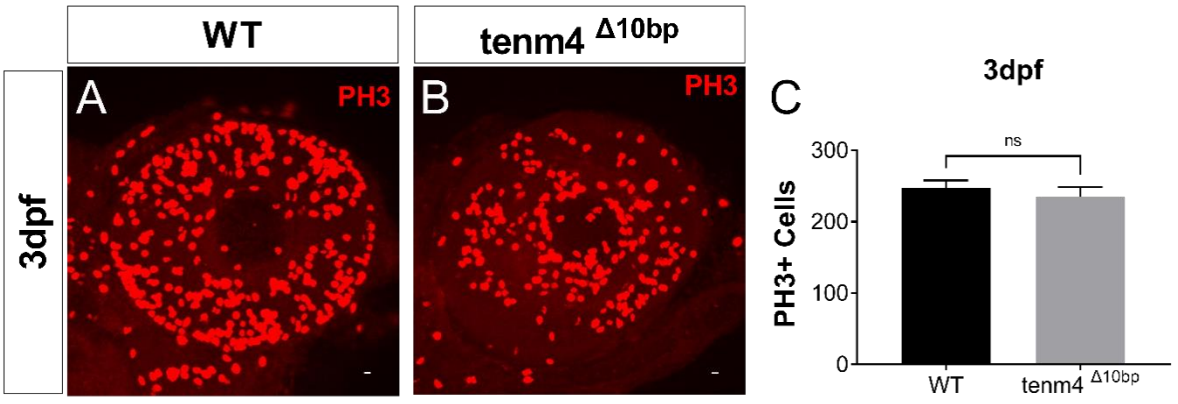

Figure 3.1 Wholemount immunolabelling for mitotic cells in 3 dpf larvae. Immunostaining of wholemount retinae with anti-PH3 (red) - which targets late G2/M phase mitotic cells. Quantification of **A**. 3 dpf WT larvae **B**. 3 dpf tenm4$^{\Delta 10bp}$ mutant larvae mitotic cells. **C.** No significant difference was observed between the number of mitotic cells within the two genotypes (WT: 247.4±10.37, n=5; Tenm4$^{\Delta 10bp}$ mutant: 235.4±12.89, n=5; p<0.7538, ns). Scale bars set at 10µm.Statistical test: t-test

By 4 dpf, RGC axons have reached the optic tectum (OT), where they are able to make synaptic connections with their synaptic partners. Visually evoked responses can be seen in larval zebrafish from 3 dpf. Considering that RGCs have already reached the OT and have begun to establish synaptic connections by 4 dpf, we analysed cell proliferation in the retina at three key developmental stages for this project: 3 dpf – stage at which you can begin to elicit visually evoked response; 4 dpf – stage at which the initial functional imaging was performed; and 5 dpf – stage at which larvae are capable of engaging in tectum-dependant complex behaviours such a prey capture.

Embryos were stained against the late G2/M phase marker phosphohistone-H3 (PH3) using immunohistochemistry to quantify retinal cells undergoing mitosis. The antibody stainings were done both in cryosections and wholemount larvae and imaged on a confocal microscope; for details on image acquisition, cell quantification, and statistical analysis, please see Material and Methods (Chapter 2).

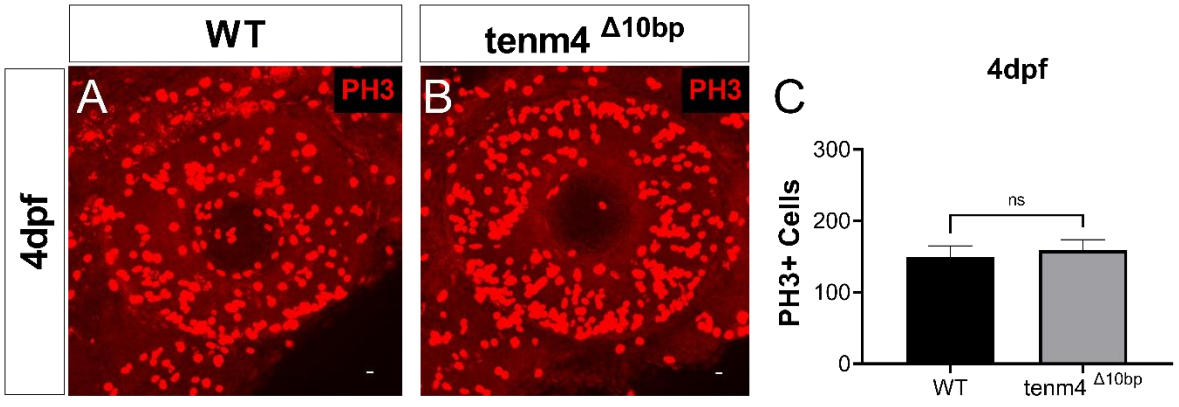

Figure 3.2 Wholemount immunolabelling for mitotic cells in 4 dpf larvae. Immunostaining of retinae with anti-PH3 (red) which targets late G2/M phase mitotic cells. Quantification of **A**. 4 dpf WT larvae **B**. 4 dpf tenm4$^{\Delta 10bp}$ mutant larvae. **C.** No significant difference observed between the two genotypes (WT:149.8±15.49, n=5; tenm4 $^{\Delta 10bp}$ mutant: 158.8±14.96, n=5; p<0.7538, ns). Scale bars set at 10µm. Statistical analysis: t-test

As seen in **Figure 3.1,** through wholemount immunohistochemistry (IHC) at 3 dpf in both the Wildtype (WT) retina (**Figure 3.1A**) and the Tenm4$^{\Delta 10bp}$ mutant retina (**Figure 3.1B)** mitotic cells were found throughout, with no significant difference observed between the two genotypes (n = 5 eyes per genotype); **Figure 3.1C).** Similarly at 4 dpf **(Figure 3.2)** and 5 dpf **(Figure 3.3)** no significant differences were observed between the two genotypes.

Looking at mitosis throughout these developmental stages **(Figure 3.4)**, it was seen that there is a higher number of cells undergoing mitosis at 3 dpf in both genotypes **(Figure 3.4A and 3.4B),** with the number of mitotic cells decreasing at 4 dpf, before stabilising by 5 dpf. This trend was followed by both genotypes throughout the specific time points chosen for the experiment (**Figure 3.4C)**. This suggests that the Tenm4 mutation does not seem to have an impact on the overall cell proliferation

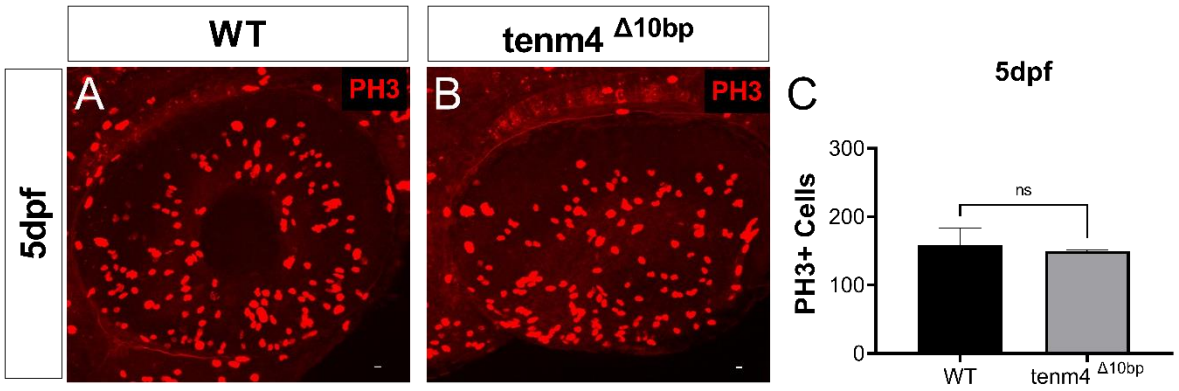

Figure 3.3 Wholemount immunolabelling for mitotic cells in 5 dpf larvae. Immunostaining of retinae with anti-PH3 (red) which targets late G2/M phase mitotic cells. Quantification of **A**. 5 dpf WT larvae **B**. 5 dpf tenm4$^{\Delta 10bp}$ mutant larvae. **C.** No significant difference observed between the two genotypes (WT:158.4±11.13, n=5; tenm4 $^{\Delta 10bp}$ mutant: 149.6±0.812, n=5; p<0.4531, ns). Scale bars set at 10µm. Statistical analysis: t-test

in the retina, and therefore could not be used to explain the increase of visual responses seen by our Tenm4$^{\Delta 10bp}$ mutant larvae at 4 dpf. Although there is a lack of cell-type specificity within the experiment, and we can therefore not be certain of the

number of RGCs and the number of ACs, we can clearly see that there is no difference in the overall number of cells undergoing mitosis. Alternative experiments to answer this question with more precise information, including cell-type specificity, are described in section **3.6.**

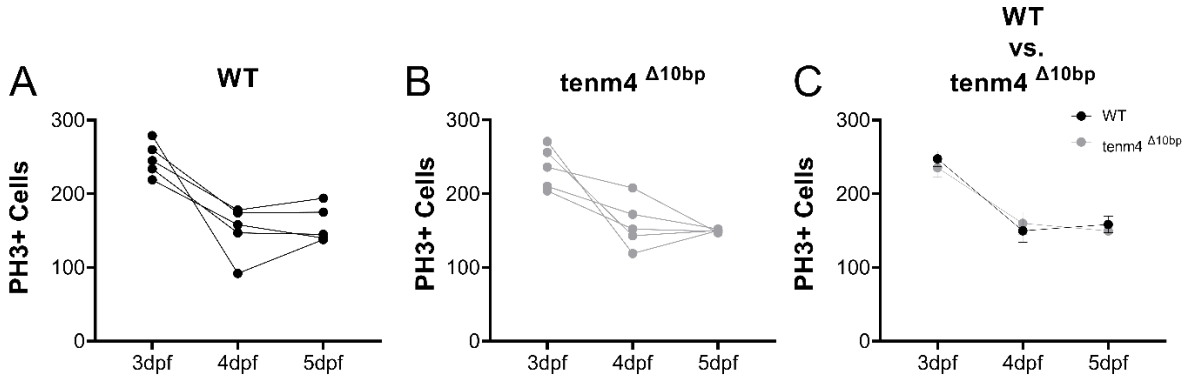

Figure 3.4 Mitosis in the retina through development. A. Average number of mitotic cells through development in WT larval retinae from 3dpf to 5dpf. **B.** Average number of mitotic cells through development in tenm4$^{\Delta 10bp}$ mutant larval retinae from 3dpf to 5dpf. **C.** Comparison of average mitotic cells through development of both WT and tenm4$^{\Delta 10bp}$ mutant larvae. (n=5 eyes per genotype).

3.3 Increase of Apoptotic Cells Upon the Deletion of Teneurin-4

As second possibility to explain the observed changes in the number of visually evoked responses between the two genotypes seen in Chapter 1, we hypothesised that there could be a change in the number of cells undergoing apoptosis within the retina. As it was described in section **3.2,** if the tenm4$^{\Delta 10bp}$ mutant retina is undergoing more AC apoptosis, or having a lower number of apoptotic RGCs, it could mean that these inhibitory cells are again, incapable of achieving their role in shaping and modulating RGC responses due to the imbalance between the two sub-population of cells. To understand this, we used the DeadEnd™ Fluorometric (TdT-mediated dUTP Nick-End Labelling) TUNEL System (Promega), which is designed for detection of apoptotic cells by measuring nuclear DNA fragmentation (see Material and Methods Chapter 2.). For details regarding the image acquisition, cell quantification, and statistical analysis, please refer to Material and Methods (Chapter 2).

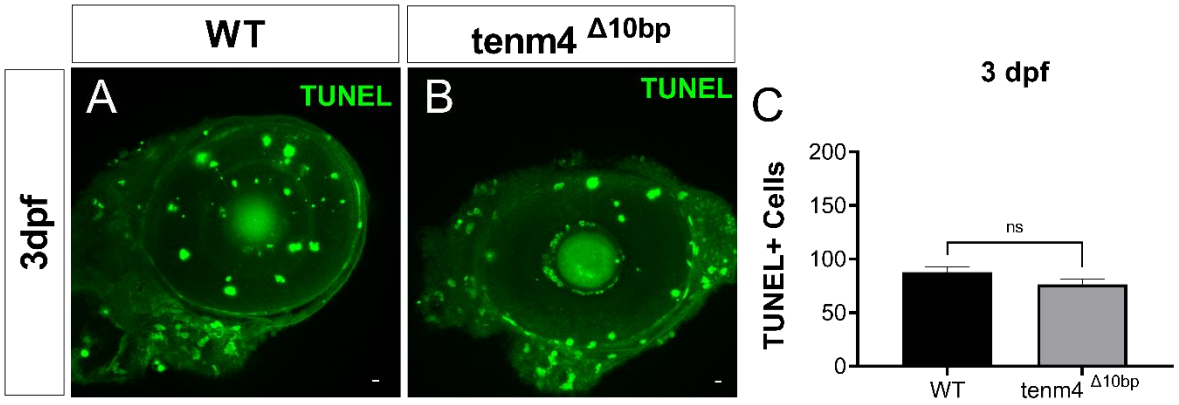

Figure 3.5 Wholemount TUNEL staining for the detection of apoptotic cells in 3 dpf larvae. A. Quantification of TUNEL positive cells in 3 dpf WT retina **B.** Quantification of TUNEL positive cells in 3 dpf tenm4$^{\Delta 10bp}$ mutant larva **C.** No significant difference observed between the two genotypes. (WT:87.80±4.93, n=5; tenm4 $^{10bp\Delta}$ mutant: 76.40±4.84, n=5; p<0.9724, ns). Scale bars set at 10µm. Statistical analysis: t-test

TUNEL positive cells were found throughout the retina at the three developmental time points chosen for this study (3 dpf, 4 dpf and 5 dpf). Previous work in zebrafish larvae has shown that during these early stages of development, apoptosis is expected to be very high (Biehlmaier et al., 2001; Schmitt & Dowling, 1999). We initially looked at 3 dpf larvae **(Figure 3.5)** where no significant difference was observed between WT larvae **(Figure 3.5A)** and Tenm4$^{\Delta 10bp}$ mutant larvae **(Figure 3.5B)**. However, once we examined the larvae at 4 dpf **(Figure 3.6)** a significant difference was observed between the two genotypes, with an increase of TUNEL+ cells within the tenm4$^{\Delta 10bp}$ mutant retinae **(Figure 3.6C)**.

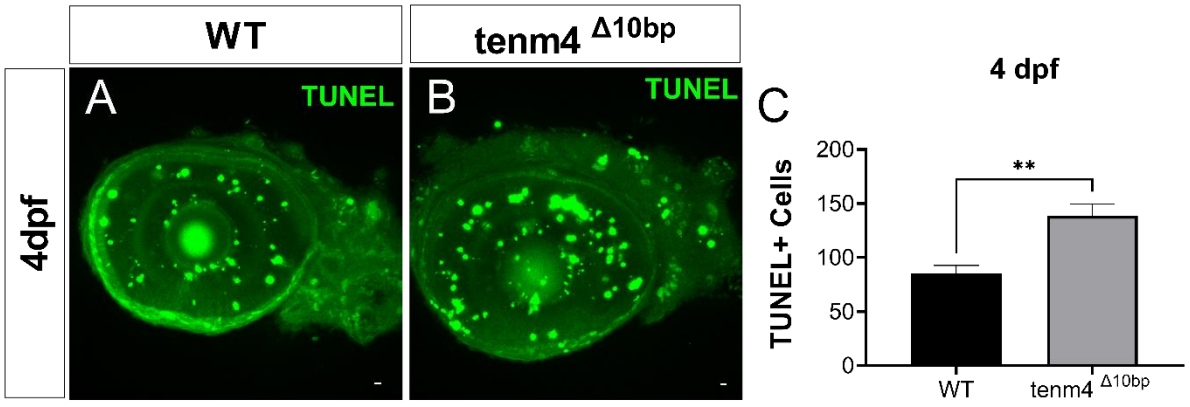

Figure 3.6 Wholemount TUNEL staining for the detection of apoptotic cells in 4 dpf larvae. A. Quantification of TUNEL positive cells in 4 dpf WT retina **B.** Quantification of TUNEL positive cells in 4 dpf tenm4$^{\Delta 10bp}$ mutant larval **C.** A significant difference was observed with the tenm4$^{\Delta 10bp}$ mutant having more TUNEL positive cells than the WT. (WT: 85.60±6.91, n=5; tenm4$^{\Delta 10bp}$ mutant: 138.60±10.99, n=5, p<0.0035 **). Scale bars set at 10µm. Statistical analysis: t-test

Due to the significant differences found at 4 dpf, we not only quantified the overall TUNEL-positive cells, but we divided the retinae anatomically and quantified cells from each layaer - for details regarding how the retina was divided for this analysis please see **Figure 2.1** in Chapter 2. Material and Methods. Following this anatomical division, TUNEL-positive cells were found in all nuclear layers of the retina

(ganglion cell layer (GCL) and the region where ACs are located, from here on forward known as amacrine cell layer (ACL)). We found a significant difference between our two genotypes **(Figure 3.7A)** in both the GCL **(Figure 3.7B)** and the ACL **(Figure 3.7C)**, but no significant difference was observed in what we considered "the rest of the retina". WT larvae showed a significant difference between TUNEL- positive cells in the GCL and the ACL **(Figure 3.7E)** with more apoptotic cells found within the GCL than in the ACL. Having set this baseline of apoptotic cells in WT larvae, we looked at our tenm4$^{\Delta 10bp}$ mutant larvae **(Figure 3.7F).** Here we found that although there is a general increase of apoptotic cells within the tenm4$^{\Delta 10bp}$ mutant, the number of cells undergoing apoptosis in both the GCL and the ACL are not significantly different **(Figure 3.7F)** as they stay within the same ranges as WT larvae **(Figure 3.7E).** The same trend is followed, where there is a higher number of apoptotic cells within the GCL than there is in the ACL. The differences between the TUNEL-positive cells in these two areas of the retina is not enough to be considered significantly different. The lack of cell-type specificity within the experiment, does not allow for specific conclusions to be made regarding the difference of apoptotic numbers in the different retinal layers and of the different retinal cells.

We then had a look at the overall quantification of apoptotic cells at 5 dpf **(Figure 3.8)** and once again found that there was no significant difference between the WT **(Figure 3.8A)** and the tenm4$^{\Delta 10bp}$ mutant **(Figure 3.8B)**. Lastly, we decided to examine how the number of TUNEL-positive cells behave throughout development, we therefore compared the three different developmental time points initially chosen for this experiment**(Figure 3.9).** It appears, as seen in **Figure 3.9A** that the number of TUNEL-positive cells in WT retinae are stable from 3 dpf to 4 dpf followed by a slight increase at 5 dpf. On the contrary, in the tenm4$^{\Delta 10bp}$ mutant retinae **(Figure 3.9B)**

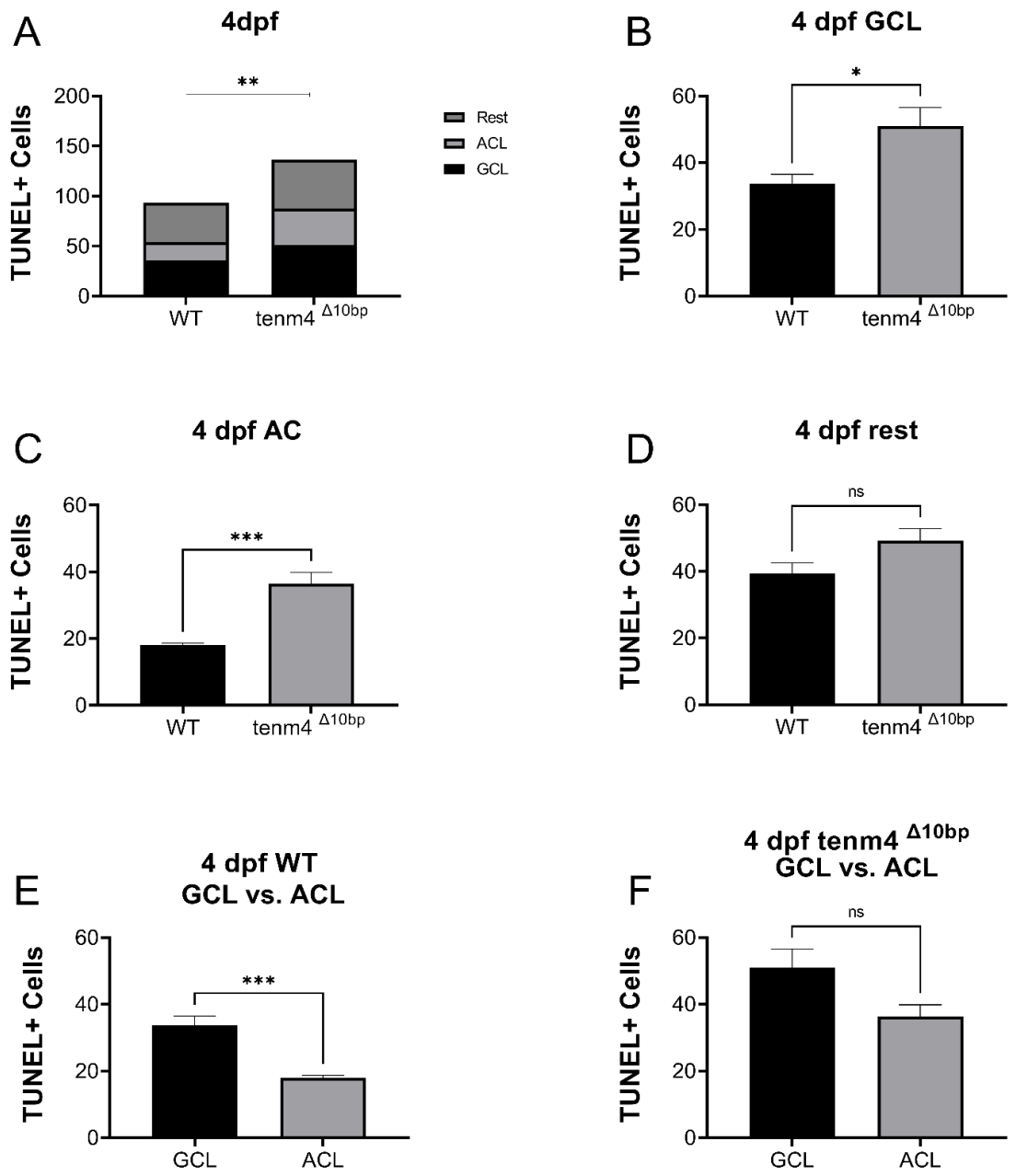

Figure 3.7 Breakdown of TUNEL positive cells in 4 dpf larvae A. Overall cell count shows a significant difference between genotypes **B.** Significant difference observed between genotypes within cells in the GCL (WT: 33.80±2.709, n=5; Tenm4$^{\Delta 10bp}$ mutant: 51.00±5.523, n=5 p<0.0233*) **C.** Significant difference observed between genotypes within cells in the ACL (WT: 18.00±0.7071, n=5; Tenm4$^{\Delta 10bp}$ mutant: 36.40±3.415, n=5 p<.0007***). **D.** No significant difference was observed when comparing TUNEL+ cells in the rest of the retina. (WT: 39.40±3.172, n=5; Tenm4$^{\Delta 10bp}$ mutant: 49.20±3.597, n=5 p<0.0753 ns). **E-F.** Comparison between TUNEL+ cells in the GCL and ACL. Significant difference observed in WT larvae (GCL: 33.80±2.709, n=5; ACL: 18.00±0.7071, n=5 p<0.0005***) but not Tenm4$^{\Delta 10bp}$ mutant larvae (GCL: 51.00±5.523, n=5; ACL: 36.40±3.415, n=5 p<0.0547 ns). Statistical analysis: t-test

3 dpf larvae have a similar number of apoptotic cells in the retina as WT, followed by a massive spike at 4 dpf, before they stabilise and reach a normal range (as WT larvae) by 5 dpf **(Figure 3.9C)**.

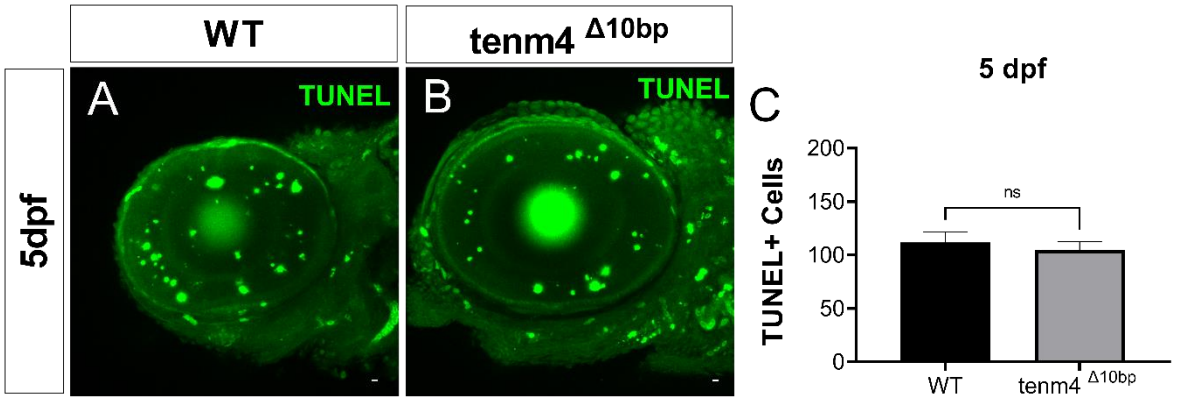

Figure 3.8 Wholemount TUNEL staining for the detection of apoptotic cells in 5 dpf larvae. A. Quantification of TUNEL-positive cells in 5 dpf WT retina **B.** Quantification of TUNEL-positive cells in 5 dpf tenm4$^{\Delta 10bp}$ mutant larval **C.** A significant difference was observed with the tenm4$^{\Delta 10bp}$ mutant having more TUNEL-positive cells than the WT. (WT: 111.8±9.805, n=5; tenm4$^{\Delta 10bp}$ mutant: 104.8±8.010, n=5, p<0.5750, ns). Scale bars set at 10µm. Statistical analysis: t-test

These results presented in this section allow us to conclude that Tenm4 seems to have a role in the development of the vertebrate retina at 4 dpf, having an impact in the number of cells undergoing apoptosis within the retina at this specific stage. Although there is an increase of apoptosis occurring in general within the Tenm4$^{\Delta 10bp}$ mutant, it can be pinpointed to a specific time point, 4 dpf, and to what anatomically seem to be specific retinal layers, the GCL and what we refer here to the ACL. Based on the data presented here, we can begin to develop a more concrete hypothesis regarding the change in visually responsive voxels between WT larvae and Tenm4$^{\Delta 10bp}$ mutant larvae. If there is a higher percentage of apoptotic cells in the ACL than in the GCL, it could mean there are not sufficient ACs to shape, modulate and

regulate RGC responses that are being sent to the OT. There are limitations to this study, by not known the specific cell types of our quantifications, and by not knowing the total number of cells that are present in the retina, we lose important data that could help build a stronger picture of Tenm4 role in the developing retina. More specific work would need to be done to be able to prove this hypothesis, such as cell counts in the retina to know the exact number of cells which could be done through a simple DAPI staining, which would therefore allow us to know the percentage of cells that are undergoing apoptosis. Using cell-type specific markers alongside the TUNEL staining which would allow us to count the true number of RGCs and ACs that are undergoing this apoptotic process. For more information regarding this, please see section **3.6.**

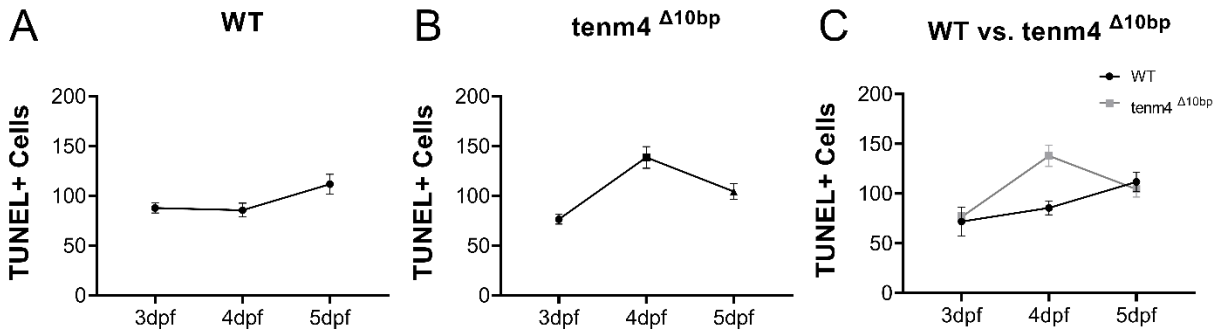

Figure 3.9 Apoptosis in the retina through development. A. Average number of apoptotic cells through development in WT larval retinae from 3 dpf to 5 dpf. **B.** Average number of apoptotic cells through development in tenm4$^{\Delta 10bp}$ mutant larval retinae from 3 dpf to 5 dpf. **C.** Comparison of average number of apoptotic cells through development of both WT and tenm4$^{\Delta 10bp}$ mutant larvae (n=5 eyes per genotype).

3.4 Intraretinal Connectivity: The Inner Plexiform Layer, RGCs and ACs

During development, precise patterns of neuronal connectivity must be established. Molecular cues are needed for the correct wiring of visual circuits during development and some of them are known to be expressed in subsets of neurons. In the vertebrate retina, some, but not all these molecules have been thoroughly studied. Although their different roles have been discovered, we are still far from having a full picture of the role they play in circuit assembly. The transmembrane molecule Tenm4 is expressed in a subset of RGCs and ACs as well as tectal neurons during a period of intense synapse formation (**Figure 1.16** and **1.17** Chapter 1.**)**, suggesting a potential role throughout this process. As described in Chapter 1, the dendrites of RGCs, ACs and BPs arborise within a specific layer of the retina called the inner plexiform layer (IPL). This layer is further subdivided into 5 different strata where synaptic connections of these retinal cells occur (S. y Cajal, 1972). These strata are positioned at 5%, 33%, 66% and 95% depth of the IPL – with 0% corresponding to the INL/IPL border, and 100% to the IPL/GCL border. These were named S5, S33, S66 and S95, respectively **(Figure 1.4** Chapter 1. Introduction**)**.

We therefore decided to measure fluorescent intensities across different stages and multiple larvae show that these strata are positioned at 5%, 33%, 66% and 95% depth of the IPL – with 0% corresponding to the INL/IPL border, and 100% to the IPL/GCL border. These were named S5, S33, S66 and S95, respectively **(Figure 1.4** Chapter 1. Introduction**)**. We hypothesise that a tenm4 mutation could cause a stratification error where RGCs within the IPL of tenm4$^{\Delta 10bp}$ mutant fish do not arborise to the correct strata, and/or where synaptic targeting errors occur. This could

subsequently have an influence on the specificity of the connections, and therefore shed light on the initial phenotype described in Chapter 1 , where an increase of visually responsive voxels was seen within the 4 dpf tenm4$^{\Delta 10bp}$ mutant when undergoing functional calcium imaging.

Previous work has demonstrated that in zebrafish larvae lacking Teneurin-3 (tenm3), RGCs tend to overshoot their target in the IPL causing aberrant stratification, this was seen starting at ~2 dpf during development (Antinucci et al., 2013). Our approach to discover if our hypothesis was correct, was to measure fluorescent intensities in the IPL across different developmental stages.

3.5 Laminar Targeting in the Inner Plexiform Layer Not Majorly Affected by Tenneurin-4 Deletion

To investigate the Tenm4 function within the developing visual system and its role in circuit assembly, specifically in RGC dendritic stratification in the IPL *in vivo*, the *tg(Isl2b:Gal4;UAS:GFP);mitfa-/-* and the *tg(Isl2b:Gal4;UAS:GFP);mitfa+/-;* Tenm4$^{\Delta 10bp}$ mutant larvae transgenic zebrafish lines (see chapter 2, Material and Methods) were used. With these lines, the fluorescent protein GFP is expressed in the majority of RGCs in the retina and their projection into the OT. This enabled us to visualise RGCs and their dendritic stratification within the IPL.

We examined wildtype (WT) and tenm4$^{\Delta 10bp}$ mutant larvae RGC dendrites and their lamination patterns within IPL at 3 dpf**(Figure 3.10)** and at 5 dpf **(Figure 3.11).** At 3 dpf a bi-laminar stratification can be expected, developing into a four layered structure by 5 dpf (**Figure 1.4;** Chapter 1)**.** *In vivo* imaging of 3 dpf *tg(Isl2b:Gal4;UAS:GFP);mitfa+/-* zebrafish larvae showed a bi-laminar stratification in the IPL (**Figure 3.10A)**, positioned at S^{95} and S^{55} respectively. The average fluorescent intensity profile shows the same two strata when imaging the 3 dpf *tg(Isl2b:Gal4;UAS:GFP);* Tenm4$^{\Delta 10bp}$ mutant larvae **(Figure 3.10B)**, proving there was no major stratification defect visible or significant difference obtained between the two genotypes in the IPL. This experiment was repeated at 5 dpf, where, as mentioned before, most RGCs have reached their targets in the appropriate IPL laminar depth (**Figure 1.4;** Chapter 1) creating four out of the five expected sub-layers (Mumm et al., 2006). Our analysis showed that, at this time point, four GFP positive strata were visible in the IPL of the WT larvae (**Figure 3.11A)**. When plotting the average

fluorescent intensity profiles taken from these larvae, it was confirmed that two new strata had appeared **(Figure 3.11C).** Strata were now visible at S^5, S^{33}, S^{66} and S^{95}. In Tenm4$^{\Delta 10bp}$ mutant larvae **(Figure 3.11B)**, the same four strata were visible and there was no significant difference between the two genotypes **(Figure 3.11C).**

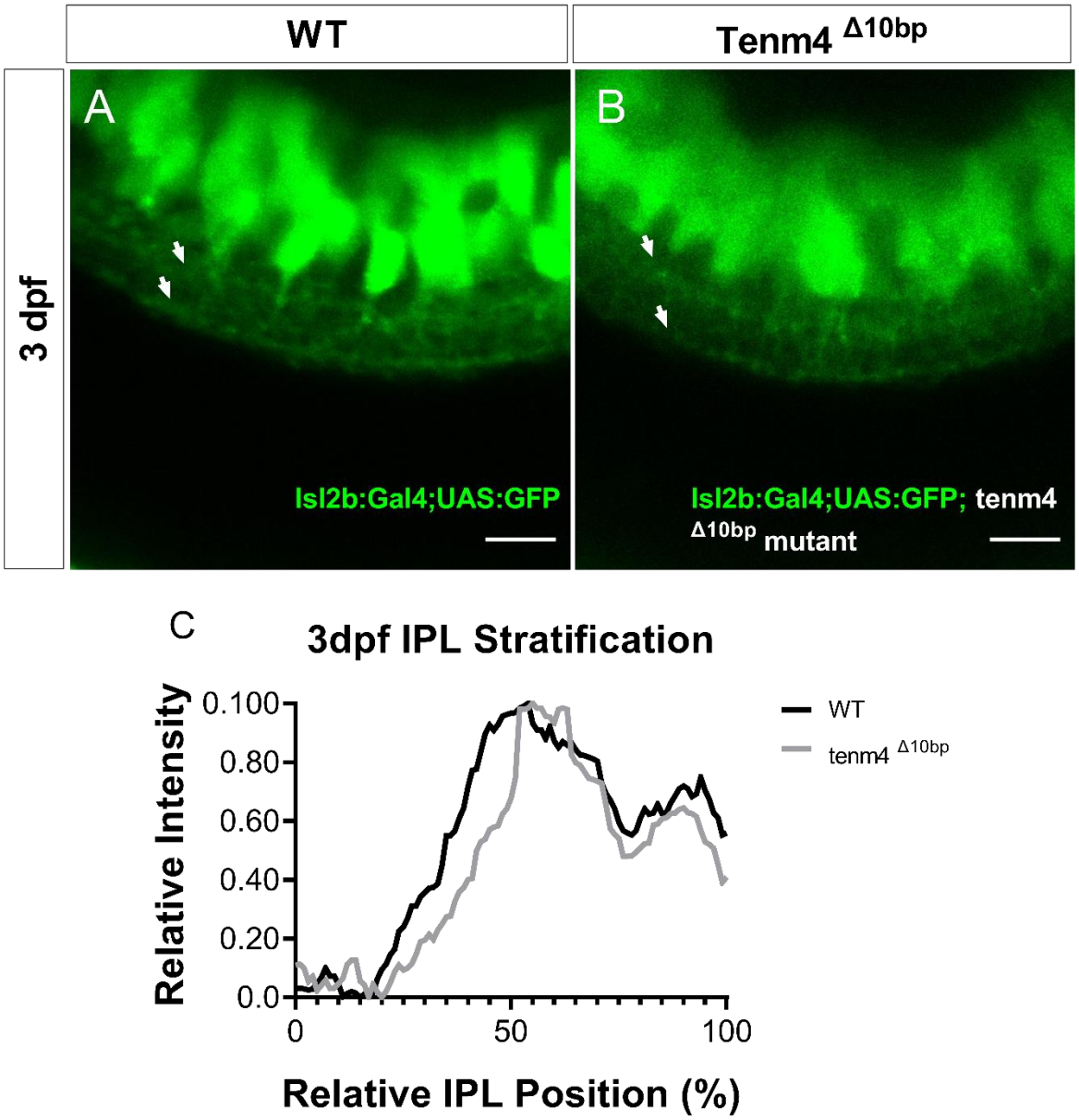

Figure 3.10 Neurite stratification of RGCs in the IPL at 3 dpf. GFP expressing RGCs in the retina of **A.** 3 dpf WT zebrafish larvae **B.** 3 dpf Tenm4$^{\Delta 10bp}$ mutant larvae **C**. Average fluorescence intensity profiles of dendritic IPL stratification in 3 dpf WT larvae (black; n=5 eyes) and Tenm4$^{\Delta 10bp}$ mutant larvae (gray; n=5 eyes). 0% corresponds to the boundary between GCL and IPL; and 100% corresponds to the boundary between IPL and INL. White arrows indicate laminae in the retina positioned at 55% and 95%. Scale bars set at 10µm.

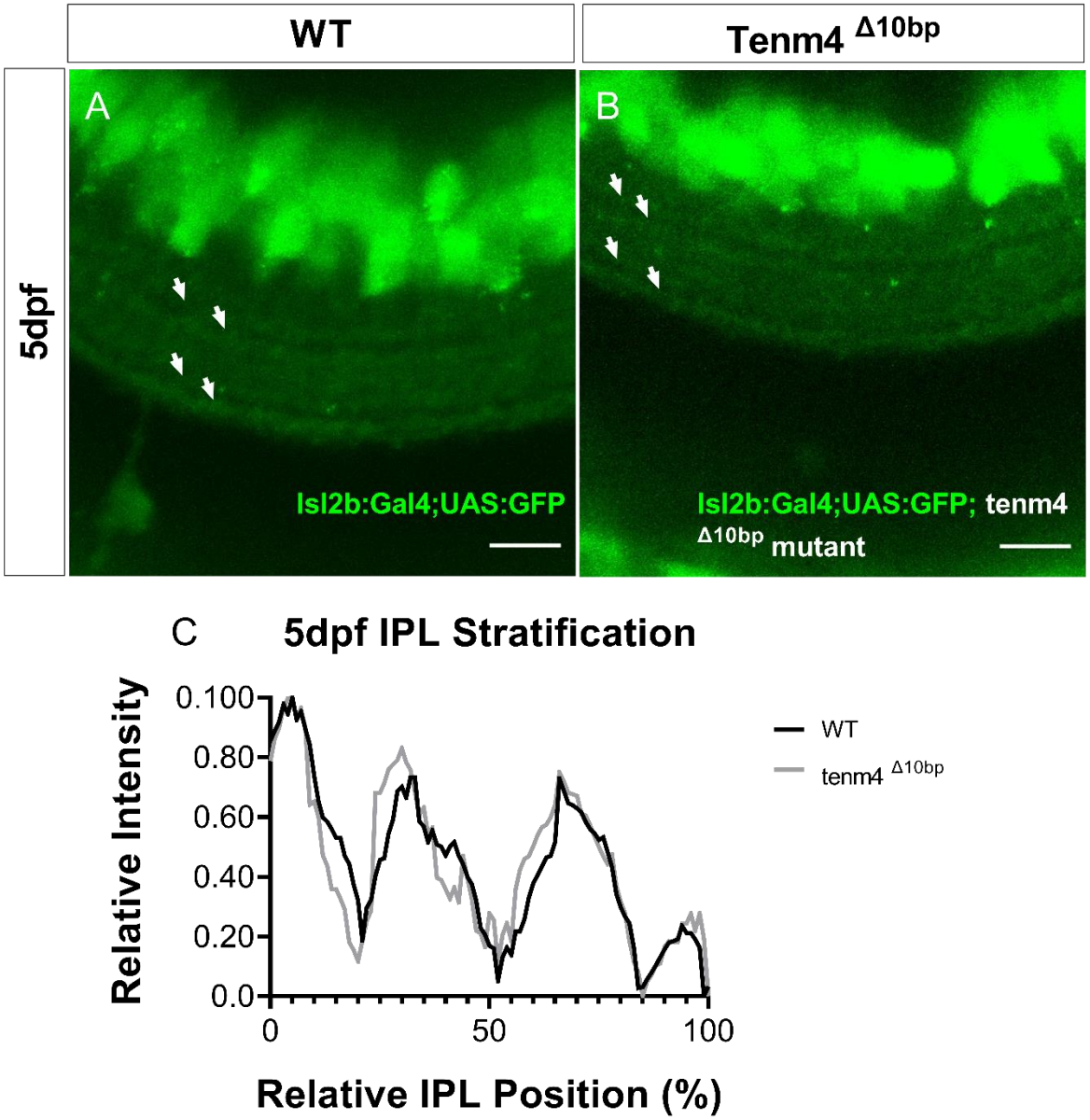

Figure 3.11 Neurite stratification of RGCs in the IPL at 5 dpf. GFP expressing RGCs in the retina of **A.** 5 dpf WT zebrafish larvae **B.** 5 dpf Tenm4$^{\Delta 10bp}$ mutant larvae **C.** Average fluorescence intensity profiles of dendritic IPL stratification in 5 dpf WT larvae (black; n=5 eyes) and Tenm4$^{\Delta 10bp}$ mutant larvae (gray; n=5 eyes). 0% corresponds to the boundary between GCL and IPL; and 100% corresponds to the boundary between IPL and INL. White arrows indicate laminae in the retina positioned at 5%, 33%. 66% and 95%. Scale bars set at 10μm.

Overall, this data suggests that loss of Tenm4 does not cause major structural irregularities in the IPL stratification of RGC dendrites and therefore does not seem to have a key instructive role in functional wiring in the IPL. In addition, because the

results showed no significant differences at both stages, we can most likely eliminate the possibility that an alteration in the stratification is the cause of the altered functional responses in mutant fish. However, minor defects in a small subset of RGCs and/or ACs is still a possibility that needs to be assessed. How these defects could be addressed is further discussed in the next section of this chapter, section **3.6.**

3.6 Conclusions and Discussion

Throughout this chapter, by comparing WT larvae to tenm4$^{\Delta 10bp}$ mutant larvae, we have characterised three aspects of the developing larval retina; quantification of cells undergoing (1) mitosis and (2) apoptosis as well as the (3) stratification of RGC dendrites within the IPL. With this characterisation we begin to take the first steps in understanding the role that Tenm4 plays in circuit assembly. Here, we have described that although Tenm4 does not seem to be a key player of mitosis in the developing retina, the loss of it leads to changes in the number of cells undergoing apoptosis at 4 dpf – with an increase of apoptotic cells in both the ACL and the GCL. We also describe through *in vivo* confocal imaging, that Tenm4 does not seem to impair gross synaptic connectivity in the retina as neurite lamination was not majorly altered in tenm4$^{\Delta 10bp}$ mutant fish.

3.6.1 Teneurins Play a Part in Cell Number Balance

Through the loss-of-function experiments performed throughout this chapter, we have identified that Tenm4 is required for what seems to be the correct balance of RGC and AC numbers by regulating apoptosis during a specific time point - 4 dpf. It is important to state that when referring to RGCs and ACs in the retina, we did not use a cell-type specific marker, we inferred the cell type by their anatomical positioning within the retina. Although no significant difference was observed with mitotic cells between 3 dpf and 5 dpf, there was an increase in the number of RGCs and ACs undergoing apoptosis at 4 dpf, with the number of apoptotic ACs almost doubling in tenm4$^{\Delta 10bp}$

mutant larvae. The data acquired in this study is similar to previous work done assessing other CAMs, such as cell adhesion molecule contactin-6 (Cntn6), where upon its deletion a significant decrease in cell survival was detected, both in *in vitro* experiments as well as in *in vivo* ones (Huang et al., 2011; Zuko et al., 2016). It is known that Teneurins are expressed during critical periods of synaptogenesis and apoptosis throughout development, as described in Chapter 1, ISH data shows that at 4 dpf there are high levels of Tenm4 expression in the retina – where RGC and AC are positioned. The high expression of Tenm4 during development and the results acquired through the TUNEL assay experiment, could imply that Tenm4 plays a regulating role in apoptosis during development. In addition, it has recently been discovered that the C-terminal domain of the Teneurin glycoprotein is cytotoxic, (Ferralli, Tucker, & Chiquet-Ehrismann, 2018) which could help explain the results uncovered in this study.

The mechanisms by which Tenm4 contributes to the prevention of cell death during development is still unknown. Previous work (Trubiani, Al Chawaf, Belsham, Barsyte-Lovejoy, & Lovejoy, 2007) has begun to show that an important function of Teneurins is mediated by the TCAP sequence; higher survivability was seen in TCAP-1 treated cells. Other studies (X. Z. Wang et al., 1998) have shown that stress-inducing circumstances such as alkylating agents or UV lights can cause Tenm-4 activation in mice. All these studies suggest that TCAP may enhance survivability. This could therefore explain the higher survivability of retinal cells in the WT larvae that have all four teneurin homologues intact.

While these experiments give us a general idea of what is happening in the developing larval retina, there are many limitations. Addressing these limitations will narrow down the role that *tenm4* plays in development. To being, a simple way to

begin to tackle these limitations would be to repeat these experiments with DAPI staining allowing us to quantify the overall number of cells in the retina, as well as the ones undergoing mitosis and/or apoptosis respectively. More complex experiments with cell-type specific markers to stain for RGCs and/or ACs alongside apoptotic and mitotic markers would give a clearer and stronger idea of the number of specific cells undergoing mitosis and/or apoptosis. It would therefore help give us a more specific understanding of the role that *tenm4* might be playing in the developing larval retina.

3.6.2 Role of Teneurins in Neural Circuit Wiring

The precise mechanisms underlying how retinal circuits are created during development is still greatly unknown. Teneurins have become exciting candidates amongst the variety of CAMs known to control precise lamination patterns and synaptic partner matching of neurites (Antinucci et al., 2013; Krishnaswamy, Yamagata, Duan, Hong, & Sanes, 2015; Masahito Yamagata & Sanes, 2008; Masahito Yamagata et al., 2002). Less than a decade ago, studies in *Drosophila* were the only ones that showed that Teneurins controlled synaptic partner matching in specific populations (W. Hong et al., 2012; Mosca et al., 2012). We have recently learnt that Tenm3 plays a critical role in specifying appropriate synaptic connections and lamination of RGC neurites in the zebrafish retina (Antinucci et al., 2013).

As an initial step to understand the potential roles of *tenm4* in retinal circuit assembly, the expression pattern of *tenm4* in the larval zebrafish visual system was characterised (see Chapter 1.), *tenm4* is highly expressed in pre- and postsynaptic targets in the retina (i.e., RGCs and ACs). The individual roles that Teneurins play

through development is still a fundamental question. Although studies in recent years have begun to narrow down individual functions for the four Teneurin members, many unknowns still remain. Advances have been made, different Teneurins have been found to be expressed in the same cell (Marta Reyes Corral, Hindges Lab, Unpublished), but individually what each Teneurin is contributing to its function and/or development is still being studied. Essentially, all teneurins are expressed in an overlapping manner across interconnected regions of the zebrafish CNS, such as retina and OT. It is known that there is a strong co-expression of tenm3 and tenm4 across many areas, which can imply a possible functional redundancy between the two teneurins – but further investigation is needed (Cheung et al., 2019). With that in mind, the fact that tenm3, which is also expressed in RGCs and ACs, leads to stratification defects, does not automatically mean that this is true for other Teneurins, such as Tenm4, and we can begin to consolidate the idea that although different Teneurins may be expressed in the same cell types, each one seems to have a specific function.

Based on the data presented here, where no stratification defects were found in the Tenm4$^{\Delta 10bp}$ mutant larvae, we can infer that *tenm4* may have alternative functions in zebrafish visual system development. This not only helps narrow down the role that tenm4 has in the developing retina and visual system, but it helps narrow down the roles that other Teneurins have in development. Although we have a general picture of the role of Tenm4 in the assembly of these fine circuits, there are many limitations to this study such as expression of the overall population which limits the capacity to study individual dendrite patterning. Mosaic labelling would allow to study precise stratification in the retina, especially when using other cell-type specific markers that would allow to see its presynaptic counterparts such as ACs and/or BCs.

Although mosaic labelling would allow a clearer picture to be formed about the minor defects in the IPL that might exist, the best way study them would be through individually labelling Tenm4 positive cells. To carry out these experiments, the generation of a Tenm4:Gal4 zebrafish transgenic line would be useful, this could be done through various gene edition techniques such as BAC transgenesis or CRISPR gene editing technology where an insertion of a Gal4 cassette is inserted alongside the Tenm4 protein.

CHAPTER 4.

CORRECT RGC DEVELOPMENT IN THE OPTIC TECTUM REQUIRES TENEURIN-4

4.1 Axon Growth, Guidance, and Arborisation

In vertebrates, growing retinal ganglion cells (RGC) axons make their way from the retina to the optic tectum (OT) – one of the ten retinorecipient targets - where they can begin to develop axonal arbors and establish synaptic connections with their postsynaptic partners, tectal cell (TC) dendrites. Molecular cues are known to guide these retinal axons to the OT. RGCs are thought to project a topographic map of information captured by the retina into the OT (Meyer & Smith, 2006; Niell, Meyer, & Smith, 2004; O'Rourke, Cline, & Fraser, 1994; Ruthazer, Akerman, & Cline, 2003).

Previous work has demonstrated that, in zebrafish, growing axons reach the OT at 2 dpf and by 3 dpf visually evoked responses can be elicited from them in the OT. Synaptic activity (Debski & Cline, 2002; O'Rourke et al., 1994), extracellular guidance cues (Debski & Cline, 2002; Hindges, McLaughlin, Genoud, Henkemeyer, & O'Leary, 2002), and inter- and intracellular signalling (A. Hall & Lalli, 2010; D. H. Hall & Treinin, 2011), are just some of the necessary factors to correctly shape axon growth and guidance as well as arbor development in vertebrates. Axonal morphology is known to have an influence in the way that information gets processed at the presynaptic sites (Debanne, 2004). This morphology is known to be highly variable from a single T-shaped branch point – in granule cells, to a complex arborisation

containing up to 275 branch(Cheung et al., 2019) points – in thalamocortical axons of the cat visual cortex (Antonini & Stryker, 1998; Debanne, 2004). Another important morphological aspect to take into consideration is the presence of synapses which are distributed along the axonal arbor (Debanne, 2004). Morphological irregularities can thus lead to functional irregularities – axons with extensive arborisations and terminal varicosities reduce the conduction velocity of their action potentials (Manor, Gonczarowski, & Segev, 1991). It is important to note that Teneurins are known to regulate fine neural wiring processes such as neurite outgrowth. The intracellular domain (ICD) of Teneurins has been shown to interact with cytoskeletal proteins such as CAP/ponsin, which itself binds to different factors which regulate the actin cytoskeleton (Nunes et al., 2005; Ribon, Herrera, Kay, & Saltiel, 1998; Scaife & Langdon, 2000). The ICD of Teneurins is also anchored to the actomyosin cytoskeleton – necessary for cell-cell adhesion, hence altering the cytoskeleton (Beckmann et al., 2013). Axonal branching is a highly dynamic process which results from the formation and elimination of nascent branches. In retinotectal projections, the retinotopic map is improved and maintained by this dynamic rearrangement of branches (McLaughlin & O'Leary, 2005; Ruthazer & Cline, 2004). RGCs in mice, for example, initially overshoot their targets and the correct elaboration of the axonal arbors is only possible through interstitial branching (Debski & Cline, 2002; Hindges et al., 2002). In fish, the retinal topography is preserved by the constant shifting of RGC axons within the OT. Furthermore, only a small fraction of initial branches is maintained throughout development, which allow for the elaboration of a mature arbor. The selective stabilisation of these branches is influenced by Hebbian mechanisms involving retrograde signalling downstream of activation of postsynaptic tectal cells (H.

T. Cline & Constantine-Paton, 1989; Hua, Li-Jian, & Ya, 2005; Ruthazer et al., 2003; Schmidt, Buzzard, Borress, & Dhillon, 2000; Schmidt & Buzzard, 1993).

The synaptotropic hypothesis, proposed over two decades ago, states that inputs from a presynaptic cell to a postsynaptic cell (synapse formation) directs the formation of axonal and dendritic arbors (H. Cline & Haas, 2008; Vaughn & Sims, 1978; Vaughn, 1989); this was later demonstrated *in vivo* (Meyer & Smith, 2006; Niell et al., 2004; Niell & Smith, 2005). RGC axons expressing a fluorescent synaptic marker were imaged *in vivo* as they arborised in the zebrafish OT. Arbor growth and synaptogenesis processes were found to be dynamic – growing branches and nascent synapses were seen to form and dissolve simultaneously (Meyer & Smith, 2006). Similarly, *in vivo* imaging on growing dendritic arbors in the zebrafish OT to visualise synapse formation. Again, synapses were found to selectively stabilise filopodia, which eventually form branches from which further growth can occur (Niell & Smith, 2005). Synaptogenesis seems to selectively stabilise branches in dendrites and axons, as well as promote branch formation solely in axons (Alsina, Vu, & Cohen-Cory, 2001; Javaherian & Cline, 2005; Meyer & Smith, 2006).

Synaptophysin (Syp) is a synaptic vesicle protein involved in exo- and endocytosis (Valtorta, Pennuto, Bonanomi, & Benfenati, 2004) that is expressed in the developing nervous system - it is the most important element of presynaptic vesicles (Meyer & Smith, 2006). Fused to GFP, Syp has been used as a marker to study synapse distribution (Meyer & Smith, 2006; Nakata et al., 1998; Valtorta et al., 2004). Cytosolic red fluorescent protein Ds-RedExpress (DsR) is a soluble space-filling marker (Valtorta et al., 2004) that when expressed with Syp:GFP can be used to simultaneously analyse Syp distribution as well as the arbors of the cell (Meyer & Smith, 2006).

The initial phenotype observed in the tenm4$^{\Delta 10bp}$ mutant larvae (see Chapter 1.), where a higher number of visually evoked responses were seen, could be explained by aberrant synapse formation in the OT. To address this directly, we performed *in vivo* imaging of RGC axons and synapses in live zebrafish.

4.2 Loss of Teneurin-4 Alters RGC Branch Morphology in Axons

To analyse the morphology of RGCs at the single-cell level, they were mosaically labelled by co-injections of Ath5:Gal4 - RGC specific promoter, and Syp:GFP-DsR constructs into one-cell stage embryos. This was followed by *in vivo* confocal microscopy at 4 dpf (see Chapter 2. Material and Methods). Using this strategy, we were able to characterise the different axonal morphologies seen in the tenm4$^{\Delta 10bp}$ mutant larvae. As an attempt to understand the initial phenotype seen, where the tenm4$^{\Delta 10bp}$ mutant larvae had more visually evoked responses, we compared the results obtained in the mutant to WT larvae. This also helped shed light on the role that *tenm-4* has in development – specifically in the vertebrate visual system.

As a first step we studied the overall structure of the RGC axonal branching in the WT larvae with specific focus on two key elements – number of branches **(Figure 4.1 A,D)** and the length of those branches **(Figure 4.3 A,D)**. This was followed by an assessment of the tenm4$^{\Delta 10bp}$ mutant larvae RGC axonal branches **(Figure 4.1 B,E; Figure 4.3 B,E)**. Leading to the final step which was the comparison of the two genotypes as a step to get an overview of possible changes that could be happening within our two genotypes (WT, n= 32; tenm4$^{\Delta 10bp}$ mutant, n = 38). During imaging, the complete length of the RGC axon was not visible, for this reason measurements began at the first branching point (**Figure 4.2;** see Chapter 2. Material and Methods).

Our focus initially was placed in analysing the number of branches per RGC in each genotype. On average, 15.63 ± 1.106 branches were present in the WT RGCs, showing a broad and even axonal branching pattern **(Figure 4.1 A)**. On the other hand, on average there were 17.42 ± 0.9205 branches in the tenm4$^{\Delta 10bp}$ mutant RGCs, with

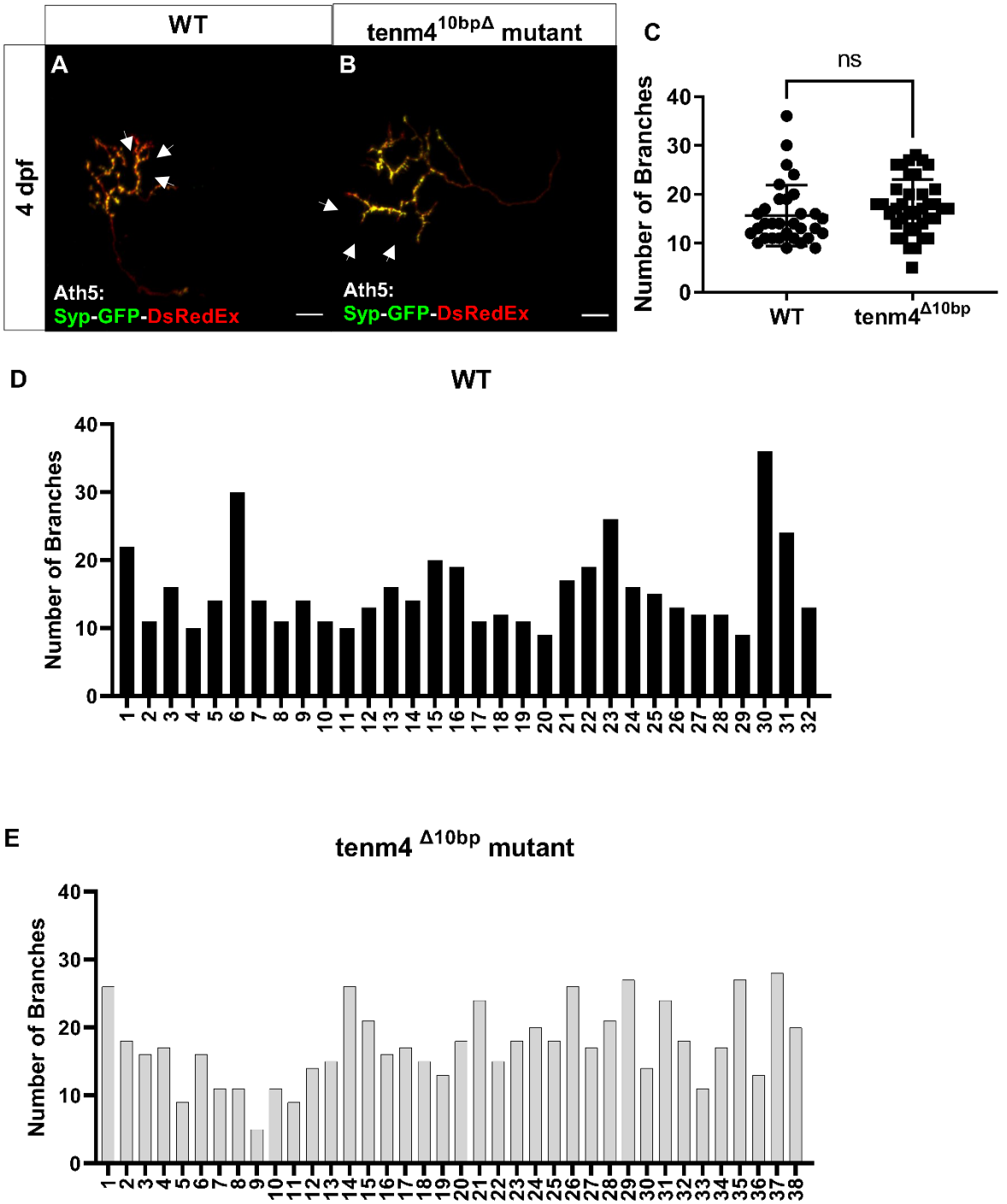

Figure 4.1 RGC branch number. Comparison of number of branches in **A.** 4 dpf WT and **B. 4dpf** tenm4 $^{\Delta 10bp}$ mutant, **C.** No significant difference was observed between the two genotypes (WT - 15.63±1.106, n=32; tenm4 $^{\Delta 10bp}$ mutant - 17.42±0.9205, n=38; p<0.2124, ns). **D.** Individual branch number of WT RGCs. Minimum number of branches 9; maximum number of branches 36.00. **E.** Individual branch number of t4 10bpΔ mutant. Minimum number of branches 5; maximum number of branches 28. White arrows pointing to examples of short branches considered in the quantification. Scale bars set at 10µm. Statistical analysis: t-test

a more disorganised axonal branching pattern **(Figure 4.3 B)**. As seen in **Figure 4.1 C**, when comparing the number of branches, there was no significant difference found between the WT larvae and the tenm4$^{\Delta 10bp}$ mutant larvae, with both genotypes having similar branch numbers in their axonal arborisations. Although no differences were seen, when looking at the graphs, there seems to be a wider range in the number of branches within WT RGCs, whereas the tenm4$^{\Delta 10bp}$ mutant RGCs seem to be more concentrated having more similar number of branches amongst all the RGCs imaged. For precise information regarding image acquisition, image analysis please see **Chapter 2.**

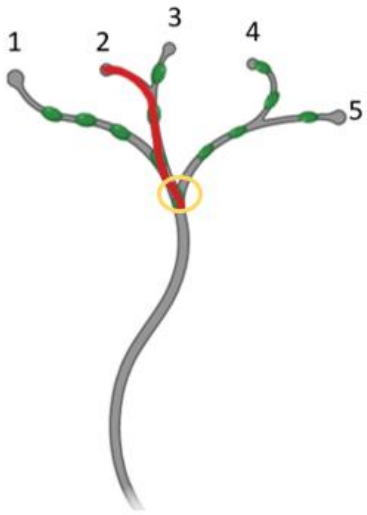

Figure 4.2 Branch length measurements. "Filament object" function used for branch measurements outlined in red. Yellow circle is marking the branching point where measurements began.

Moving forward we wanted to find out if there was a possibility that there was a difference in the length of these branches even though there was no significant difference in the number of branches per RGC. As previously mentioned, the total branch length was measured from the first branching point in the crossing axon (**Figure 4.2;** see Chapter 2. Material and Methods for specifics). WT RGCs had an average total length of 290.0 µm ± (WT, n= 32; **(Figure 4.3 A,D)** whereas tenm4$^{\Delta 10bp}$ mutant RGCs had an average total length of 253.4± 13.28 µm (tenm4$^{\Delta 10bp}$ mutant, n = 38; **Figure 4.3 B,E)**. When comparing the

two genotypes, we found not only that there was a significant difference in the total length of the branching **(Figure 4.3 C)**, but that the tenm4$^{\Delta 10bp}$ mutant seemed to be divided into two different sub-groups. The first one, having branch lengths within the range of WT RGCs (labelled in grey); and the second, displaying shorter branch lengths (labelled in red; **Figure 4.3 E**).

All this data put together, helps deepen our understanding of tenm-4's role in the development of axonal branching. Although no differences were seen in the number of branches, the difference seen in the branch lengths leads us to believe that it could be playing a role in axon growth.

4.3 Complexity of RGC Axonal Arborisations Modified in Teneurin-4 Knock-Out

Diving deeper into our attempt to understand the morphological differences, we looked at the complexity of arborisations of these RGCs in the OT. This was accomplished through Sholl analysis. Sholl analysis is a method used to quantitatively compare the morphological characteristics of imaged neurons. It was initially used to describe morphological differences between the dendritic arborisation of neurons in the visual and motor cortices of cats (Sholl, 1953), but since then has evolved and is most used to look at complexity of dendritic arborisations, as well as dendritic length and diameter. In brief, it counts the number of dendritic intersections that happen at specific distance from the cell body in concentric circles (we adjusted this analysis for the analysis of axonal arborisations - for specific information about this type of analysis, as well as the statistical analysis involved, please see Chapter 2).

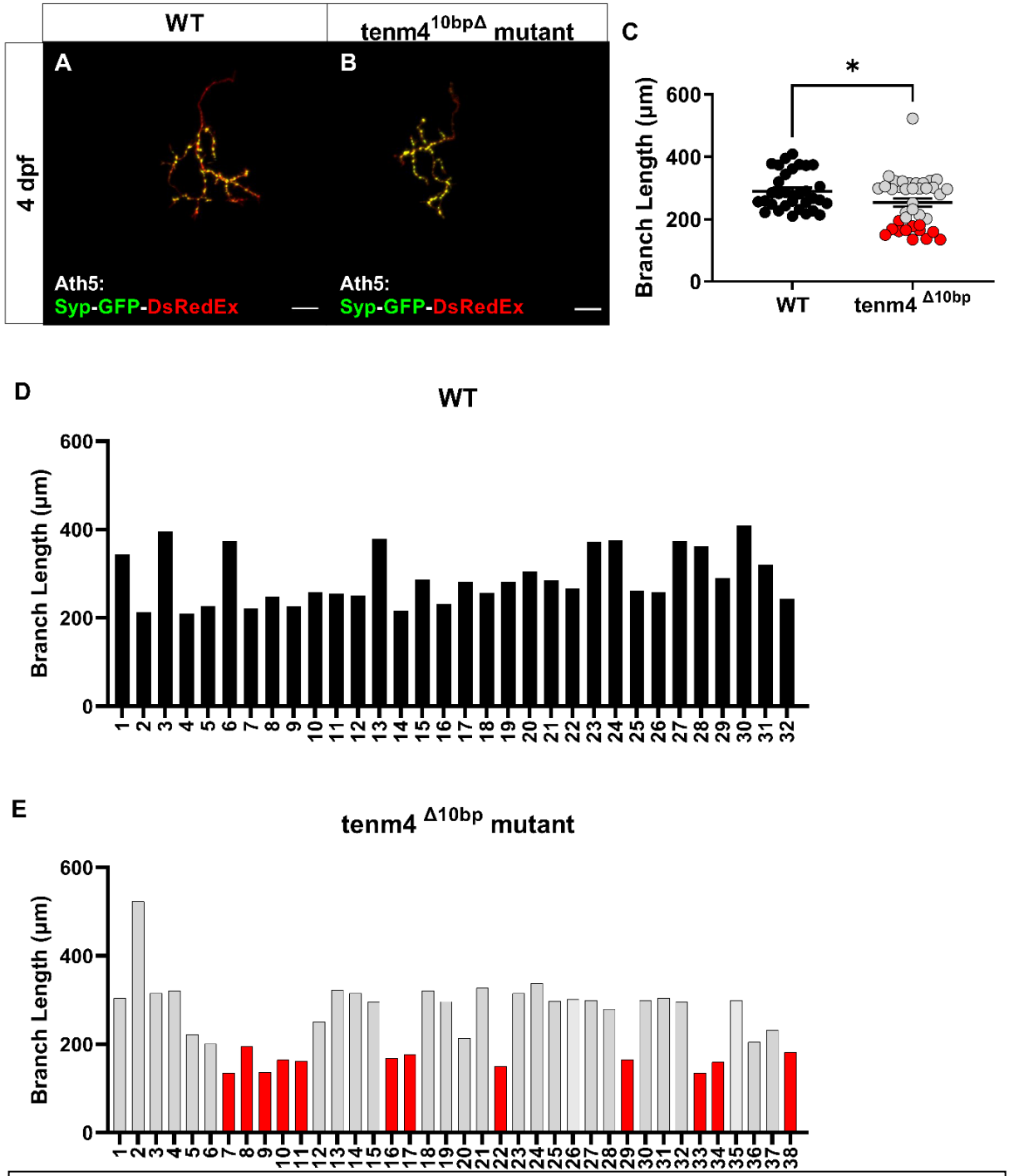

Figure 4.3 RGC branch lengths. Comparison of branch lengths in **A.** 4 dpf WT and **B.** 4 dpf tenm4$^{\Delta 10bp}$ mutant, **C.** A significant difference was observed between the two genotypes (WT - 290±10.80, n=32; tenm4$^{\Delta 10bp}$ mutant - 253.4±13.28, n=38; p<0.0406*). Red dots represent branch lengths which are shorter than WT branch lengths. **D.** Individual branch length of WT RGCs. **E.** Individual branch length of tenm4$^{\Delta 10bp}$ mutant. Red bars indicate the same cells as indicated with dots in **C.** White arrows pointing at the first branch point where measurement began. Scale bars set at 10µm. Statistical analysis: t-test

Based on our analysis, we know that tenm4$^{\Delta 10bp}$ mutant RGCs have the same number of branches as WT RGCs but that they are shorter in their overall length, so we hypothesised that the complexity of these arborisations would also vary between our two genotypes. When evaluating this complexity of axonal arborisations between our WT RGCs (WT, n=32; **Figure 4.4 A)** and tenm4$^{\Delta 10bp}$ mutant RGCs (tenm4$^{\Delta 10bp}$ mutant, n = 38; **Figure 4.4 B)**, a significant difference was found between the two genotypes. WT RGC axonal arbors have a higher complexity - towards the middle of the cell (sholl radius 20 µm. and 25 µm.), than those of the tenm4$^{\Delta 10bp}$ mutant RGCs (WT (20) - 5±0.5688, n=32; tenm4$^{\Delta 10bp}$ mutant (20) – 3.26±0.5646, n=38); (WT (25) – 4.412±0.6006, n=32; tenm4$^{\Delta 10bp}$ mutant (25) – 2.20±0.4899) **(Figure 4.4 C)**.

Taking into consideration all the information we have gathered on the branching of WT and tenm4$^{\Delta 10bp}$ mutant RGCs, the results presented here shorten the gap of understanding tenm-4 and its role in axonal morphogenesis. Although we found no evidence of a change in the number of branches, the decreased length, which in turn leads to less complex arborisations, strengthens the idea that there is a direct link between tenm-4, axon growth and overall axonal morphogenesis.

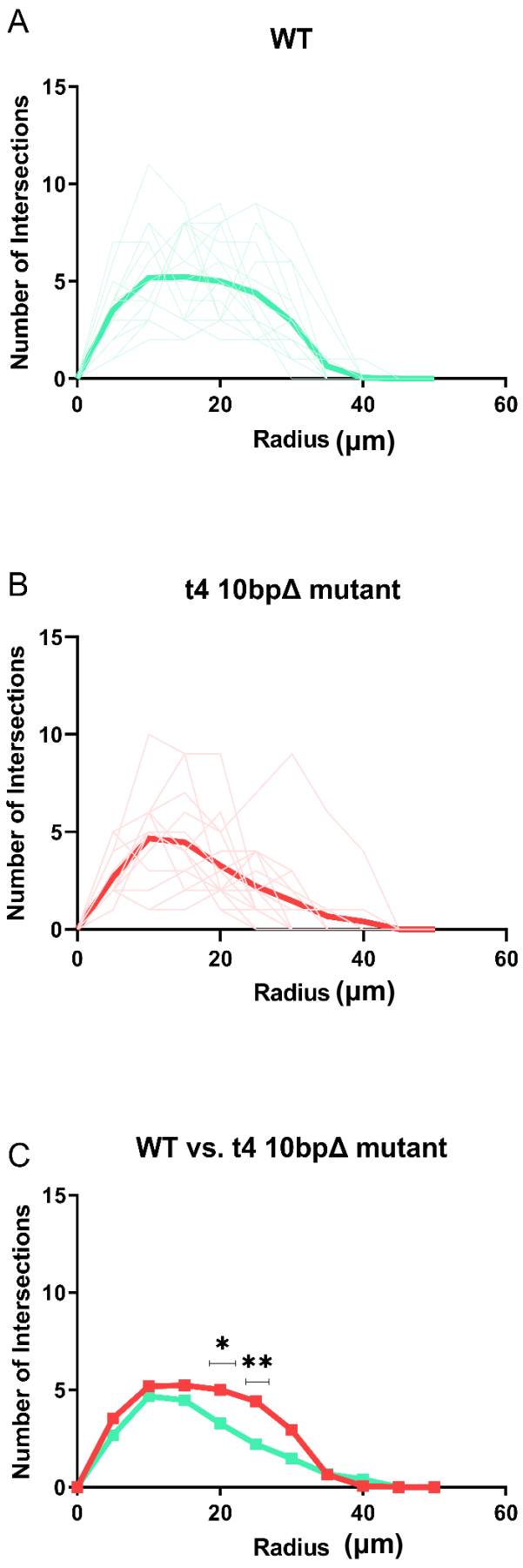

Figure 4.4 Complexity of RGC axonal arborisations. Sholl analysis of **A.** 4 dpf WT RGCs showed that they were more complex at 20 µm and 25 µm than **B.** 4 dpf tenm4$^{\Delta 10bp}$ mutant **C.** Comparison between WT and tenm4$^{\Delta 10bp}$ mutant axonal arborisations (WT - 5±0.5688, n=32; tenm4$^{\Delta 10bp}$ mutant – 3.26±0.5646, n=38; p<0.0395*); (WT – 4.412±0.6006, n=32; tenm4$^{\Delta 10bp}$ mutant – 2.20±0.4899, n=38; p<0.0.0087*). Statistical analysis: t-test

4.4 RGC Synaptic Markers Decrease Upon Teneurin-4 Deletion

Understanding synaptic organisation is an essential step to understanding how sensory information is received and processed so it can be sent to the brain. Prior work identified that the *Drosophila* teneurin homologues, ten-m and ten-a, are important regulators of synaptic partner matching, synapse number, and synaptic organisation (W. Hong et al., 2012; Mosca et al., 2012). Previous studies also described a close relationship between synaptogenesis and axon arbor growth (Meyer & Smith, 2006). Taking this information into consideration and including the data already obtained from this study, we wondered if the difference observed in the axonal branch lengths and arborisations amongst WT and tenm4$^{\Delta 10bp}$ mutant RGCs could be related to the number of synapses upon them. To begin to investigate this, we quantified the number of puncta[10] in single cells by using co-injections of Ath5:Gal4 and Syp:GFP-DsR constructs. A change in the number of puncta could also help understand our initial phenotype of an increased number of visually responsive voxels upon visual stimulation in the tenm4$^{\Delta 10bp}$ mutant (see Chapter 1. Introduction).

Quantification of Syp-GFP-positive puncta was done through the “Spots Object” function in IMARIS 8.0 (Bitplane). For specifics regarding image acquisition, image analysis and statistical test, please see **Chapter 2.**. WT RGCs **(Figure 4.5 A)** contained on average 57.53 ± 2.585 puncta per cell, whilst the tenm4$^{\Delta 10bp}$ mutant RGCs **(Figure 4.5 B)** 42.63 ± 2.457 puncta per cell. A significant difference was

[10] Throughout this chapter the word **puncta** will be used instead of synapse as up to this point, we do not know if they are active synapses or just accumulation of the fluorescently labelled presynaptic protein synaptophysin.

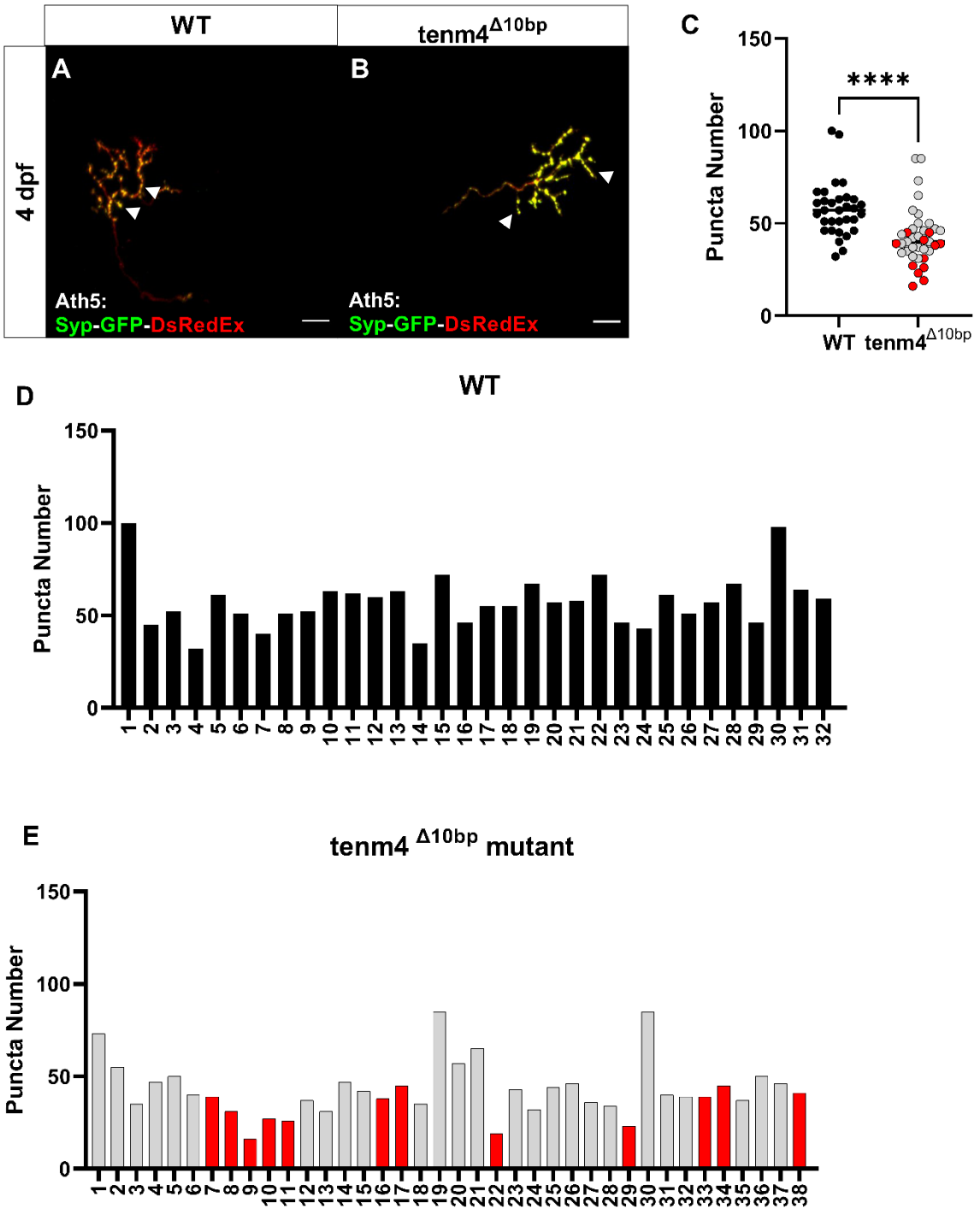

Figure 4.5 RGC puncta number A. 4 dpf WT RGC. **B** 4 dpf tenm4$^{\Delta 10bp}$ mutant RGC. **C.** WT RGCs have a significantly larger number of puncta per RGCs than tenm4$^{\Delta 10bp}$ mutant RGCs (WT - 57.53±2.58, n=32; tenm4$^{\Delta 10bp}$ mutant - 42.63±2.457, n=38; p<0.001****). Red dots represent same RGCs that presented shorter branch lengths in Figure 4.2. **D.** Individual puncta number of WT RGCs. **E.** Individual puncta number of tenm4$^{\Delta 10bp}$ mutant RGCs. Red bars indicate the same cells as indicated with dots in **C.** White arrows pointing at two different puncta that are separated by a very small distance. Scale bars set at 10µm. Statistical test: t-

observed when comparing the data obtained from the two genotypes, with tenm4$^{\Delta 10bp}$ mutant larvae having a significant lower number of puncta per cell than the WT **(Figure 4.5 C)**.

Previous work has demonstrated that new axon branches arise preferentially from synaptic sites (Alsina et al., 2001; Javaherian & Cline, 2005) and that a developmental regulation of axonal filopodia motility by individual synaptic activity exists, proving that most axonal growth occurs from branch tips where nascent synapses on a growing arbor are located (Meyer & Smith, 2006; Tashiro & Yuste, 2003). The reduced branch lengths seen in the tenm4$^{\Delta 10bp}$ mutant, could be caused by the decreased number of puncta being formed. Combining this knowledge with the data obtained so far, helps explain why although branch numbers are the same, puncta number and branch length are decreased in the tenm4$^{\Delta 10bp}$ mutant.

4.5 Teneurin-4 Knock-Out Leads to Enlarged Puncta in a Subset of RGCs

Synapses are specialised cell-cell connections permitting the transfer of chemical or electrical signals between neurons. CAMs function as upstream signals to allow the first cell-cell contact. Because of this, during the past years, CAMs have become a topic of interest in synaptogenesis research. Studies have shown that these molecules are involved in more than just initial contact formation (Washbourne et al., 2004), including triggering synapse formation (Biederer et al., 2002), specific target recognition (Masahito Yamagata et al., 2002) and regulation of synaptic size (Scheiffele, 2003). Our results thus far have shown that WT larvae and tenm4$^{\Delta 10bp}$ mutant larvae have significant differences in aspects such as branch length and

number of puncta per cell, so naturally we wondered whether there was a difference in the size of these puncta between the different genotypes. We focused on two specific aspects regarding puncta size: first, the length – from point “a” to point “b” on an axonal branch; and second, the volume it occupies within this axonal branch (**Figure 4.6;** see Chapter 2. Material and Methods).

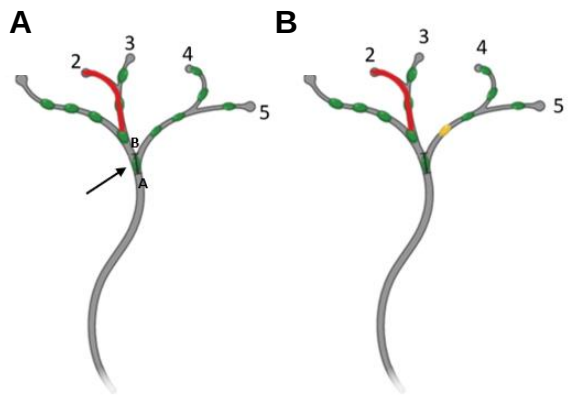

Figure 4.6 Branch puncta measurements. A. “Filament object” function used for puncta length marked by black arrow. **B.** “Surface object” function used for puncta volume measurements represented by yellow dot.

Individual puncta length measurements were taken from 70 different RGCs (WT, n=32; tenm4$^{\Delta 10bp}$ mutant, n=38). All puncta within WT RGCs had a length of no more than 5 µm, with the largest WT puncta reaching 4.95 µm **(Figure 4.7 A,D)**, on average each punctum was 1.500 µm ± 0.04364 long. When analysing tenm4$^{\Delta 10bp}$ mutant puncta **(Figure 4.7 B,E)**, we found that some RGCs exhibited larger puncta, with the largest puncta reaching 11.78 µm, on average each punctum was 1.678 µm ± 0.05625 long. Once again, we not only found a significant difference between the average length amongst the two genotypes - with individual puncta length increased in tenm4$^{\Delta 10bp}$ mutant puncta, but we found a sub-division within our tenm4$^{\Delta 10bp}$ mutant group. Consistent with branch length data **(Figure 4.3)**, there are two sub-groups of puncta length **(Figure 4.7 B,C,E)**, one of them reaching similar puncta length to the WT puncta (labelled in grey), and the other having significantly increased size in puncta length (labelled in red).

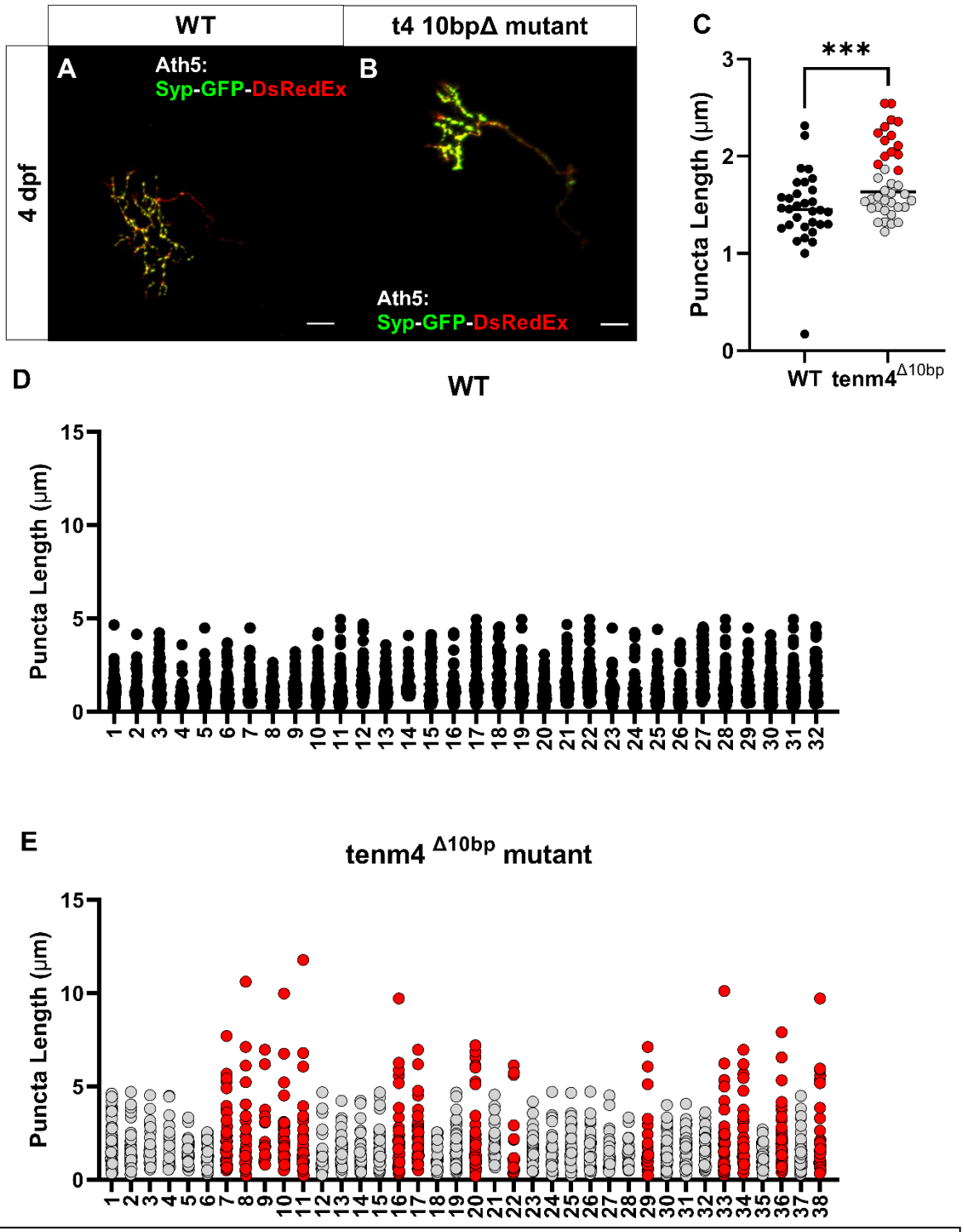

Figure 4.7 RGC puncta length. A. 4 dpf WT RGC. **B.** 4 dpf tenm4$^{\Delta 10bp}$ mutant RGC. **C.** WT RGCs have a significantly smaller length in their puncta than the tenm4$^{\Delta 10bp}$ mutant RGCs (WT - 1.456±0.066, n=32; tenm4$^{\Delta 10bp}$ mutant - 1.766±0.060, n=38; p<0.0010***). Red dots represent same RGCs that presented shorter branch lengths in Figure 4.3. **D.** Individual puncta lengths of WT RGCs. **E.** Individual puncta lengths of tenm4$^{\Delta 10bp}$ mutant RGCs. Red bars indicate the same cells as indicated with dots in **C.** For puncta length measurements please refer to Figure **4.6.** Scale bars set at 10µm. Statistical analysis: t-test

We then moved on to analyse the volume that these individual puncta take in the axonal branch. For volume measurements, the “surfaces object” function was used in IMARIS 8.0 (Bitplane) software. A 3D surface was created over every punctum and the volume data was extracted for statistical analysis. For precise details about image acquisition, image analysis and statistical analysis, please refer to **Chapter 2.** The average WT puncta volume was 1.539 μm^3 ± 0.1821 **(Figure 4.8 A,D)** while the tenm4$^{\Delta 10bp}$ mutant puncta volume reached 2.971 μm^3 ± 0.3488 **(Figure 4.8 A,E)** once again showing a significant difference between the two genotypes **(Figure 4.8 C)**. As described above, we were able to find two very distinct sub-groups within our tenm4$^{\Delta 10bp}$ mutant groups **(Figure 4.8 E)**, with approximately half of RGCs having similar volumetric measurements as the WT RGCs puncta (labelled in grey), but the other sub-group presenting puncta with much larger volumes (labelled in red).

These results once again strengthen the idea that *tenm-4* plays an essential role in a subset of developing RGCs with specific focus on synaptogenesis and/or synaptic organisation within vertebrate visual system assembly. Our results thus far show that by eliminating *tenm-4*, a subset of RGCs do not undergo normal development. This subset of RGCs present shorter branches and less complex arborisation patterns, a smaller number of puncta within these branches as well as the puncta being larger in both size and volume. A summary and comparison of the findings can be seen in **Figure 4.9.**

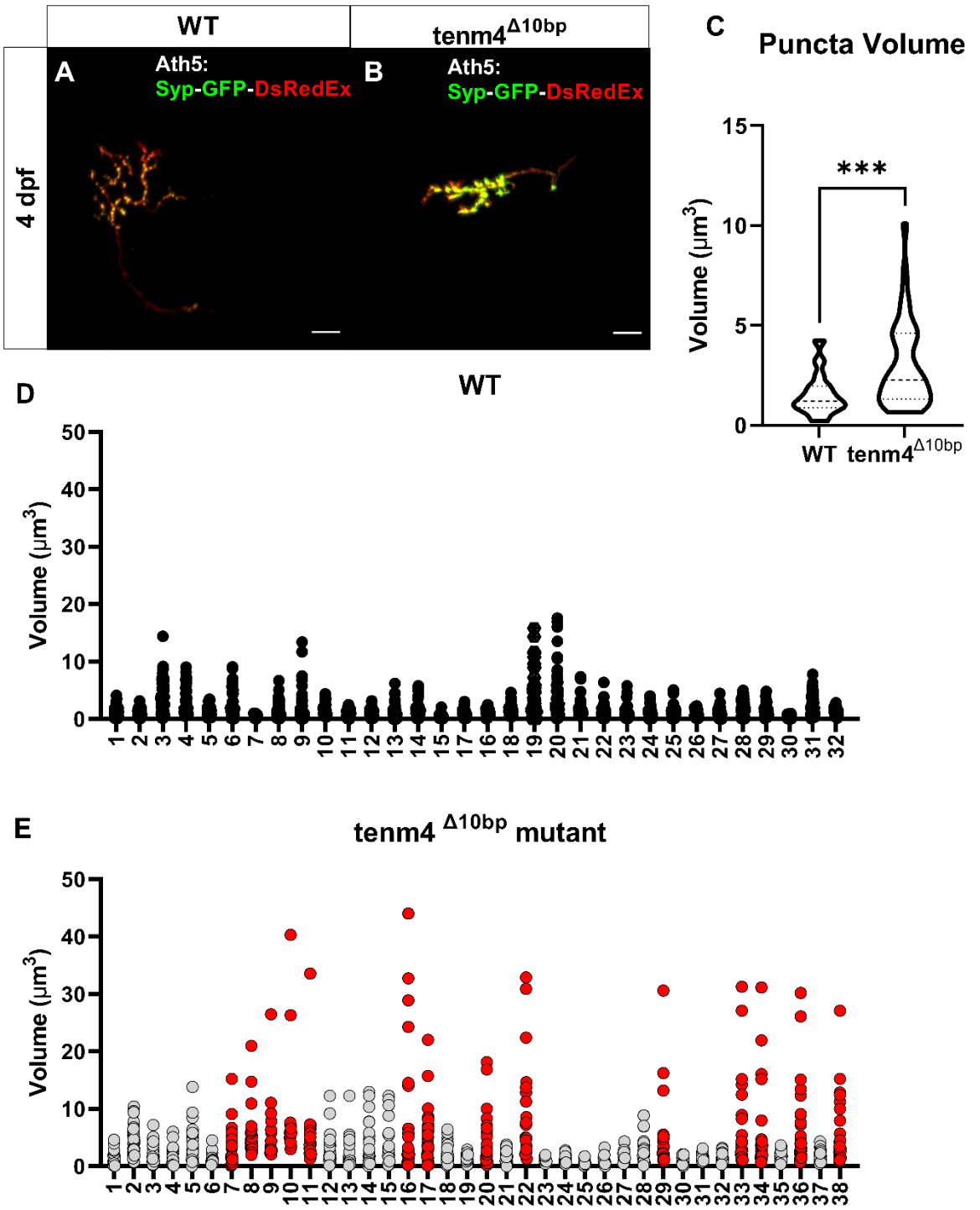

Figure 4.8 RGC puncta volume. A. 4 dpf WT RGC. **B.** 4 dpf tenm4$^{\Delta 10bp}$ mutant RGC. **C.** WT RGCs have a significantly smaller volume in their puncta than the tenm4$^{\Delta 10bp}$ mutant RGCs (WT - 1.539±0.1821, n=32; tenm4$^{\Delta 10bp}$ mutant - 2.971±0.3488, n=38; p<0.0009***). Red dots represent same RGCs that presented shorter branch lengths in Figure 4.3. **D.** Individual puncta volume of WT RGCs. **E.** Individual puncta volume of tenm4$^{\Delta 10bp}$ mutant RGCs. Red bars indicate the same cells as indicated with dots in **C.** For puncta volume measurements please refer to Figure **4.6.** Scale bars set at 10µm. Statistical analysis: t-test

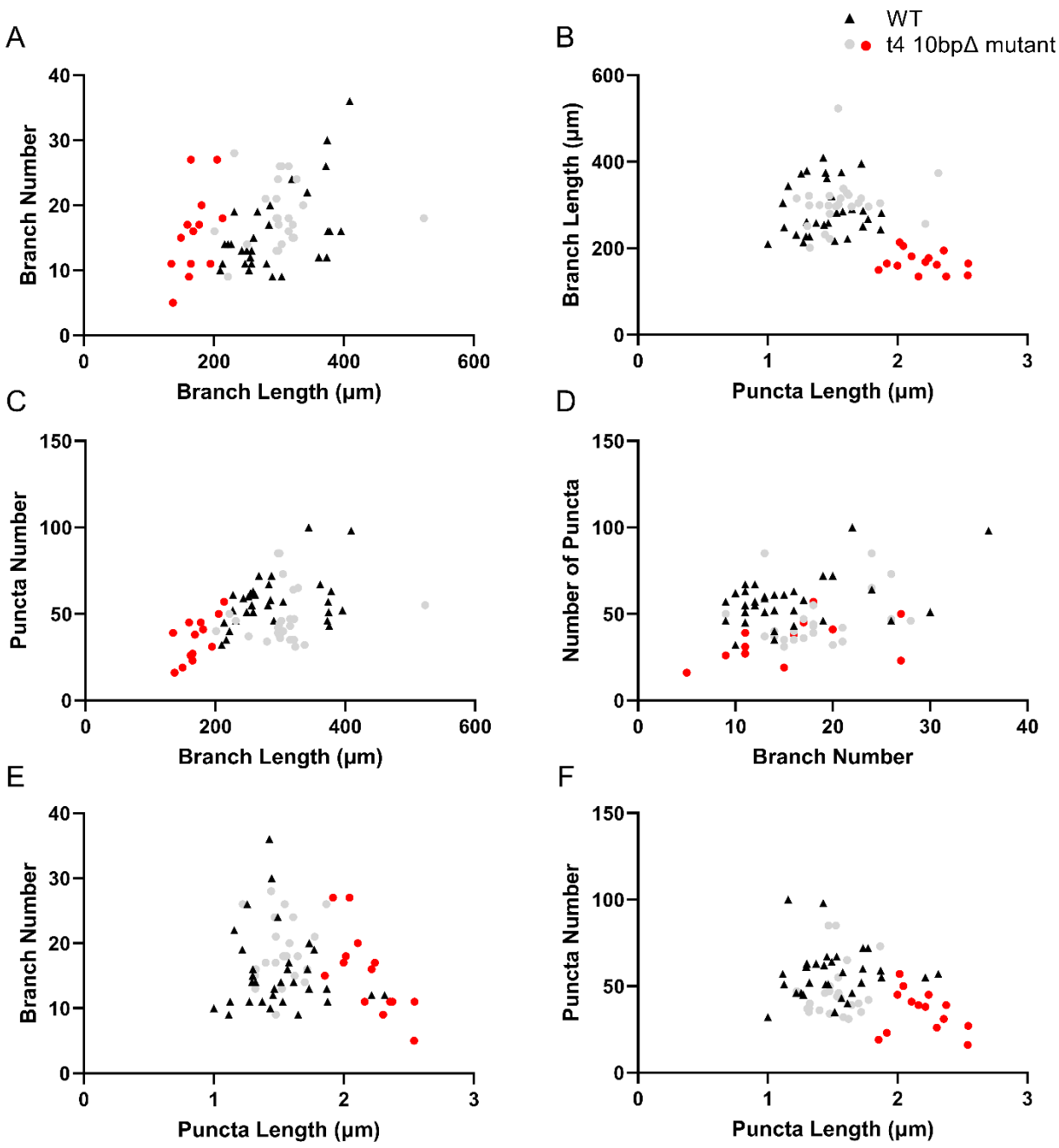

Figure 4.9 Comparisons between measured parameters. A. When comparing branch number against branch length a clear sub-group is seen within the tenm4$^{\Delta 10bp}$ mutant genotype showing shorter branch lengths. **B.** Branch length compared against puncta length, a clear group within the tenm4$^{\Delta 10bp}$ mutant is seen showing shorter branch lengths but larger puncta lengths. **C.** A sub-group within the tenm4$^{\Delta 10bp}$ mutant can be seen when comparing the number of puncta against the branch length, with them having shorter branch lengths and a smaller puncta number. **D.** No clear sub-groups could be distinguished when comparing number of puncta vs branch number. **E.** Clear sub-group of tenm4$^{\Delta 10bp}$ mutant can be seen having larger puncta lengths than the WT RGCs. **F.** Puncta number compared to puncta length showing a distinguished sub-group within the tenm4$^{\Delta 10bp}$ mutant RGCs having a smaller puncta number, but larger puncta lengths.

4.6 Teneurin-4 is Needed for Correct RGC Development

Lastly, we were interested in looking at RGCs as they developed to try and pinpoint the developmental stage at which the phenotypes described above begin to appear. As mentioned in the introduction, the first RGC axons reach the OT at 2 dpf, where they begin to develop and elaborate axonal arbors as they create synaptic connections with their postsynaptic partners - the TCs. Previous hippocampal slice studies have demonstrated that the motility of these developing axonal arbors has a direct correlation with free extracellular space that exists around them (Tashiro & Yuste, 2003). Within the OT, as well as in other areas of the developing embryo, the extracellular space decreases over time because of the developing axonal and dendritic branches, therefore slowing branch motility down as time goes on and branch maturity is reached. Taking all of this into consideration, we chose our first developmental imaging time point at 2.5 dpf - to make sure that RGC axons had already reached the OT - and continued until 5 dpf. For specifics of how imaging , image analysis and statistical test were carried out, please see **Chapter 2.**

For this, we took the same approach as the previous analysis. As a first step we looked at the number of branches per cell at each developmental time point. At 2.5 dpf we found a significant difference between WT larvae (WT, n=5; **Figure 4.10 A, I; Figure 4.11 A**) and the tenm4$^{\Delta 10bp}$ mutant (tenm4$^{\Delta 10bp}$ mutant, n=5; **Figure 4.10 E, I; Figure 4.11 A),** with WT larvae having a higher number of branches. The average number of branches seen in WT were 4 ± 0.4472, whereas in the tenm4$^{\Delta 10bp}$ mutant it was 2 ± 0.4472. We then imaged and analysed the same cells again at 3 dpf **(Figure 4.10 B,F,I; Figure 4.11 B)**, at this time point branch numbers had evened out and

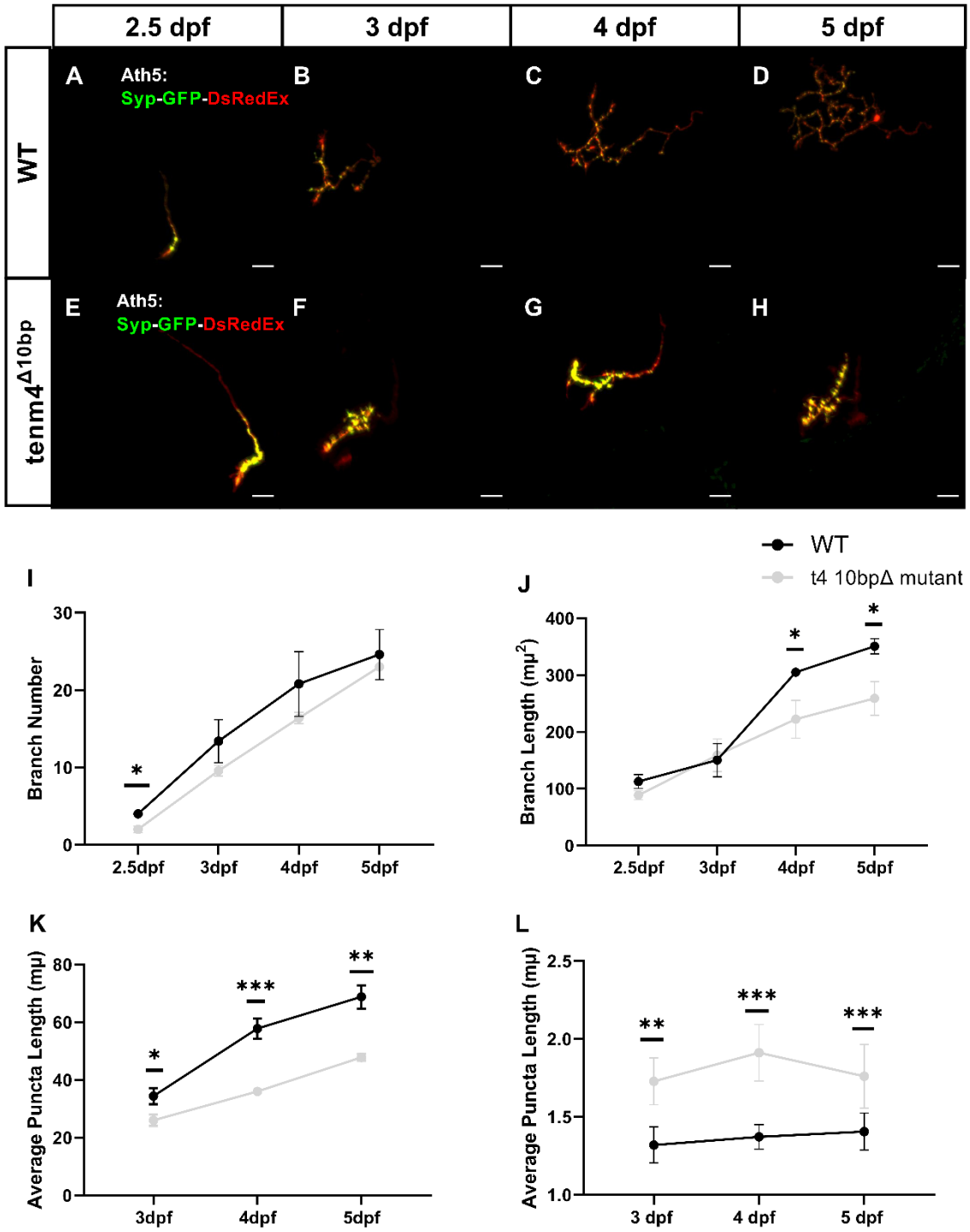

Figure 4.10 RGCs through development. **A.** 2.5 dpf **B.** 3 dpf **C.** 4 dpf **D.** 5 dpf WT RGCs in the OT. **E.** 2.5 dpf **F.** 3 dpf **G**. 4 dpf **H.** 5 dpf tenm4$^{\Delta 10bp}$ mutant RGCs in the OT. **I.** Number of branches per developmental time point, only difference observed at 2.5 dpf. **J.** Branch length per developmental time point significant differences observed at 4 dpf and 5 dpf. **K.** Number of puncta per cell per developmental time point. Significant difference observed at all developmental time points. **L.** Average puncta lengths per developmental time point. Significant difference observed at all developmental time points. Scale bars set at 10μm. Statistical analysis: t-test. For all statistical results please see **Figure 4.11** and **4.12.**

there was no longer a significant difference between the two genotypes (WT average branch number 13.4 ± 2.786 , tenm4$^{\Delta 10bp}$ mutant average branch number 9.60 ± 0.6782). This continued through the rest of our chosen developmental stages with no significant difference observed at 4 dpf (WT average branch number 20.8 ± 4.188, tenm4$^{\Delta 10bp}$ mutant average branch number 16.4 ± 0.7483) **(Figure 4.10 C, G, I; Figure 4.11 C)** and 5 dpf (WT average branch number 24.6 ± 3.250, tenm4$^{\Delta 10bp}$ mutant average branch number 23 ± 1.703) **(Figure 4.10 D, H, I; Figure 4.11 D)**.

We then analysed the length of these branches, from our previous experiment, we know that by 4 dpf **(Figure 4.3 D)** there is already a significant difference that can be seen with WT RGCs having larger branches than tenm4$^{\Delta 10bp}$ mutant RGCs. Our focus was therefore to try and pinpoint the developmental onset of our phenotype. F At 2.5 dpf no significant difference was observed between the two groups **(Figure 4.10 A, E, J; Figure 4.11 A')**. WT larvae at this developmental time point had an average length of 112.8 µm ± 12.36 tenm4$^{\Delta 10bp}$ mutant RGCs had an average branch length of 88.54 µm ± 7.8. At 3 dpf, still no significant difference could be observed between the branch lengths of these two genotypes (WT average branch length 150.4 µm ± 29.29 and tenm4$^{\Delta 10bp}$ mutant average branch lengths being 159 µm ± 28.71; **Figure 4.10 B, F, J; Figure 4.11 B')**. Unsurprisingly, when analysing these cells at 4 dpf, we found that there was a significant difference between the lengths of the branches, with WT **(Figure 4.10 C ,J; Figure 4.11 C')** having larger branch lengths (average of 305.20 µm ± 7.561) than those of the tenm4$^{\Delta 10bp}$ mutant (average of 222.4 µm ± 33.08) **(Figure 4.10 G, J; Figure 4.11 C;)**, in line with our previous data **(Figure 4.3D).** This branching difference continued on until our last developmental time point - at 5 dpf - with WT RGCs having larger branch lengths (average 350.8 µm ± 13.31) than

tenm4$^{\Delta 10bp}$ mutant RGCs (average 259.1 µm ± 29.68) throughout **(Figure 4.10 D, H, J; Figure 4.11 D')**.

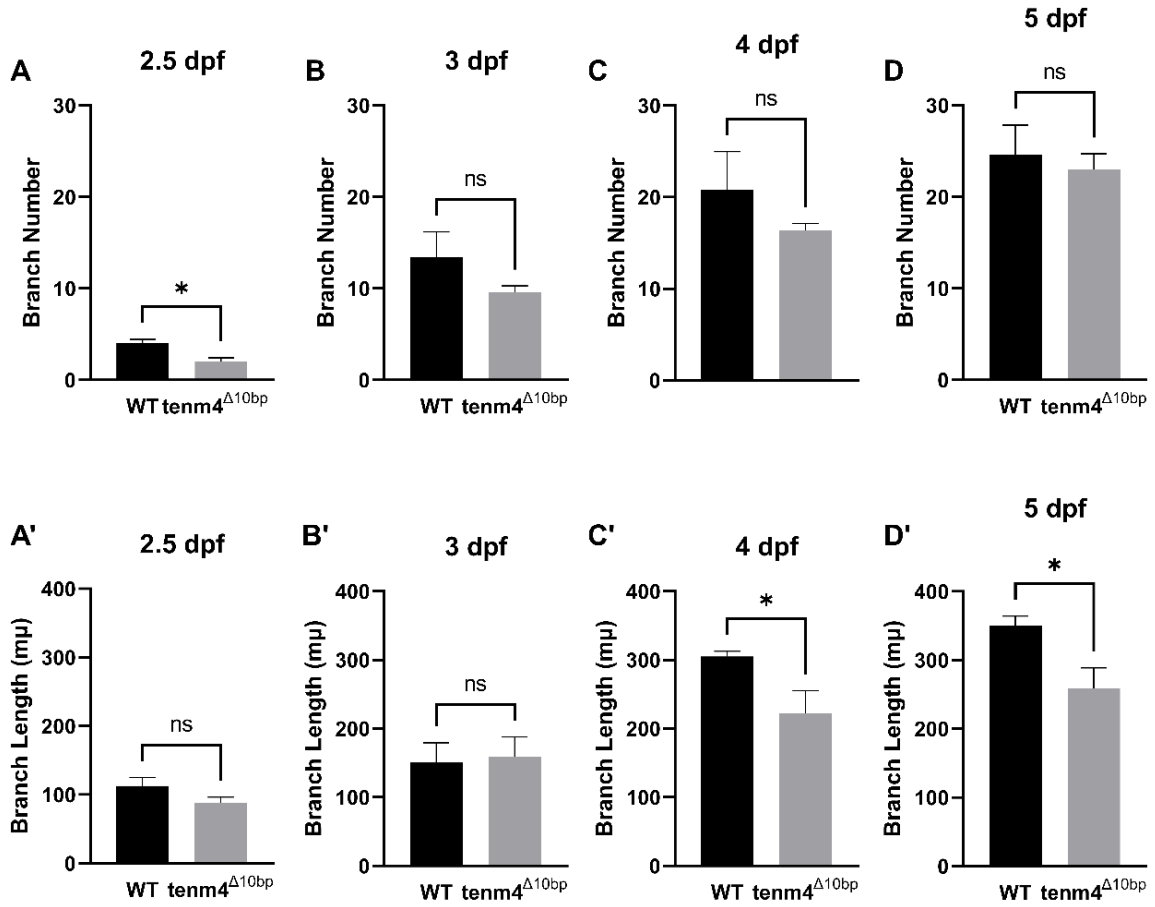

Figure 4.11 Individual RGC branch measurements through development. WT and tenm4$^{\Delta 10bp}$ mutant comparisons at different developmental stages. **A.** 2.5 dpf branch number. Regarding branch number, this was the only developmental time point in which there was a significant difference observed, with tenm4$^{\Delta 10bp}$ mutant having a smaller number of branches than WT (WT - 4±0.4472, n=5; tenm4$^{\Delta 10bp}$ mutant - 2±0.4472, n=5; p<0.0133*). **B.** 3 dpf branch number (WT - 13.40±2.786, n=5; tenm4$^{\Delta 10bp}$ mutant - 9.60±0.6782, n=5; p<0.2216, ns). **C.** 4 dpf branch number (WT - 20.80±4.188, n=5; tenm4$^{\Delta 10bp}$ mutant - 16.40±0.7483, n=5; p<0.3313, ns). **D.** 5 dpf branch number (WT - 24.60±3.250, n=5; tenm4$^{\Delta 10bp}$ mutant - 23±1.703, n=5; p<0.6743, ns). **A'.** 2.5 dpf branch length (WT - 112.8±12.36, n=5; tenm4$^{\Delta 10bp}$ mutant - 88.54±7.8, n=5, p<0.1361, ns). **B'.** 3 dpf branch length (WT - 150.4±29.29, n=5; tenm4$^{\Delta 10bp}$ mutant - 159±28.71, n=5; p<0.8386, ns). **C'.** 4 dpf branch length, WT RGCs have significantly larger branch lengths than the tenm4$^{\Delta 10bp}$ mutant (WT - 305.2±7.561, n=5; tenm4$^{\Delta 10bp}$ mutant - 222.4±33.08, n=5; p<0.0405*). This difference continued at **D'.** 5 dpf where the branch lengths of WT RGCs were still significantly larger (WT - 350.8±13.31, n=5; tenm4$^{\Delta 10bp}$ mutant - 259.1±29.68, n=5; p<0.0225*). Statistical analysis: t-test

We moved our focus to the number of puncta at these different developmental stages . No clear punctum was visible at 2.5 dpf and it is more likely that at this time

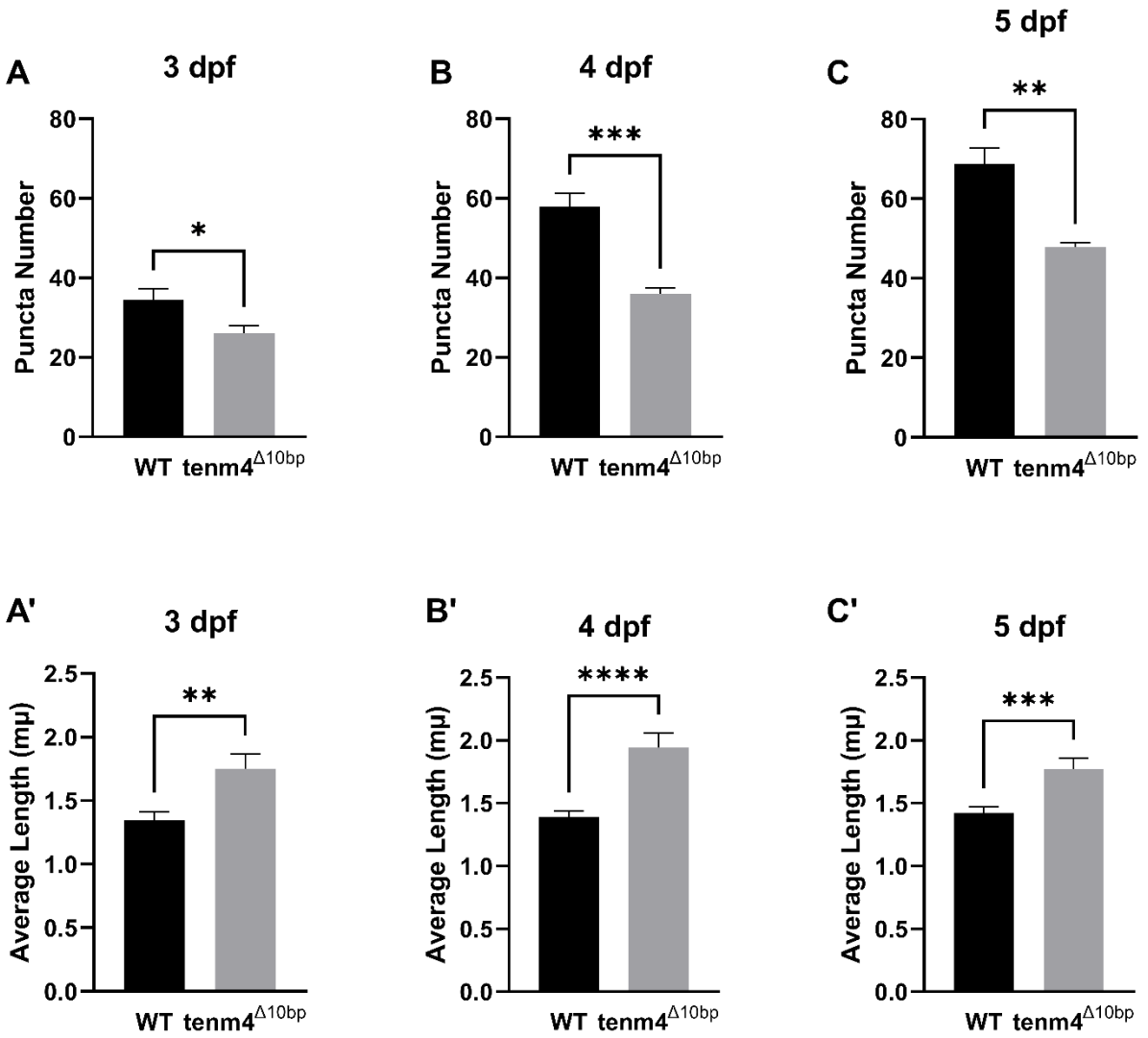

Figure 4.12 Individual RGC puncta measurements through development. WT and tenm4$^{\Delta 10bp}$ mutant comparisons at different developmental stages. A significant difference in the number of puncta was observed at **A.** 3 dpf (WT - 34.40±2.83, n=5; tenm4$^{\Delta 10bp}$ mutant - 26±1.949, n=5; p<0.0406*). **B.** 4 dpf (WT - 57.8±3.47, n=5; tenm4$^{\Delta 10bp}$ mutant - 36±1.517, n=5; p<0.0004***). and **C.** 5 dpf (WT - 68.80±4.030, n=5; tenm4$^{\Delta 10bp}$ mutant - 47.80±1.158, n=5; p<0.001**). With WT larvae having more puncta per RGCs the tenm4$^{\Delta 10bp}$ mutant larvae. Although there were a smaller number of puncta in the tenm4$^{\Delta 10bp}$ mutant, the length of these was larger throughout development. At **A'.** 3 dpf (WT - 1,349±0.06341, n=5; tenm4$^{\Delta 10bp}$ mutant - 1.751±0.1155, n=5; p<0.0014**), **B'**. 4 dpf (WT - 1.388±0.0513, n=5; tenm4$^{\Delta 10bp}$ mutant - 1.942±0.1182, n=5; p<0.0001****) and **C'**. 5 dpf (WT - 1.421±0.04974, n=5; tenm4$^{\Delta 10bp}$ mutant - 1.774±0.08530, n=5;p<0.0002***).

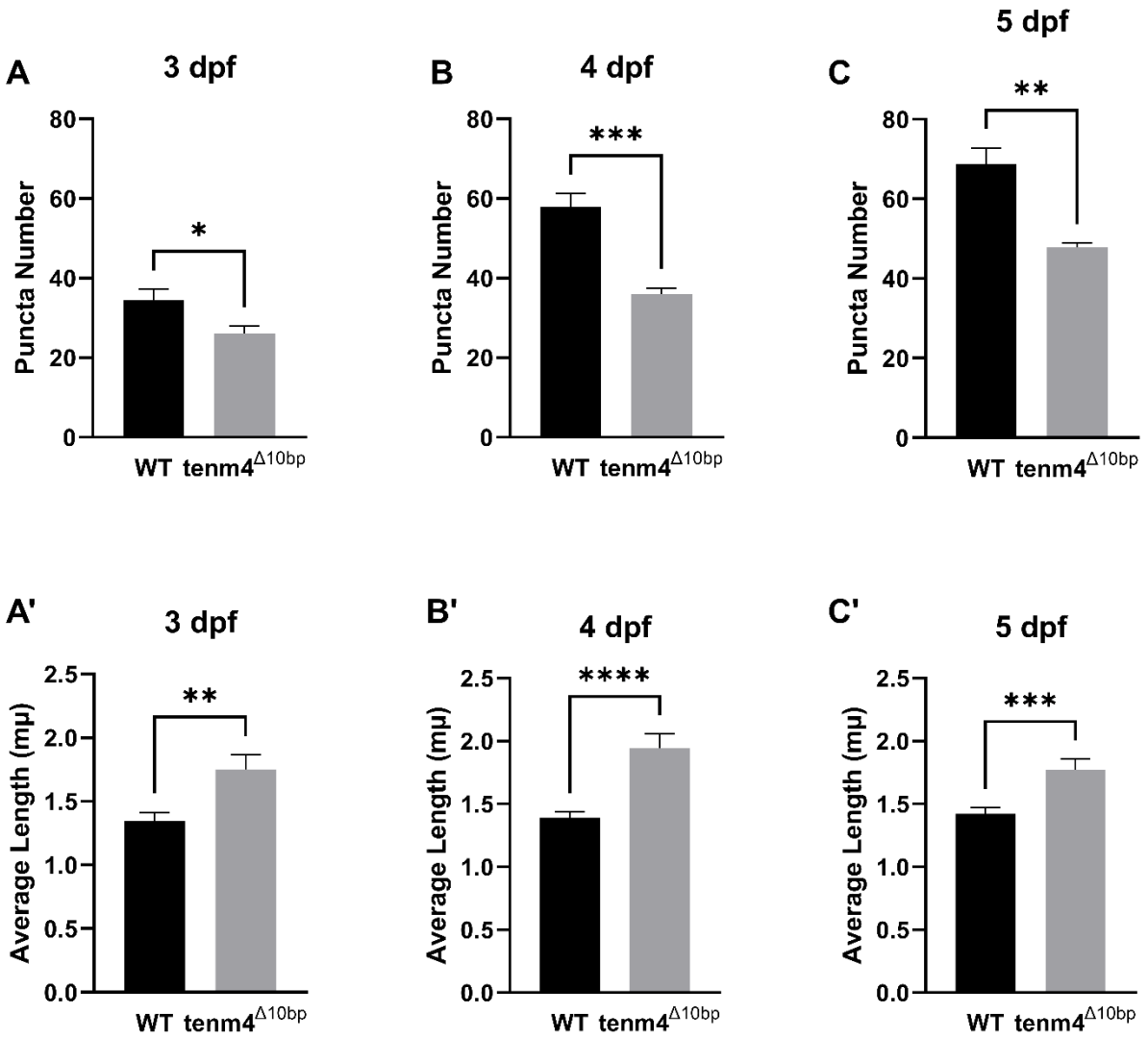

Figure 4.12 Individual RGC puncta measurements through development. WT and tenm4$^{\Delta 10bp}$ mutant comparisons at different developmental stages. A significant difference in the number of puncta was observed at **A.** 3 dpf (WT - 34.40±2.83, n=5; tenm4$^{\Delta 10bp}$ mutant - 26±1.949, n=5; p<0.0406*). **B.** 4 dpf (WT - 57.8±3.47, n=5; tenm4$^{\Delta 10bp}$ mutant - 36±1.517, n=5; p<0.0004***). and **C.** 5 dpf (WT - 68.80±4.030, n=5; tenm4$^{\Delta 10bp}$ mutant - 47.80±1.158, n=5; p<0.001**). With WT larvae having more puncta per RGCs the tenm4$^{\Delta 10bp}$ mutant larvae. Although there were a smaller number of puncta in the tenm4$^{\Delta 10bp}$ mutant, the length of these was larger throughout development. At **A'.** 3 dpf (WT - 1,349±0.06341, n=5; tenm4$^{\Delta 10bp}$ mutant - 1.751±0.1155, n=5; p<0.0014**), **B'**. 4 dpf (WT - 1.388±0.0513, n=5; tenm4$^{\Delta 10bp}$ mutant - 1.942±0.1182, n=5; p<0.0001****) and **C'**. 5 dpf (WT - 1.421±0.04974, n=5; tenm4$^{\Delta 10bp}$ mutant - 1.774±0.08530, n=5;p<0.0002***).

point synaptophysin has not stabilised yet **(Figure 4.10 A,E)**; because of this we began the punctum analysis at 3 dpf. We found that at this initial time point - 3 dpf, a significant difference could already be observed **(Figure 4.10 B,F,K; Figure 4.12 A)**, with WT larvae having higher number of puncta per cell (WT average punctum number was 34.4 ± 2.83, tenm4$^{\Delta 10bp}$ mutant average punctum number 26 ± 1.949) continuing to 4 dpf (WT average punctum number was 57.8 ± 3.47, tenm4$^{\Delta 10bp}$ mutant average punctum number 36 ± 1.517) **Figure 4.10 C,G,K; Figure 4.12 B)** and 5dpf larvae (WT average punctum number was 68.8 ± 4.030, tenm4$^{\Delta 10bp}$ mutant average punctum number 47.8 ± 1.158; **Figure 4.10 D,H,K; Figure 4.12 C)**.

Lastly, we analysed the individual lengths of these punctum, the analysis began at 3 dpf **(Figure 4.10 B, F; Figure 4.12 A')**. At this stage, our tenm4$^{\Delta 10bp}$ mutant larvae already start to show the occasional enlarged punctum **(Figure 4.13 A)** and when comparing the two genotypes we see that at this developmental time point there is already a significant difference between the two (WT - 34.40 ± 2.83; tenm4$^{\Delta 10bp}$ mutant - 26 ± 1.949) **(Figure 4.10 L)**. When looking at these cells at 4 dpf we can see that this phenotype continues, with puncta still being larger in tenm4$^{\Delta 10bp}$ mutant RGCs than in WT RGCs **(Figure 4.10 C, G, L; Figure 4.12 B'; Figure 4.13 B, B')**. These enlarged puncta continue to be visible up until our last developmental time point, 5 dpf, with a significant difference observed throughout **(Figure 4.10 D, H, L; Figure 4.12 C'; Figure 4.13 C, C').** Whether this phenotype continues after this time point is still unknown.

In conclusion **(Table 4.1)** at 2.5 dpf, cells in both genotypes develop in a similar fashion. They have comparable average branch numbers, and their branch lengths are almost identical. At this stage puncta are not properly differentiated therefore quantification of these was not possible. At 3 dpf, RGCs have no significant

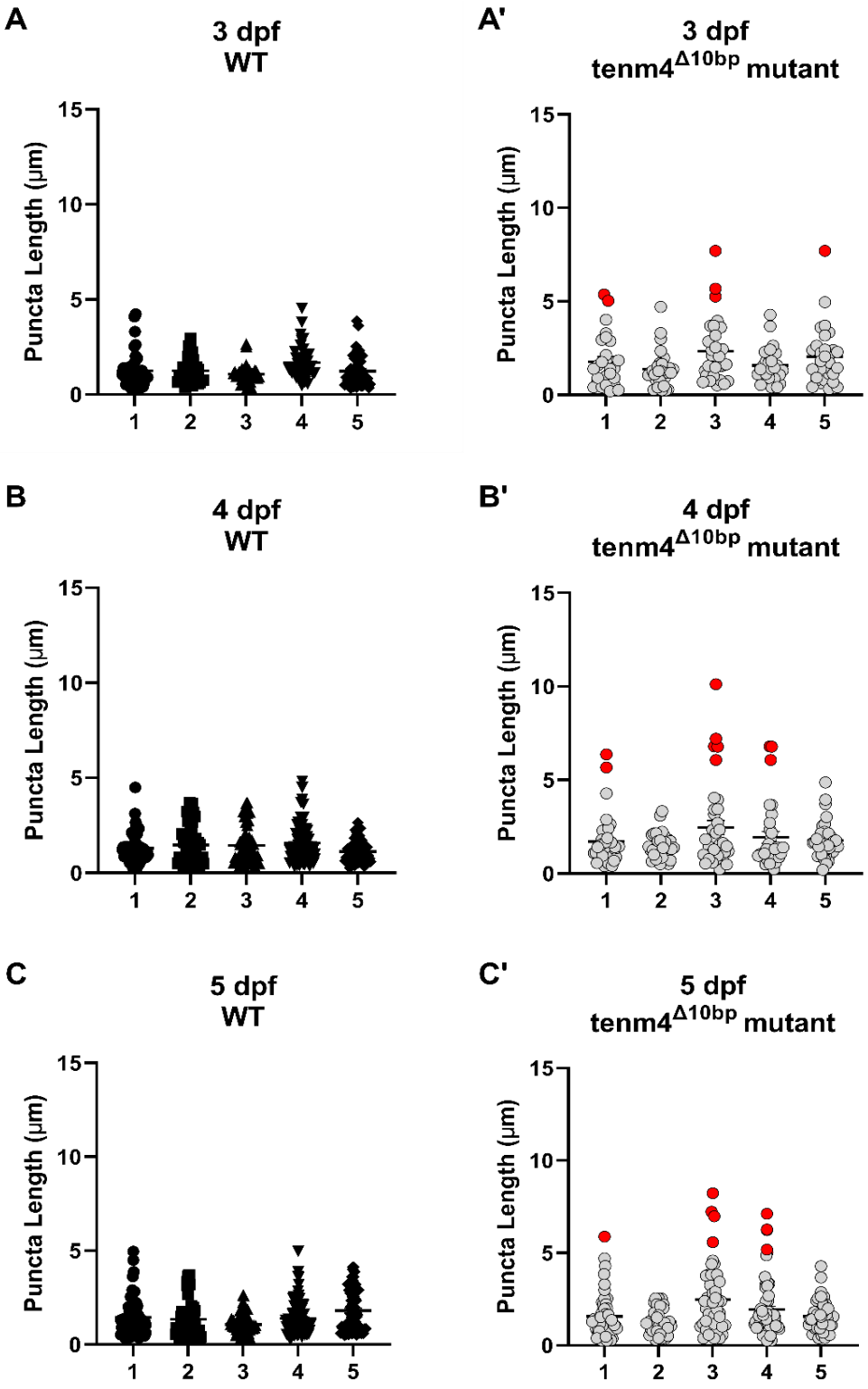

Figure 4.13 Individual puncta lengths through development of **A.** 3 dpf WT (n=5), **A'.** 3 dpf tenm4$^{\Delta 10bp}$ mutant (n=5), B. 4 dpf WT (n=5), B'. 4 dpf tenm4$^{\Delta 10bp}$ mutant (n=5), **C.** 5 dpf WT, and **C'.** 5 dpf tenm4$^{\Delta 10bp}$ mutant (n=5) larvae. Enlarged punctum can be seen since **A'.** 3 dpf throughout development in the tenm4$^{\Delta 10bp}$ mutant larvae. Red dots represent enlarged punctum.

difference in the number of branches or the length of these branches, but they do show a significant difference in the number of puncta, with tenm4$^{\Delta 10bp}$ mutant RGCs having less puncta than WT RGCs. At 4 dpf results are comparable to those described in previous sections above. No significant difference was observed in the number of

branches, but the branches appear to be shorter in length. There is also a decrease in the number of puncta per cell when compared to WT larvae. Lastly, at 5 dpf we can see that the number of branches is still comparable between the two phenotypes, and that there is still a significant difference in the length of these branches with WT having longer branch lengths than the tenm4$^{\Delta 10bp}$ mutants. Similarly, there is a higher number of puncta in WT RGCs than in tenm4$^{\Delta 10bp}$ mutant RGCs.

Table 4.1 Summary of RGC development

	2.5 dpf		**3 dpf**		**4 dpf**		**5 dpf**	
Branch Number	4 ± 0.4472	2.6 ± 0.2449	13.40 ± 2.786	9.6 ± 0.6783	20.80 ± 4.188	16.20 ± 0.5831	24.60 ± 3.250	23 ± 1.703
Branch Length (µm)	110.8 ± 13.12	88.54 ± 7.8	150.4 ± 29.29	159 ± 28.71	294.7 ± 3.361	228 ± 36.38	336.4 ± 9.346	287.1 ± 35.25
Puncta Number	N/A	N/A	37 ± 3.178	31.20 ± 1.497	57.8 ± 3.470	47.6 ± 3.586	70.6 ± 3.326	61.60 ± 2.926
Puncta Length (µm)	N/A	N/A	1.322 ± 0.0582	1.825 ± 0.1133	1.388 ± 0.051	1.858 ± 0.112	1.421 ± 0.0497	1.782 ± 0.0832

From this data we can pinpoint the developmental onset of our phenotype between 3 dpf and 4 dpf and we can see that it continues very strongly at 5 dpf. When and if this phenotype disappears is still unknown. It can also be seen, within our tenm4$^{\Delta 10bp}$ mutant larvae that the RGCs that present these early on phenotypic behaviours are the ones that end up developing into full phenotypic cells. This reinforces our hypothesis that not all RGCs are tenm-4 positive, as well as tenm-4

being necessary for the correct morphological development of RGCs and synaptogenesis or synaptic organisation.

4.7 Conclusions and Discussion

In conclusion, here we report that deletion of teneurin-4 leads to a morphological phenotype in a subset of RGCs, with tenm4$^{\Delta 10bp}$ mutant larvae presenting shorter RGC axonal branches and less complex arborisation patterns in the OT. Furthermore, we detect fewer puncta per RGC in the tenm4$^{\Delta 10bp}$ mutant fish, but these puncta seem to be larger in size as well as volume. We have also pinpointed the onset of these changes which occur between 2.5 dpf and 3 dpf. We show that by eliminating tenm-4 a structural alteration in the overall morphology of RGCs is produced, suggesting an instructive role of this CAM in RGC morphogenesis in the vertebrate visual system. Interestingly, the phenotypes observed throughout this analysis appeared to be constrained to a specific group of RGCs. ISH data **(Figure 1.16;1.17;** Chapter 1. Introduction) shows that *tenm-4* seems to be expressed in some but not all RGCs and ACs in the retina. We therefore think that not all RGCs are *tenm-4* positive and therefore only the sub-group of RGCs that are *tenm-4* positive are being affected by the mutation in the tenm4$^{\Delta 10bp}$ mutant larvae.

Studies in *Drosophila* and zebrafish have demonstrated that Teneurins have an active role in establishing specific synaptic circuits (Mosca et al., 2012) and correct structural and functional development of RGCs (Antinucci et al., 2013). However, there is very little known about teneurin-4 and its role in development. Here we report that teneurin-4 controls the shape of RGC axonal arbors and the number and size of presynaptic puncta. A structural phenotype was observed in the puncta of the tenm4$^{\Delta 10bp}$ mutant larvae, suggesting a possible instructive role during synaptogenesis in the vertebrate visual system. Interestingly, these alterations appeared to be

constrained to a specific subpopulation of RGCs, hinting, as previously mentioned (Chapter 1. Introduction), that not all RGCs are tenm-4 positive and therefore these phenotypes are not visible in tenm-4 negative RGCs. This is also evident in the scatter plots showing the two non-overlapping populations of RGCs for the tenm4$^{\Delta 10bp}$ mutant phenotypes. As reported by Meyer and Smith (Meyer & Smith, 2006), synaptogenesis has been implicated in shaping axonal outgrowth; based on these findings we think that tenm-4 not only has an impact in the distribution of synaptophysin protein through RGCs but has a direct impact on the length of its axons and the complexity of their arborisations.

CHAPTER 5.

TC DEVELOPMENT DEFECTS UPON THE DELETION OF TENEURIN-4

5.1 Dendritic Development

Retinal ganglion cells (RGCs) – sole output neurons of the retina – project to the optic tectum (OT) where they make synaptic connections with tectal cells (TCs). The OT, the main retinorecipient area in the brain of nonmammalian vertebrates, is homologous to the superior colliculus in mammals. It is a highly laminar structure, with RGC axons forming well-defined sublayers of the tectal neuropil (Baier, 2013).

Developmentally, dendrites of neurons are constantly changing, branches grow, complexity increases and lastly, they form synaptic connections. This development occurs in three main stages. During the first step, there is an initial outgrowth and primary dendrites are formed, these dendrites are tipped with growth cones – which will allow them to find their synaptic partners. Although no synapses are formed during this step, the axonal arbors are in proximity. During the second stage, the dendritic arborisations increase their complexity, and the branches are covered with filopodia which allows synaptogenesis to occur between axonal arbors and dendritic arbors. During the last phase, the dendritic tree has reached morphological maturity and the synaptic connections it made are now stabilised (McAllister, 2000).

Postsynaptic densities (PSD) are the primary sites of synaptic transmitter action at all chemical synapses (Kennedy, 2000), they can be either inhibitory or excitatory. Retinotectal synapses are glutamatergic, and through different biochemical and molecular studies it has been shown that the PSD at glutamatergic synapses consists of over 80 different proteins (Husi, Ward, Choudhary, Blackstock, & Grant, 2000; Walikonis et al., 2000; Yamauchi, 2002). One of these proteins, PSD-95, is a postsynaptic scaffolding protein that belongs to a family of membrane-associated guanylate kinases (MAGUKs) which contain multiple protein-protein interaction domains (Meyer, Trimmer, Gilthorpe, & Smith, 2005). By interacting with other scaffolding proteins, MAGUKs help organise PSDs. MAGUKs bind directly to the PDZ-binding region of the C-termini of many CAMs and receptor proteins. The N-terminal mRNA splicing is known to have important functional consequences for MAGUK trafficking and for their specialised roles in synaptic function (Zheng, Seabold, Horak, & Petralia, 2011).

In *Drosophila* a PSD-95 homologue known as *disc large* is known to be a key player in the development of neuromuscular junctions (NMJ). When motor nerve terminals (presynaptic boutons) contact the muscle, clustering of *disc large* at synapses begins with the contact of motor nerve terminals (presynaptic boutons) with the muscle. These boutons release glutamate, which is the primary neurotransmitter at the NMJ (Zheng et al., 2011). In vertebrates, both mammals and zebrafish, PSD-95 is known to participate in synapse development, it is the first protein to arrive and cluster at the synapse. PSD-95 drives synaptic maturation not only of postsynaptic components, but of presynaptic terminals as well, this is thought to be done through retrograde signalling (El-Husseini, Schnell, Chetkovich, Nicoll, & Bredt, 2000).

The correct wiring of retinotectal synaptic connections are essential for normal development. As previously discussed, (Chapter 1.), the first axons reach the OT between 46-48 hpf. Once there, and in a short period of time (~30 hours), they innervate the tectal neuropil (TNP), the retinotopic map and create the first functional connections (Easter & Nicola, 1996; Niell & Smith, 2005; Stuermer, 1988; Zheng et al., 2011). Once RGCs enter the TNP they are restricted to a specific layer, the specific lamina that they target depends on the particular RGC subtype, although most of them innervate the most superficial laminae in the TNP, the stratum opticum (SO) (Chapter 1.) (Gabriel, Trivedi, Maurer, Ryu, & Bollmann, 2012; Huberman et al., 2008, 2009; Nikolaou & Meyer, 2012; Xiao, Roeser, Staub, & Baier, 2005; M Yamagata & Sanes, 1995). RGC axons and TC dendrites use CAMs to sort themselves into these laminae and to find their synaptic partners (Nevin, Taylor, & Baier, 2008). Both RGC axonal arbors and TC dendritic arbor growth is complete by 6 dpf (Meyer & Smith, 2006; Niell et al., 2004).

Synapses within the CNS most commonly form between the axons of one neuron and the cell soma or dendrites of other neurons. The dynamic mobility of axonal and dendritic branches is accompanied by the turnover of emerging synapses (Meyer & Smith, 2006; Niell et al., 2004). These dynamic movements and rearrangements of the arbors allow for the sampling of many potential synaptic partners. Because of this, a large number of nascent synaptic connections are formed, although only a few are kept. For this to occur, synaptic vesicles dock, fuse and release neurotransmitters into the synaptic cleft at the active zone (Chapter 1). Directly opposite to the active zone, the PSD is found. During periods of circuit assembly, a vast number of synaptic connections are assembled in a short period of time (Nikolaou & Meyer, 2012; Waites et al., 2005)

As seen in Chapter 1., ISH data shows tenm4 expression in both the retina – GCs and ACs – as well as in the OT. Based on this expression pattern and previously acquired data (Chapter 4.) we wanted to investigate the potential role that *tenm4* has on the development of TCs postsynaptic structures as well as retinotectal circuits.

5.2 Teneurin-4 Deletion Impacts TC Dendrite Morphology

In the previous chapter (Chapter 4.) we described that Teneurin-4 seems to be required for correct synaptogenesis and synaptic organisation at presynaptic sites. Based on these results as well as the previously mentioned *tenm4* ISH expression patterns in the OT (Chapter 1.), we wondered if the changes observed on the axonal arbors and at the presynaptic sites could be influencing the morphology of the dendritic arbors and postsynaptic sites. For this, we mosaically labelled tectal cells in WT and Tenm4$^{\Delta 10bp}$ mutant embryos by co-injecting FoxP2:Gal4 and UAS:PSD-95-GFP-Zfn-mKate2 – a postsynaptic density marker, and subsequently did *in vivo* confocal imaging (see Chapter 2. Material and Methods). Forkhead (Fox) domain transcription factors are a large gene family with multiple roles in development such as regulation of embryonic patterning and tissue specific gene expression. *FoxP2* is a member of this family of genes with expression in zebrafish. This gene is first expressed at the 20-somite stage in the area that will develop into the telencephalon but by 72 hpf its expression is more complex. By this time point, the developing OT becomes the main expression area for this gene (Bonkowsky & Chien, 2005; Shah, Medina-Martinez, Chu, Samaco, & Jamrich, 2006) and thus has become an avidly used TC driver. By using these two expression plasmids, we were able to individually label TCs and therefore characterise and compare the different morphologies in WT and Tenm4$^{\Delta 10bp}$ mutant larvae. It is important to note that by using the FoxP2:Gal4 plasmid, a large variety of TC subtypes were labelled; the analysis presented here is an average of all these subtypes.

For the analysis of these cells, we followed the same strategy as we did with the RGCs in Chapter 4. We first studied the overall structure of the dendritic branches

of both 4 dpf WT and tenm4$^{\Delta 10bp}$ mutant TCs by looking at the number of branches **(Figure 5.1)** and the length of these branches **(Figure 5.2)** – measurements were done following the same criteria as in **Figure 4.2**. We also analysed the complexity of the dendritic arborisations to see if there was a difference between the overall morphology in our two genotypes **(Figure 5.3)**. We then focused on the postsynaptic sites, quantifying the number of PSD puncta per cell **(Figure 5.4)**, assessing the PSD puncta volume **(Figure 5.5)** and lastly had a close look at the distribution patterns of these puncta **(Figure 5.6)** – measurements were done following the same criteria as in **Figure 4.6.** This specific developmental stage was chosen due to an initial phenotype found through functional imaging, where at 4 dpf, the tenm4$^{\Delta 10bp}$ mutant larvae had more visually responsive voxels than WT larvae.

We initially looked at the number of branches per TC in both of our genotypes. On average, 26.93 ± 2.874 branches were present in the WT TCs (n=15 cells), **(Figure 5.1 A,D)**, on the other hand, there were an average of 16.73 ± 1.406 branches in the Tenm4$^{\Delta 10bp}$ mutant (n=15 cells) TCs **(Figure 5.1 B,E).** As seen in **Figure 5.1 C**, when comparing the number of branches, there was a significant difference found between the WT and the Tenm4$^{\Delta 10bp}$ mutant larvae, with WT TCs having more branches per TC than those of the Tenm4$^{\Delta 10bp}$ mutant ones.

As a next step, we wanted to find out if there was also a significant difference in the length of these branches. Using IMARIS 8.0, the total branch length was measured starting at the cell body (see Chapter 2). WT TCs had an average total length of 434.9 ± 38.45 µm (WT, n= 15; **(Figure 5.2 A,D)** whereas Tenm4$^{\Delta 10bp}$ mutant TCs had an average total length of 338.8 ± 26.83 µm (Tenm4$^{\Delta 10bp}$ mutant, n = 15; **Figure 5.2 B,E)**. As described with the number of branches per cell, although we find a few TCs with shorter branches than WT – represented in red **(Figure 5.2 D,E)**. When

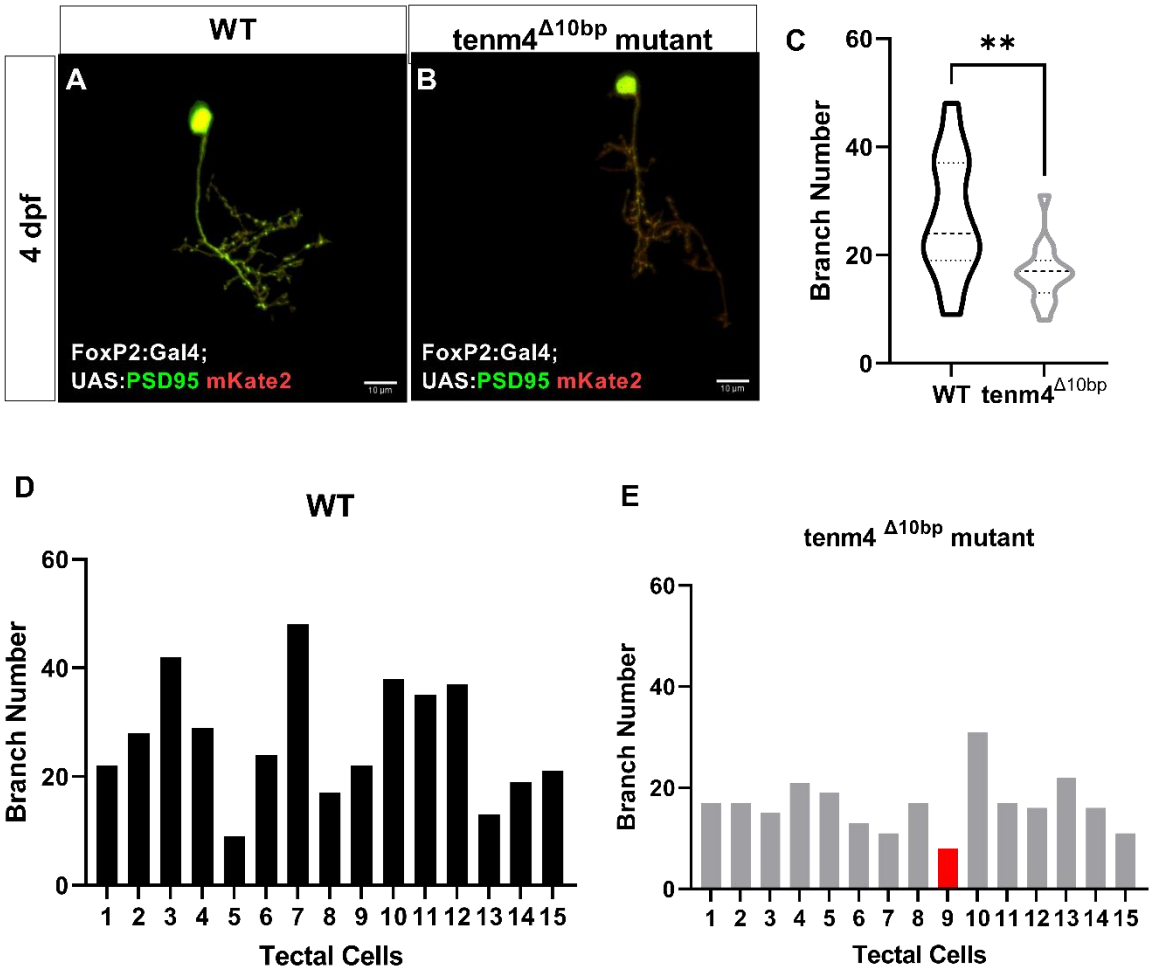

Figure 5.1 Tectal cell branch number. Comparison of number of branches in **A.** 4 dpf WT and **B.** 4 dpf tenm4$^{10bp\Delta}$ mutant, **C.** A significant difference was observed between the two genotypes (WT - 26.93±2.874, n=15; tenm4$^{10bp\Delta}$ mutant - 16.73±1.406, n=15; p<0.0035**). **D.** Individual branch number of WT TCs. Minimum number of branches 9; maximum number of branches 48. **E.** Individual branch number of tenm4$^{10bp\Delta}$ mutant. Minimum number of branches 8; maximum number of branches 23. Red bar represents TC with a smaller number of branches than the WT. Scale bars set at 10µm. Statistical analysis: t-test

comparing branch lengths between the two genotypes we found that Tenm4$^{\Delta 10bp}$ mutant TCs have overall significantly shorter branches than those of the WT larvae **(Figure 5.2 C)**. For precise information regarding image acquisition, analysis and statistical analysis please refer to **Chapter 2.**

Although significant differences were found between the genotypes in both the number of branches and the length of the branches, there is no specific pattern seen of a specific subtype or number of TC affected by the Tenm4$^{\Delta 10bp}$ mutation. It appears as if the mutation causes an alteration in the overall population of TCs. Overall, the Tenm4$^{\Delta 10bp}$ mutant TCs have fewer **(Figure 5.1)** and shorter **(Figure 5.2)** branches.

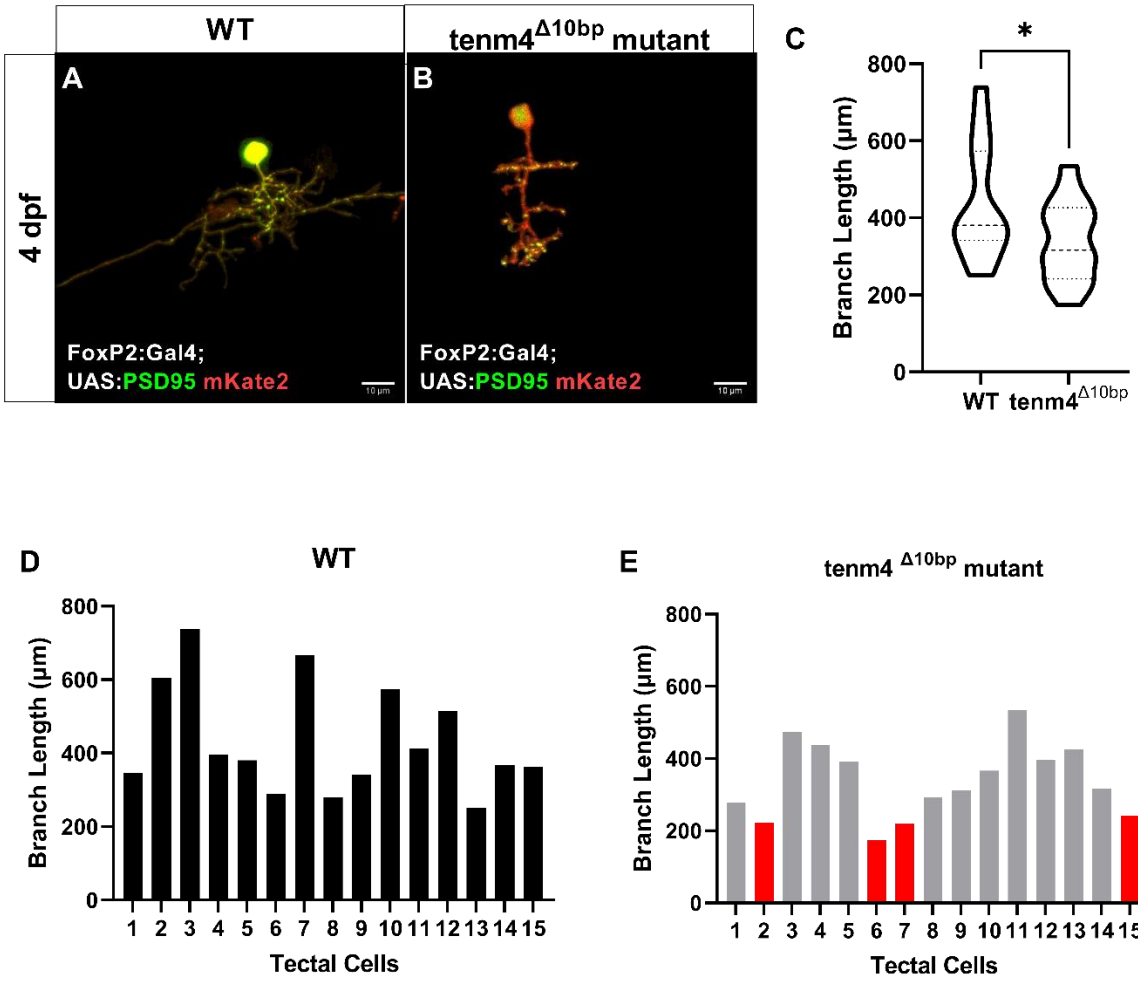

Figure 5.2 Tectal cell branch length. Comparison of branch length in **A.** 4 dpf WT and **B.4 dpf** tenm4$^{10bp\Delta}$ mutant, **C.** A significant difference was observed between the two genotypes (WT - 434.9±28.45, n=15; tenm4$^{10bp\Delta}$ mutant – 338.8±26.83, n=15; p<0.0498*). **D.** Individual branch lengths of WT TCs. **E.** Individual branch lengths of tenm4$^{10bp\Delta}$ mutant. Red bar represents TC with branch lengths which are shorter than WT branch lengths. Scale bars set at 10µm. Statistical analysis: t-test

5.3 TC Dendritic Arborisation Complexity Modified Upon Teneurin-4 Deletion

Moving forward, we looked at the arborisations of TCs to better understand the effect that tenm-4 deletion has. As previously mentioned we used Sholl analysis as a method to quantitatively compare the morphological characteristics of imaged neurons. Based on our earlier analysis, we know that the Tenm4$^{\Delta 10bp}$ mutant TCs have a significantly lower number of branches and that these branches are significantly shorter in length, we can therefore infer that the dendritic arborisations will be less complex than those of the WT TCs.

When evaluating and comparing the dendritic arborisations of our WT TCs (WT, n=15, **Figure 5.3 A)** and the Tenm4$^{\Delta 10bp}$ mutant TCs (Tenm4$^{\Delta 10bp}$ mutant n=15, **Figure 5.3 B)**, no significant difference was found between the two genotypes. Although no significant difference was observed, Tenm4$^{\Delta 10bp}$ mutant TC dendritic arbors have a tendency of higher complexity closer to the cell body, becoming less complex the further away they are from the cell body; whereas WT TCs seem to have a tendency of less complex arborisations when they are closer to the cell body, but gain complexity the further away they are from it **(Figure 5.3 C).** For information regarding the image analysis and statistical analysis please refer to **Chapter 2.**

Based on this morphological assessment of TC branching, we can conclude that tenm-4 is a key player in the morphogenesis of dendritic branching. Tenm4$^{\Delta 10bp}$ mutant TCs present a smaller number of branches, which are overall shorter in length.

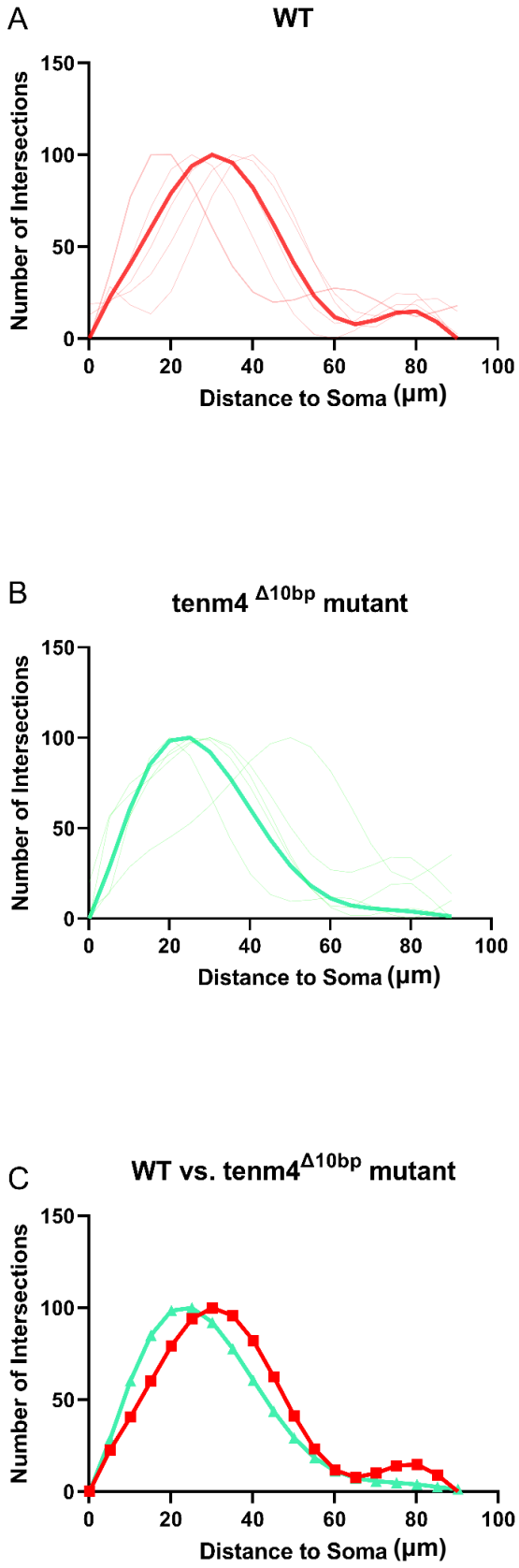

Figure 5.3 Complexity of tectal cell dendritic arborisations. Sholl analysis of **A.** 4 dpf WT TCs and **B.** 4 dpf tenm4$^{10bp\Delta}$ mutant **C.** Comparison between WT and tenm4$^{10bp\Delta}$ mutant dendritic arborisations show that although there is a tendency for mutant cells to be more complex the closer, they are to the soma, there is no significant difference between the complexity of these arborisations. Statistical analysis: t-test

The smaller number of branches, as well as the decreased lengths that are seen in the tenm4$^{\Delta 10bp}$ mutant TCs lead to these fewer complex arborisations. Tenm4 seems

to have an effect on the development of dendritic arbors in the OT.

5.4 Teneurin-4 Knock-Out Leads to Lower Numbers of Postsynaptic Sites on TCs.

The development of dendritic arbors and the creation of the correct synaptic connections upon that arbor, are crucial for neural circuit development. Scaffolding proteins are key players in synapse organisation and function (Funke, Dakoji, & Bredt, 2005). The previously mentioned PSD-95 has been thoroughly studied over the years because of its involvement within the CNS as an essential component of excitatory PSDs (Chen et al., 2005). It has also been discovered that PSD-95 has a direct impact on synaptic plasticity (Miguad et al., 1998). Furthermore, PSD-95 is known to have an influence on synapse maturation and stabilisation (De Roo, Klauser, Garcia, Poglia, & Muller, 2008; Ehrlich, Klein, Rumpel, & Malinow, 2007; El-Husseini et al., 2000; Won, Levy, Nicoll, & Roche, 2017) and therefore on synapse number. We wondered if the differences observed within the dendritic branches of our Tenm4$^{\Delta 10bp}$ mutant larvae could be influenced by the PSD puncta of our TCs. A change at these sites could also help broaden our understanding of not only the presynaptic phenotypes that were found (see Chapter 4) but the role that Teneurin-4 is playing postsynaptically. If RGCs and TCs aren't establishing appropriate synaptic connections, it could also help explain the initial phenotype observed where Tenm4$^{\Delta 10bp}$ mutant larvae had an increase in the number of visually responsive voxels (see Chapter 1. Introduction).

The quantification of PSD puncta was done through the "spots object" function in IMARIS 8.0); for information regarding image acquisition, image analysis and statistical analysis please refer to **Chapter 2** and **Figure 4.6**. WT TCs **(Figure 5.4 A)** contained on average 55.80 ± 5.33 PSD puncta per cell, whilst the Tenm4$^{\Delta 10bp}$ mutant

TCs **(Figure 5.4 B)** 39.20 ± 5.343 PSD puncta per cell. A significant difference was observed when comparing the data obtained from the two genotypes, with Tenm4$^{\Delta 10bp}$ mutant larvae having a significantly lower number of PSD puncta per cell than the WT **(Figure 5.4 C).** When looking at the individual measurements of both genotypes (WT – **Figure 5.4 D**, Tenm4$^{\Delta 10bp}$ mutant – **Figure 5.4 E)**, we again found that some of our Tenm4$^{\Delta 10bp}$ mutant TCs (represented with red bars on **Figure 5.4 E**) had a smaller number of puncta than those of the WT TCs. Based on ISH data (Chapter 1.) we know

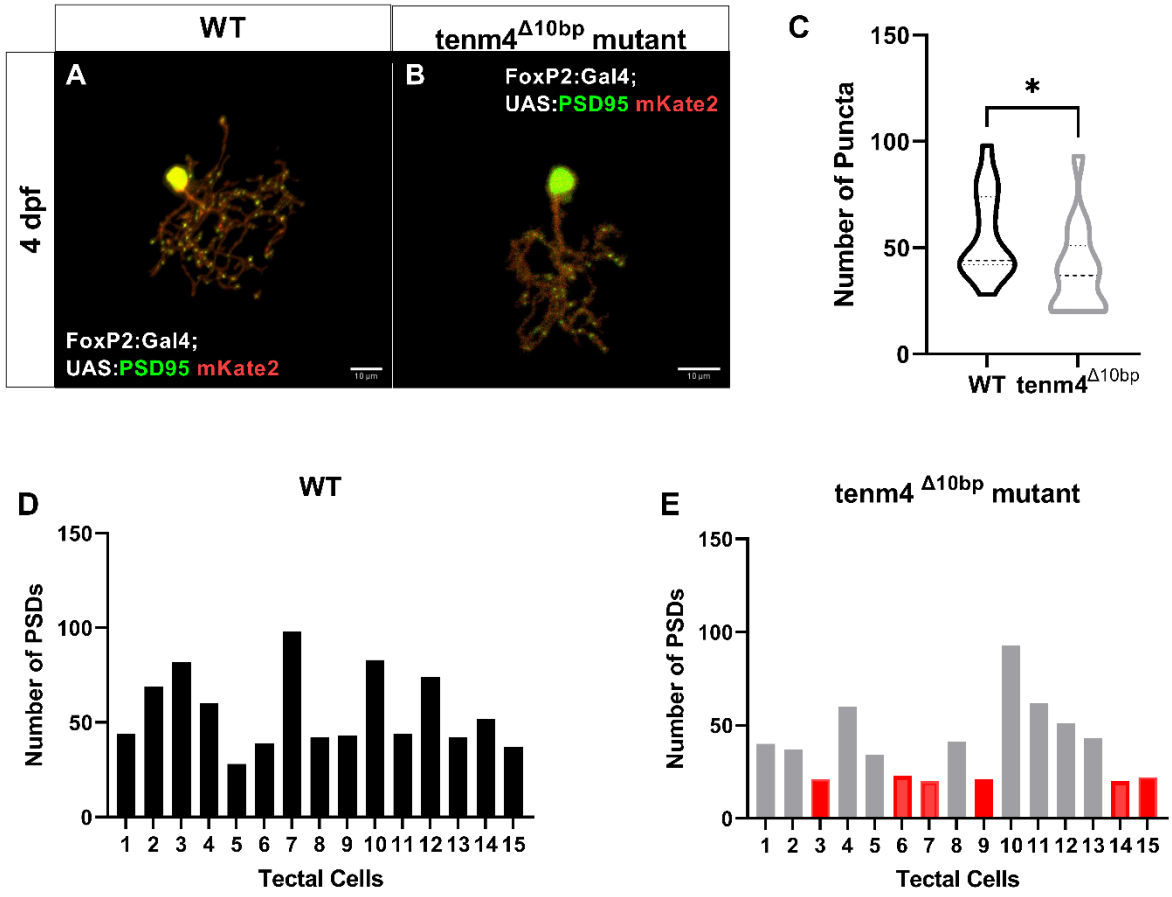

Figure 5.4 Number of PSD puncta per tectal cell. A. 4 dpf WT TC and **B.** 4 dpf tenm4$^{10bp\Delta}$ mutant TC **C.** WT TCs have a significantly larger number of PSD positive puncta per TC than tenm4$^{10bp\Delta}$ mutant TCs (WT - 55.80±5.335, n=15; tenm4$^{10bp\Delta}$ mutant – 39.20±5.343, n=15; p<0.0363*). **D.** Individual number of PSD positive puncta of WT TCs **E.** Individual number of PSD positive puncta of tenm4$^{10bp\Delta}$ mutant. Red bar represents TC with a smaller number of PSD positive puncta than the average WT. Scale bars set at 10µm. Statistical analysis: t-test.

that teneurin-4 is expressed in a subset of TCs. We hypothesise that these cells, which exhibit a smaller number of puncta, could be tenm4 positive cells. There does not seem to be a specific correlation between the number of branches, the length of these branches and the number of PSD puncta per TC in the Tenm4$^{\Delta 10bp}$ mutant.

5. 5 Postsynaptic Sites on TCs Enlarged Upon Deletion of Teneurin-4

Before synaptogenesis can begin, the pre- and postsynaptic cells must find each other (DePew, Aimino, & Mosca, 2019). PSD-95 is localised at dendritic filopodia – whose main role is probing the environment for their targets (Dunaevsky & Mason, 2003; Wong & Wong, 2000). Direct links between CAMs, synaptic partner matching and synaptogenesis has been found (Missaire & Hindges, 2015; Masahito Yamagata & Sanes, 2008; Masahito Yamagata et al., 2002). Over recent years, Teneurins have been found to be involved in a variety of neurodevelopmental processes such as synaptic partner matching and synapse organisation (W. Hong et al., 2012; Mosca et al., 2012; Mosca & Luo, 2014; Zheng et al., 2011). Our results thus far have shown that WT larvae and Tenm4$^{\Delta 10bp}$ mutant larvae have significant differences in morphological aspects such as branch length and number of PSD puncta per cell, so we wondered whether there was a difference in the volume of these PSD puncta.

Individual PSD puncta volume measurements were taken from 30 different TCs (WT, n=15; Tenm4$^{\Delta 10bp}$ mutant, n=15). The measurements were taken using the “surfaces object” function on IMARIS 8.0 software. A 3D surface was created over every PSD punctum and the volume data was extracted for statistical analysis. For more information regarding image acquisition, image analysis and statistical analysis please refer to **Chapter 2** and **Figure 4.6.**

All PSD puncta within WT TCs had a volume of no more than 4.824 μm^3, with an average WT PSD puncta reaching 0.6308 μm^3 ± 0.02081 **(Figure 5.5 A,D)**. When analysing the Tenm4$^{\Delta 10bp}$ mutant PSD puncta **(Figure 5.5 B,E)**, we found that some

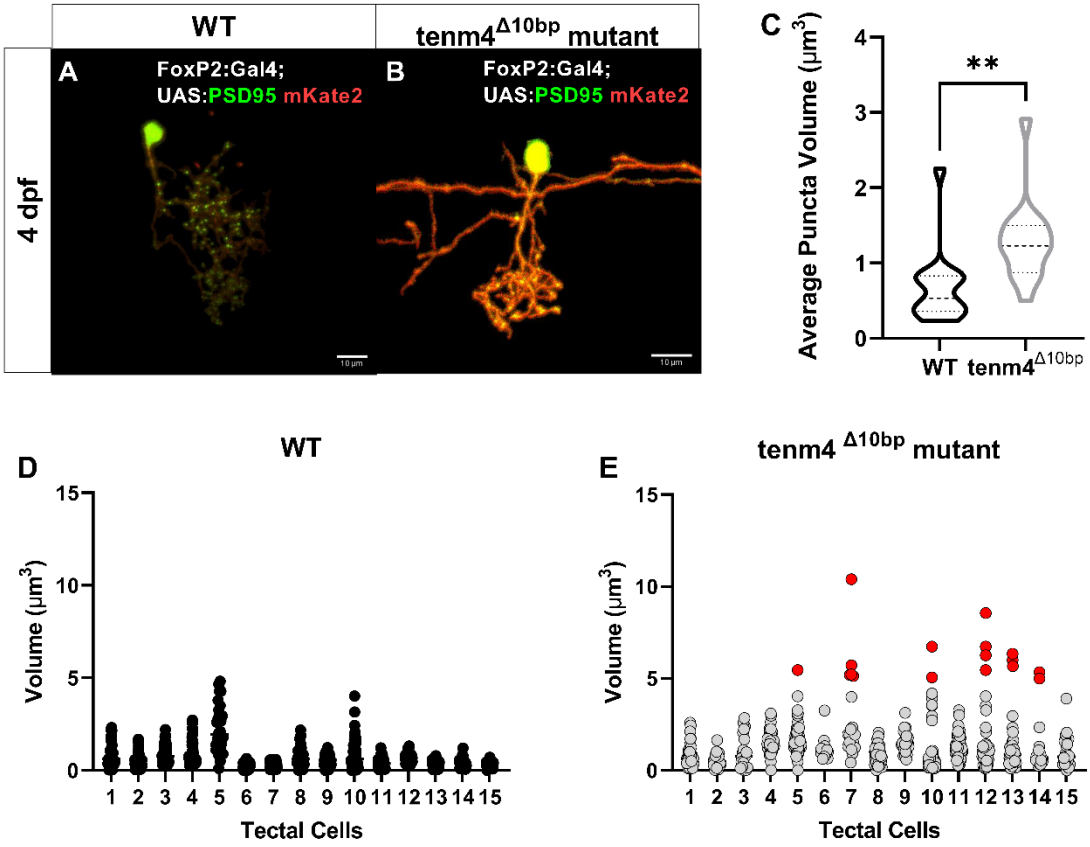

Figure 5.5 PSD puncta volumes. A. 4 dpf WT TC and **B.** 4 dpf tenm4$^{10bp\Delta}$ mutant TC **C.** WT TCs have a significantly smaller volume in their PSD puncta per TC than tenm4$^{10bp\Delta}$ mutant TCs (WT – 0.6667±0.1278, n=15; tenm4$^{10bp\Delta}$ mutant – 1.284±0.1417, n=15; p<0.0031**). **D.** Individual PSD positive puncta volumes of WT TCs **E.** Individual PSD positive puncta volumes of tenm4$^{10bp\Delta}$ mutant TCs. The red dots represent PSD positive puncta with a larger volume than the average WT PSD positive puncta. Scale bars set at 10μm. Statistical analysis: t-test

TCs exhibited larger volumes, with the largest one reaching 10.39 μm^3, on average each PSD puncta had a volume of 1.221 μm^3 ± 0.04639. When comparing our two genotypes, we not only found a significant difference between the average volume - with individual PSD puncta volumes increased in tenm4 10bpΔ mutant **(Figure 5.5 C)**, but we found a sub-division where within our Tenm4$^{\Delta 10bp}$ mutant group there

were PSD puncta with similar volumes to WT PSD puncta and another group with larger volumes **(Figure 5.5 E)**. These results were similar to those observed in RGCs of tenm4$^{\Delta 10bp}$ mutant larvae in Chapter 4. For more information regarding the statistical analysis please refer to **Chapter 2.**

Lastly, we looked at the frequency distribution of these PSD puncta **(Figure 5.6)**. Within the WT TCs there was a higher frequency of smaller volume PSD puncta than in the Tenm4$^{\Delta 10bp}$ mutant TCs. Although the Tenm4$^{\Delta 10bp}$ mutant TCs have a similar frequency distribution pattern to WT TCs - having a higher frequency of smaller volume PSD puncta - they seem to be: (1) shifted slightly towards larger volumes than the WT TCs; and (2) having a wider distribution pattern than their WT counterparts. These results concur with the previously discussed data, where WT larvae have more

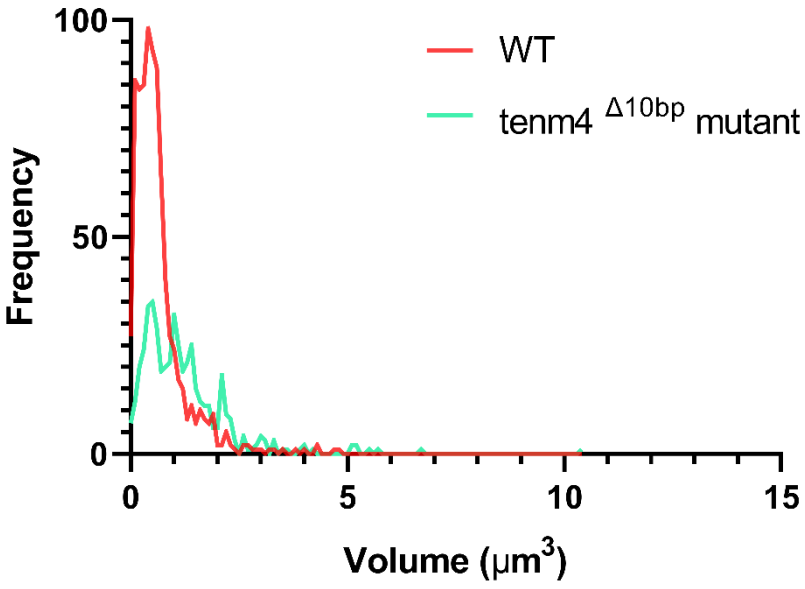

Figure 5.6 Frequency distribution of PSD puncta volumes. Frequency distribution of PSD positive puncta volumes in 4 dpf WT TCs (red) and 4 dpf tenm4$^{\Delta 10bp}$ mutant TCs (green). There is a higher frequency of smaller volume PSD puncta in WT TCs, but a higher frequency of larger volume PSD puncta in tenm4$^{\Delta 10bp}$ mutants TCs.

PSD puncta per cell than Tenm4$^{\Delta 10bp}$ mutants **(Figure 5.4)**, but those PSD puncta being smaller in size **(Figure 5.5).**

5.6 Conclusions and Discussion

Research done on *Drosophila* and zebrafish have shown that Teneurins are implicated in establishing precise synaptic circuits, both structurally and functionally (Antinucci et al., 2013; W. Hong et al., 2012; Mosca et al., 2012). Here we report that upon the deletion of teneurin-4, FoxP2-positive TCs are affected morphologically. A change in branch number and length as well as complexity of the dendritic arbor can be seen in the Tenm4$^{\Delta 10bp}$ mutant larvae. Additionally, a decrease in the number of PSD puncta and an increase in the volume of these can be seen in the mutant genotype. The phenotypes observed in TCs are matching those we identified in RGCs (Chapter 4); this strengthens our hypothesis that Teneurin-4 plays an essential role in synaptogenesis and synapse organisation and therefore in the development of these retinotectal circuits.

Through the characterisation done here, we can begin to create a clearer picture of the different roles that tenm-4 has in the developing system. Teneurin-3 is known to be required for proper dendrite morphogenesis and axon targeting in the vertebrate visual system (Antinucci et al., 2013, 2016; Berns et al., 2018; Dharmaratne et al., 2012; Leamey et al., 2007). *In situ* hybridisation analysis done by our lab (Cheung et al., 2019) revealed expression patterns of overlapping Teneurin members in the developing visual system. *Tenm3* and *tenm4* in particular, have similar expression patterns. Based on the results reported here, and previously reported *tenm3* data, we could therefore infer that they have a similar role in visual circuit wiring.

Although the phenotype reported here mimics closely that of the phenotype discovered in RGCs (Chapter 4.), there are important differences. The most important

being that there is no clear sub-group of TCs that is affected by the tenm4$^{\Delta 10bp}$ mutation as there was with RGCs (identified by the segregation of the data in two populations). With TCs, there is an alteration of the overall morphology of the cell. The underlying cause could lay in phenotypic RGCs making aberrant connections with all TCs and not with a specific sub-group. This will be further discussed in the next chapter.

CHAPTER 6.

CONCLUSIONS AND DISCUSSION

6.1 Summary

In this study, the mechanisms of visual circuit assembly have been investigated in the larval zebrafish. Specific focus has been placed on the role that cell adhesion molecule, Teneurin-4, has in shaping the connectivity in the vertebrate visual system. Initial work done through functional calcium imaging on the Tenm4$^{\Delta 10bp}$ mutant larvae (Isl2b:Gal4;UAS:SyGCaMP3;tenm4$^{\Delta 10bp}$ mutant) showed that there was an increase of visually responsive voxels in RGCs when comparing them to WT larvae (Isl2b:Gal4;UAS:SyGCaMP3). We hypothesised that these changes could be a result of various factors, including a decrease in apoptosis or increase in proliferation of RGCs; errors in intraretinal connectivity – specifically in the IPL; or incorrect development of RGC axonal arbors, TC dendritic arbors and/or synaptogenesis/synaptic partner matching between the two sub-type population of cells.

Throughout this research project, several key findings were made; (1) loss of tenm-4 results in a significant increase of apoptotic cells within the developing retina at 4 dpf. (2) Tenm-4 is required for the correct development of axonal and dendritic branches in RGCs and TCs respectively. Specifically, for their growth and overall arborisation patterns. (3) Tenm-4 is necessary for synaptogenesis and synapse organisation to occur correctly, both pre- and postsynaptically. (4) Only a subset of

RGCs present the observed phenotype – proving that not all RGCs are tenm-4 positive.

Throughout this chapter, a summary of the three main result chapters will be reviewed, followed by the relevance of the study as well as a discussion of potential limitations to the study and alternative methodologies that could have been used. Lastly, suggestions for future work regarding the role that teneurin-4 has in the developing visual system will be presented.

6.2 Role of Teneurin-4 in the Developing Vertebrate Retina

The retina, a sensory neural structure formed by multiple cell types, has become a valuable model in which to study developmental aspects such as cell cycle, neurogenesis, and circuit assembly. The synchronisation of cell growth, division and death are some of the essential steps necessary for correct circuit wiring, tissue development and therefore embryonic development (Hipfner & Cohen, 2004). Teneurins have been shown to be expressed by interconnected populations of neurons in the developing central nervous system (CNS) (Chapter 1). The timing of this expression typically concurs with periods of axon outgrowth, synaptogenesis, pruning, and apoptosis (Antinucci et al., 2013; Berns et al., 2018; W. Hong et al., 2012; Beatrix P. Rubin et al., 2002).

In Chapter 3, we examine the role of tenm-4 in retinal development with specific focus on proliferating and apoptotic cells as well as circuit assembly in the inner plexiform layer. In line with the hypothesis, we found Tenm-4 is required for what appears to be the correct balance of RGCs and ACs -judging by their anatomical

positioning - undergoing apoptosis during a specific timepoint in development - 4 dpf. An increase of apoptotic cells was seen in the GCL and in the ACL at this developmental stage (for layer specifics please see Chapter 2 and Chapter 3). Previous work has demonstrated that the C-terminal domain of Teneurins is cytotoxic and promotes cells *in vitro* to rapidly undergo apoptosis (Ferralli et al., 2018). Although the physiological stimuli which triggers its release is still unknown, the domain was proposed to model neural networks through selective induction of apoptosis. In the context that Teneurins and apoptosis could be linked, an increase of apoptosis could be considered. This could begin to widen our scientific curiosity about teneurin-4's "teneurin C-terminal associated peptide" (TCAP) (Reid, Freij, Maples, & Biga, 2019) and its function *in vivo* in development. Furthermore, it has been shown that CAMs promote cell survival by inhibiting apoptotic effects of transmembrane receptors. Through *in vivo* and *in vitro* experiments, it was shown that by binding to G-protein coupled receptor (GPCR) Latrophilin-1 *(Lphn1)*, contactin-6 (Cntn6) modulates its activity and inhibits an apoptosis response. *Lphn1* has a more widely expressed pattern than Cntn6, which allows for other ligands to regulate its activity. Such ligands could potentially include Teneurins which have previously been demonstrated to interact with Lphn (Burbach & Meijer, 2019; Del Toro et al., 2020; Zuko et al., 2016). Interestingly, it was recently proved through *in vitro* work (Husić, Barsyte-Lovejoy, & Lovejoy, 2019) that the tenm/lphn interaction is accomplished by the TCAP. The TCAP region of teneurins associates directly with latrophilins, and, as a diffusible peptide, can modulate cell-to-cell adhesion, which strengthens the hypothesis of a tenm4 role in the inhibition of *lphn1* and thus inhibiting apoptosis.

Considering that an increase of apoptosis is only seen at a single developmental stage, and that the number of apoptotic cells in the GCL and the ACL seem to be

affected evenly, an increase of apoptosis does not seem to explain the difference in visually evoked responses (Chapter 1). However, the reliability of this data is impacted by a variety of factors. First, the number of samples used was very low (n=5 per genotype). Second, DAPI staining was not used alongside TUNEL staining, therefore the total number of cells in our samples was unknown as well as not using cell-type specific markers, or transgenic zebrafish lines that would allow for the visualisation of RGCs and ACs specifically (i.e. isl2b:Gal4;UAS;GFP). Lastly, we relied on only one method to detect apoptosis. Because of this, further research is needed to assess the role of tenm4 in the developing retina. By first increasing the sample size the data obtained could be more reliable as it increases the statistical power and therefore the probability of finding a true statistically significant result. Secondly, by co-staining with DAPI the total number of cells in the retina could be quantified, giving us a more precise number of apoptotic cells in the overall population. By using cell-type specific markers alongside DAPI and TUNEL we could have a better understanding and a clearer picture of the number of cells as well as the specificity of the cell type undergoing apoptosis. Finally, apoptosis occurs via a complex signalling cascade, by using alternative apoptotic markers, cells at different stages of the apoptotic process can be detected – giving a more precise picture of apoptosis in the retina. Overall although these experiments are beginning to tell a story about apoptosis in the retina in relation to the deletion of tenm4, there are various limitations with the study – described above – that need addressing. When these limitations are addressed, stronger conclusions will be able to be drawn from the study.

6.3 Correct RGC and TC Development in the Optic Tectum require Teneurin-4

A functional nervous system relies on complex regulated processes such as neurite outgrowth, axon guidance and synaptogenesis. During development, neural circuits are formed through a multitude of molecular cues controlling different wiring processes. Several molecules have been identified in visual circuit assembly (Chapter 1). These molecules are expressed in specific subtypes of retinal cells, and have particular developmental roles - such as neurite attraction and repulsion, self-avoidance, adhesion as well as synaptic partner matching (Matsuoka et al., 2011; Rheaume et al., 2018; Visser et al., 2015). Additionally, arbor growth and synaptogenesis are dynamic processes – nascent branches and putative nascent synapses form and disappear concurrently, proving to be a closely couples process. Through these *in vivo* experiments, synaptogenesis was found to guide the growth of axonal arbors by promoting the formation of nascent branches as well as selectively stabilising them (Meyer & Smith, 2006; Niell et al., 2004). Therefore, factors that regulate synaptogenesis and the stability of these newly formed synapses, may have an effect of axon arbor growth. Furthermore, work in cells, *Drosophila,* zebrafish and mice have shown that Teneurins are involved in establishing specific synaptic circuits, such as tenm-3 within the IPL of larval zebrafish (Chapter 1 and Chapter 4) (Antinucci et al., 2013; W. Hong et al., 2012; Mosca et al., 2012). Moreover, Teneurins are known to influence axon guidance during early development and once they reach their target regions, they enable partner matching and synapse formation. These processes are achieved by transsynaptic interactions as well as membrane stabilisation through the interaction with and the regulation of the cytoskeleton. Work

done in *Drosophila* has shown Teneurins may control how neurons move and match with their postsynaptic targets by interactions with the cytoskeleton. Pre- or postynaptic perturbations in *Drosophila* Teneurins are known to cause severe synapse loss as well as impair facets of organisation trans-synaptically – including defects in the active zone apposition, release sites, membrane, and vesicle organisation as well as synaptic transmission. Presysnaptic microtubules and posynaptic spectrin cytoskeleton were seen to be severely disrupted upon the deletion of one of the two *Drosophila* Teneurins (Mosca et al., 2012; Mosca & Luo, 2014; Zheng et al., 2011).

In this context, the results presented in Chapter 4 indicate that teneurin-4 is required for the morphological development of RGCs. Through *in vivo* single cell imaging, we found that the tenm4$^{\Delta 10bp}$ mutant develops shorter RGC axonal branches, less complex arborisation patterns, fewer presynaptic puncta as well as a larger size and volume of these puncta. All this data combined, suggests an instructive role of the CAM teneurin-4 in RGC morphogenesis in the vertebrate visual system. The onset of this phenotype appears to be between 2.5 dpf and 3 dpf, continuing through to (at least) 5 dpf – this reinforces the supposition of teneurin-4's function in RGCs morphogenesis. Remarkably, these results appear to be constrained to a specific subset of RGCs **(Figure 4.9)**, which corresponds to the zebrafish salt and pepper ISH expression patterns observed in the developing retina **(Figure 1.19; Figure 1.20)**. We therefore infer that not all RGCs are tenm4 positive, and thus a KO of this glycoprotein does not affect all RGCs. Similarly, in Chapter 5, we see that TCs in the tenm4$^{\Delta 10bp}$ mutant present a smaller number of shorter length branches, less complex arborisations, as well as fewer PSD puncta with larger volume. Once again, these results support the theory of teneurin-4's role in regulating neurite morphogenesis in

the vertebrate visual system and the previous findings of Teneurins having an influence on axon guidance and synaptic partner matching that was observed in cell culture, *Drosophila* and zebrafish (Antinucci et al., 2013; W. Hong et al., 2012; Y. K. Hong et al., 2011; Mosca et al., 2012; Mosca & Luo, 2014). Furthermore it provides more evidence for the recent hypothesis that arbor growth and synaptogenesis are dynamic processes (Meyer & Smith, 2006; Meyer et al., 2005; Niell et al., 2004; Nikolaou & Meyer, 2012). Lastly, Teneurins have been found to be colocalised with α-spectrin, a cytoskeletal protein. Upon teneurin deletion, pre- or postsynaptic perturbations have been observed including the number of synaptic puncta suggesting that Teneurins organise synapses through interactions with the cytoskeleton. The phenotypes described throughout this research may bring us a step closer to proving this hypothesis. Previous findings in *Drosophila* teneurin research, such as synaptic morphology upon the deletion of teneurin, or the distribution of these synapses, have now been corroborated by this study. There is therefore a possibility that by eliminating tenm4, there is a disruption in the interaction of α-spectrin, which might lead to the perturbation of cytoskeletal structures and therefore to the RGC and TC phenotype discussed throughout this thesis. Moreover, by having a role in synaptogenesis and synapse organisation, Teneurins may also play a role in arbor growth - as described by Meyer and Smith (Meyer & Smith, 2006).

Due to the lack of data on the functionality of these pre- and postsynaptic puncta, the results cannot confirm that these enlarged puncta are indeed fully functional synapses. These pre- and postsynaptic puncta could simply be the distribution of presynaptic protein synaptophysin as well as the distribution of postsynaptic protein PSD-95 being transported through the arbors. For a puncta to be considered a synapse, functionality must be seen; by taking advantage of the recently

created fluorescent glutamate sensor, iGluSnFR (Johnston et al., 2019; Marvin et al., 2013) the functionality of these pre- and postsynaptic puncta could be assessed. Driven by Ath5:Gal4, RGC specific promoter or FoxP2:Gal4/Y308:Gal4 tectal cell drivers, iGluSnFR could be used to compare the synaptic output from individual tenm4$^{\Delta 10bp}$ mutant cells to WT cells. Consequently, by assessing the functionality of these puncta, it could confirm if the phenotype presented in this study actually indicates teneurin-4's role in synaptogenesis and synaptic organisation, or if its impact is in the distribution of the synaptic proteins, both presynaptically as well as postsynaptically.

Lastly, the development of RGCs as well as the establishment of puncta upon them was briefly studied. Although the RGC time-lapse imaging data presented throughout this project does not allow us to see arbor growth dynamics or the formation of puncta by the presynaptic protein, it allowed us to set a time point for the onset of this phenotype. Time-lapse imaging over an extended period of time, between 3 dpf and 4 dpf, would enable the observation and analysis of axon growth dynamics as well as puncta formation during the onset of the developmental phenotype. Because of its high-quality imaging speed, performing this experiment on a light sheet microscope at the timepoints mentioned above, would allow for higher resolution imaging, and the ability to see the dynamics behind these processes. Light sheet microscopy would also allow for less photobleaching of the labelled cells – a problem commonly encountered with confocal time-lapse imaging performed for this project. Additionally, expanding this experiment to look at the dynamics of TC development, would not only help understand how these cells and the postsynaptic phenotype develop, but could begin to explain the relationship and/or influence between the presynaptic and the postsynaptic phenotype.

Further enrichment to the study could come from considering the use of alternative tectal cell drivers. Although FoxP2:Gal4 is a reliable TC driver, it is known to label only a specific subset of TC, limiting the possibility of seeing teneurin-4's impact on all TC sub-types. Moreover, the exact types and variety of TCs labelled by FoxP2 have not been fully characterised – reducing the conclusions that could be drawn from this experiment. The use of different TC driver lines, such as a Y308:Gal4 line - which labels a larger variety of tectal cell subtypes, could increase the quality of data acquisition and therefore we could have a better understanding of the implications of tenm4 in the development of tectal cells and visual system circuit assembly.

Future studies regarding the impact of tenm4 on the retinotectal circuit could benefit from the creation of tenm4 specific zebrafish lines. By taking advantage of gene editing tools such as CRISPR or bacterial artificial chromosome (BAC), tenm4 could be fluorescently tagged. Doing so, would allow a full characterisation of tenm4-positive cells in both the retina and the tectum throughout development. The repetition of the experiments presented in these thesis with a tagged tenm4 zebrafish line would lead to more precise conclusions regarding the role of tenm4 in the developing zebrafish visual system. Lastly, although in Chapter one we present ISH data which allows for the identification of the mRNA expression pattern, it does not allow us to quantify the number of Teneurin-positive cells or draw accurate information regarding the presence of tenm4 in the zebrafish. By taking advantage of more recent techniques, such as fluorescent ISH (FISH) we would be able to in addition to the FISH stain with DAPI and study the colocalisation of the two, therefore allowing us to quantify the number of Teneurin-positive cells. This would in turn, lead to a better understanding of the phenotype presented here, where a subgroup of tenm4$^{\Delta 10bp}$ mutant RGCs present a phenotype whilst the ones that do not, stay within WT ranges.

6.4 Conclusions and Future Directions

Throughout this chapter we have not only summarised the key findings of this research study, but we have outlined the limitations within it. Our findings thus far have demonstrated a potential contribution of tenm-4 in synaptogenesis, synaptic partner matching as well as axon growth within the zebrafish visual system. Determining the exact role that teneurin-4 plays in synaptic formation and function, as well as its action in specific cell types is still a fundamental priority. Although further experiments are needed to achieve this specificity of knowledge, the results presented here strengthen the idea that Teneurins have an important role in the development of vertebrate neural circuit specificity. Taken together, our findings support a role for tenm4 in correct visual circuit morphogenesis in vertebrates as well as the correct formation of retinotectal circuits.

So far, we have established that the deletion of tenm-4 leads to a subpopulation of RGCs presenting shorter branches, with a higher number of puncta which are larger both in size and volume. The precise timepoint at which this phenotype appears is not known, but it seems to be between 3 dpf and 4 dpf. Its synaptic counterparts, the TCs, upon the deletion of tenm-4 present a higher number of branches, which are shorter in length. They seem to have a lower number of puncta, which are larger in size. Both RGC and TC arborisation patterns are less complex upon the deletion of tenm-4. The exact mechanisms involved in the formation of these phenotypes are still largely unknown.

Understanding if the puncta we are imaging are functional synapses or just accumulation of the synaptic proteins, it an essential step would be do single-cell functional imaging. As previously mentioned, the best way to go about this would be by taking advantage of the recently created fluorescent glutamate sensor, iGluSnFR (intensity-based glutamate-sensing fluorescent reporter) (Johnston et al., 2019; Marvin et al., 2013). Single-wavelength fluorescent reporters allow the visualisation of specific neurotransmitters, in this case glutamate, with high spatial and temporal resolutions. By doing so we would be able to detect submicromolar to millimolar amounts of glutamate, and finally know if these puncta are functional synapses or not. Using iGluSnFR instead of SyGCaMP3 would allow more precise synaptic imaging. Genetically encoded calcium indicators allow for repeated, non-invasive measurements of neural activity in defined populations of neurons, but because of the precision needed in imaging the specific functionality of these puncta, the speed at which you can detect the iGluSnFR, makes it a better candidate than the SyGCaMP3.

We would then need to address the question of whether the phenotypes we are seeing in this study are cell autonomous or not. This could be done by taking advantage of single-cell transplants as a tool to track RGCs and TCs development in different environments. Transplanting single cells from the tenm4$^{\Delta 10bp}$ mutant to WT and vice versa would allow us to observe this. This could be accomplished, for example, by co-injecting mCerulean mRNA and Syp:GFP-DsRed into a tg(isl2b:Gal4) zebrafish line and transplanting single cells into a tenm4$^{\Delta 10bp}$ mutant at the 10- to 12-somite stage, would give way for the healthy adaptation of these cells into their new environment and tracking the development in the different environments. Possible outcomes from this experiment could be normal cell development - which would insinuate, for instance, (1) an intrinsic mechanism of the cell for correct development;

(2) aberrant cell development – which would strengthen the already set teneurin homophilic interaction mechanism or help explain an extrinsic mechanism such as environmental factors.

As mentioned throughout this thesis, other experiments that would help fill in the knowledge gaps would be the repetition of the apoptotic and mitotic experiments with newly defined parameters. These parameters could include things like cell-type specific markers to stain for RGCs and ACs specifically, using DAPI staining to quantify the total number of cells present in the retina, as well as using different apoptotic and mitotic markers to corroborate and deepen the results found here.

To conclude, this study constitutes a significant advancement in bridging the knowledge gap in the underlying mechanisms in retinotectal circuit assembly. Specifically, the role of CAM teneurin-4 in morphogenesis and synaptogenesis within these developing circuits. By taking advantage of a CRISPR knockout zebrafish line we were able to assess the role of teneurin-4 in the assembly of defined retinal circuits, specifically in the correct morphological development of RGC axonal arbors in the tectum as well as the development of its synaptic partners the TCs. Furthermore, we detect an aberrant distribution of the presynaptic protein synaptophysin in RGC axonal arbors, as well as the postsynaptic protein PSD-95, suggesting a role for this protein in synaptogenesis and/or synaptic organisation. If the experiments suggested in this section were completed, we would have a clear picture of the role that tenm4 plays in development. Lastly, we have also mentioned that mutations in human TENM4 have been linked to neuropsychiatric disorders such as bipolar disorder as well as schizophrenia. Our findings therefore have the potential to lead to a better understanding of the aetiology of this disorder, as well as the general mechanisms involved in the creation of functional synaptic networks in healthy states.

BIBLIOGRAPHY

Adriano, F., Caltagirone, C., & Spalletta, G. (2012). Hippocampal volume reduction in first-episode and chronic schizophrenia: a review and meta-analysis. *The Neuroscientist*, *18*(2), 180–200. https://doi.org/10.1177/1073858410395147

Agathocleous, M., & Harris, W. A. (2009). From progenitors to differentiated cells in the vertebrate retina. *Annual Review of Cell and Developmental Biology*, *25*, 45–69. https://doi.org/10.1146/annurev.cellbio.042308.113259

Ahmari, S. E., Buchanan, J., & Smith, S. J. (2000). Assembly of presynaptic active zones from cytoplasmic transport packets. *Nature Neuroscience*, *3*(5), 445–451. https://doi.org/10.1038/74814

Alsina, B., Vu, T., & Cohen-Cory, S. (2001). Visualizing synapse formation in arborizing optic axons in vivo: dynamics and modulation by BDNF. *Nature Neuroscience*, *4*(11), 1093–1101. https://doi.org/10.1038/nn735

Ament, S. A., Szelinger, S., Glusman, G., Ashworth, J., Hou, L., Akula, N., … Roach, J. C. (2015). Rare variants in neuronal excitability genes influence risk for bipolar disorder. *Proceedings of the National Academy of Sciences of the United States of America*, *112*(11), 3576–3581. https://doi.org/10.1073/pnas.1424958112

Amini, R., Rocha-Martins, M., & Norden, C. (2017). Neuronal migration and lamination in the vertebrate retina. *Frontiers in Neuroscience*, *11*, 742. https://doi.org/10.3389/fnins.2017.00742

Anishchenko, A., Greschner, M., Elstrott, J., Sher, A., Litke, A. M., Feller, M. B., & Chichilnisky, E. J. (2010). Receptive field mosaics of retinal ganglion cells are established without visual experience. *Journal of Neurophysiology*, *103*(4), 1856–1864. https://doi.org/10.1152/jn.00896.2009

Antinucci, P., Nikolaou, N., Meyer, M. P., & Hindges, R. (2013). Teneurin-3 specifies morphological and functional connectivity of retinal ganglion cells in the

vertebrate visual system. *Cell reports*, *5*(3), 582–592. https://doi.org/10.1016/j.celrep.2013.09.045

Antinucci, P., Suleyman, O., Monfries, C., & Hindges, R. (2016). Neural mechanisms generating orientation selectivity in the retina. *Current Biology*, *26*(14), 1802–1815. https://doi.org/10.1016/j.cub.2016.05.035

Antonini, A., & Stryker, M. P. (1998). Effect of sensory disuse on geniculate afferents to cat visual cortex. *Visual Neuroscience*, *15*(3), 401–409.

Ardiles, A. O., Grabrucker, A. M., Scholl, F. G., Rudenko, G., & Borsello, T. (2017). Molecular and cellular mechanisms of synaptopathies. *Neural plasticity*, *2017*, 2643943. https://doi.org/10.1155/2017/2643943

Ault, S. J., & Leventhal, A. G. (1994). Postnatal development of different classes of cat retinal ganglion cells. *The Journal of Comparative Neurology*, *339*(1), 106–116. https://doi.org/10.1002/cne.903390110

Badea, T. C., & Nathans, J. (2004). Quantitative analysis of neuronal morphologies in the mouse retina visualized by using a genetically directed reporter. *The Journal of Comparative Neurology*, *480*(4), 331–351. https://doi.org/10.1002/cne.20304

Baden, T., Berens, P., Franke, K., Román Rosón, M., Bethge, M., & Euler, T. (2016). The functional diversity of retinal ganglion cells in the mouse. *Nature*, *529*(7586), 345–350. https://doi.org/10.1038/nature16468

Bae, J. A., Mu, S., Kim, J. S., Turner, N. L., Tartavull, I., Kemnitz, N., … Eyewirers. (2018). Digital Museum of Retinal Ganglion Cells with Dense Anatomy and Physiology. *Cell*, *173*(5), 1293–1306.e19. https://doi.org/10.1016/j.cell.2018.04.040

Bagutti, C., Forro, G., Ferralli, J., Rubin, B., & Chiquet-Ehrismann, R. (2003). The intracellular domain of teneurin-2 has a nuclear function and represses zic-1-mediated transcription. *Journal of Cell Science*, *116*(Pt 14), 2957–2966. https://doi.org/10.1242/jcs.00603

Baier, H. (2013). Synaptic laminae in the visual system: molecular mechanisms forming layers of perception. *Annual Review of Cell and Developmental Biology*, *29*, 385–416. https://doi.org/10.1146/annurev-cellbio-101011-155748

Barnett, J. H., & Smoller, J. W. (2009). The genetics of bipolar disorder. *Neuroscience*, *164*(1), 331–343. https://doi.org/10.1016/j.neuroscience.2009.03.080

Baumgartner, S., & Wides, R. (2019). Discovery of Teneurins. *Frontiers in Neuroscience*, *13*, 230. https://doi.org/10.3389/fnins.2019.00230

Becker, C. G., Schweitzer, J., Feldner, J., Becker, T., & Schachner, M. (2003). Tenascin-R as a repellent guidance molecule for developing optic axons in zebrafish. *The Journal of Neuroscience*, *23*(15), 6232–6237.

Beckmann, J., Schubert, R., Chiquet-Ehrismann, R., & Müller, D. J. (2013). Deciphering teneurin domains that facilitate cellular recognition, cell-cell adhesion, and neurite outgrowth using atomic force microscopy-based single-cell force spectroscopy. *Nano Letters*, *13*(6), 2937–2946. https://doi.org/10.1021/nl4013248

Ben-Zur, T., Feige, E., Motro, B., & Wides, R. (2000). The mammalian Odz gene family: homologs of a Drosophila pair-rule gene with expression implying distinct yet overlapping developmental roles. *Developmental Biology*, *217*(1), 107–120. https://doi.org/10.1006/dbio.1999.9532

Benson, D. L., Colman, D. R., & Huntley, G. W. (2001). Molecules, maps and synapse specificity. *Nature Reviews. Neuroscience*, *2*(12), 899–909. https://doi.org/10.1038/35104078

Berns, D. S., DeNardo, L. A., Pederick, D. T., & Luo, L. (2018). Teneurin-3 controls topographic circuit assembly in the hippocampus. *Nature*, *554*(7692), 328–333. https://doi.org/10.1038/nature25463

Biederer, T., Sara, Y., Mozhayeva, M., Atasoy, D., Liu, X., Kavalali, E. T., & Südhof, T. C. (2002). SynCAM, a synaptic adhesion molecule that drives synapse assembly. *Science*, *297*(5586), 1525–1531. https://doi.org/10.1126/science.1072356

Biehlmaier, O., Neuhauss, S. C., & Kohler, K. (2001). Onset and time course of apoptosis in the developing zebrafish retina. *Cell and Tissue Research*, *306*(2), 199–207. https://doi.org/10.1007/s004410100447

Bilotta, J., & Saszik, S. (2001). The zebrafish as a model visual system. *International Journal of Developmental Neuroscience*, *19*(7), 621–629. https://doi.org/10.1016/S0736-5748(01)00050-8

Bonkowsky, J. L., & Chien, C.-B. (2005). Molecular cloning and developmental expression of foxP2 in zebrafish. *Developmental Dynamics*, *234*(3), 740–746. https://doi.org/10.1002/dvdy.20504

Bosco, A., & Linden, R. (1999). BDNF and NT-4 differentially modulate neurite outgrowth in developing retinal ganglion cells. *Journal of Neuroscience Research*.

Boucard, A. A., Maxeiner, S., & Südhof, T. C. (2014). Latrophilins function as heterophilic cell-adhesion molecules by binding to teneurins: regulation by alternative splicing. *The Journal of Biological Chemistry*, *289*(1), 387–402. https://doi.org/10.1074/jbc.M113.504779

Bowden, C. L., Swann, A. C., & Calabrese, J. R. (1997). Maintenance clinical trials in bipolar disorder: design implications of the divalproex-lithium-placebo study. *Psychopharmacology bulletin, 33*, *33*(4), 693.

Bukalo, O., & Dityatev, A. (2012). Synaptic cell adhesion molecules. *Advances in Experimental Medicine and Biology*, *970*, 97–128. https://doi.org/10.1007/978-3-7091-0932-8_5

Burbach, J. P. H., & Meijer, D. H. (2019). Latrophilin's social protein network. *Frontiers in Neuroscience*, *13*, 643. https://doi.org/10.3389/fnins.2019.00643

Burrill, J. D., & Easter, S. S. (1994). Development of the retinofugal projections in the embryonic and larval zebrafish (Brachydanio rerio). *The Journal of Comparative Neurology*, *346*(4), 583–600. https://doi.org/10.1002/cne.903460410

Burrill, J. D., & Easter, S. S. (1995). The first retinal axons and their microenvironment in zebrafish: cryptic pioneers and the pretract. *The Journal of Neuroscience*, *15*(4), 2935–2947.

Bury, L. A. D., & Sabo, S. L. (2010). How it's made: the synapse. *Molecular Interventions*, *10*(5), 282–292. https://doi.org/10.1124/mi.10.5.5

Cajal, S. y. (1972). The structure of the retina. *The structure of the retina*.

Cajal, S. R. y. (1893). La rétine des vertébrés. *La cellule, 9*, *9*, 119–259.

Carvalho, A. F., Firth, J., & Vieta, E. (2020). Bipolar Disorder. *The New England Journal of Medicine*, *383*(1), 58–66. https://doi.org/10.1056/NEJMra1906193

Centanin, L., & Wittbrodt, J. (2014). Retinal neurogenesis. *Development*, *141*(2), 241–244. https://doi.org/10.1242/dev.083642

Cepko, C. L., Austin, C. P., Yang, X., Alexiades, M., & Ezzeddine, D. (1996). Cell fate determination in the vertebrate retina. *Proceedings of the National Academy of Sciences of the United States of America*, *93*(2), 589–595. https://doi.org/10.1073/pnas.93.2.589

Chalupa, L. M., & Günhan, E. (2004). Development of On and Off retinal pathways and retinogeniculate projections. *Progress in Retinal and Eye Research*, *23*(1), 31–51. https://doi.org/10.1016/j.preteyeres.2003.10.001

Chen, X., Vinade, L., Leapman, R. D., Petersen, J. D., Nakagawa, T., Phillips, T. M., … Reese, T. S. (2005). Mass of the postsynaptic density and enumeration of three key molecules. *Proceedings of the National Academy of Sciences of the United States of America*, *102*(32), 11551–11556. https://doi.org/10.1073/pnas.0505359102

Cheung, A., Trevers, K. E., Reyes-Corral, M., Antinucci, P., & Hindges, R. (2019). Expression and roles of teneurins in zebrafish. *Frontiers in Neuroscience*, *13*, 158. https://doi.org/10.3389/fnins.2019.00158

Cline, H. (2003). Sperry and Hebb: oil and vinegar? *Trends in Neurosciences*, *26*(12), 655–661. https://doi.org/10.1016/j.tins.2003.10.005

Cline, H., & Haas, K. (2008). The regulation of dendritic arbor development and plasticity by glutamatergic synaptic input: a review of the synaptotrophic hypothesis. *The Journal of Physiology*, *586*(6), 1509–1517. https://doi.org/10.1113/jphysiol.2007.150029

Cline, H. T., & Constantine-Paton, M. (1989). NMDA receptor antagonists disrupt the retinotectal topographic map. *Neuron*, *3*(4), 413–426. https://doi.org/10.1016/0896-6273(89)90201-8

Cole, L. K., & Ross, L. S. (2001). Apoptosis in the developing zebrafish embryo. *Developmental Biology*, *240*(1), 123–142. https://doi.org/10.1006/dbio.2001.0432

Cook, T. (2003). Cell diversity in the retina: more than meets the eye. *Bioessays: News and Reviews in Molecular, Cellular and Developmental Biology*, *25*(10), 921–925. https://doi.org/10.1002/bies.10356

Coombs, J., van der List, D., Wang, G. Y., & Chalupa, L. M. (2006). Morphological properties of mouse retinal ganglion cells. *Neuroscience*, *140*(1), 123–136. https://doi.org/10.1016/j.neuroscience.2006.02.079

Daly, F. J., & Sandell, J. H. (2000). Inherited retinal degeneration and apoptosis in mutant zebrafish. *The Anatomical Record Part B: The New Anatomist*, *258*(2), 145–155. https://doi.org/10.1002/(SICI)1097-0185(20000201)258:2<145::AID-AR4>3.0.CO;2-G

Dann, J. F., Buhl, E. H., & Peichl, L. (1988). Postnatal dendritic maturation of alpha and beta ganglion cells in cat retina. *The Journal of Neuroscience*, *8*(5), 1485–1499.

De Roo, M., Klauser, P., Garcia, P. M., Poglia, L., & Muller, D. (2008). Spine dynamics and synapse remodeling during LTP and memory processes.

Progress in Brain Research, *169*, 199–207. https://doi.org/10.1016/S0079-6123(07)00011-8

Debanne, D. (2004). Information processing in the axon. *Nature Reviews. Neuroscience*, *5*(4), 304–316. https://doi.org/10.1038/nrn1397

Debski, E. A., & Cline, H. T. (2002). Activity-dependent mapping in the retinotectal projection. *Current Opinion in Neurobiology*, *12*(1), 93–99. https://doi.org/10.1016/S0959-4388(02)00295-7

Del Toro, D., Carrasquero-Ordaz, M. A., Chu, A., Ruff, T., Shahin, M., Jackson, V. A., … Seiradake, E. (2020). Structural Basis of Teneurin-Latrophilin Interaction in Repulsive Guidance of Migrating Neurons. *Cell*, *180*(2), 323–339.e19. https://doi.org/10.1016/j.cell.2019.12.014

DeMarco, E., Xu, N., Baier, H., & Robles, E. (2020). Neuron types in the zebrafish optic tectum labeled by an id2b transgene. *The Journal of Comparative Neurology*, *528*(7), 1173–1188. https://doi.org/10.1002/cne.24815

Demb, J. B., & Singer, J. H. (2015). Functional circuitry of the retina. *Annual review of vision science*, *1*, 263–289. https://doi.org/10.1146/annurev-vision-082114-035334

DePew, A. T., Aimino, M. A., & Mosca, T. J. (2019). The tenets of teneurin: conserved mechanisms regulate diverse developmental processes in the drosophila nervous system. *Frontiers in Neuroscience*, *13*, 27. https://doi.org/10.3389/fnins.2019.00027

Dhande, O. S., & Huberman, A. D. (2014). Retinal ganglion cell maps in the brain: implications for visual processing. *Current Opinion in Neurobiology*, *24*(1), 133–142. https://doi.org/10.1016/j.conb.2013.08.006

Dhande, O. S., Stafford, B. K., Lim, J.-H. A., & Huberman, A. D. (2015). Contributions of retinal ganglion cells to subcortical visual processing and behaviors. *Annual review of vision science*, *1*, 291–328. https://doi.org/10.1146/annurev-vision-082114-035502

Dharmaratne, N., Glendining, K. A., Young, T. R., Tran, H., Sawatari, A., & Leamey, C. A. (2012). Ten-m3 is required for the development of topography in the ipsilateral retinocollicular pathway. *Plos One*, *7*(9), e43083. https://doi.org/10.1371/journal.pone.0043083

Dickson, B. J. (2002). Molecular mechanisms of axon guidance. *Science*, *298*(5600), 1959–1964. https://doi.org/10.1126/science.1072165

Dreher, B., & Robinson, S. R. (1991). *Neuroanatomy of the visual pathways and their development*. Macmillan.

Duan, Y., Wang, S.-H., Song, J., Mironova, Y., Ming, G., Kolodkin, A. L., & Giger, R. J. (2014). Semaphorin 5A inhibits synaptogenesis in early postnatal- and adult-born hippocampal dentate granule cells. *eLife*, *3*. https://doi.org/10.7554/eLife.04390

Dunaevsky, A., & Mason, C. A. (2003). Spine motility: a means towards an end? *Trends in Neurosciences*, *26*(3), 155–160. https://doi.org/10.1016/S0166-2236(03)00028-6

Dyer, M. A., & Cepko, C. L. (2001). p27Kip1 and p57Kip2 regulate proliferation in distinct retinal progenitor cell populations. *The Journal of Neuroscience*, *21*(12), 4259–4271.

Easter, S. S., & Nicola, G. N. (1996). The development of vision in the zebrafish (Danio rerio). *Developmental Biology*, *180*(2), 646–663. https://doi.org/10.1006/dbio.1996.0335

Ehrlich, I., Klein, M., Rumpel, S., & Malinow, R. (2007). PSD-95 is required for activity-driven synapse stabilization. *Proceedings of the National Academy of Sciences of the United States of America*, *104*(10), 4176–4181. https://doi.org/10.1073/pnas.0609307104

El-Husseini, A. E., Schnell, E., Chetkovich, D. M., Nicoll, R. A., & Bredt, D. S. (2000). PSD-95 involvement in maturation of excitatory synapses. *Science*, *290*(5495), 1364–1368.

Famiglietti, E. V., & Kolb, H. (1976). Structural basis for ON-and OFF-center responses in retinal ganglion cells. *Science*, *194*(4261), 193–195. https://doi.org/10.1126/science.959847

Fanous, A. H., Middleton, F. A., Gentile, K., Amdur, R. L., Maher, B. S., Zhao, Z., … Pato, C. N. (2012). Genetic overlap of schizophrenia and bipolar disorder in a high-density linkage survey in the Portuguese Island population. *American Journal of Medical Genetics. Part B, Neuropsychiatric Genetics*, *159B*(4), 383–391. https://doi.org/10.1002/ajmg.b.32041

Faraone, S. V., Glatt, S. J., & Tsuang, M. T. (2003). The genetics of pediatric-onset bipolar disorder. *Biological Psychiatry*, *53*(11), 970–977. https://doi.org/10.1016/s0006-3223(02)01893-0

Feng, K., Zhou, X.-H., Oohashi, T., Mörgelin, M., Lustig, A., Hirakawa, S., … Fässler, R. (2002). All four members of the Ten-m/Odz family of transmembrane proteins form dimers. *The Journal of Biological Chemistry*, *277*(29), 26128–26135. https://doi.org/10.1074/jbc.M203722200

Ferralli, J., Tucker, R. P., & Chiquet-Ehrismann, R. (2018). The teneurin C-terminal domain possesses nuclease activity and is apoptogenic. *Biology open*, *7*(3). https://doi.org/10.1242/bio.031765

Fleisch, V. C., & Neuhauss, S. C. F. (2006). Visual behavior in zebrafish. *Zebrafish*, *3*(2), 191–201. https://doi.org/10.1089/zeb.2006.3.191

Friedman, H. V., Bresler, T., Garner, C. C., & Ziv, N. E. (2000). Assembly of new individual excitatory synapses: time course and temporal order of synaptic molecule recruitment. *Neuron*, *27*(1), 57–69. https://doi.org/10.1016/s0896-6273(00)00009-x

Fu, Z., Washbourne, P., Ortinski, P., & Vicini, S. (2003). Functional excitatory synapses in HEK293 cells expressing neuroligin and glutamate receptors. *Journal of Neurophysiology*, *90*(6), 3950–3957. https://doi.org/10.1152/jn.00647.2003

Funke, L., Dakoji, S., & Bredt, D. S. (2005). Membrane-associated guanylate kinases regulate adhesion and plasticity at cell junctions. *Annual Review of*

Biochemistry, *74*, 219–245. https://doi.org/10.1146/annurev.biochem.74.082803.133339

Furrer, M.-P., Vasenkova, I., Kamiyama, D., Rosado, Y., & Chiba, A. (2007). Slit and Robo control the development of dendrites in Drosophila CNS. *Development*, *134*(21), 3795–3804. https://doi.org/10.1242/dev.02882

Gabriel, J. P., Trivedi, C. A., Maurer, C. M., Ryu, S., & Bollmann, J. H. (2012). Layer-specific targeting of direction-selective neurons in the zebrafish optic tectum. *Neuron*, *76*(6), 1147–1160. https://doi.org/10.1016/j.neuron.2012.12.003

Garcia-Lopez, P., Garcia-Marin, V., & Freire, M. (2010). The histological slides and drawings of cajal. *Frontiers in Neuroanatomy*, *4*, 9. https://doi.org/10.3389/neuro.05.009.2010

Garner, C. C., Zhai, R. G., Gundelfinger, E. D., & Ziv, N. E. (2002). Molecular mechanisms of CNS synaptogenesis. *Trends in Neurosciences*, *25*(5), 243–251. https://doi.org/10.1016/s0166-2236(02)02152-5

Gebhardt, C., Baier, H., & Del Bene, F. (2013). Direction selectivity in the visual system of the zebrafish larva. *Frontiers in Neural Circuits*, *7*, 111. https://doi.org/10.3389/fncir.2013.00111

Glücksmann, A. (1965). Cell death in normal development. *Archives de biologie*, *76*(2), 419–437.

Gollisch, T., & Meister, M. (2010). Eye smarter than scientists believed: neural computations in circuits of the retina. *Neuron*, *65*(2), 150–164. https://doi.org/10.1016/j.neuron.2009.12.009

Gordon-Weeks, P. R., & Fischer, I. (2000). MAP1B expression and microtubule stability in growing and regenerating axons. *Microscopy Research and Technique*, *48*(2), 63–74. https://doi.org/10.1002/(SICI)1097-0029(20000115)48:2<63::AID-JEMT2>3.0.CO;2-1

Hadjieconomou, D., Timofeev, K., & Salecker, I. (2011). A step-by-step guide to visual circuit assembly in Drosophila. *Current Opinion in Neurobiology*, *21*(1), 76–84. https://doi.org/10.1016/j.conb.2010.07.012

Hall, A., & Lalli, G. (2010). Rho and Ras GTPases in axon growth, guidance, and branching. *Cold Spring Harbor Perspectives in Biology*, *2*(2), a001818. https://doi.org/10.1101/cshperspect.a001818

Hall, D. H., & Treinin, M. (2011). How does morphology relate to function in sensory arbors? *Trends in Neurosciences*, *34*(9), 443–451. https://doi.org/10.1016/j.tins.2011.07.004

Harvard University Press, 1987. (n.d.). *The Retina: An Approachable Part of the Brain - John E. Dowling - Google Books*.

He, J., Zhang, G., Almeida, A. D., Cayouette, M., Simons, B. D., & Harris, W. A. (2012). How variable clones build an invariant retina. *Neuron*, *75*(5), 786–798. https://doi.org/10.1016/j.neuron.2012.06.033

Helmchen, F. (2009). Two-Photon Functional Imaging of Neuronal Activity. In R. D. Frostig, R. D. Frostig, R. D. Frostig, R. D. Frostig, & R. D. Frostig (eds.), *In Vivo Optical Imaging of Brain Function* (2nd ed.). Boca Raton (FL): CRC Press/Taylor & Francis.

Hindges, R., McLaughlin, T., Genoud, N., Henkemeyer, M., & O'Leary, D. D. M. (2002). EphB forward signaling controls directional branch extension and arborization required for dorsal-ventral retinotopic mapping. *Neuron*, *35*(3), 475–487. https://doi.org/10.1016/s0896-6273(02)00799-7

Hipfner, D. R., & Cohen, S. M. (2004). Connecting proliferation and apoptosis in development and disease. *Nature Reviews. Molecular Cell Biology*, *5*(10), 805–815. https://doi.org/10.1038/nrm1491

Holt, C. E. (1989). A single-cell analysis of early retinal ganglion cell differentiation in Xenopus: from soma to axon tip. *The Journal of Neuroscience*, *9*(9), 3123–3145.

Hong, W., Mosca, T. J., & Luo, L. (2012). Teneurins instruct synaptic partner matching in an olfactory map. *Nature*, *484*(7393), 201–207. https://doi.org/10.1038/nature10926

Hong, Y. K., Kim, I.-J., & Sanes, J. R. (2011). Stereotyped axonal arbors of retinal ganglion cell subsets in the mouse superior colliculus. *The Journal of Comparative Neurology*, *519*(9), 1691–1711. https://doi.org/10.1002/cne.22595

Hoogenraad, C. C., Milstein, A. D., Ethell, I. M., Henkemeyer, M., & Sheng, M. (2005). GRIP1 controls dendrite morphogenesis by regulating EphB receptor trafficking. *Nature Neuroscience*, *8*(7), 906–915. https://doi.org/10.1038/nn1487

Hosen, M. J., Vanakker, O. M., Willaert, A., Huysseune, A., Coucke, P., & De Paepe, A. (2013). Zebrafish models for ectopic mineralization disorders: practical issues from morpholino design to post-injection observations. *Frontiers in genetics*, *4*, 74. https://doi.org/10.3389/fgene.2013.00074

Hua, M., Li-Jian, Y., & Ya, J. (2005). A Quantitative Analysis of Modulation of the Fast Excitatory Postsynaptic Potential of Neurons in Rat Sympathetic Ganglia by a Low-Intensity Laser. *Chinese Physics Letters*, *22*(9), 2433–2436. https://doi.org/10.1088/0256-307X/22/9/081

Huang, X., Sun, J., Zhao, T., Wu, K.-W., Watanabe, K., Xiao, Z.-C., … Fan, M. (2011). Loss of NB-3 aggravates cerebral ischemia by impairing neuron survival and neurite growth. *Stroke*, *42*(10), 2910–2916. https://doi.org/10.1161/STROKEAHA.110.609560

Huberman, A. D., Clandinin, T. R., & Baier, H. (2010). Molecular and cellular mechanisms of lamina-specific axon targeting. *Cold Spring Harbor Perspectives in Biology*, *2*(3), a001743. https://doi.org/10.1101/cshperspect.a001743

Huberman, A. D., Feller, M. B., & Chapman, B. (2008). Mechanisms underlying development of visual maps and receptive fields. *Annual Review of Neuroscience*, *31*, 479–509. https://doi.org/10.1146/annurev.neuro.31.060407.125533

Huberman, A. D., Wei, W., Elstrott, J., Stafford, B. K., Feller, M. B., & Barres, B. A. (2009). Genetic identification of an On-Off direction-selective retinal ganglion cell subtype reveals a layer-specific subcortical map of posterior motion. *Neuron*, *62*(3), 327–334. https://doi.org/10.1016/j.neuron.2009.04.014

Husi, H., Ward, M. A., Choudhary, J. S., Blackstock, W. P., & Grant, S. G. (2000). Proteomic analysis of NMDA receptor-adhesion protein signaling complexes. *Nature Neuroscience*, *3*(7), 661–669. https://doi.org/10.1038/76615

Husić, M., Barsyte-Lovejoy, D., & Lovejoy, D. A. (2019). Teneurin C-Terminal Associated Peptide (TCAP)-1 and Latrophilin Interaction in HEK293 Cells: Evidence for Modulation of Intercellular Adhesion. *Frontiers in endocrinology*, *10*, 22. https://doi.org/10.3389/fendo.2019.00022

Jackson, V. A., Meijer, D. H., Carrasquero, M., van Bezouwen, L. S., Lowe, E. D., Kleanthous, C., … Seiradake, E. (2018). Structures of Teneurin adhesion receptors reveal an ancient fold for cell-cell interaction. *Nature Communications*, *9*(1), 1079. https://doi.org/10.1038/s41467-018-03460-0

Jan, Y.-N., & Jan, L. Y. (2010). Branching out: mechanisms of dendritic arborization. *Nature Reviews. Neuroscience*, *11*(5), 316–328. https://doi.org/10.1038/nrn2836

Javaherian, A., & Cline, H. T. (2005). Coordinated motor neuron axon growth and neuromuscular synaptogenesis are promoted by CPG15 in vivo. *Neuron*, *45*(4), 505–512. https://doi.org/10.1016/j.neuron.2004.12.051

Johnston, J., Seibel, S.-H., Darnet, L. S. A., Renninger, S., Orger, M., & Lagnado, L. (2019). A retinal circuit generating a dynamic predictive code for oriented features. *Neuron*, *102*(6), 1211–1222.e3. https://doi.org/10.1016/j.neuron.2019.04.002

Jontes, J. D., & Phillips, G. R. (2006). Selective stabilization and synaptic specificity: a new cell-biological model. *Trends in Neurosciences*, *29*(4), 186–191. https://doi.org/10.1016/j.tins.2006.02.002

Karlstrom, R. O., Trowe, T., Klostermann, S., Baier, H., Brand, M., Crawford, A. D., … Bonhoeffer, F. (1996). Zebrafish mutations affecting retinotectal axon pathfinding. *Development*, *123*, 427–438.

Katz, L. C., & Shatz, C. J. (1996). Synaptic activity and the construction of cortical circuits. *Science*, *274*(5290), 1133–1138. https://doi.org/10.1126/science.274.5290.1133

Kennedy, M. B. (2000). Signal-processing machines at the postsynaptic density. *Science*, *290*(5492), 750–754. https://doi.org/10.1126/science.290.5492.750

Kenzelmann, D., Chiquet-Ehrismann, R., Leachman, N. T., & Tucker, R. P. (2008). Teneurin-1 is expressed in interconnected regions of the developing brain and is processed in vivo. *BMC Developmental Biology*, *8*, 30. https://doi.org/10.1186/1471-213X-8-30

Kenzelmann-Broz, D., Tucker, R. P., Leachman, N. T., & Chiquet-Ehrismann, R. (2010). The expression of teneurin-4 in the avian embryo: potential roles in patterning of the limb and nervous system. *The International Journal of Developmental Biology*, *54*(10), 1509–1516. https://doi.org/10.1387/ijdb.103139dk

Kim, I.-J., Zhang, Y., Meister, M., & Sanes, J. R. (2010). Laminar restriction of retinal ganglion cell dendrites and axons: subtype-specific developmental patterns revealed with transgenic markers. *The Journal of Neuroscience*, *30*(4), 1452–1462. https://doi.org/10.1523/JNEUROSCI.4779-09.2010

Kinoshita, M., & Ito, E. (2006). Roles of periventricular neurons in retinotectal transmission in the optic tectum. *Progress in Neurobiology*, *79*(2), 112–121. https://doi.org/10.1016/j.pneurobio.2006.06.002

Kinoshita, M., Ito, E., Urano, A., Ito, H., & Yamamoto, N. (2006). Periventricular efferent neurons in the optic tectum of rainbow trout. *The Journal of Comparative Neurology*, *499*(4), 546–564. https://doi.org/10.1002/cne.21080

Kölsch, Y., Hahn, J., Sappington, A., Stemmer, M., Fernandes, A. M., Helmbrecht, T. O., … Baier, H. (2020). Molecular classification of zebrafish retinal ganglion

cells links genes to cell types to behavior. *BioRxiv*. https://doi.org/10.1101/2020.07.29.226050

Kong, J.-H., Fish, D. R., Rockhill, R. L., & Masland, R. H. (2005). Diversity of ganglion cells in the mouse retina: unsupervised morphological classification and its limits. *The Journal of Comparative Neurology*, *489*(3), 293–310. https://doi.org/10.1002/cne.20631

Krishnaswamy, A., Yamagata, M., Duan, X., Hong, Y. K., & Sanes, J. R. (2015). Sidekick 2 directs formation of a retinal circuit that detects differential motion. *Nature*, *524*(7566), 466–470. https://doi.org/10.1038/nature14682

LaVail, J. H., & Cowan, W. M. (1971). The development of the chick optic tectum. II. Autoradiographic studies. *Brain Research*, *28*(3), 421–441. https://doi.org/10.1016/0006-8993(71)90054-0

Leachman, N. T. (2010). The processing and expression of teneurin-3 and a related protein during development. *The processing and expression of teneurin-3 and a related protein during development*.

Leamey, C. A., Glendining, K. A., Kreiman, G., Kang, N.-D., Wang, K. H., Fassler, R., … Sur, M. (2008). Differential gene expression between sensory neocortical areas: potential roles for Ten_m3 and Bcl6 in patterning visual and somatosensory pathways. *Cerebral Cortex*, *18*(1), 53–66. https://doi.org/10.1093/cercor/bhm031

Leamey, C. A., Merlin, S., Lattouf, P., Sawatari, A., Zhou, X., Demel, N., … Fässler, R. (2007). Ten_m3 regulates eye-specific patterning in the mammalian visual pathway and is required for binocular vision. *PLoS Biology*, *5*(9), e241. https://doi.org/10.1371/journal.pbio.0050241

Leamey, C. A., & Sawatari, A. (2014). The teneurins: new players in the generation of visual topography. *Seminars in Cell & Developmental Biology*, *35*, 173–179. https://doi.org/10.1016/j.semcdb.2014.08.007

Lee, H. O., & Norden, C. (2013). Mechanisms controlling arrangements and movements of nuclei in pseudostratified epithelia. *Trends in Cell Biology*, *23*(3), 141–150. https://doi.org/10.1016/j.tcb.2012.11.001

Lettvin, J., Maturana, H., McCulloch, W., & Pitts, W. (1959). What the Frog's Eye Tells the Frog's Brain. *Proceedings of the IRE*, *47*(11), 1940–1951. https://doi.org/10.1109/JRPROC.1959.287207

Levine, A., Bashan-Ahrend, A., Budai-Hadrian, O., Gartenberg, D., Menasherow, S., & Wides, R. (1994). Odd Oz: a novel Drosophila pair rule gene. *Cell*, *77*(4), 587–598. https://doi.org/10.1016/0092-8674(94)90220-8

Lichtenstein, P., Yip, B. H., Björk, C., Pawitan, Y., Cannon, T. D., Sullivan, P. F., & Hultman, C. M. (2009). Common genetic determinants of schizophrenia and bipolar disorder in Swedish families: a population-based study. *The Lancet*, *373*(9659), 234–239. https://doi.org/10.1016/S0140-6736(09)60072-6

Linden, R., Rehen, S. K., & Chiarini, L. B. (1999). Apoptosis in developing retinal tissue. *Progress in Retinal and Eye Research*, *18*(2), 133–165. https://doi.org/10.1016/s1350-9462(98)00020-2

Lipton, S. A., Frosch, M. P., Phillips, M. D., Tauck, D. L., & Aizenman, E. (1988). Nicotinic antagonists enhance process outgrowth by rat retinal ganglion cells in culture. *Science*, *239*(4845), 1293–1296. https://doi.org/10.1126/science.3344435

Livesey, F. J., & Cepko, C. L. (2001). Vertebrate neural cell-fate determination: lessons from the retina. *Nature Reviews. Neuroscience*, *2*(2), 109–118. https://doi.org/10.1038/35053522

Livesey, R., & Cepko, C. (2001). Developing order. *Nature*, *413*(6855), 471–473. https://doi.org/10.1038/35097186

Lom, B., & Cohen-Cory, S. (1999). Brain-derived neurotrophic factor differentially regulates retinal ganglion cell dendritic and axonal arborization in vivo. *The Journal of Neuroscience*, *19*(22), 9928–9938.

Maletic, V., & Raison, C. (2014). Integrated neurobiology of bipolar disorder. *Frontiers in psychiatry*, *5*, 98. https://doi.org/10.3389/fpsyt.2014.00098

Manji, H. K., Quiroz, J. A., Payne, J. L., Singh, J., Lopes, B. P., Viegas, J. S., & Zarate, C. A. (2003). The underlying neurobiology of bipolar disorder. *World psychiatry : official journal of the World Psychiatric Association (WPA)*, *2*(3), 136–146.

Manor, Y., Gonczarowski, J., & Segev, I. (1991). Propagation of action potentials along complex axonal trees. Model and implementation. *Biophysical Journal*, *60*(6), 1411–1423. https://doi.org/10.1016/S0006-3495(91)82178-6

Martersteck, E. M., Hirokawa, K. E., Evarts, M., Bernard, A., Duan, X., Li, Y., … Harris, J. A. (2017). Diverse central projection patterns of retinal ganglion cells. *Cell reports*, *18*(8), 2058–2072. https://doi.org/10.1016/j.celrep.2017.01.075

Marvin, J. S., Borghuis, B. G., Tian, L., Cichon, J., Harnett, M. T., Akerboom, J., … Looger, L. L. (2013). An optimized fluorescent probe for visualizing glutamate neurotransmission. *Nature Methods*, *10*(2), 162–170. https://doi.org/10.1038/nmeth.2333

Masland, R. H. (2012). The neuronal organization of the retina. *Neuron*, *76*(2), 266–280. https://doi.org/10.1016/j.neuron.2012.10.002

Matsuoka, R. L., Nguyen-Ba-Charvet, K. T., Parray, A., Badea, T. C., Chédotal, A., & Kolodkin, A. L. (2011). Transmembrane semaphorin signalling controls laminar stratification in the mammalian retina. *Nature*, *470*(7333), 259–263. https://doi.org/10.1038/nature09675

McAllister, A. K. (2000). Cellular and molecular mechanisms of dendrite growth. *Cerebral Cortex*, *10*(10), 963–973. https://doi.org/10.1093/cercor/10.10.963

McLaughlin, T., & O'Leary, D. D. M. (2005). Molecular gradients and development of retinotopic maps. *Annual Review of Neuroscience*, *28*, 327–355. https://doi.org/10.1146/annurev.neuro.28.061604.135714

Meek, J., & Schellart, N. A. (1978). A Golgi study of goldfish optic tectum. *The Journal of Comparative Neurology*, *182*(1), 89–122. https://doi.org/10.1002/cne.901820107

Melnattur, K. V., & Lee, C.-H. (2011). Visual circuit assembly in Drosophila. *Developmental Neurobiology*, *71*(12), 1286–1296. https://doi.org/10.1002/dneu.20894

Merlin, S., Horng, S., Marotte, L. R., Sur, M., Sawatari, A., & Leamey, C. A. (2013). Deletion of Ten-m3 induces the formation of eye dominance domains in mouse visual cortex. *Cerebral Cortex*, *23*(4), 763–774. https://doi.org/10.1093/cercor/bhs030

Mey, J., & Thanos, S. (2000). Development of the visual system of the chick. *Brain Research Reviews*, *32*(2-3), 343–379. https://doi.org/10.1016/S0165-0173(99)00022-3

Meyer, M. P., & Smith, S. J. (2006). Evidence from in vivo imaging that synaptogenesis guides the growth and branching of axonal arbors by two distinct mechanisms. *The Journal of Neuroscience*, *26*(13), 3604–3614. https://doi.org/10.1523/JNEUROSCI.0223-06.2006

Meyer, M. P., Trimmer, J. S., Gilthorpe, J. D., & Smith, S. J. (2005). Characterization of zebrafish PSD-95 gene family members. *Journal of Neurobiology*, *63*(2), 91–105. https://doi.org/10.1002/neu.20118

Mieda, M., Kikuchi, Y., Hirate, Y., Aoki, M., & Okamoto, H. (1999). Compartmentalized expression of zebrafish ten-m3 and ten-m4, homologues of the Drosophila ten(m)/odd Oz gene, in the central nervous system. *Mechanisms of Development*, *87*(1-2), 223–227. https://doi.org/10.1016/s0925-4773(99)00155-0

Minet, A. D., Rubin, B. P., Tucker, R. P., Baumgartner, S., & Chiquet-Ehrismann, R. (1999). Teneurin-1, a vertebrate homologue of the Drosophila pair-rule gene ten-m, is a neuronal protein with a novel type of heparin-binding domain. *Journal of Cell Science*.

Missaire, M., & Hindges, R. (2015). The role of cell adhesion molecules in visual circuit formation: from neurite outgrowth to maps and synaptic specificity. *Developmental Neurobiology*, *75*(6), 569–583. https://doi.org/10.1002/dneu.22267

Missler, M., Südhof, T. C., & Biederer, T. (2012). Synaptic cell adhesion. *Cold Spring Harbor Perspectives in Biology*, *4*(4), a005694. https://doi.org/10.1101/cshperspect.a005694

Montague, P. R., & Friedlander, M. J. (1991). Morphogenesis and territorial coverage by isolated mammalian retinal ganglion cells. *The Journal of Neuroscience*, *11*(5), 1440–1457.

Mosca, T. J. (2015). On the Teneurin track: a new synaptic organization molecule emerges. *Frontiers in Cellular Neuroscience*, *9*, 204. https://doi.org/10.3389/fncel.2015.00204

Mosca, T. J., Hong, W., Dani, V. S., Favaloro, V., & Luo, L. (2012). Trans-synaptic Teneurin signalling in neuromuscular synapse organization and target choice. *Nature*, *484*(7393), 237–241. https://doi.org/10.1038/nature10923

Mosca, T. J., & Luo, L. (2014). Synaptic organization of the Drosophila antennal lobe and its regulation by the Teneurins. *eLife*, *3*, e03726. https://doi.org/10.7554/eLife.03726

Mumm, J. S., Williams, P. R., Godinho, L., Koerber, A., Pittman, A. J., Roeser, T., … Wong, R. O. L. (2006). In vivo imaging reveals dendritic targeting of laminated afferents by zebrafish retinal ganglion cells. *Neuron*, *52*(4), 609–621. https://doi.org/10.1016/j.neuron.2006.10.004

Nakata, T., Terada, S., & Hirokawa, N. (1998). Visualization of the dynamics of synaptic vesicle and plasma membrane proteins in living axons. *The Journal of Cell Biology*, *140*(3), 659–674. https://doi.org/10.1083/jcb.140.3.659

Nava, C., Lamari, F., Héron, D., Mignot, C., Rastetter, A., Keren, B., … Depienne, C. (2012). Analysis of the chromosome X exome in patients with autism spectrum disorders identified novel candidate genes, including TMLHE. *Translational psychiatry*, *2*, e179. https://doi.org/10.1038/tp.2012.102

Nawrocki, L. W. (1985). Development of the neural retina in the zebrafish, Brachydanio rerio (neurogenesis). Retrieved April 20, 2021, from https://www.elibrary.ru/item.asp?id=7452023

Neary, J. L., Perez, S. M., Peterson, K., Lodge, D. J., & Carless, M. A. (2017). Comparative analysis of MBD-seq and MeDIP-seq and estimation of gene expression changes in a rodent model of schizophrenia. *Genomics*, *109*(3-4), 204–213. https://doi.org/10.1016/j.ygeno.2017.03.004

Nevin, L. M., Robles, E., Baier, H., & Scott, E. K. (2010). Focusing on optic tectum circuitry through the lens of genetics. *BMC Biology*, *8*, 126. https://doi.org/10.1186/1741-7007-8-126

Nevin, L. M., Taylor, M. R., & Baier, H. (2008). Hardwiring of fine synaptic layers in the zebrafish visual pathway. *Neural Development*, *3*, 36. https://doi.org/10.1186/1749-8104-3-36

Nguyen-Ba-Charvet, K. T., & Chédotal, A. (2014). Development of retinal layers. Comptes Rendus Biologies, 337(3), 153–159. https://doi.org/10.1016/j.crvi.2013.11.010

Niell, C. M., Meyer, M. P., & Smith, S. J. (2004). In vivo imaging of synapse formation on a growing dendritic arbor. *Nature Neuroscience*, *7*(3), 254–260. https://doi.org/10.1038/nn1191

Niell, C. M., & Smith, S. J. (2005). Functional imaging reveals rapid development of visual response properties in the zebrafish tectum. *Neuron*, *45*(6), 941–951. https://doi.org/10.1016/j.neuron.2005.01.047

Nikolaou, N., Lowe, A. S., Walker, A. S., Abbas, F., Hunter, P. R., Thompson, I. D., & Meyer, M. P. (2012). Parametric functional maps of visual inputs to the tectum. *Neuron*, *76*(2), 317–324. https://doi.org/10.1016/j.neuron.2012.08.040

Nikolaou, N., & Meyer, M. P. (2012). Imaging circuit formation in zebrafish. *Developmental Neurobiology*, *72*(3), 346–357. https://doi.org/10.1002/dneu.20874

Nunes, S. M., Ferralli, J., Choi, K., Brown-Luedi, M., Minet, A. D., & Chiquet-Ehrismann, R. (2005). The intracellular domain of teneurin-1 interacts with MBD1 and CAP/ponsin resulting in subcellular codistribution and translocation to the nuclear matrix. *Experimental Cell Research*, *305*(1), 122–132. https://doi.org/10.1016/j.yexcr.2004.12.020

O'Rourke, N. A., Cline, H. T., & Fraser, S. E. (1994). Rapid remodeling of retinal arbors in the tectum with and without blockade of synaptic transmission. *Neuron*, *12*(4), 921–934. https://doi.org/10.1016/0896-6273(94)90343-3

Olsen, T. K., & Baryawno, N. (2018). Introduction to Single-Cell RNA Sequencing. *Current Protocols in Molecular Biology*, *122*(1), e57. https://doi.org/10.1002/cpmb.57

Oohashi, T., Zhou, X. H., Feng, K., Richter, B., Mörgelin, M., Perez, M. T., … Fässler, R. (1999). Mouse ten-m/Odz is a new family of dimeric type II transmembrane proteins expressed in many tissues. *The Journal of Cell Biology*, *145*(3), 563–577. https://doi.org/10.1083/jcb.145.3.563

Oppenheim, R. W., Flavell, R. A., Vinsant, S., Prevette, D., Kuan, C. Y., & Rakic, P. (2001). Programmed cell death of developing mammalian neurons after genetic deletion of caspases. *The Journal of Neuroscience*, *21*(13), 4752–4760.

Paoloni-Giacobino, A., Bottani, A., & Dahoun, S. P. (1999). Pure partial trisomy 5q33-->5q35 resulting from the adjacent-1 segregation of a paternal (5;14)(q33;p12) translocation. *Annales de genetique*, *42*(3), 166–169.

Peng, Y.-R., Shekhar, K., Yan, W., Herrmann, D., Sappington, A., Bryman, G. S., … Sanes, J. R. (2019). Molecular classification and comparative taxonomics of foveal and peripheral cells in primate retina. *Cell*, *176*(5), 1222–1237.e22. https://doi.org/10.1016/j.cell.2019.01.004

Perez, R. G., & Halfter, W. (1993). Tenascin in the developing chick visual system: distribution and potential role as a modulator of retinal axon growth. *Developmental Biology*, *156*(1), 278–292. https://doi.org/10.1006/dbio.1993.1076

Perry, V. H., Henderson, Z., & Linden, R. (1983). Postnatal changes in retinal ganglion cell and optic axon populations in the pigmented rat. *The Journal of Comparative Neurology*, *219*(3), 356–368. https://doi.org/10.1002/cne.902190309

Pinto-Costa, R., & Sousa, M. M. (2021). Microtubules, actin and cytolinkers: how to connect cytoskeletons in the neuronal growth cone. *Neuroscience Letters*, *747*, 135693. https://doi.org/10.1016/j.neulet.2021.135693

Potts, R. A., Dreher, B., & Bennett, M. R. (1982). The loss of ganglion cells in the developing retina of the rat. *Developmental Brain Research*, *3*(3), 481–486. https://doi.org/10.1016/0165-3806(82)90013-X

Psychiatric GWAS Consortium Bipolar Disorder Working Group. (2011). Large-scale genome-wide association analysis of bipolar disorder identifies a new susceptibility locus near ODZ4. *Nature Genetics*, *43*(10), 977–983. https://doi.org/10.1038/ng.943

Psychology Press, 2005. (n.d.). *The Organization of Behavior: A Neuropsychological Theory - D.O. Hebb - Google Books*.

Ramoa, A. S., Campbell, G., & Shatz, C. J. (1988). Dendritic growth and remodeling of cat retinal ganglion cells during fetal and postnatal development. *The Journal of Neuroscience*, *8*(11), 4239–4261.

Reid, R. M., Freij, K. W., Maples, J. C., & Biga, P. R. (2019). Teneurins and Teneurin C-Terminal Associated Peptide (TCAP) in Metabolism: What's Known in Fish? *Frontiers in Neuroscience*, *13*, 177. https://doi.org/10.3389/fnins.2019.00177

Remé, C. E., Grimm, C., Hafezi, F., Wenzel, A., & Williams, T. P. (2000). Apoptosis in the Retina: The Silent Death of Vision. *News in physiological sciences : an international journal of physiology produced jointly by the International Union of Physiological Sciences and the American Physiological Society*, *15*, 120–124. https://doi.org/10.1152/physiologyonline.2000.15.3.120

Ren, J. Q., McCarthy, W. R., Zhang, H., Adolph, A. R., & Li, L. (2002). Behavioral visual responses of wild-type and hypopigmented zebrafish. *Vision Research*, *42*(3), 293–299. https://doi.org/10.1016/s0042-6989(01)00284-x

Rheaume, B. A., Jereen, A., Bolisetty, M., Sajid, M. S., Yang, Y., Renna, K., … Trakhtenberg, E. F. (2018). Single cell transcriptome profiling of retinal ganglion cells identifies cellular subtypes. *Nature Communications*, *9*(1), 2759. https://doi.org/10.1038/s41467-018-05134-3

Ribon, V., Herrera, R., Kay, B. K., & Saltiel, A. R. (1998). A role for CAP, a novel, multifunctional Src homology 3 domain-containing protein in formation of actin stress fibers and focal adhesions. *The Journal of Biological Chemistry*, *273*(7), 4073–4080. https://doi.org/10.1074/jbc.273.7.4073

Richardson, R., Tracey-White, D., Webster, A., & Moosajee, M. (2017). The zebrafish eye-a paradigm for investigating human ocular genetics. *Eye*, *31*(1), 68–86. https://doi.org/10.1038/eye.2016.198

Robles, E., Filosa, A., & Baier, H. (2013). Precise lamination of retinal axons generates multiple parallel input pathways in the tectum. *The Journal of Neuroscience*, *33*(11), 5027–5039. https://doi.org/10.1523/JNEUROSCI.4990-12.2013

Robles, E., Laurell, E., & Baier, H. (2014). The retinal projectome reveals brain-area-specific visual representations generated by ganglion cell diversity. *Current Biology*, *24*(18), 2085–2096. https://doi.org/10.1016/j.cub.2014.07.080

Rodieck. (n.d.). The First Steps in Seeing.

Rosso, S. B., Sussman, D., Wynshaw-Boris, A., & Salinas, P. C. (2005). Wnt signaling through Dishevelled, Rac and JNK regulates dendritic development. *Nature Neuroscience*, *8*(1), 34–42. https://doi.org/10.1038/nn1374

Rouse, H. (2015). tectum growth in zebrafish.

Rubin, B P, Tucker, R. P., Martin, D., & Chiquet-Ehrismann, R. (1999). Teneurins: a novel family of neuronal cell surface proteins in vertebrates, homologous to the Drosophila pair-rule gene product Ten-m. *Developmental Biology*, *216*(1), 195–209. https://doi.org/10.1006/dbio.1999.9503

Rubin, Beatrix P., Tucker, R. P., Brown-Luedi, M., Martin, D., & Chiquet-Ehrismann, R. (2002). Teneurin 2 is expressed by the neurons of the thalamofugal visual system in situ and promotes homophilic cell-cell adhesion in vitro. *Development*.

Ruthazer, E. S., Akerman, C. J., & Cline, H. T. (2003). Control of axon branch dynamics by correlated activity in vivo. *Science*, *301*(5629), 66–70. https://doi.org/10.1126/science.1082545

Ruthazer, E. S., & Cline, H. T. (2004). Insights into activity-dependent map formation from the retinotectal system: a middle-of-the-brain perspective. *Journal of Neurobiology*, *59*(1), 134–146. https://doi.org/10.1002/neu.10344

Sabo, S. L., Gomes, R. A., & McAllister, A. K. (2006). Formation of presynaptic terminals at predefined sites along axons. *The Journal of Neuroscience*, *26*(42), 10813–10825. https://doi.org/10.1523/JNEUROSCI.2052-06.2006

Sakurai, T. (2017). The role of cell adhesion molecules in brain wiring and neuropsychiatric disorders. *Molecular and Cellular Neurosciences*, *81*, 4–11. https://doi.org/10.1016/j.mcn.2016.08.005

Sanes, J R, & Yamagata, M. (1999). Formation of lamina-specific synaptic connections. *Current Opinion in Neurobiology*, *9*(1), 79–87. https://doi.org/10.1016/S0959-4388(99)80010-5

Sanes, Joshua R, & Masland, R. H. (2015). The types of retinal ganglion cells: current status and implications for neuronal classification. *Annual Review of Neuroscience*, *38*, 221–246. https://doi.org/10.1146/annurev-neuro-071714-034120

Sanes, Joshua R, & Yamagata, M. (2009). Many paths to synaptic specificity. *Annual Review of Cell and Developmental Biology*, *25*, 161–195. https://doi.org/10.1146/annurev.cellbio.24.110707.175402

Sanes, Joshua R, & Zipursky, S. L. (2010). Design principles of insect and vertebrate visual systems. *Neuron*, *66*(1), 15–36. https://doi.org/10.1016/j.neuron.2010.01.018

Scaife, R. M., & Langdon, W. Y. (2000). c-Cbl localizes to actin lamellae and regulates lamellipodia formation and cell morphology. *Journal of Cell Science*.

Scheiffele, P. (2003). Cell-cell signaling during synapse formation in the CNS. *Annual Review of Neuroscience*, *26*, 485–508. https://doi.org/10.1146/annurev.neuro.26.043002.094940

Schmidt, J. T., & Buzzard, M. (1993). Activity-driven sharpening of the retinotectal projection in goldfish: development under stroboscopic illumination prevents sharpening. *Journal of Neurobiology*, *24*(3), 384–399. https://doi.org/10.1002/neu.480240310

Schmidt, J. T., Buzzard, M., Borress, R., & Dhillon, S. (2000). MK801 increases retinotectal arbor size in developing zebrafish without affecting kinetics of branch elimination and addition. *Journal of Neurobiology*, *42*(3), 303–314. https://doi.org/10.1002/(SICI)1097-4695(20000215)42:3<303::AID-NEU2>3.0.CO;2-A

Schmitt, E. A., & Dowling, J. E. (1999). Early retinal development in the zebrafish, Danio rerio: light and electron microscopic analyses. *The Journal of Comparative Neurology*, *404*(4), 515–536. https://doi.org/10.1002/(SICI)1096-9861(19990222)404:4<515::AID-CNE8>3.0.CO;2-A

Schulte, D., & Bumsted-O'Brien, K. M. (2008). Molecular mechanisms of vertebrate retina development: implications for ganglion cell and photoreceptor patterning. *Brain Research*, *1192*, 151–164. https://doi.org/10.1016/j.brainres.2007.04.079

Sekar, A., Bialas, A. R., de Rivera, H., Davis, A., Hammond, T. R., Kamitaki, N., … McCarroll, S. A. (2016). Schizophrenia risk from complex variation of complement component 4. *Nature*, *530*(7589), 177–183. https://doi.org/10.1038/nature16549

Sernagor, E., Eglen, S. J., & Wong, R. O. (2001). Development of retinal ganglion cell structure and function. *Progress in Retinal and Eye Research*, *20*(2), 139–174. https://doi.org/10.1016/S1350-9462(00)00024-0

Seung, H. S., & Sümbül, U. (2014). Neuronal cell types and connectivity: lessons from the retina. *Neuron*, *83*(6), 1262–1272. https://doi.org/10.1016/j.neuron.2014.08.054

Shah, R., Medina-Martinez, O., Chu, L.-F., Samaco, R. C., & Jamrich, M. (2006). Expression of FoxP2 during zebrafish development and in the adult brain. *The International Journal of Developmental Biology*, *50*(4), 435–438. https://doi.org/10.1387/ijdb.052065rs

Shapira, M., Zhai, R. G., Dresbach, T., Bresler, T., Torres, V. I., Gundelfinger, E. D., … Garner, C. C. (2003). Unitary assembly of presynaptic active zones from Piccolo-Bassoon transport vesicles. *Neuron*, *38*(2), 237–252. https://doi.org/10.1016/s0896-6273(03)00207-1

Shapiro, L., & Colman, D. R. (1999). The diversity of cadherins and implications for a synaptic adhesive code in the CNS. *Neuron*, *23*(3), 427–430. https://doi.org/10.1016/s0896-6273(00)80796-5

Shen, K. (2004). Molecular mechanisms of target specificity during synapse formation. *Current Opinion in Neurobiology*, *14*(1), 83–88. https://doi.org/10.1016/j.conb.2004.01.007

Shen, K., & Bargmann, C. I. (2003). The immunoglobulin superfamily protein SYG-1 determines the location of specific synapses in C. elegans. *Cell*, *112*(5), 619–630. https://doi.org/10.1016/s0092-8674(03)00113-2

Shen, K., & Scheiffele, P. (2010). Genetics and cell biology of building specific synaptic connectivity. *Annual Review of Neuroscience*, *33*, 473–507. https://doi.org/10.1146/annurev.neuro.051508.135302

Sholl, D. A. (1953). Dendritic organization in the neurons of the visual and motor cortices of the cat. *Journal of Anatomy*, *87*(4), 387–406.

Sklar, P., Ripke, S., Scott, L. J., Andreassen, O. A., & Cichon, S. (2011). Psychiatric GWAS Consortium Bipolar Disorder Working Group. Large-scale genome-wide association analysis of bipolar disorder identifies a new …. N*at Genet, 43, 43,* 977–983.

Sperry, R. W. (1963). CHEMOAFFINITY IN THE ORDERLY GROWTH OF NERVE FIBER PATTERNS AND CONNECTIONS. *Proceedings of the National Academy of Sciences of the United States of America*, *50*, 703–710. https://doi.org/10.1073/pnas.50.4.703

Stevens, C. F. (1998). Neuronal diversity: too many cell types for comfort? *Current Biology*, *8*(20), R708–10. https://doi.org/10.1016/s0960-9822(98)70454-3

Storey, E., Bahlo, M., Fahey, M., Sisson, O., Lueck, C. J., & Gardner, R. J. M. (2009). A new dominantly inherited pure cerebellar ataxia, SCA 30. *Journal of Neurology, Neurosurgery, and Psychiatry*, *80*(4), 408–411. https://doi.org/10.1136/jnnp.2008.159459

Stuermer, C. A. (1988). Retinotopic organization of the developing retinotectal projection in the zebrafish embryo. *The Journal of Neuroscience*, *8*(12), 4513–4530.

Sun, W., Li, N., & He, S. (2002). Large-scale morphological survey of mouse retinal ganglion cells. *The Journal of Comparative Neurology*, *451*(2), 115–126. https://doi.org/10.1002/cne.10323

Suzuki, N., Mizuniwa, C., Ishii, K., Nakagawa, Y., Tsuji, K., Muneta, T., … Akazawa, C. (2014). Teneurin-4, a transmembrane protein, is a novel regulator that suppresses chondrogenic differentiation. *Journal of Orthopaedic Research*, *32*(7), 915–922. https://doi.org/10.1002/jor.22616

Tan, L. A., Chand, D., De Almeida, R., Xu, M., De Lannoy, L., & Lovejoy, D. A. (2012). Modulation of neuroplastic changes and corticotropin-releasing factor-associated behavior by a phylogenetically ancient and conserved peptide family. *General and Comparative Endocrinology*, *176*(3), 309–313. https://doi.org/10.1016/j.ygcen.2011.11.011

Tashiro, A., & Yuste, R. (2003). Structure and molecular organization of dendritic spines. *Histology and Histopathology*, *18*(2), 617–634. https://doi.org/10.14670/HH-18.617

Taylor, R. C., Cullen, S. P., & Martin, S. J. (2008). Apoptosis: controlled demolition at the cellular level. *Nature Reviews. Molecular Cell Biology*, *9*(3), 231–241. https://doi.org/10.1038/nrm2312

Thapar, A., Cooper, M., & Rutter, M. (2017). Neurodevelopmental disorders. *The Lancet. Psychiatry*, *4*(4), 339–346. https://doi.org/10.1016/S2215-0366(16)30376-5

Tran, H., Sawatari, A., & Leamey, C. A. (2015). The glycoprotein Ten-m3 mediates topography and patterning of thalamostriatal projections from the parafascicular nucleus in mice. *The European Journal of Neuroscience*, *41*(1), 55–68. https://doi.org/10.1111/ejn.12767

Tran, N. M., Shekhar, K., Whitney, I. E., Jacobi, A., Benhar, I., Hong, G., … Sanes, J. R. (2019). Single-Cell Profiles of Retinal Ganglion Cells Differing in Resilience to Injury Reveal Neuroprotective Genes. *Neuron*, *104*(6), 1039–1055.e12. https://doi.org/10.1016/j.neuron.2019.11.006

Trubiani, G., Al Chawaf, A., Belsham, D. D., Barsyte-Lovejoy, D., & Lovejoy, D. A. (2007). Teneurin carboxy (C)-terminal associated peptide-1 inhibits alkalosis-associated necrotic neuronal death by stimulating superoxide dismutase and catalase activity in immortalized mouse hypothalamic cells. *Brain Research*, *1176*, 27–36. https://doi.org/10.1016/j.brainres.2007.07.087

Tucker, R P, & Chiquet-Ehrismann, R. (2006). Teneurins: a conserved family of transmembrane proteins involved in intercellular signaling during development. *Developmental Biology*, *290*(2), 237–245. https://doi.org/10.1016/j.ydbio.2005.11.038

Tucker, Richard P, Kenzelmann, D., Trzebiatowska, A., & Chiquet-Ehrismann, R. (2007). Teneurins: transmembrane proteins with fundamental roles in development. *The International Journal of Biochemistry & Cell Biology*, *39*(2), 292–297. https://doi.org/10.1016/j.biocel.2006.09.012

Tucker, Richard P, Martin, D., Kos, R., & Chiquet-Ehrismann, R. (2000). The expression of teneurin-4 in the avian embryo. *Mechanisms of Development*, *98*(1-2), 187–191. https://doi.org/10.1016/S0925-4773(00)00444-5

Valtorta, F., Pennuto, M., Bonanomi, D., & Benfenati, F. (2004). Synaptophysin: leading actor or walk-on role in synaptic vesicle exocytosis? *Bioessays: News and Reviews in Molecular, Cellular and Developmental Biology*, *26*(4), 445–453. https://doi.org/10.1002/bies.20012

Vaughn, J. E. (1989). Fine structure of synaptogenesis in the vertebrate central nervous system. *Synapse*, *3*(3), 255–285. https://doi.org/10.1002/syn.890030312

Vaughn, J. E., & Sims, T. J. (1978). Axonal growth cones and developing axonal collaterals form synaptic junctions in embryonic mouse spinal cord. *Journal of Neurocytology*, *7*(3), 337–363. https://doi.org/10.1007/BF01176998

Vecino, E., Hernández, M., & García, M. (2004). Cell death in the developing vertebrate retina. *The International Journal of Developmental Biology*, *48*(8-9), 965–974. https://doi.org/10.1387/ijdb.041891ev

Visser, J. J., Cheng, Y., Perry, S. C., Chastain, A. B., Parsa, B., Masri, S. S., … Wojtowicz, W. M. (2015). An extracellular biochemical screen reveals that FLRTs and Unc5s mediate neuronal subtype recognition in the retina. *eLife*, *4*, e08149. https://doi.org/10.7554/eLife.08149

Waites, C. L., Craig, A. M., & Garner, C. C. (2005). Mechanisms of vertebrate synaptogenesis. *Annual Review of Neuroscience*, *28*, 251–274. https://doi.org/10.1146/annurev.neuro.27.070203.144336

Walikonis, R. S., Jensen, O. N., Mann, M., Provance, D. W., Mercer, J. A., & Kennedy, M. B. (2000). Identification of proteins in the postsynaptic density fraction by mass spectrometry. *The Journal of Neuroscience*, *20*(11), 4069–4080.

Wang, L., Rotzinger, S., Al Chawaf, A., Elias, C. F., Barsyte-Lovejoy, D., Qian, X., … Lovejoy, D. A. (2005). Teneurin proteins possess a carboxy terminal sequence with neuromodulatory activity. *Brain research. Molecular brain research*, *133*(2), 253–265. https://doi.org/10.1016/j.molbrainres.2004.10.019

Wang, X. Z., Kuroda, M., Sok, J., Batchvarova, N., Kimmel, R., Chung, P., … Ron, D. (1998). Identification of novel stress-induced genes downstream of chop.

The EMBO Journal, *17*(13), 3619–3630. https://doi.org/10.1093/emboj/17.13.3619

Washbourne, P. (2015). Synapse assembly and neurodevelopmental disorders. *Neuropsychopharmacology*, *40*(1), 4–15. https://doi.org/10.1038/npp.2014.163

Washbourne, P., Bennett, J. E., & McAllister, A. K. (2002). Rapid recruitment of NMDA receptor transport packets to nascent synapses. *Nature Neuroscience*, *5*(8), 751–759. https://doi.org/10.1038/nn883

Washbourne, P., Dityatev, A., Scheiffele, P., Biederer, T., Weiner, J. A., Christopherson, K. S., & El-Husseini, A. (2004). Cell adhesion molecules in synapse formation. *The Journal of Neuroscience*, *24*(42), 9244–9249. https://doi.org/10.1523/JNEUROSCI.3339-04.2004

Wässle, H. (2004). Parallel processing in the mammalian retina. *Nature Reviews. Neuroscience*, *5*(10), 747–757. https://doi.org/10.1038/nrn1497

Watanabe, Y., & Nakamura, H. (2000). Control of chick tectum territory along dorsoventral axis by Sonic hedgehog. *Development*.

Weinberg, D., Lenroot, R., Jacomb, I., Allen, K., Bruggemann, J., Wells, R., … Weickert, T. W. (2016). Cognitive subtypes of schizophrenia characterized by differential brain volumetric reductions and cognitive decline. *JAMA psychiatry*, *73*(12), 1251–1259. https://doi.org/10.1001/jamapsychiatry.2016.2925

Werblin, F. S., & Roska, B. M. (2004). Parallel visual processing: a tutorial of retinal function. *International Journal of Bifurcation and Chaos*, *14*(02), 843–852. https://doi.org/10.1142/S0218127404009508

Williams, M. A., Piñon, L. G., Linden, R., & Pinto, L. H. (1990). The pearl mutation accelerates the schedule of natural cell death in the early postnatal retina. *Experimental Brain Research*, *82*(2), 393–400. https://doi.org/10.1007/BF00231258

Won, S., Levy, J. M., Nicoll, R. A., & Roche, K. W. (2017). MAGUKs: multifaceted synaptic organizers. *Current Opinion in Neurobiology*, *43*, 94–101. https://doi.org/10.1016/j.conb.2017.01.006

Wong, W. T., & Wong, R. O. (2000). Rapid dendritic movements during synapse formation and rearrangement. *Current Opinion in Neurobiology*, *10*(1), 118–124. https://doi.org/10.1016/s0959-4388(99)00059-8

Wu, S. M. (2010). Synaptic organization of the vertebrate retina: general principles and species-specific variations: the Friedenwald lecture. *Investigative Ophthalmology & Visual Science*, *51*(3), 1263–1274. https://doi.org/10.1167/iovs.09-4396

Xiao, T., & Baier, H. (2007). Lamina-specific axonal projections in the zebrafish tectum require the type IV collagen Dragnet. *Nature Neuroscience*, *10*(12), 1529–1537. https://doi.org/10.1038/nn2002

Xiao, T., Roeser, T., Staub, W., & Baier, H. (2005). A GFP-based genetic screen reveals mutations that disrupt the architecture of the zebrafish retinotectal projection. *Development*, *132*(13), 2955–2967. https://doi.org/10.1242/dev.01861

Xiao, T., Staub, W., Robles, E., Gosse, N. J., Cole, G. J., & Baier, H. (2011). Assembly of lamina-specific neuronal connections by slit bound to type IV collagen. *Cell*, *146*(1), 164–176. https://doi.org/10.1016/j.cell.2011.06.016

Xu, B., Tang, X., Jin, M., Zhang, H., Du, L., Yu, S., & He, J. (2020). Unifying developmental programs for embryonic and postembryonic neurogenesis in the zebrafish retina. *Development*, *147*(12). https://doi.org/10.1242/dev.185660

Xu, H.-P., & Tian, N. (2007). Retinal ganglion cell dendrites undergo a visual activity-dependent redistribution after eye opening. *The Journal of Comparative Neurology*, *503*(2), 244–259. https://doi.org/10.1002/cne.21379

Xue, C.-B., Xu, Z.-H., Zhu, J., Wu, Y., Zhuang, X.-H., Chen, Q.-L., … Chen, J.-H. (2018). Exome Sequencing Identifies TENM4 as a Novel Candidate Gene for

Schizophrenia in the SCZD2 Locus at 11q14-21. *Frontiers in genetics*, *9*, 725. https://doi.org/10.3389/fgene.2018.00725

Yamagata, M, & Sanes, J. R. (1995). Lamina-specific cues guide outgrowth and arborization of retinal axons in the optic tectum. *Development*.

Yamagata, Masahito, & Sanes, J. R. (2008). Dscam and Sidekick proteins direct lamina-specific synaptic connections in vertebrate retina. *Nature*, *451*(7177), 465–469. https://doi.org/10.1038/nature06469

Yamagata, Masahito, Sanes, J. R., & Weiner, J. A. (2003). Synaptic adhesion molecules. *Current Opinion in Cell Biology*, *15*(5), 621–632. https://doi.org/10.1016/s0955-0674(03)00107-8

Yamagata, Masahito, Weiner, J. A., & Sanes, J. R. (2002). Sidekicks. *Cell*, *110*(5), 649–660. https://doi.org/10.1016/S0092-8674(02)00910-8

Yamauchi, T. (2002). Molecular constituents and phosphorylation-dependent regulation of the post-synaptic density. *Mass spectrometry reviews*, *21*(4), 266–286. https://doi.org/10.1002/mas.10033

Yan, W., Peng, Y.-R., van Zyl, T., Regev, A., Shekhar, K., Juric, D., & Sanes, J. R. (2020). Cell atlas of the human fovea and peripheral retina. *Scientific Reports*, *10*(1), 9802. https://doi.org/10.1038/s41598-020-66092-9

Young, T. R., Bourke, M., Zhou, X., Oohashi, T., Sawatari, A., Fässler, R., & Leamey, C. A. (2013). Ten-m2 is required for the generation of binocular visual circuits. T*he Journal of Neuroscience,* 3*3(*30), 12490–12509. https://doi.org/10.1523/JNEUROSCI.4708-12.2013

Young, T. R., & Leamey, C. A. (2009). Teneurins: important regulators of neural circuitry. *The International Journal of Biochemistry & Cell Biology*, *41*(5), 990–993. https://doi.org/10.1016/j.biocel.2008.06.014

Zhai, R. G., Vardinon-Friedman, H., Cases-Langhoff, C., Becker, B., Gundelfinger, E. D., Ziv, N. E., & Garner, C. C. (2001). Assembling the presynaptic active

zone: a characterization of an active one precursor vesicle. *Neuron*, *29*(1), 131–143. https://doi.org/10.1016/s0896-6273(01)00185-4

Zheng, C.-Y., Seabold, G. K., Horak, M., & Petralia, R. S. (2011). MAGUKs, synaptic development, and synaptic plasticity. *The Neuroscientist*, *17*(5), 493–512. https://doi.org/10.1177/1073858410386384

Zhou, X.-H., Brandau, O., Feng, K., Oohashi, T., Ninomiya, Y., Rauch, U., & Fässler, R. (2003). The murine Ten-m/Odz genes show distinct but overlapping expression patterns during development and in adult brain. *Gene Expression Patterns*, *3*(4), 397–405. https://doi.org/10.1016/S1567-133X(03)00087-5

Zuko, A., Oguro-Ando, A., Post, H., Taggenbrock, R. L. R. E., van Dijk, R. E., Altelaar, A. F. M., … Burbach, J. P. H. (2016). Association of Cell Adhesion Molecules Contactin-6 and Latrophilin-1 Regulates Neuronal Apoptosis. *Frontiers in Molecular Neuroscience*, *9*, 143. https://doi.org/10.3389/fnmol.2016.00143